MEMBRANE FOULING: INFLUENCE OF NATURAL ORGANIC MATTER PROPERTIES AND MEMBRANE SURFACE TREATMENT ON NANOFILTRATION PERFORMANCE

Rensselaer Polytechnic Institute
Troy, New York

Agreement No. 98-FC-81-0061

Desalination Research and Development
Program Report No. 83

September 2002

U.S. Department of the Interior
Bureau of Reclamation
Denver Office
Technical Service Center
Environmental Resources Team
Water Treatment Engineering and Research Group

REPORT DOCUMENTATION PAGE

Form Approved
OMB No. 0704-0188

1. AGENCY USE ONLY *(Leave Blank)*	2. REPORT DATE	3. REPORT TYPE AND DATES COVERED
	September 2002	

4. TITLE AND SUBTITLE

Membrane Fouling: Influence of Natural Organic Matter Properties and Membrane Surface Treatment on Nanofiltration Performance

5. FUNDING NUMBERS

Agreement No. 98-FC-81-0061

6. AUTHOR(S)

James E. Kilduff, Assistant Professor and George Belfort, Professor

7. PERFORMING ORGANIZATION NAME(S) AND ADDRESS(ES)

Department of Environmental and Energy Engineering
Rensselaer Polytechnic Institute
Troy, New York

Howard P. Isermann Department of Chemical Engineering
Rensselaer Polytechnic Institute
Troy, New York

9. SPONSORING/MONITORING AGENCY NAME(S) AND ADDRESS(ES)

Bureau of Reclamation
Denver Federal Center
PO Box 25007
Denver CO 80225-0007

10. SPONSORING/MONITORING AGENCY REPORT NUMBER

Desalination Research and Development Program
Report No. 83

11. SUPPLEMENTARY NOTES

12a. DISTRIBUTION/AVAILABILITY STATEMENT

Available from the National Technical Information Service, Operations Division, 5285 Port Royal Road, Springfield, Virginia 22161

12b. DISTRIBUTION CODE

13. ABSTRACT ***(Maximum 200 words)***

Membrane Fouling: Influence of Natural Organic Matter Properties and Membrane Surface Treatment on Nanofiltration Performance

New membrane technology has improved water flux and salt rejection and lowered operating pressures. However, membrane fouling can significantly reduce membrane performance, increase operating costs, and shorten membrane life.

This research calculated how natural organic matter properties influence membrane fouling. Natural aquatic organic matter was isolated from surface water sources to simulate fouling that might occur during potable water treatment. As natural organic matter from different feed waters has different properties, the study used three water sources. Experimental results revealed that membrane fouling depended on the membrane characteristics, the polarity of the natural organic matter, molecular weight, and feed solution chemistry.

14. SUBJECT TERMS--

membrane fouling, nanofiltration, NOM solution protocol, membrane characterization

15. NUMBER OF PAGES

145

16. PRICE CODE

17. SECURITY CLASSIFICATION OF REPORT	18. SECURITY CLASSIFICATION OF THIS PAGE	19. SECURITY CLASSIFICATION OF ABSTRACT	20. LIMITATION OF ABSTRACT
UL	UL	UL	UL

MEMBRANE FOULING: INFLUENCE OF NATURAL ORGANIC MATTER PROPERTIES AND MEMBRANE SURFACE TREATMENT ON NANOFILTRATION PERFORMANCE

James E. Kilduff, Assistant Professor
Department of Environmental and Energy Engineering
Rensselaer Polytechnic Institute

George Belfort, Professor
Howard P. Isermann Department of Chemical Engineering
Rensselaer Polytechnic Institute
Troy, New York

Agreement No. 98-FC-81-0061

Desalination Research and Development
Program Report No. 83

September 2002

U.S. Department of the Interior
Bureau of Reclamation
Denver Office
Technical Service Center
Environmental Resources Team
Water Treatment Engineering and Research Group

Mission Statements

U.S. Department of the Interior

The mission of the Department of the Interior is to protect and provide access to our Nation's natural and cultural heritage and honor out trust responsibilities to tribes.

Bureau of Reclamation

The mission of the Bureau of Reclamation is to manage, develop, and protect water and related resources in an environmentally and economically sound manner in the interest of the American public.

Federal Disclaimer

The information contained in this report regarding commercial products of firms may not be used for advertising or promotional purposes and is not to be construed as an endorsement of any product or firm by the Bureau of Reclamation.

The information contained in this report was developed for the Bureau of Reclamation: no warranty as to the accuracy, usefulness, or completeness is expressed or implied.

Acknowledgements

We gratefully acknowledge the support of the Bureau of Reclamation's Science and Technology Program and Desalination and Water Purification Research Program, in funding this research. We also gratefully acknowledge the efforts of Graduate and Undergraduate Student Research Assistants, for their role in conducting many of the experiments described in this report.

Graduate Student Research Assistants

Supatpong Mattaraj (Doctoral)
Jason E. Sensibaugh (Masters)
John P. Pieracci (Doctoral)
Andrew Wigton (Doctoral)
Krisidee Sirikrai (Masters)
Laurence Welch (Masters)

Undergraduate Student Research Assistants

Alicia Dunne

List Of Publications

Journal Articles:

Kilduff, J.E.; Mattaraj, S.; Sensibaugh, J.; Pieracci, J.P.; Belfort, G. Photochemical Modification of Poly(ether sulfone) and Sulfonated Poly(sulfone) Nanofiltration Membranes for Control of Fouling by Natural Organic Matter. *Desalination*, 132: 133-142 (2000).

Conference Proceedings:

Kilduff, J.E.; Mattaraj, S.; Pieracci, J.P.; Belfort, G. Photochemical Modification of poly(ether sulfone) and sulfonated poly(sulfone) nanofiltration membranes for Control Of Fouling by Natural Organic Matter. Proceedings of the International Water Association conference on Membranes in Drinking and Industrial Water Production, Paris, France, October 2000.

Mattaraj, S. and Kilduff, J.E. Effects of Natural Organic Matter Properties on Flux and Rejection in Nanofiltration Systems. Presented at the 32nd Mid-Atlantic Hazardous and Industrial Wastes Conference, Rensselaer Polytechnic Institute, Troy, NY, June 25-26, 2000.

Mattaraj, S.; Kilduff, J.E. Crossflow Membrane Filtration for Removing Natural Organic Matter: Factors Affecting Flux Reduction. Presented at the 74th Colloid and Surface Science Symposium, American Chemical Society, Lehigh University, Bethlehem, Pennsylvania, June 18-21, 2000.

Mattaraj, S.; Sensibaugh, J. Pieracci, J.P.; Belfort, G. and Kilduff J.E. "Effects of Natural Organic Matter on Membrane Processes for Pollution Control" Presented at the 1999 Annual Meeting of the American Institute of Chemical Engineers, Dallas, TX, October 31 - November 5, 1999.

Oral and poster presentations:

Mattaraj, S.; Sensibaugh, J.E.; Pieracci, J.P.; Belfort, G. ; Kilduff, J.E. Modification of Nanofiltration Membranes for Control of NOM Fouling. Presented at the AWWA Annual Conference, Washington, DC, June 17-21, 2001. (Oral Presentation).

Mattaraj, S.; Kilduff, J.E. Nanofiltration of Surface Waters: Factors Affecting Flux and Rejection. Presented at the NY Section, American Water Works Association, Syracuse University, Syracuse, NY, April 13, 2000.

Table of Contents

List of Tables

List of Figures

Executive Summary

Poly(ether sulfone) and sulfonated poly(sulfone) nanofiltration membranes were modified by UV irradiation and UV-assisted graft polymerization of N-vinyl-2-pyrrolidinone (NVP) as a strategy for increasing the wettability of membrane surfaces and mitigating fouling by naturally-occurring organic compounds present in surface waters. The UV-assisted graft polymerization approach with a reaction time of 60 s increased the wettability (increased cos θ) of membrane surfaces, which exhibited a significantly lower propensity to foul. For this reaction time, clean water permeability and solute rejection (as organic carbon) were maintained close to that of the as-received membranes. Graft polymerization was carried out using two different methods. Using the dip method, membrane coupons coated with a 3% N-vinyl-2-pyrrolidinone solution were UV irradiated under nitrogen. Using the immersion method, membrane coupons were irradiated directly in nitrogen-purged 3% NVP solution. Both techniques increased membrane wettability; however, the immersion technique required much longer reaction times resulting from the absorption of UV radiation by the monomer solution.

The influence of natural organic matter (NOM) properties on the fouling potential of NOM in nanofiltration systems was investigated using a crossflow bench-scale test cell. Three different water sources (Tomhannock (TMK) reservoir, NY; Intercoastal Waterway Myrtle beach (MB), SC; and Edisto River Charleston (CT), SC), were isolated by a field reverse osmosis (RO) membrane. The concentrated NOM solution was then fractionated by adsorption to XAD8 resin (to yield hydrophobic and hydrophilic fractions) and by ultrafiltration (to yield several molecular weight fractions). Membrane performance including permeate flux decline and rejection were observed during filtration experiments. Experimental results revealed that membrane fouling was dependent on the NF membrane characteristics, NOM polarity, molecular weight, and feed solution chemistry. The tightest NF membrane (NF-70) showed the worst membrane fouling and highest dissolved organic carbon (DOC) rejection. Increased membrane openness (NTR7450) and decreased wettability (NF-PES-10) increased irreversible fouling, possibly due to NOM trapped in the membrane pores. Solutions having higher ionic strength exhibited more membrane fouling and decreased DOC rejection, possibly due to a combination of decreased electrostatic charge repulsion between a negatively charged NOM macromolecules, and conformational changes tending to decrease NOM size. At high ionic strength, the hydrophobic NOM fraction exhibited the greatest flux decline for most natural water sources. However, at low ionic strength, the hydrophilic MB- and CT-NOM fractions caused more membrane fouling and increased "irreversible" fouling on the membrane. The hydrophobic fractions of MB-and CT-NOM solution showed less membrane fouling than the hydrophilic fractions, possibly due to larger molecular weight from hydrophobic components, thus producing a looser cake layer on the membrane surface. It was observed that larger NOM molecular weight fractions (those retained by a 5 kDa UF membrane) of the MB- and CT waters exhibited less membrane fouling, increased DOC rejection and decreased irreversible fouling. However, the larger NOM molecular weight fractions of the TMK water caused more membrane fouling, and increased irreversible fouling. For the TMK-NOM solution, large TMK-NOM molecular weight (5-K UF membrane) showed the worst membrane fouling and caused irreversible fouling.

1.0 Introduction

New membrane technology has resulted in materials offering improved water flux, improved salt rejection, and lower operating pressures. However, membrane fouling by colloidal substances can significantly reduce membrane performance, increase operating costs, and shorten membrane life (Nilson and DiGiano, 1996). Understanding fouling mechanisms and developing ways to control them are critical for the economical development of water treatment technologies. Naturally occurring dissolved and colloidal organic matter (NOM) is considered a major contributor to membrane fouling in water treatment applications, including microfiltration (Kaiya, et al., 1996; Yuan and Zydney, 1999a;Yuan and Zydney, 1999b), ultrafiltration (Mallevialle et al., 1989; Jucker and Clark, 1994; Cho et al., 1999; Kabsch-Korbutowicz et al. 1999; Lin et al., 1999; Cho et al., 2000a; Cho et al., 2000b; Maartens et al., 2000) and nanofiltration (Nilson and DiGiano, 1996; Hong and Elimelech, 1997; Braghetta et al., 1997; Braghetta et al., 1998; Alborzfar et al., 1998; Yoon et al., 1998; Combe et al., 1999 Manttari et al., 2000). In addition, removal of natural organic matter prior to disinfection of potable water represents one of the primary strategies to control the formation of disinfection by-products, including trihalomethanes and haloacetic acids that form when chlorine reacts with NOM. Disinfection by-products in drinking water are suspected to be toxic, carcinogenic and mutagenic to humans (Glaze et al., 1993; Putnam and Graham, 1993), and are regulated by the EPA through the Disinfectants/ Disinfection By-products (D/DBP) Rule (Federal Register, 1994). In Stage I of this Rule, the maximum contaminant level (MCL) will be lowered from 100 to 80 μg/l for total trihalomethanes, and an MCL of 60 μg/l will be set for the total of five haloacetic acids (HAA_5: monochloro-, dichloro-, trichloro-, monobromo-, and dibromo-acetic acids); in Stage II, the MCLs are expected to be further decreased to 40 and 30 μg/l for total trihalomethanes and the five haloacetic acids respectively. Membrane processes have been shown to be effective for disinfection by-product precursor removal, and their economics are becoming increasingly competitive (Blau et al., 1992; Allegeir and Summers, 1995;Visvanathan et al., 1998; Chellam, 2000).

Natural organic matter is present in all surface and ground waters, with total organic carbon concentrations generally ranging from 1 to 8 mg/l and median concentrations of 3.4 mg/l and 0.8 mg/l in surface water and ground water, respectively (Symons et al., 1975; Krasner et al., 1995; Lawrence, 1989). NOM is a heterogeneous mixture of complex organic materials including humic substances, hydrophilic acids, proteins, lipids, carboxylic acids, amino acids, and hydrocarbons. Humic substances comprise the bulk of organic substances in natural systems; estimates range from 30 to 80% (Thurman and Malcolm, 1981; Thurman, et al., 1982 & 1985; Morel, 1983; Kim, 1988; Buffle, 1990; Aiken et al., 1995; Krasner et al. 1996). Carbohydrates and proteinaceous materials may be adsorbed or covalently bonded to a humic substance "core" (Malcom, 1990; Schnitzer, 1991; Schulten and Schnitzer, 1993). The molecular size and weight of humic substances have been estimated using a variety of techniques, and reported weight-averaged molecular weights (M_w) for aquatic humic substances generally range from 1500 to 5000 g/mol for humic acids and from 600 to 2000 for fulvic

acids (Thurman et al., 1982; Beckett et al., 1987;Aiken et al., 1987; Reid et al., 1990; Chin and Gschwend, 1991; Chin et al., 1994). Estimated radii of gyration of humic substances fall in the range of 4.5 to 30 Å (Thurman et al., 1982; Cameron et al., 1972; Cornel et al., 1986).

One primary objective of this research was to evaluate how natural organic matter properties influence fouling mechanisms. Natural aquatic organic matter was isolated from a surface water source, to simulate the fouling that might occur during potable water treatment. It is important that the organic matter composition of filtration solutions employed to study membrane performance is representative of feed waters encountered in practice, because it has been shown that NOM from different environments (e.g. soil, surface water, and groundwater) have significantly different properties (Malcolm, 1990; Malcolm and MacCarthy, 1986). For example, it has been shown that the composition of saccaride, phenolic, methoxyl, aromatic, hydrocarbon, amino acid and nitrogen moieties of each type of humic substance depends, to some degree, on whether the source was a surface water, marine, or soil environment (Malcolm, 1990). For example, aromaticity increases in the order marine < stream < soil for both humic and fulvic acids. NOM was isolated from surface water sources using a field RO system, and fractionated according to molecular weight and polarity. Isolates and fractions were characterized by total organic carbon, UV spectroscopy, molecular weight distributions, and acidity. Fouling characteristics of NOM and NOM fractions were measured in a bench-scale test cell designed to provide hydrodynamics similar to full-scale spiral-wound membrane elements.

Several approaches to mitigate the negative effects of NOM fouling on nanofiltration membrane performance have been described (Potts et al., 1981). These include (i) selecting a membrane material that minimizes attractive interactions between NOM and the membrane surface (Childress and Elimelech, 1996), (ii) improved pretreatment to selectively remove the most adhesive components in NOM (Rautenbach et al., 1997), and (iii) enhanced module design and operation that reduces fouling through more effective hydrodynamics (Chellam and Wiesner, 1997; Mallubhotla et al., 1998). An important variant of (i) above is to tailor membrane surface chemistry for particular applications. Modifications to polymer substrates can be made through homogeneous reaction in solution with subsequent preparation as a synthetic membrane via phase inversion (Nabe et al., 1997). However, an easier, inexpensive, and scalable approach involves surface modification of commercial membranes. One approach based on low-temperature plasma and plasma-initiated graft polymerization has been described (Ulbricht and Belfort, 1996). Belfer and coworkers have recently modified commercial composite polyamide reverse osmosis membranes via radical grafting of hydrophilic monomers initiated using a potassium persulfate-sodium metabisulfite chemical redox system (Belfer et al., 1998). Recently, a general method for modifying poly(aryl sulfone) membranes was developed (Yamagishi et al., 1995a; Yamagishi et al., 1995b; Pieracci et al., 2000). The membranes are UV-irradiated in the presence of either water or methanol-soluble monomers, which chemically bond to poly(aryl sulfone) chains; a mechanism involving a photochemically induced free radical cleavage of the polymer chain was proposed (Yamagishi et al., 1995a). This method, which is described more

fully in a US Patent (Yamagishi et al., 1995), takes advantage of the intrinsic photosensitivity of poly(aryl sulfones), which precludes the need for a photoinitiator.

Poly(aryl sulfone) membranes offer attractive features for water treatment applications, including good chemical stability. Such stability results from electronic deactivation of the aromatic rings by the adjacent sulfone ($-SO_2$) groups, and steric hindrance to rotation around the polymer backbone created by the repeating aromatic rings (Zeeman and Zydney, 1996). Poly(aryl sulfone) membranes exhibit wide pH tolerance (1 to13); good resistance to oxidants, including chlorine under water treatment conditions (i.e., < 50 ppm); and high temperature limits (operation at 75 °C and limited exposure to temperatures up to 125 °C) (Zeeman and Zydney, 1996). This is in contrast to widely used aromatic polyamide membranes, which are susceptible to oxidative degradation, cannot tolerate exposure to free chlorine because of their amide functionality, and have relatively low temperature thresholds (e.g. < 40 °C).

A possible disadvantage of poly(aryl sulfone) membranes is that they generally exhibit lower wettability ($\cos\theta \approx 0.50$ to 0.60) than both regenerated cellulose ($\cos\theta >$ 0.80) and commercially available aromatic polyamide ($\cos\theta > 0.80$) membranes. Previous research has correlated low surface wettability with non-specific sorption of both detergents and proteins (Sigal et al., 1998). Therefore, poly(aryl sulfone) membranes are potentially more susceptible to fouling by natural organic matter and other colloidal material.

A second primary objective of this research was to develop a UV-assisted photochemical graft polymerization technique to increase the wettability of commercially-available poly(aryl sulfone) nanofiltration membrane surfaces. The goal is to produce more wettable surfaces that lack the ability to interact with hydrophobic moieties present on natural organic molecules, as a route to reducing the fouling caused by NOM. Photochemical graft polymerization offers a promising approach to developing physically and chemically robust materials that exhibit lower fouling by NOM than the native polymers. An additional objective was to compare two different techniques for carrying out the graft polymerization. In the first ("dip") technique, the membrane surface was coated with monomer solution, and irradiated through an inert gas atmosphere. In the second ("immersion") technique, the membrane surface was submerged in a monomer solution, and irradiated through this solution. As-received and surface modified membranes were tested. As-received and fouled membranes were characterized by contact angle, and attenuated total reflection infrared spectroscopy.

2.0 Field Scale RO System for Organic Matter Isolation

2.1 Introduction

One approach to studying the role of NOM in environmental processes is to use source waters directly. Another approach involves isolating NOM from source waters. The objective of isolation is to concentrate organic constituents from source waters with minimal chemical alteration (Jolley and Suffet, 1987). Isolating and concentrating NOM provides several advantages over direct use of source waters, including:

1) reduced storage requirements;

2) providing a consistent supply for long-term studies;

3) providing sufficient mass of NOM to investigate concentration effects; and,

4) providing sufficient mass of NOM to investigate behavior of components through fractionation techniques, including adsorption by XAD resins (Thurman and Malcolm, 1981) and molecular weight fractionation by ultrafiltration (UF) (Buffle et al., 1978).

Several methods have been used to isolate NOM, including vacuum evaporation (Beck et al., 1974), chemical precipitation (Weber and Wilson, 1975), adsorption on XAD resins (Mantoura and Riley, 1975; Thurman and Malcolm, 1981), and adsorption by DEAE cellulose (Miles et al., 1983). However, these each isolation technique has a characteristic limitation. For example, vacuum evaporation can be slow and inconvenient for processing large volumes of solution; chemical precipitation uses aggressive reagents, may cause alteration of the NOM structure, and may exhibit low recovery; processing large volumes of water through adsorbent beds can be slow, and recovery is limited (e.g., recovery from XAD resins is on the order of 75 to 92%; recovery from activated carbon can be much lower) (Serkiz and Perdue, 1990). A desirable feature of any isolation process is near complete recovery of organic constituents from source waters with minimal chemical alteration (Jolley and Suffet, 1987).

Reverse osmosis (RO) is a pressure-driven membrane process that has many advantages as an isolation technique. Reverse osmosis has been used as a water treatment process to remove humic substances because RO membranes exhibit high NOM rejection (Kim et al., 1989; Odegaard and Koottatep, 1982). Advantages of RO include the ability to process large volumes of source water, recover organic carbon efficiently and in large quantities over relatively short periods of time, and isolate NOM without the need for strong chemical reagents (Serkiz and Perdue, 1990; Sun et al., 1995). Field-scale reverse osmosis systems have been used to isolate DOM from surface and ground waters with good success (Kim et al., 1989; Serkiz and Perdue, 1990; Clair et al., 1991; Sun et al., 1995). While it is expected that the RO isolation process will cause minimal alteration of the NOM, few studies have addressed this issue in any detail. Possible mechanisms contributing to alteration of the NOM include changes in solution composition; *i.e.*, increases in both organic and inorganic constituent concentrations.

The objectives of this chapter describes are to:

1. Develop a protocol to characterize the hydraulics of the RO system (pump and headloss) and the membrane permeability, to provide data for evaluating membrane integrity and the extent of fouling in field applications. Incorporate relationships between transmembrane pressure, feed flowrate, product water recovery, rejection, and temperature into mass-balance models that can be used to predict process operation.

2. Evaluate the effects of transmembrane pressure, solution flux, and crossflow velocity on the recovery of DOC under controlled laboratory conditions. Evaluate the effectiveness of hydrodynamic cleaning in recovering NOM that accumulates on the membrane surface during operation.

3. Compare the performance of the system, under field conditions, for isolating several surface waters with significantly different organic carbon concentrations and hydrophobic/hydrophilic characteristics.

4. Confirm that RO isolation does not change DOC reactivity in terms of molecular weight distribution and adsorption properties.

2.2 Experimental

2.2.1 RO System

Figure 2-1 is a schematic of the field RO system custom-built in our laboratory. During operation, water was pumped from the source, pretreated, and then fed to a 200-L stainless-steel sample reservoir. Pretreated sample water was concentrated across the RO membrane, and then recirculated back to the reservoir, forming a closed loop. The membrane module consists of a 10 cm × 100 cm (7.44 m^2) spiral-wound aromatic polyamide thin-layer composite membrane (Fastek™ TLC) housed in a stainless steel pressure vessel (Osmonics, Inc., Minnetonka, MN, USA). This membrane was chosen based on it's high salt rejection characteristics (99% at 2000 ppm NaCl, 225 psig), and the success of polyamide thin-layer composite membranes in water treatment applications (Taylor et al., 1987). Membrane specifications are summarized in Table 2-1.

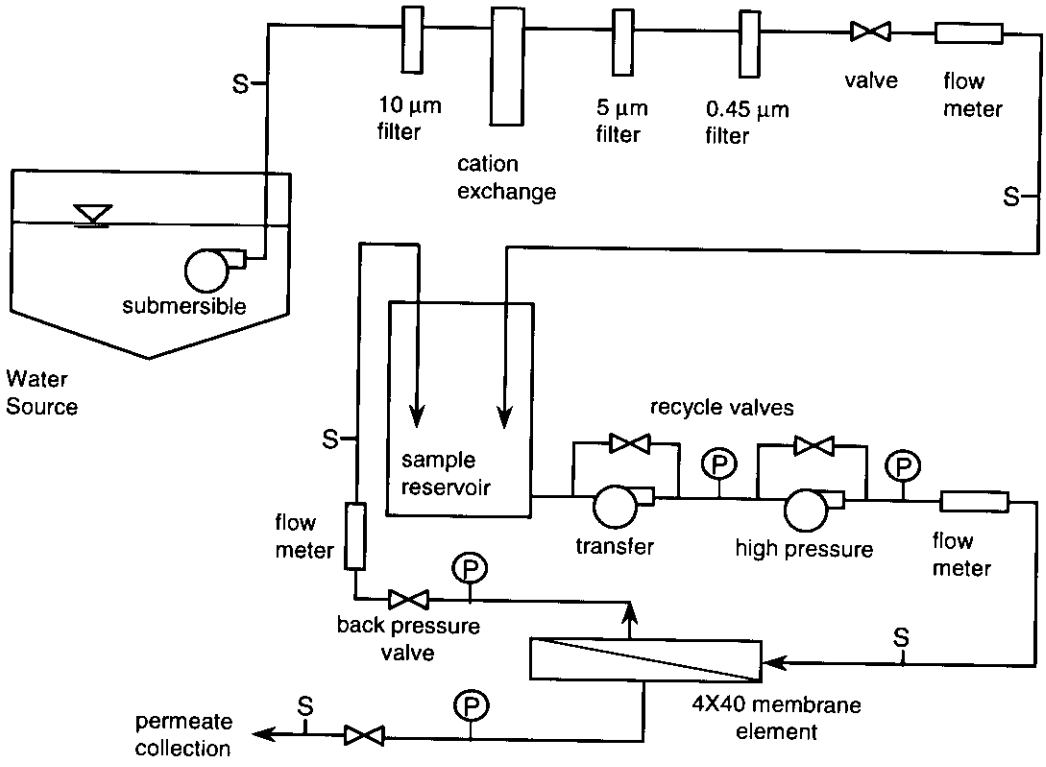

Figure 2-1. Process schematic of the field-scale RO system. "P" represents a pressure guage. "S" represents a sampling tap.

Table 2-1. Characteristics and Specifications - Field-Scale RO System

Parameter	Specification
Membrane size	S4040 (3.9 inch x 40 inch)
Membrane type	Spiral wound cross flow
Membrane material	Aromatic polyamide
Total surface area	80 ft^2
Maximum operating pressure	250 psig
Silt density index (15 min)	less than 5
pH range	3-11
Maximum feed water temperature	10-30 °C
Maximum feed chlorine	less than 0.1 mg/L
Maximum feed flow	6 gpm
Feed turbidity	less than 1 NTU
Salt rejection @ 225 psig (2000 ppm NaCl)	99% (typical)

System pressure is generated using a high-pressure stainless-steel multi-stage centrifugal pump (Tonkaflo, Osmonics, Inc.) capable of providing 15 L/m (4 gpm) against 1447 kPa (210 psig). The multi-stage centrifugal pump requires an inlet pressure of about 200 kPa; this was provided using a centrifugal transfer pump mounted on a separate hand truck. The high-pressure pump was chosen to meet membrane module design specifications; *i.e.*, a feed flow (Q_f) of about 15 L/min, a permeate flow (Q_p) of about 2 L/min and a concentrate flow (Q_c) of about 13 L/min.

Both the RO membrane and the high-pressure pump were mounted together on a single hand-truck; all interconnections were made using either 0.5-inch or 0.75-inch O.D. stainless-steel tubing. The larger size achieves a good balance between system head loss and cost of fittings, valves, and appurtenances. A needle valve was provided in the concentrate line to control the operating (transmembrane) pressure. Two flowmeters (Great Plains Industries) calibrated between 4 and 40 L/min were provided to monitor feed and concentrate flow rates. Pressure gauges were provided to continuously monitor feed and concentrate pressure.

2.2.2 Pretreatment of raw water

Water was pumped by a stainless steel submersible pump (Grundfos, Inc.) from the source (*i.e.*, lake, river etc.) through a series of pretreatment steps. Pretreatment of raw waters consisted of two steps. The first pretreatment step included a virgin polypropylene 10-μm pre-filter to remove larger particles, in series with a sodium-form cation exchange softener (Osmonics, Inc.) to remove multivalent cations (mainly Ca^{++} and Mg^{++}, Fe^{++}, and Mn^{++}) and thus minimize precipitation (scaling) on the membrane surface. The softener was sized to have a capacity of 10 L/min to provide the capability of filling the 200-L sample reservoir in less than one hour. Softened source water was then microfiltered through two cartridge filters in series (glass fiber or virgin polypropylene) (Osmonics or U.S. Filter, Inc.). Two cartridge filters, a ball valve, and a totalizing flow meter were constructed with the transfer pump (discussed above) on a single hand-truck. The cation exchange resin is salt-regenerable in the field.

2.2.3 NOM Isolation Protocol

Prior to NOM isolation, the sample reservoir was filled with filtered and softened source water. Next, using the transfer pump, the RO system was flushed with at least 20-L (3 void volumes) of filtered and softened source water. With the transfer pump primed and running, and the concentrate valve fully open, the high-pressure pump was started. Then, the backpressure valve (in the concentrate line) was closed slowly to adjust the operating pressure to the desired value. Typically, transmembrane pressure was maintained in the range of 414 to 1000 kPa (60 to 145 psi) during NOM isolation.

During NOM isolation, filtered and softened water was continuously added to the sample reservoir to keep a constant volume of 200-L. Keeping the sample reservoir full facilitates subsequent modeling, and provides a large heat sink that limits increases in sample temperature. Sample temperature was controlled with a stainless-steel cooling coil immersed in the sample

reservoir. Part of the source water flow to the sample pretreatment train was diverted to flow through the cooling coil.

At regular intervals, feed and permeate water was sampled for DOC, UV absorbance and conductivity analysis. Water temperature, concentrate pH, and permeate flow were monitored at regular intervals in the field. A single isolation run concludes by allowing the sample to concentrate to a final volume of approximately 20 liters. After recovering the sample from a drain in the sample reservoir, the system was flushed with about 10 L of permeate water (about 1.5 void volumes). The membrane was then cleaned with 10-L of permeate adjusted to pH of 10 (using NaOH) which was recirculated for 20 minutes to remove NOM that had accumulated on the membrane surface. After chemical cleaning, the system was again flushed with permeate water until the original permeate pH (about 6) is recovered. Overall NOM mass recovery was calculated from DOC measurements and the volumes of recovered NOM solutions (including isolated sample water, analytical samples, flush, and NaOH wash):

$$\%\ \text{Total Mass Recovery} = \frac{V_c C_c + \sum V_{sample} C_{sample} + V_{flush} C_{flush} + V_{NaOH} C_{NaOH}}{V_{initial} C_{initial}} \qquad (1)$$

Where, V_c and C_c are the volume and concentration of isolate (~20 L), the sum of $V_{sample} \times C_{sample}$ is the mass organic carbon (mg) present in samples taken for analysis; $V_{flush} \times C_{flush}$ is the mass organic carbon (mg) present in the clean water flush after processing; and $V_{NaOH} \times C_{NaOH}$ is the mass organic carbon (mg) present in the NaOH cleaning solution. Where possible, sample volumes were measured gravimetrically using an electronic bench scale (Ohaus Inc.).

2.2.4 Source Water characteristics

Source waters selected for this study were the Tomhannock reservoir, drinking water supply for the city of Troy, NY; the Intercoastal Waterway, drinking water supply for Myrtle Beach, SC; and the Edisto River, drinking water supply for Charleston, SC. For isolations not carried out on-site, source waters were collected in 20-L glass carboys and/or fluorinated polyethylene jerricans. These vessels were pre-cleaned in the laboratory, followed by exhaustive rinsing with clean DI water. Clean carboys were rinsed with raw water in the field prior to sample collection. Raw waters were transported to the laboratory and were stored at 4 °C in the dark. The characteristics of these raw waters are tabulated in Table 2-2.

2.2.5 Sample Analysis

Sample analysis was conducted in the Keck Water Quality Laboratory at Rensselaer Polytechnic Institute, and in the Department of Environmental Engineering and Science at Clemson University. The samples analyzed included source water, filtered source water, permeate, and concentrate waters. UV absorbance was measured using a diode-array spectrophotometer (HP8452A, Hewlett Packard, Menlo Park, CA). Samples were analyzed in duplicate. A 5-cm cell was used for low concentration samples (including membrane permeate) while a 1-cm cell was used for all other samples. Organic carbon was measured using an analyzer employing a high-temperature persulfate oxidation process (Model 1010, OI

Analytical, College Station, TX). Reagant grade I water was used as a blank and as dilution water. It was prepared by filtering tap water through an activated carbon filter and two mixed-bed ion exchange columns; this was followed by processing through a Milli-Q system (Millipore, Bedford MA) consisting of an activated carbon bed, two beds containing a mixture of strong acid and strong base ion-exchange resins, and a 0.20 micron microfilter. This water had a DOC of approximately 0.10 mg/L. For organic carbon analysis, at least three sample injections were made, and reported values are averages of at least two replicates (*i.e.*, data falling outside the 95% confidence interval were treated as outliers and were discarded). Analytical precision was consistently within 3%. The analytical procedures followed for other water quality parameters, including hardness, Ca^{++}, Mg^{++}, Cl^{-}, pH, temperature, turbidity, conductivity, and alkalinity, are described in Standard Methods (Eaton et al., 1995). Temperature, pH, turbidity, and conductivity readings were taken after stable meter readings had been achieved, generally 1 to 2 minutes. Before samples were analyzed, each instrument was calibrated using external standards as outlined in Standard Methods.

Specific conductivity (AP50, Denver Instruments Company) was measured as a surrogate parameter for ionic strength. A calibration between conductivity ($\mu S/cm$) and the ionic strength was developed:

$$I.S. = \frac{1}{2}\sum C_i Z_i^2 = 9.5\times10^{-6} \times (\mu S/cm) \qquad (2)$$

where C_i is the molar concentration and Z_i is the ionic valence.

Table 2-2. Raw Water Characteristics.

Parameter	Tomhannock	Myrtle Beach	Charleston
DOC (mg/L)	2.99	23.8	3.44
$UV_{254\ nm}$ (cm^{-1})	0.074	1.06	0.162
SUVA (L/mg-C.m)	2.5	4.5	4.7
Acidity at pH 7 meq/mg-C)	11.4	9.4	8.4
Alkalinity mg$CaCO_3$/L)	35	94	66
Hardness (mg$CaCO_3$/L)	76	40	27
pH	7.2	7.8	7.8

Note: values reported are the average of triplicate measurements. DOC is dissolved organic carbon. SUVA is specific UV absorbance.

2.3 Modeling

Overall system mass balance equations are written under the assumption that the density of water remains constant. These equations, written for water and solute, respectively, are:

$$Q_f = Q_p + Q_c \tag{3}$$

$$Q_f C_f = Q_p C_p + Q_c C_c \tag{4}$$

$$r = \frac{Q_p}{Q_f} \tag{5}$$

where Q_f, Q_p and Q_c are the feed, permeate, and concentrate (retentate) flows [L min^{-1}]; C_f, C_p and C_c are the feed, permeate, and concentrate concentrations [mg L^{-1}]; and r is recovery.

The volumetric solution flux, J_v, of water passing through the membrane surface is proportional to the water mass transfer coefficient (or permeability), L_p [L m^{-2} hr^{-1} kPa^{-1}], and the net transmembrane pressure gradient (ΔP-$\Delta\pi$) [kPa]:

$$J_v = L_p(\Delta P - \Delta\pi) = \frac{Q_p}{A_m} \tag{6}$$

where ΔP is the average transmembrane pressure [$(P_{feed} + P_{concentrate})/2 - P_{permeate}$], $\Delta\pi$ is the osmotic pressure, and A_m is the membrane area [m^2]. Solute flux is proportional to the concentration differential between the membrane surface (C_m) and the permeate, but is often expressed phenomenologically in terms of feed and permeate concentrations:

$$J_s = K_s(C_m - C_p) = K_s'\left\{\left[\frac{C_f + C_c}{2}\right] - C_p\right\} \tag{7}$$

where K_s is a solute mass transfer coefficient [m min^{-1}], which incorporates solute diffusivity and a membrane distribution coefficient, while K_s' is a phenomenological coefficient.

By continuity, the solute flux must also equal the product of the volumetric solution flux and the permeate concentration:

$$J_s = \frac{Q_p C_p}{A} = J_v C_p \tag{8}$$

Solute rejection, R, is defined as:

$$R = 1 - \frac{C_p}{C_f} \tag{9}$$

A mass balance relationship can be written on the sample reservoir under the assumption of complete mixing in the reservoir. Input to the sample reservoir included the pretreated source water ($Q_s C_s$) and the recycled concentrate (retentate) stream ($Q_c C_c$). Output from the sample reservoir is the feed stream to the membrane ($Q_f C_f$). The mass balance is:

$$C_f \frac{dV_r}{dt} + V_r \frac{dC_f}{dt} = Q_c C_c + Q_s C_s - Q_f C_f \tag{10}$$

where V_r is the volume of the sample reservoir [m^3]. Eliminating $Q_c C_c$ in favor of feed and permeate values using Eq. 4, and expressing C_p in terms of C_f and rejection using Eq. 9, the mass balance can be written:

$$C_f \frac{dV_r}{dt} + V_r \frac{dC_f}{dt} = Q_s C_s - Q_p (1-R) C_f \tag{11}$$

This makes the assumption that accumulation (loss) of mass on the membrane surface is negligible. If the sample reservoir volume is maintained constant, by either sample feed or buffer feed, the time derivative of volume goes to zero. The resulting solution for the feed concentration as a function of time is then:

$$C_f = C_{f,o} e^{-\beta t} + \frac{Q_s C_s}{Q_p (1-R)} \left[1 - e^{-\beta t}\right] \tag{12}$$

where $\beta = Q_p (1-R)/V_{r,o}$ and $V_{r,o}$ is the initial (and constant) reservoir volume. Note that this is a more general form of Eq. 9 as reported by Kilduff and Weber (1992); if the volume is maintained constant by using a buffer feed ($Q_{buffer} = Q_p$), then Q_s is zero and the second term on the right hand side of the equation goes to zero. The buffer flow rate does not appear directly in equation 12 because it does not involve an input or removal of dissolved carbon from the system. If the volume is allowed to vary, then:

$$\frac{dV_r}{dt} = Q_s + Q_c - Q_f = Q_s - Q_p \tag{13}$$

Therefore, upon integration, $V_r = V_{r,o} + (Q_s - Q_p)t$. Substituting into Eq. 11,

$$\frac{dC_f}{dt} + \left[\frac{Q_s - RQ_p}{V_{r,o} + (Q_s - Q_p)t}\right] C_f = \frac{Q_s C_s}{V_{r,o} + (Q_s - Q_p)t} \tag{14}$$

Solution of this differential equation with the initial condition that $C_f = C_{f,o}$ when $t = 0$ yields:

$$C_f = \frac{Q_s C_s}{Q_s - RQ_p} + \frac{V_{r,o}^{\alpha}}{\left(V_{r,o} + (Q_s - Q_p)t\right)^{\alpha}} \left[C_{f,o} - \frac{Q_s C_s}{Q_s - RQ_p}\right] \tag{15}$$

where $\alpha = (Q_s - RQ_p)/(Q_s - Q_p)$. Note that this is a more general form of Eq. 11 as reported by Kilduff and Weber (1992), which can be recovered by setting Q_s equal to zero.

2.4 Results and Discussion

2.4.1 Pretreatment of Source Water

Two pretreatment experiments were conducted using Tomhannock water to provide a rational basis for selecting pretreatment filters. The first experiment evaluated the performance of a stainless-steel 10-μm prefilter in series with a cation exchanger followed by 5 μm and 0.45 μm cartridge filters. Turbidity was used as the primary measure of pretreatment efficiency, but other water quality parameters were also measured. As illustrated in Figure 2-2, the initial raw water turbidity of 2.1 NTU was reduced to 0.62 NTU (71 % reduction) by the 10-μm pre-filter and the cation exchange softener combination. The pH increased from 6.74 to 7.43, most likely as a result of CO_2 degassing, but alkalinity remained unchanged. After further microfiltration through two cartridge filters in series (5 and 0.45 μm), the turbidity was further reduced to 0.44 NTU (about 80% removal based on raw water turbidity) while the final pH was increased to 7.84. The removal of cations (e.g., mainly Ca^{2+} and Mg^{2+}) by the ion exchanger was greater than 95%. This is expected to significantly reduce precipitation of divalent ions and destabilized natural organic matter on the membrane surface. Because sodium ions were exchanged, the conductivity remained the same after softening. Table 2-3 shows the overall performance of pretreatment before concentrating NOM.

In a second set of experiments, the *silt density index* (SDI) was used as a membrane-fouling criterion. SDI measurements were made for raw water, and raw water filtered sequentially. The sequence used in this set of experiments was the 10-μm filter followed by 5, 1, 0.45-μm filters and finally including ion exchange. Samples were collected after each pretreatment step. The SDI test involves passing the water sample through a 0.45-μm Millipore filter with a 47-mm internal diameter at a constant pressure of 30 psig. The filtration volume analyzed is chosen as the volume of sample water that can be filtered within 10% of the time required to filter a non-fouling reference water (Milli-Q reagent-grade water). In this study, a volume of 100 ml was chosen based on this criteria. The time to collect the first 100 ml (t_i- t_o) is recorded. Filtration is continued for 5 minutes, and the time required to collect a second 100 ml (beginning at t = 5) is recorded (t_f). Filtration is continued for another 5 minutes, and the measurement is repeated. Filtration is then continued for a final 5 minutes, and the measurement is repeated once again. The final SDI is calculated using:

$$SDI_T = \frac{\left[1 - \frac{t_i}{t_f}\right] \cdot 100}{T} \qquad (16)$$

where, t_i is the time to collect the initial 100 ml of sample, t_f is the time to collect final 100 ml of sample, and T is total running time of the test (min). Three values of t_f will be available, one each beginning at 5, 10, and 15 minutes of filtration. The t_f chosen to calculate the SDI is the value which satisfies the following criteria:

$$\left[1-\frac{t_i}{t_f}\right] < 0.75 \qquad (17)$$

The value chosen is indicated by a subscript after the SDI acronym; i.e., if the t_f beginning at 10 minutes is chosen, the SDI is indicated as SDI_{10}. Table 2-4 shows the results from all SDI tests.

Most of the SDI calculations were made using the t_f beginning at 5 minutes, because data for t_f beginning at 10 and 15 minutes did not meet the test criteria ($1-t_i/t_f <$ 0.75). Most published criteria for membrane fouling specifies an $SDI_{15} < 5$. However, it was not possible to determine the SDI_{15} for the samples tested. In light of the observation that the SDI decreases significantly as the starting time for the t_f measurement increases from 5 to 10 minutes, it is likely that the microfiltered water meets the SDI_{15} criteria, as would be expected.

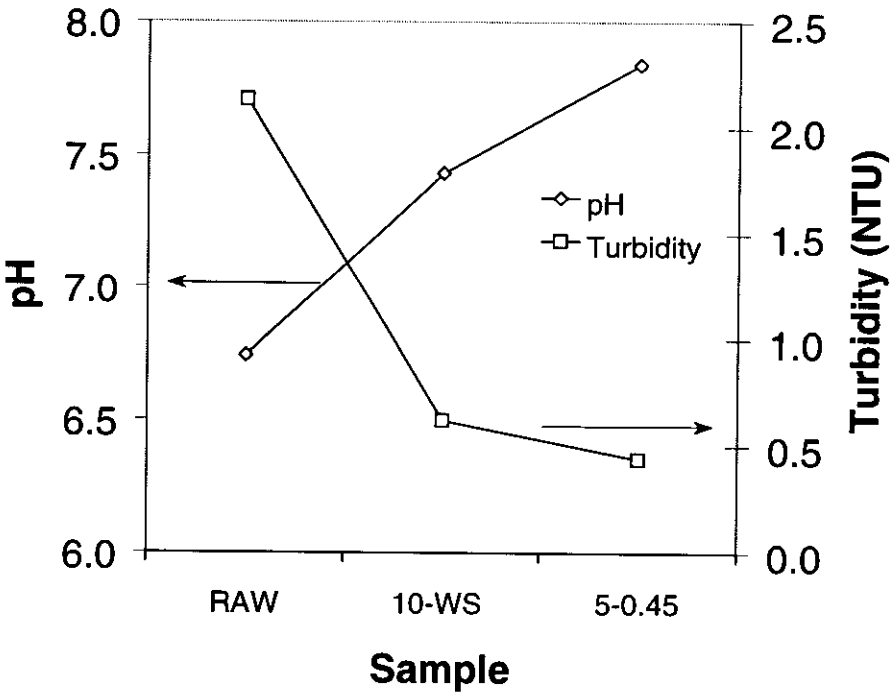

Figure 2-2. Effect of pretreatment on raw water (Tomhannock) turbidity. Raw TMK water was passed through a 10-μm prefilter and cation exchange softener, followed with 5- and 0.45-μm prefilters.

Table 2-3. Performance of Pretreatment (Tomhannock Reservoir Water).

Parameters	Raw water (11/4/98)	Raw water (1/23/99)	10μm-IX (1/23/99)	5-0.45 μm (1/23/99)
UV (pH 2.5)	0.082	0.090	NA	0.0779
DOC (mg/L)	2.80	2.77	NA	2.70
pH	6.74	7.47	7.43	7.82
Alkalinity (mg $CaCO_3$/L)	37	39	39	39
Turbidity (NTU)(filtered)	2.1	1.2	0.62	0.48
Temperature (°C)	19.8	17.9	18.0	20.5
Conductivity (μS/cm) 25 °C	152	168	151	155
Ionic strength	0.0024	0.0027	0.0026	0.0025
Hardness (mg $CaCO_3$/L)	50	54	ND	ND
Ca^{++} (mg $CaCO_3$/L)	36	39	ND	ND
Mg^{++} (mg $CaCO_3$/L)	14	15	ND	ND

NA: Not analyzed; ND: Below detection limit.

Table 2-4. SDI Test for Different Pretreatment

Sample	SDI-1	SDI-2	Average
Raw water	ND	ND	-
10 μm	ND	ND	-
5 μm	SDI_5 : 14	SDI_5 : 14	SDI_5 : 14
1 μm	SDI_5 : 13.6	SDI_5 : 13.9	SDI_5 : 13.8
0.45 μm	SDI_5 : 12.7	SDI_5 : 11.6	SDI_5 : 12.2
	SDI_{10} : 7.3	SDI_{10} : 7.3	SDI_{10} : 7.3
Ion Exchange	SDI_5 : 13.6	SDI_5 : 12.8	SDI_5 : 13.2

Note: ND means "not defined"; data for t_f beginning at 5 minutes did not meet test criteria. Tests conducted at ambient temperature (22 °C)

It is somewhat surprising that the SDI of the softened water is not lower, and that data could not be obtained for the SDI_{10}. Because the values obtained after 0.45-μm filtration and softening are within experimental error, results are inconclusive. It is possible that there was some particle shedding from the exchanger; however, this will not cause a problem during system operation because in practice the microfilters are located downstream of the softener and should provide a barrier to such particles.

Membrane fouling criteria based on turbidity alone (<1 NTU) would suggest that the 10 μm prefilter in combination with the cation exchanger would suffice as pretreatment steps. While the data is not conclusive, the SDI tests suggest that further filtration may be beneficial. We have chosen to use final filtration of 0.45 μm to provides 1) further reductions in turbidity; 2) a degree of filter sterilization to reduce microbial activity in the concentrate and on the membrane surface, and 3) operational separation of source water into dissolved and particulate fractions (Danielsson, 1982). Therefore, sample pretreatment includes a 10 μm stainless-steel or virgin polypropylene prefilter, a sodium-form cation exchange softener to remove multivalent cations (mainly Ca^{++} and Mg^{++}, Fe^{++}, and Mn^{++}) and thus prevent precipitation (scaling) on the RO membrane surface, and two cartridge filters (5-μm or 1μm (Osmonics Flotrex FPN011EGV) and 0.45-μm (Osmonics Flotrex FPN941EGV)). The cartridge filters, a ball valve, and a totalizing flow meter were constructed on a single hand-truck. Flow rates of approximately 2.4 gpm (10 L/min) are typical. After pretreatment, sample water is pumped to a 55-gal stainless steel drum that serves as a sample reservoir.

The membrane manufacturer requires a feedwater with a turbidity of less than 1 NTU. This could be achieved with a 10-μm pre-filter in combination with the cation exchanger. The removal of cations (mainly Ca^{2+} and Mg^{2+}) by the ion exchanger was greater than 95%. This is expected to significantly reduce precipitation of divalent ions and destabilized natural organic matter on the membrane surface. Previous studies have shown that the presence of calcium cation can facilitate severe fouling of the membrane surface (Hong and Elimelech, 1997; Schafer et al., 1998; Visvanathan et al. 1998).

2.4.2 Water flux and mass-transfer coefficient

Water flux was determined as a function of transmembrane pressure. Clean permeate water and distilled (DI) water were both used to determine water flux and membrane permeability (L_p). In these experiments, the osmotic pressure is effectively zero because both RO permeate and DI water has a negligible concentration of ionic species. As shown in Figure 2-3, permeate flow does not deviate significantly from linearity with increasing operating-pressures (up to 1200 kPa), as supported by a high r^2 (> 0.99) over the operating pressure range. Furthermore, there was no statistically significant difference between RO-permeate water and DI water. Because the temperature varied over a narrow range during these measurements (19.4 to 21.9 °C), temperature effects were assumed to be negligible.

We can conclude that any decreases in water permeability resulting from changes in membrane morphology (*i.e.,* compaction) appear to be small. Solution flux while filtering Tomhannock water was significantly (based on non-overlapping 95% confidence limits on the slope of the flux versus pressure curve) lower than the flux obtained using RO-permeate water, as expected. However, after chemical cleaning, flux recovery was complete. Cleaning protocols will be discussed in greater detail below.

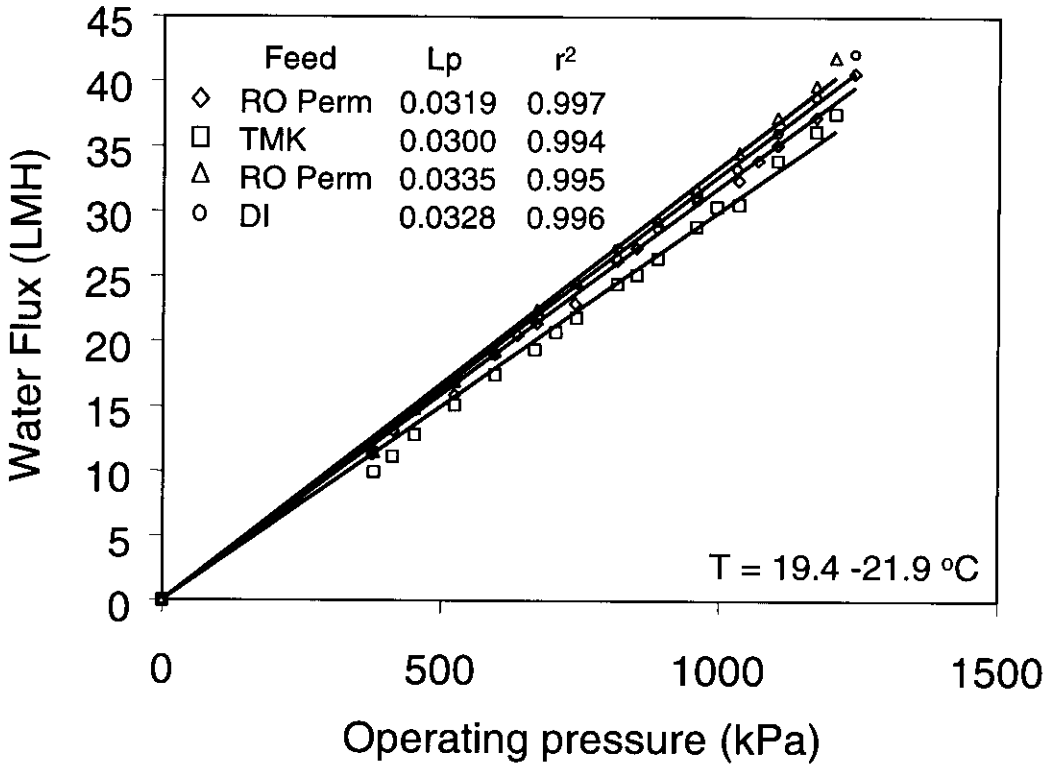

Figure 2-3. Effect of water source on the permeability of the Fastek RO Membrane. The second RO permeate and the final DI experiments were conducted after membrane cleaning, following pretreated Tomhannock filtration.

2.4.3 Effect of Operating Pressure on Feed Flowrate and Water Recovery

A second set of experiments was conducted to characterize the hydraulics of the RO system to identify operating conditions that meet manufacturer recommendations for maintaining crossflow velocity, and thus minimizing membrane fouling. Experiments were conducted using 200 L of either RO permeate or pretreated Tomhannock water. Both the concentrate and permeate were recycled to keep the system mass constant. As transmembrane pressure increases (*i.e.*, by closing the backpressure valve), permeate flux increases according to the relationship shown in Figure 3. Increasing the operating pressure from 414 to 1000 kPa (60 to 145 psig) increased permeate production from 83 to 225 L/h. Increasing the operating pressure also decreased feed flowrate, in response to higher head loss, in accordance with the pump performance curve. As shown in Figure 2-4, this relationship was linear over the range of pressure investigated, and did not depend on feed composition. As pressure and permeate flow increase, the feed flow decreases, and water recovery (Q_p/Q_f) tends to increase. As pressure increases and feed flowrate decreases, the crossflow velocity and shear rate at the membrane surface decreases significantly. A Q_c/Q_p ratio of 5 to 7 is recommended by the manufacturer to provide adequate crossflow velocity to minimize membrane fouling; this criterion corresponds to a water recovery, on an *element* basis, of about Q_p/Q_f = 12 to 15%.

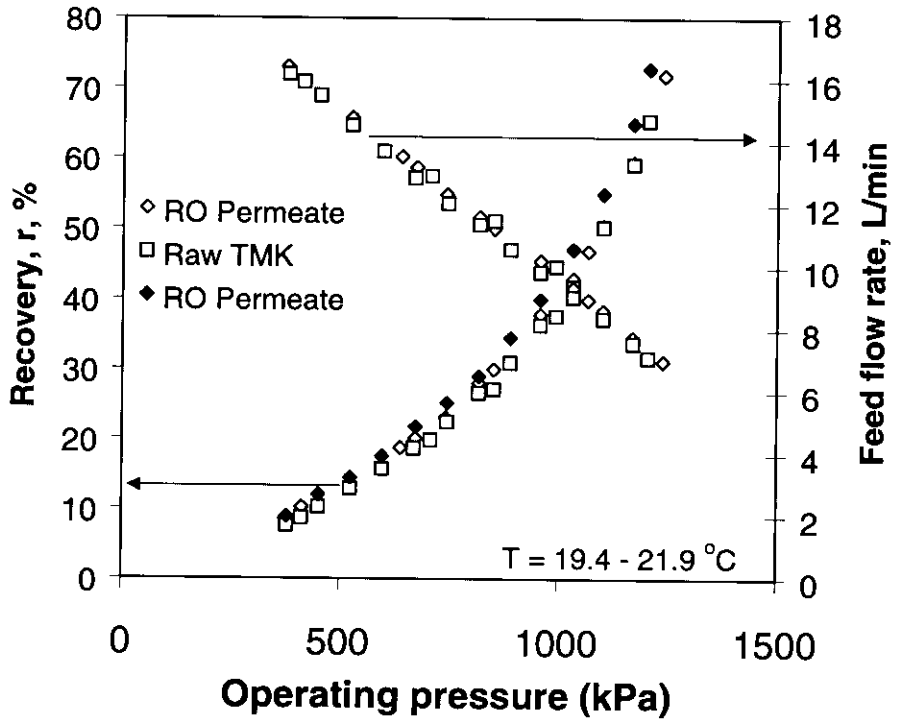

Figure 2-4. Effect of operating pressure on feed flowrate and water recovery, using RO permeate water before and after filtering and cleaning.

Note that on a *system* basis, the recovery is much higher, because the concentrate line is returned to the sample reservoir, forming a closed loop.

The maximum operating pressure that meets specified recovery criteria can be quantified by combining the definition of recovery (Eq. 5), the expression for solution flux (Eq. 6), and an empirical (linear) expression for feed flow as a function of pressure (derived from the data shown in Figure 2-4) of the form $Q_f = a\Delta P + b$:

$$\Delta P_{allowable} = \frac{r_{max} b + L_p A_m \Delta\pi}{L_p A_m - r_{max} a} \quad (18)$$

For our system, using $r_{max} = 0.15$, $L_p = 0.03$ [L m^{-2} hr^{-1} kPa^{-1}], $A_m = 7.436$ m^2, a = -0.6461 [L hr^{-1} kPa^{-1}], and b = 1226 [L hr^{-1}], and neglecting $\Delta\pi$, $\Delta P_{allowable} = 575$ kPa (83 psi).

2.4.4 Effect of temperature on water flux

Feed temperature is an important parameter governing membrane performance. It especially relevant to the isolation of natural organic matter because 1) temperatures in the field may vary considerably on a seasonal basis, and from site to site; and, 2) by returning concentrate to the sample reservoir in a closed loop, the temperature in the system has a tendency to increase. Figure 2-5 shows the effect of feed temperature on water flux. In these experiments, pressure was maintained at approximately 130 psig with 22% water recovery. Feed water temperature was varied from 15.7 °C to 25.3 °C. The water flux increased from 18.3 to 20.8 L $m^{-2} h^{-1}$ over the temperature range studied, a finding consistent with Cadotte et al. (1980).

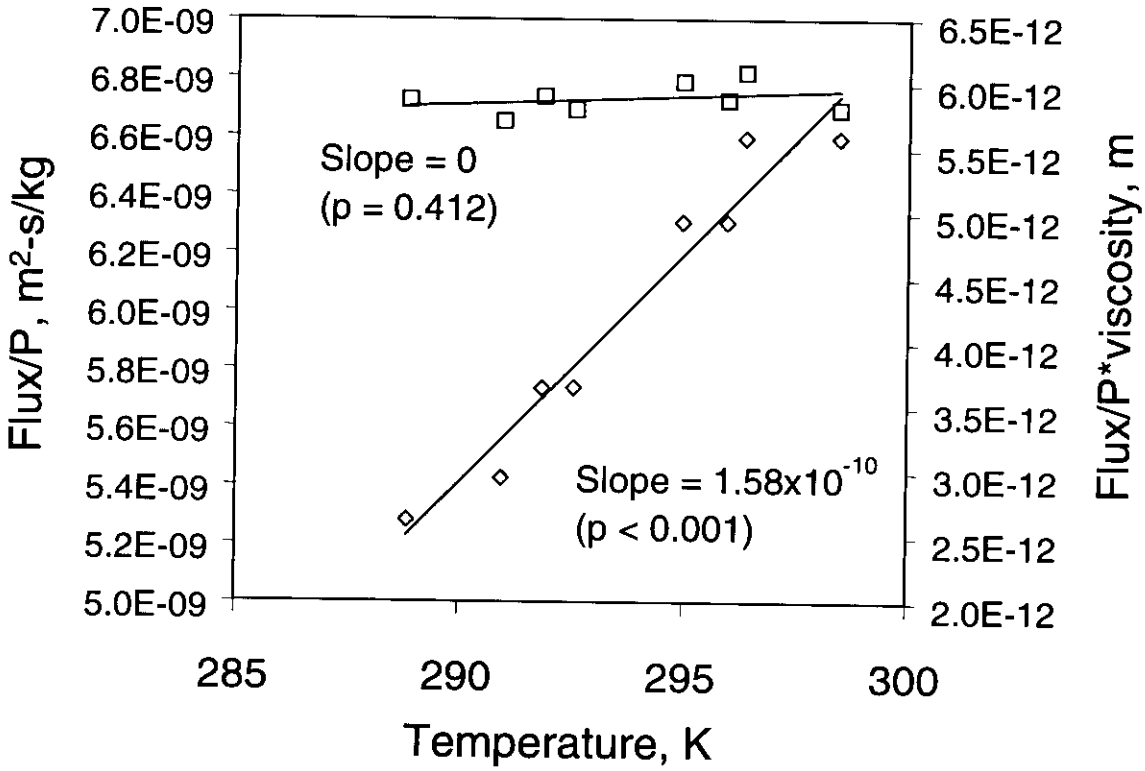

Figure 2-5. Effect of temperature on water flux. Average pressure = 900 kPa (130 psi); Feedwater: filtered Tomhannock reservoir water; recovery = 22%.

In general, water flux may increase as a result of decreases in water viscosity, increases in water diffusivity through the membrane, changes in membrane morphology, or some combination. As shown in Figure 2-5, when the pressure-normalized flux is multiplied by the temperature-dependent viscosity, there is no statistically significant effect of temperature. This finding suggests that most of the increase in flux over the temperature range measured was related to a decrease in the viscosity of water. We can therefore readily incorporate the effect of temperature on the maximum allowable transmembrane pressure (Eq. 18). The membrane permeability, L_p, at any temperature T, can be estimated as L_p measured at a reference temperature (e.g., 20 °C), multiplied by the ratio of viscosity:

$$L_{p,T} = L_{p,T_{ref}} \frac{\mu_{T_{ref}}}{\mu_T} \qquad (19)$$

The viscosity of water [Pa s] can be estimated from the polynomial regression $\mu = -0.0077T^3 + 1.0344T^2 - 57.283T + 1790.8$ with μ in [Pa s] and T in °C for $0 > T > 50$ °C. Incorporating the effect of temperature on membrane permeability into (Eq. 18) yields:

$$\Delta P_{allowable} = \frac{r_{max} b + \dfrac{1002 L_p A_m \Delta\pi}{-0.0077T^3 + 1.0344T^2 - 57.283T + 1790.8}}{\dfrac{1002 L_p A_m}{-0.0077T^3 + 1.0344T^2 - 57.283T + 1790.8} - r_{max} a} \qquad (20)$$

Therefore, as temperature increases, the transmembrane pressure should be lowered to maintain recovery within acceptable limits. For example, increasing the temperature to 30 °C reduces the allowable transmembrane pressure to about 487 kPa from 575 kPa. The extent to which this reduction in pressure is necessary is mitigated to some degree by the fact that head losses in the system are smaller at higher temperature, therefore, increases in pressure cause smaller reductions in Q_f. This effect could be explicitly accounted for in Eq. 18 by measuring the temperature dependence of coefficients a and b.

To keep the system operation as simple as possible, it is desirable to maintain the recirculating solution at constant temperature. We have designed a simple cooling system that consists of a stainless steel coil through which cooling water is continuously pumped. Typically, the cooling water is either tap water (if the system is operated in the laboratory) or raw sample water (if the system is operated in the field). While this strategy is intended to keep temperature constant during a single isolation run, site-to-site and seasonal variations will still occur.

2.4.5 System void volume and cleaning procedure

An optimal membrane cleaning and flushing protocol should use enough cleaning and rinsing solution to effectively recover organic matter that has accumulated on the membrane surface, while diluting the isolate solution as little as possible. Such an optimization requires knowledge of the system void volume. This was estimated by conducting a conservative tracer experiment using sodium chloride with conductivity detection. Levenspiel (1972) describes the analysis of such tracer tests, used to measure reactor residence time distributions (RTDs). The cumulative residence time distribution (F-curve) for the RO system is shown in Figure 2-6.

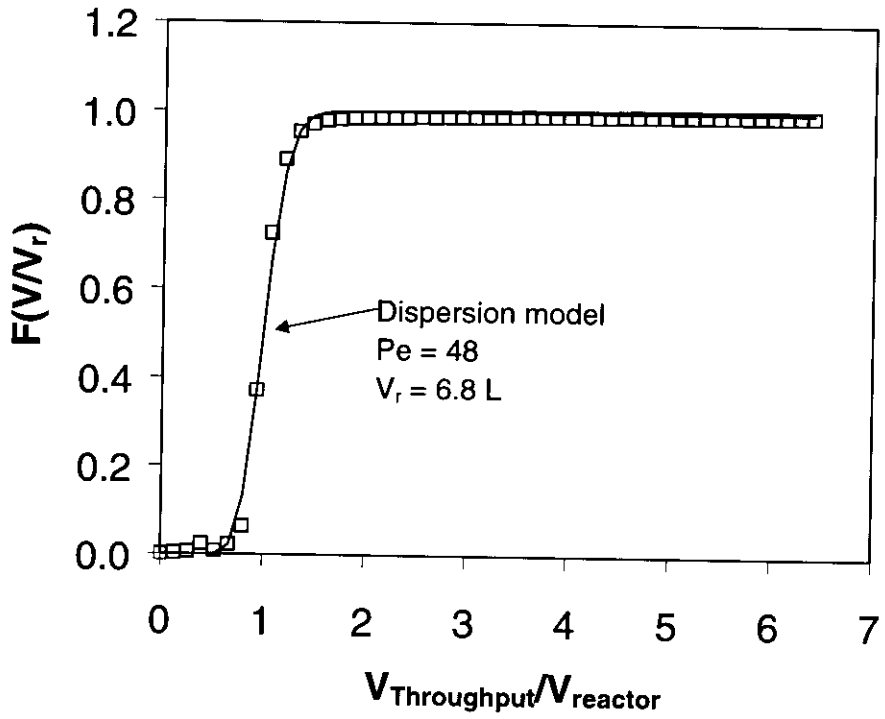

Figure 2-6. Residence time distribution of the field RO system.

The experimental data were fitted with plug-flow-with-dispersion model, which requires two fitting parameters, the Peclet number and a mean residence time (or void volume, since flowrate, Q, is known). A Peclet number of 48 and a void volume of 6.8 liters provided a good fit to the data based on a least-squares minimization. This void volume includes all piping, the booster and high-pressure pump, and the membrane module. The system can be effectively flushed with a volume equal to about 1.5 times the void volume; therefore, approximately 10 liters were required.

2.4.6 Effect of Pressure on NOM Rejection

For NOM isolation applications, the rejection ($1-C_p/C_f$) and total mass recovery of DOC were determined to characterize the overall performance of the RO system. NOM was concentrated by using the field-scale RO system, with the NOM isolation protocol previously described.

Reverse osmosis theory predicts that rejection should increase with increasing pressure, reaching a plateau at high pressures. For example, combining Eq. 6 through 9, the effect of pressure on rejection can be predicted from:

$$R = \left[1 + \left(\frac{K_s}{L_p}\right)\left(\frac{1}{\Delta P - \Delta\pi}\right)\right]^{-1} \quad (21)$$

As explained by Eriksson (1988), increasing pressure causes relatively more solvent to pass through the membrane than solute, thus increased rejection. This behavior was observed by Visvanathan *et al.* (1998). The rejection of dissolved organic carbon measured in this research is shown in Figure 7. Under all conditions rejection was greater than 99%, and over the range investigated, no significant effect of pressure was observed. This is consistent with the findings of Odegaard and Koottatep (1982). Examination of Eq. 16 shows that it is possible for rejection to remain essentially constant over large ranges of pressure when $L_p >> K_s$. In other words, the plateau region is reached at low pressures; as suggested by the data in Figure 2-7, the plateau region is reached prior to 414 kPa (60 psi).

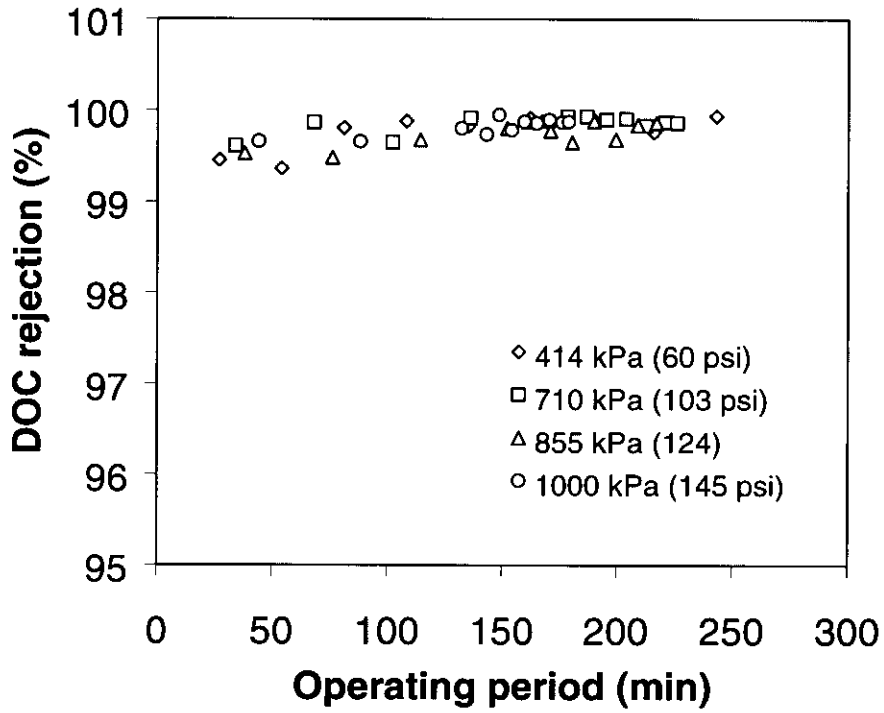

Figure 2-7. Effect of pressure on rejection of DOC from Tomhannock water.

2.4.7 Modeling NOM accumulation in the Sample Reservoir

Figure 2-8 illustrates the accumulation of NOM in the sample reservoir during an isolation run. As is typical of isolation runs in the field, during the first part of the run, the volume in the RO system was held constant by adding pretreated source water at regular intervals. During this period, the concentration of NOM in the system increased in response to the additional NOM mass in the system (at constant volume). The increase in NOM concentration was modeled using Eq. 12, and independently measured model parameters $C_{f,o}, V_{r,o}, Q_s, C_s, Q_p$, and R. After a period of constant volume operation, the feed of source water was stopped, and the NOM solution was concentrated to a final solution volume of about 25 liters. During this period, the concentration of NOM in the system increased in response to a reduction in the system volume (at constant NOM mass). The increase in NOM concentration

was modeled using Eq. 15, with $Q_s = 0$ and an updated value of $C_{f,o}$. As shown in Figure 8, the model(s) capture the trends in DOC concentration quite well. A sensitivity analysis was done to evaluate the sensitivity of the model to the value of rejection, R. Relatively small changes in R, (< 10%) result in significant deviations from the observed behavior.

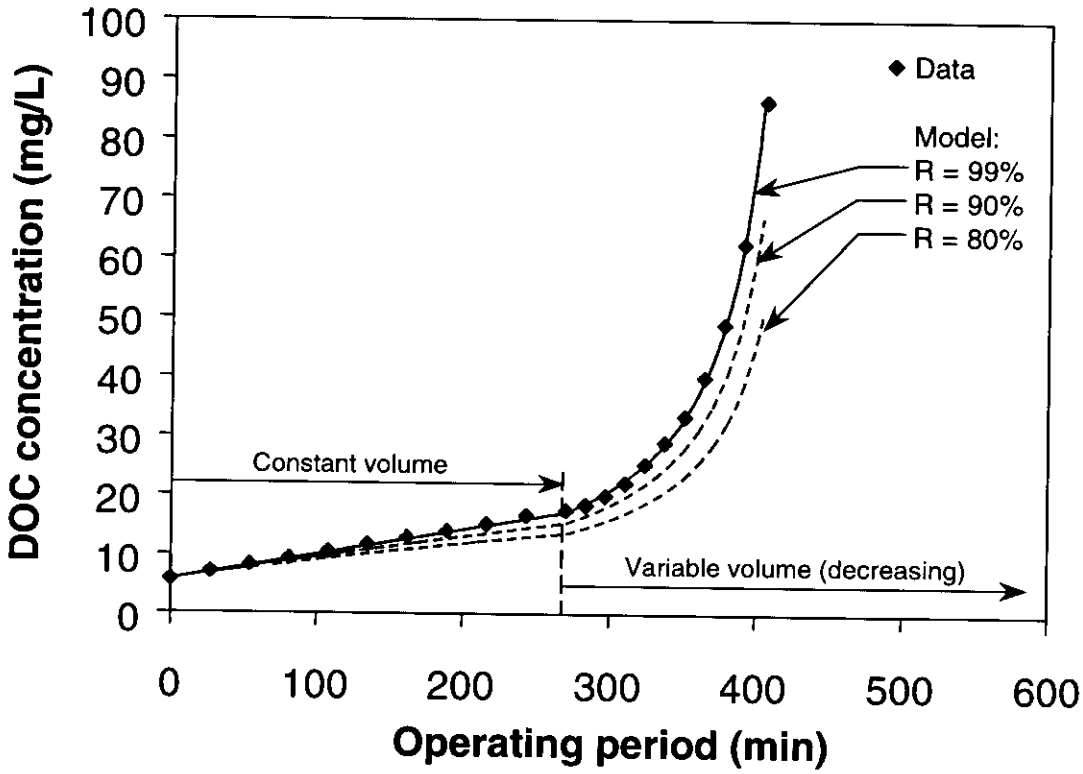

Figure 2-8. Pretreated Tomhannock NOM accumulation in the RO system during an isolation run. Symbols represent experimental data, solid line represents a model prediction based on an independently measured value of rejection (assumed to be constant); broken lines represent a sensitivity analysis to illustrate the effect of rejection on NOM accumulation. Operating conditions: pressure = 414 kPa (60 psig); constant volume of 200 L; T = 23 °C; recovery = 8.6%.

2.4.8 NOM Mass Recovery

Optimizing mass recovery is important for NOM characterization, and subsequent use in reactivity studies. Mass recovery experiments were conducted in the laboratory, and results were compared to mass recoveries calculated during field operation of the RO system. Conducting recovery experiments in the laboratory has the advantage of optimal control of operating variables, and maximum accuracy in the measurement of process volumes. For example, accurate feed solution rates could be computed from gravimetric measurements made with a platform balance.

Laboratory continuous flow experiments were conducted to investigate the effect of pressure (and recovery) on NOM recovery. Temperature was maintained constant at

about 20 °C using a cooling coil fed with cold tap water. The total mass flux to the membrane surface was the same in all experiments; *i.e.*, the higher-pressure experiments were conducted for a shorter period of time. Initially, pretreated Tomhannock water (200-L) was transferred to the sample reservoir, and 20-L aliquots source water was added at regular intervals to keep the reservoir volume approximately constant. Table 2-5 illustrates the calculated NOM mass recovery using Eq. 8. The overall mass balance for these experiments is nearly 100%, demonstrating that near-complete recovery is possible using a combination of membrane flushing (hydrodynamic cleaning) followed by chemical (NaOH) cleaning of the membrane system. Therefore, minimal NOM fractionation due to loss of fouling components occurred. The total mass recovered using this approach did not depend on pressure; *i.e.*, membrane fouling during the isolation run was reversible after chemical cleaning. However, the mass recovered in the concentrate water (and the subsequent clean water flush) decreases with increasing pressure. The concomitant increase in the mass recovered in the NaOH wash suggests that at higher pressures, a larger or more dense fouling layer formed, which contains an increasingly greater proportion of the total mass (up to 6.5 % at 1000 kPa). This is consistent with the lower cross-flow velocities in the system at higher operational pressures.

Mass recovery analysis of isolation runs from field experiments was conducted to investigate the effect of NOM source and temperature. These experiments were not designed to investigate these variables in a systematic manner; rather, they document operational experience for a range of conditions encountered in the field. In these experiments, the volume processed ranged from approximately 600 to 1200 L. The temperature during isolation was maintained relatively constant using a cooling coil fed with source water; however, the temperature varied depending on the source and the season. NOM from the southern waters (MB, CT and SP) was isolated at temperatures ranging from 25 to 30 °C, while NOM from the Tomhannock (TMK) water was isolated at a temperature of 15 to 20 °C. Most runs employed a transmembrane pressure of about 550 kPa (80 psig).

Table 2-6 shows the effect of water source on NOM mass recovery. The overall recovery of mass (mass balance) achieved in field experiments is considered acceptable, but is both more variable and somewhat lower than that achieved in more controlled laboratory experiments. In part, this is because it is more difficult to accurately measure process volume in a field setting; *i.e.*, accurate gravimetric determination was not possible. In part, this is also because while hydrodynamic cleaning was done after every run, chemical cleaning was not. In part, the variability of the results depends on operator experience (*e.g.*, compare runs TMK1, TMK2, and TMK3), and the facilities available at each field site (typically water treatment plant intake buildings). The results confirm, however, that mass recoveries greater than 95% are possible in a field setting. There does not seem to be a significant effect of water quality on NOM mass recovery for the four different waters tested, even though such parameters as source water organic carbon concentrations and specific UV absorbance vary over wide ranges.

Table 2-5. Effect of Pressure on Mass Recovery

Sample Mass, % of Total Applied	Operating pressure 414 kPa (60 psi)	530 kPa (77 psi)	703 kPa (102 psi)	855 kPa (124 psi)	993 kPa (144 psi)
Concentrate & flush	95.40	92.66	93.55	93.57	90.80
Sampling	3.60	3.38	2.68	2.23	2.22
NaOH wash	0.45	3.31	3.41	3.89	6.57
Total DOC recovered	99.45	99.36	99.64	99.69	99.59

Table 2-6. Effect of Water Source on Mass Recovery

Mass, mg	Source Water/Run MB 1	MB 2	CH 1	CH 2	SP 1	TMK 1	TMK 2	TMK 3
Applied	8665	11012	3346	3470	1247	2398	3329	2764
Recovered	8312	10600	3287	3259	1173	2172	3190	*2695
Permeate	27.8	81.5	117.3	74.4	100.9	25.6	25.6	28.8
Recovery, %	95.9	96.3	98.2	93.9	94.0	90.6	95.8	97.5
Balance, %	96.2	97.0	101.7	96.1	102.1	91.6	96.6	98.5

All masses expressed as dissolved organic carbon, DOC. Mass recovered: concentrate + flush.
Mass Balance: mass recovered + mass in permeate.
*Mass recovered from TMK run 3 includes a final base wash, others do not.

2.5 Conclusions

Field RO system including a pretreatment and RO isolation can be employed as a strategy for isolating NOM from natural waters. Using this technique, large quantities of permeate water production, high NOM removal, and mass recoveries were obtained. A pretreatment technique (using cation exchange softener and prefilters in series) can be used to meet membrane fouling criteria based on turbidity (<1 NTU). Cation exchange softener was sufficient to remove multivalent cations (mainly Ca^{++} and Mg^{++}) (> 95%), and thus prevent precipitation (scaling) on the RO membrane surface. Increased operating pressure decreased feed flow rate, thus decreased crossflow velocity on the membrane surface but increased recovery and the rate of permeate water production. The solution flux from NOM solution was lower than the flux obtained using RO permeate water, and the flux recovery was relatively high after chemical cleaning, corresponding to high NOM mass recovery. System void volume determination is an optimization technique for membrane cleaning and flushing protocol. To meet the design standards, low-pressure operation (less 700 kPa or 100 psig) would be required to achieve typical module-based recoveries of about 15%.

As expected, the overall recovery of mass (mass balance) achieved in field experiments is both more variable and somewhat lower than that achieved in more controlled laboratory experiments. In part, this is because it is more difficult to accurately measure process volume in a field setting; i.e., accurate gravimetric determination was not possible. In part, this is also because while a clean water rinse was done after every run, a base-wash was not. In part, the variability of the results depends on operator experience, and the facilities available at each field site (typically water treatment plant intake buildings). The results confirm, however, that mass recoveries greater than 95% are possible in a field setting.

3.0 Organic Matter Fractionation by Ultrafiltration

3.1 Introduction

Membrane performance experiments have been designed to examine the influence of molecular weight on nanofiltration membrane fouling and the ability of surface modification to mitigate fouling. Ultrafiltration (UF) fractionation was employed to produce well-resolved molecular weight fractions having organic carbon concentrations high enough (on the order of 8 to 10 mg/L) to carry out membrane performance experiments. In this section, the development of an ultrafiltration fractionation protocol and representative results are presented.

3.2 Modeling Fractionation of NOM Solutions by Ultrafiltration

The ultrafiltration system can be operated in different distinct modes, and each mode has different operating characteristics. In the concentration mode (also called ultrafiltration), the feed solution reservoir is kept under atmospheric pressure, and an initial volume of solution, V_o, is concentrated to a final retentate volume, V_{reten}. The permeate volume leaving the system, V_{perm}, is then $V_o - V_{reten}$. In this mode of operation, the concentration of completely rejected molecules increases in proportion to V_o/V_{reten}. The concentrations of all molecules having rejection less than unity also increase over time, in both the feed solution reservoir and the permeate. In the diafiltration mode, the feed solution reservoir is closed to the atmosphere. The initial volume of solution, V_o, is maintained constant by replacing the volume lost as permeate with either solute-free buffer solution or feed solution. Loss of volume from the system as permeate creates a vacuum in the solution reservoir, which then initiates flow from the diafiltration reservoir. During diafiltration with buffer feed, the concentration of retained molecules remains constant, because the volume of feed solution in the system is constant. In contrast, the concentration of permeating molecules ($R < 1$) decreases over time in both the reservoir and the permeate. The ultrafiltration system is operated until a chosen filtration volume has permeated the membrane.

3.2.1 Model Development

Mass distribution within the reactor and the transport of both solute and solvent across the membrane must be characterized to model molecular weight fractionation in ultrafiltration systems. The scale over which the mass distribution within the reactor system is characterized establishes a distinction between "microscopic" and "macroscopic" models. In this research, a macroscopic model is employed. In this approach, no attempt is made to characterize the distribution of mass as a function of position within a hollow fiber. Rather, transport is characterized using effective model coefficients based on readily measured macroscopic concentrations: reactor inlet concentration and permeate concentration. Advantages of macroscopic modeling are that fewer model coefficients are required, and the resulting mass-balance equations can be

solved analytically. However, the transport parameters measured depend on operating conditions, and must be considered phenomenological.

Using the fact that permeate concentration is the ratio of solute flux (J_s) and volumetric solution flux (J_v), and the definition of solute rejection (Eq. 10), the solute flux can be written:

$$J_s = (1-R)J_v C_{feed} \qquad (22)$$

Equations describing solute transport in batch ultrafiltration systems were developed by incorporating the solute flux expression into a system mass balance relationship. The recycle configuration of the semi-batch system configuration allows operational flexibility to obtain backmixing conditions which approximate completely mixed flow, thereby simplifying the system mass-balance equations. Backmixing conditions were verified using residence time distribution analysis. It should be noted that while the macroscopic system is modeled as a completely mixed reactor, the microscopic hydrodynamic conditions at the membrane surface are not characterized. Equating mass accumulation within the system to the rate of mass permeation through the membrane, the general differential mass-balance can be written:

$$V_{sys}\frac{dC_{feed}}{dt} + C_{feed}\frac{dV_{sys}}{dt} = -J_s A_m = -J_v A C_{perm} = -J_v A_m (1-R) C_{feed} \qquad (23)$$

where A_m is the membrane surface area, V_{sys} is the volume of solution in the system, and other terms are as defined previously. It is generally assumed that both J_v and membrane characteristics remain constant, which requires that the dilute organic matter solutions studied here do not give rise to significant concentration polarization effects. The validity of this assumption may depend, to varying degrees, on several physicochemical parameters including concentration, ionic strength, and pH. Logan (1990) states that such accumulation is minimized at dissolved organic carbon concentrations below 100 mg/L, a criterion satisfied for most natural waters. Aggregation of natural organic matter (e.g. fulvic acids) should not occur at concentrations below about 200 mg/L in the absence of divalent cations.

It is further assumed that the solute does not undergo transformation and that adsorption to the membrane surface is negligible.

In the diafiltration mode, the system volume is maintained constant and equal to V_o; therefore, the volume derivative in Equation 23 is equal to zero. Integrating the mass-balance equation with the initial condition $C_{feed} = C_{feed,o}$ when t = 0 and making the substitution $J_v A_m t = V_{perm}$ yields:

$$C_{feed} = C_{feed,o} \exp\left(-(1-R)\frac{V_{perm}}{V_o}\right) \qquad (24)$$

If the ultrafiltration system is operated in the concentration mode, the system volume, V_{sys}, is a function of time, or permeate volume throughput, V_{perm}:

$$V_{sys} = V_o - J_v A_m t = V_o - V_{perm} \quad (25)$$

In addition, the time derivative of the system volume is equal to $J_v A_m$. Integrating the mass-balance equation with the initial condition $C_f = C_{fo}$ when t = 0 yields:

$$C_{feed} = C_{feed,o}\left(\frac{V_o}{V_o - V_{perm}}\right)^R \quad (26)$$

The rejection may be determined from the log-linearized forms of the integrated mass-balance equations, or from non-linear regression. For the diafiltration mode, a plot of $\ln(C_{feed}/C_{feed,o})$ vs. V_{perm}/V_o yields a slope equal to $(R - 1)$, and for the concentration mode, a plot of $\ln(C_{feed}/C_{feed,o})$ vs. $\ln[V_o/(V_o - V_{perm})]$ yields a slope equal to R. Alternative forms that allow the determination of $C_{feed,o}$ from the intercept of the linearized plot can also be employed.

3.3 Materials and Methods

An increase in solution ionic strength causes charged macromolecules to coil, compress or otherwise reduce their size in solution, influencing their retention on a given membrane. Therefore, it is important to 1) use a consistent ionic strength for all samples; and, 2) keep ionic strength relatively constant during the fractionation process. An ionic strength of 0.01 M was chosen for this work. RO concentrated waters will be diluted until the conductivity is reduced to that of a 0.01 M NaCl solution, and salt will be added to waters having a lower conductivity.

The ultrafiltration system is shown in Figure 3-1. The system was obtained from A/G Technology Corporation (Needham, MA) as a package consisting of several hollow fiber membrane modules, a peristaltic pump (Cole-Parmer Masterflex I/P), and feed reservoirs. All system tubing is peroxide-cured silicone (Cole-Parmer) chosen for low organic leachables and acid/base stability characteristics. The hollow fiber modules (A/G Technology Corporation), are 31.8 cm in length by 3.2 cm in diameter. The fibers are polysulfone with inner diameter of 0.5 mm with a total surface area of 0.2 m^2. Modules are held in place with 1.5-in. tri-clamp sanitary fittings. Modules were pre-cleaned according to manufacturers recommendations including a 24-hour ethanol pre-soak followed by clean water (DI) rinse. Process solution is pumped from the reservoir into the membrane cartridge; permeate flow is diverted to a collection line, and the flow which does not permeate the membrane (retentate) is recycled back to the reservoir. Pressure drop across the membrane is controlled by a valve on the retentate line and by the pump speed (flowrate).

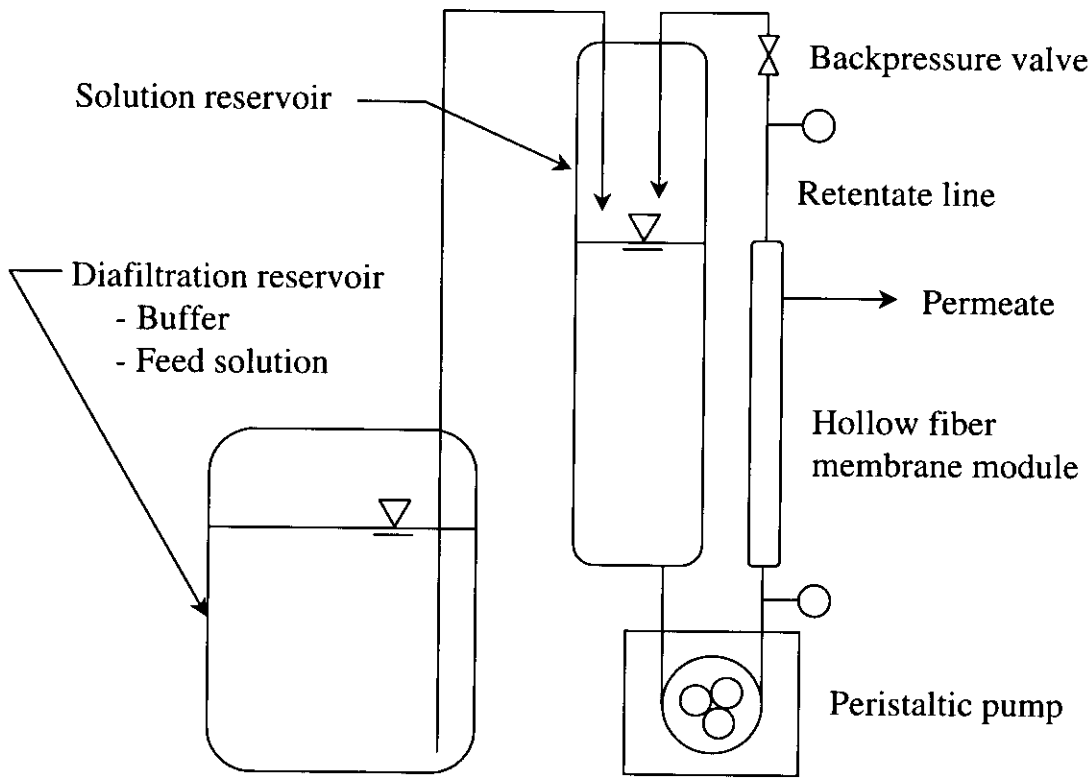

Figure 3-1. Schematic depiction of the ultrafiltration system.

The feed solution is recirculated through the system at a rate of 4 l/min, providing high cross-flow and shear rates of about 8,000 sec^{-1} to minimize accumulation of organic matter at the membrane surface. The corresponding transmodule pressure drop is on the order of 2 psi, and increases to 4 psi at a recirculation rate of 7 L/min. The system can be operated at transmembrane pressures up to 20 psi; this upper value is constrained by pressure limits of the peristaltic pump tubing. Ultrafiltration membranes employed included 1, 3, 5, 10, 30 and 100-kDa molecular weight cutoff (MWCO), calibrated by the manufacturer using polyvinylpyrrolidone. Following sample application, modules were cleaned using 0.1N NaOH solution at cross flow rate of 4 liters per minute for a minimum of one hour, followed by clean water rinse (without recycle) until retentate and permeate pH matched clean water pH (~6). Following base and clean water rinse, modules were stored in 100mg/L sodium azide, refrigerated in the dark to prevent microbial growth. Prior to subsequent sample application, modules were clean-water rinsed (without recycle) until retentate and permeate UV absorbance matched clean water absorbance (λ=254nm) to ensure flushing of all sodium azide.

3.4 System Characterization

A residence time distribution study was performed with the 1, 5 and 30 kDa MWCO membranes to verify the conditions (recirculation rates) under which the mass distribution within the ultrafiltration system approached well-mixed conditions. The reservoir was filled with a solution of NaCl, a non-rejected solute, which was then diafiltered with several liters of salt-free water. Under the assumption of complete mixing, Eq. 14 should describe the change in feed concentration (as measured by conductivity). Representative results are plotted in Figure 3-2. The goodness-of-fit demonstrates that the behavior of the system closely approaches completely mixed conditions. A recirculation rate of 4 L/min was sufficient to approximate well-mixed conditions for the 1, 3 and 5 kDa membranes; larger MWCO membranes (having higher flux) required higher recirculation rates on the order of 7 to 8 L/min.

The exclusion of ions by the membrane and subsequent accumulation at the membrane surface could influence the transport of charged macromolecules and could result in a time-dependent ionic strength effect. Retentate and permeate conductivities were monitored for the 1, 5 and 30 kDa membranes and it was found that rejection of NaCl by the tighter membranes was measurable, but less than a few percent, which is considered negligible. No rejection of NaCl by the 30-kDa membrane was observed.

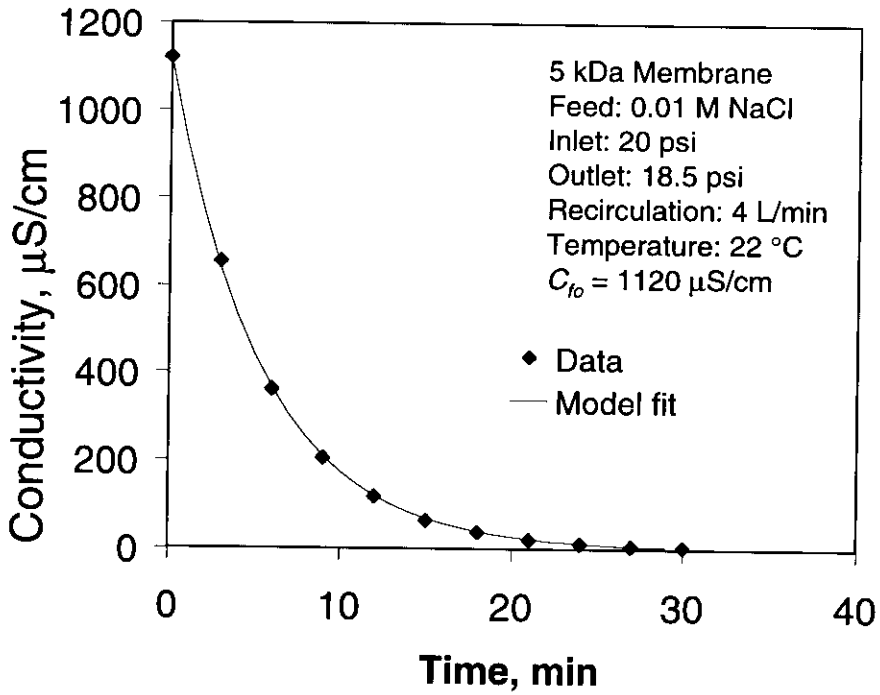

Figure 3-2. Verification of well-mixed conditions using NaCl, a conservative, non-rejected tracer.

3.5 Macromolecule Solution Fractionation

The permeation model was used to evaluate alternative fractionation procedures for preparing different size fractions of natural organic macromolecules, to identify an optimal fractionation procedure. For a given initial volume, the mass throughput depends on the initial mass present, $C_{fo}V_o$, membrane rejection, and the permeate volume throughput, V_p. Model calculations demonstrate that the most efficient mass throughput is achieved 1) at high feed concentrations, and 2) in the concentration mode. However, an important objective of any fractionation procedure is to minimize the effects of concentration polarization, solute accumulation on the membrane surface, and variations in membrane rejection. Therefore, attempting to achieve separation by using very high concentration factors is not a practical strategy.

The diafiltration mode has several advantages over the concentration mode from an operational point of view. The original solution volume is kept constant by the continuous addition of buffer solution containing the same inorganic matrix as the feed. The effects of concentration polarization are minimized, therefore, because the concentration of retained molecules is kept constant, while the concentrations of permeating molecules decrease as a function of permeate volume throughput. Further, as a matter of operational convenience, the diafiltration mode can be operated continuously. Model calculations indicated that the efficiency of the concentration mode and the operational benefits of the diafiltration mode could be combined by employing a sequential mode of operation. Under this scenario, the sample is first concentrated to enhance mass-throughput efficiency and reduce sample volume. The concentration mode is followed by a period of operation in the diafiltration mode; the smaller sample volume maximizes the value of V_p/V_o for a given total throughput volume. Figure 3-3 illustrates model calculations of the feed concentration and mass throughput for this combined operation. It can be seen that maximizing mass throughput (i.e., separation of molecular weight components) requires fairly large V_p/V_o values, which then reduce the concentration of non-rejected components in the permeate. There is a trade-off between controlling concentration at the membrane surface, achieving a high degree of separation, and maintaining a reasonable permeate concentration to facilitate further experimentation. Based on these considerations, a general cascade-type fractionation protocol was designed.

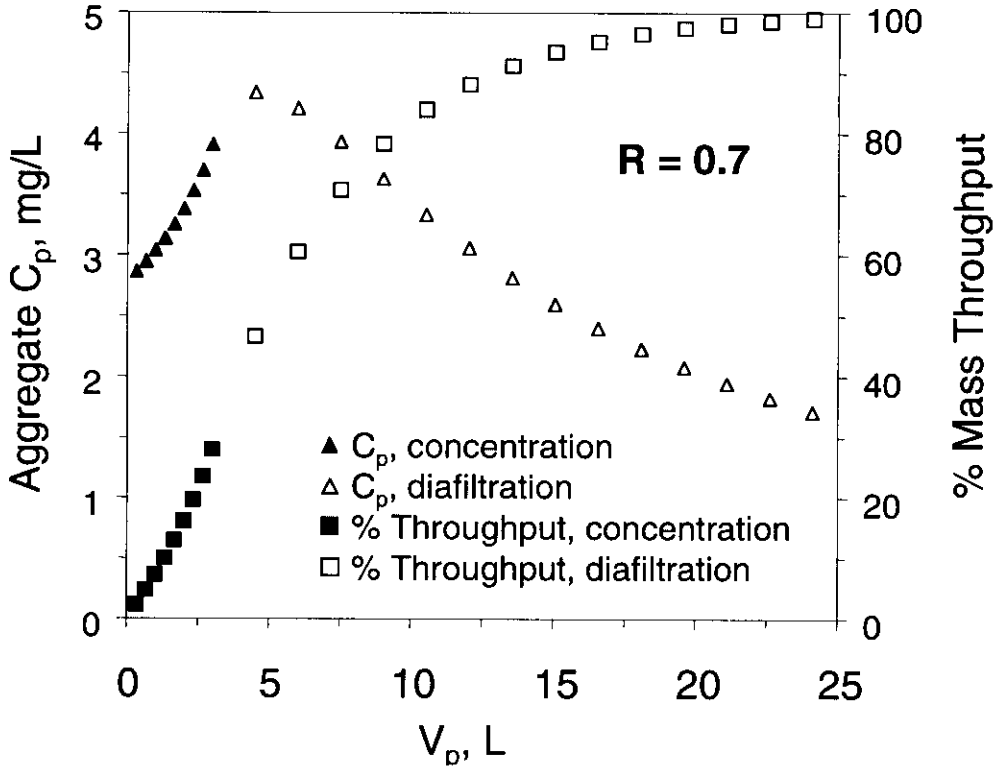

Figure 3-3. The effect of operation protocol on aggregate permeate concentration and mass throughput (molecular weight separation).

One approach to cascade fractionation is to apply the starting solution on the highest MWCO membrane, and allow smaller molecules to permeate during a concentration and subsequent diafiltration step. This permeate could then be concentrated on the next lower MWCO membrane, followed by a second diafiltration step. The volume of permeate from the second membrane in the cascade is thus approximately equal to the volume of permeate from the first membrane, plus the second diafiltration volume. The volume of permeate increases in this manner until the smallest MWCO membrane is employed. The permeate volume from this final step is the highest, and the concentration of this fraction would be too small to be useful. Therefore, this approach is not recommended. A solution to this problem is to start the cascade with the lowest MWCO membrane. A protocol based on this concept is shown in Figure 3.4.

As shown in Figure 3-4, the whole NOM solution is first applied to the 1 kDa membrane, which has the smallest MWCO. The whole solution is concentrated, then diafiltered with buffer solution, yielding the <1 kDa fraction. A high diafiltration volume can be chosen to maximize separation, or a lower volume can be chosen to keep the NOM concentration within some specified value.

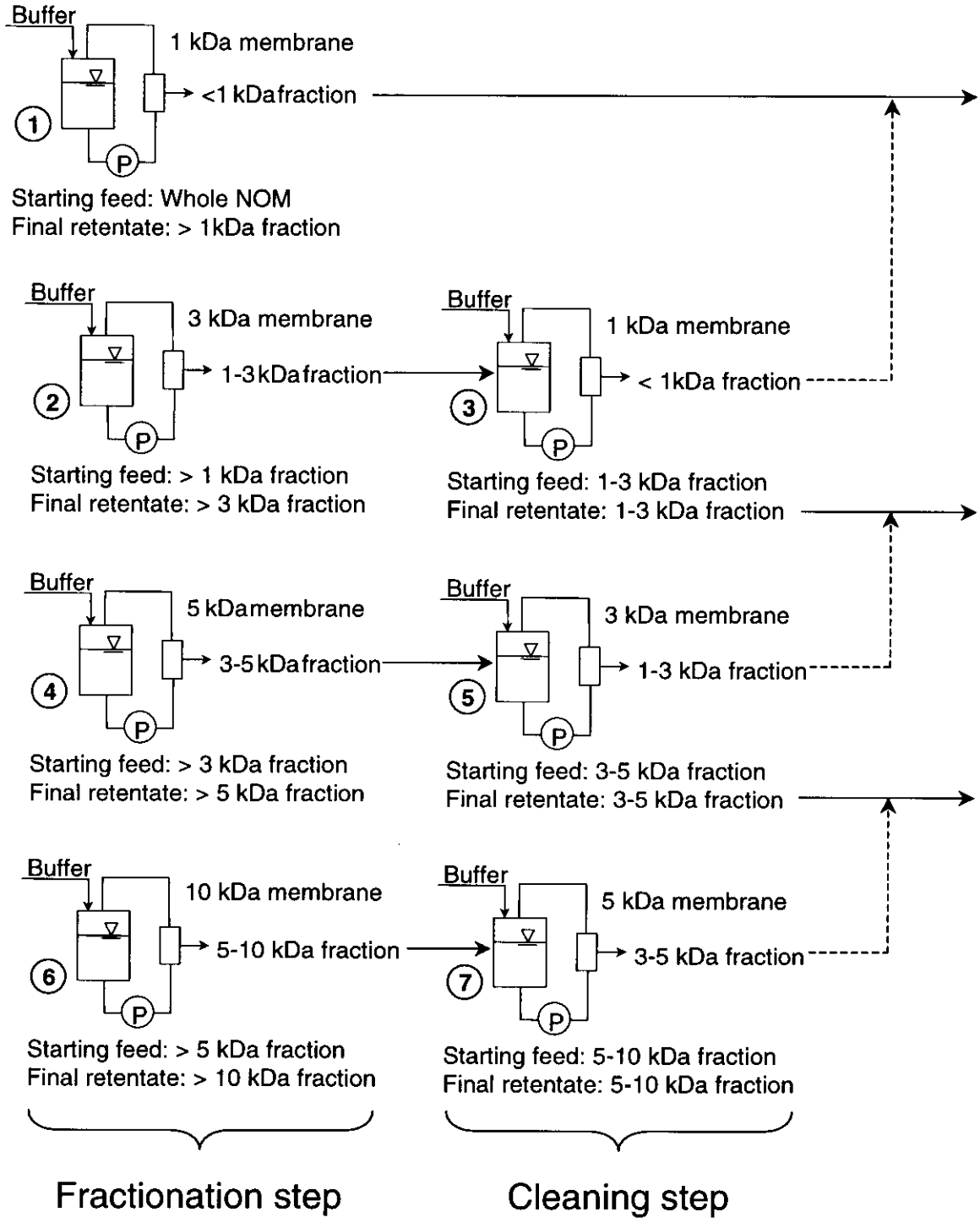

Figure 3-4. Ultrafiltration fractionation protocol showing fractionation and cleanup steps.

The retentate is then fractionated on the next higher MWCO membrane (3 kDa), using the same concentration/diafiltration technique. This yields a dilute solution of the 1-3 kDa fraction. This solution is then concentrated on the 1 kDa membrane, to reduce the fraction volume and increase its concentration. This step also serves to clean the 1-3 kDa fraction, further removing <1 kDa components that did not permeate the 1 kDa membrane in the first fractionation. The retentate from the fractionation on the 3K membrane is then applied to the next larger membrane and the process is repeated. For membranes with higher MWCO (i.e. 5, 10, 30, 100kDa), the clean up process "steps back" two membrane series. For example, permeate from the 5kDa membrane is applied to the 3kDa membrane, and the permeate from this step is applied to the 1kDa membrane.

Starting the cascade process with the smallest membrane has several advantages. In general, the fraction that passes the smallest MWCO membrane is necessarily the most dilute, because there are no smaller membranes on which to concentrate this fraction. By starting with the smallest membrane, the degree of dilution is minimized. Furthermore, as a result of subsequent concentration steps, the likelihood of low-molecular size fractions contaminating larger size fractions is minimal. Each fraction is concentrated on the next lower membrane size (i.e., the 3-5 kDa fraction is concentrated on the 3 kDa membrane), which allows smaller molecules to pass freely, thus enhancing the separation. The protocol for UF molecular size fractionation is summarized below.

3.5.1 Protocol for UF Fractionation/Cleanup Step

1. Sample was adjusted to pH 7.0 using HCL, and an ionic strength of 0.01 M (as NaCl) by adjusting sample conductivity to match a 0.01M NaCl standard at the same temperature by either adding NaCl or, sample dilution with DI water.

2. Sample volume was reduced to 1 to 2 liters in concentration mode followed by diafiltration using 0.01 M NaCl (in DI) to a "diafiltration factor," V_p/V_s, equal to or greater than 6. For components having a rejection of 0.50, a removal of 95% is predicted using this protocol. For components having higher rejection, smaller percentage removals can be expected however, additional removal will occur in subsequent concentration steps; e.g. components that do not pass the 1 kDa membrane during the initial diafiltration get a "second and third chance" during subsequent concentrations of the permeate from the 3 kDa membrane.

3. In order to keep TOC concentrations below the onset of aggregation, the maximum concentration in the UF system was kept below 200 mg/L.

4. For modeling and mass balance calculations, DOC concentration, UV absorbance, and volume data was collected for initial and final, retentate and permeate reservoir volumes, and for base wash solution. During a run, permeate DOC/UV data was recorded as a function of volume throughput rather than time to control for any variations in membrane flux caused by fouling, pressure variations, and pump tubing wear.

3.6 Solute Transport Model Verification

The permeation of natural organic matter from Tomhannock water in the polysulfone hollow fiber ultrafiltration system was modeled in both the concentration and

diafiltration modes. Representative results are shown in Figures 3.5 and 3.6 for Tomhannock hydrophobic fraction (TMK-HPO) on the 1 kDa membrane. The model parameters were calibrated in the concentration step (Figure 3-5), and these parameters were used to predict the diafiltration feed concentration as a function of permeate volume during diafiltration. These results suggest that the mode of operation, for the range of volume throughputs used in this experiment, does not significantly affect solute transport characteristics.

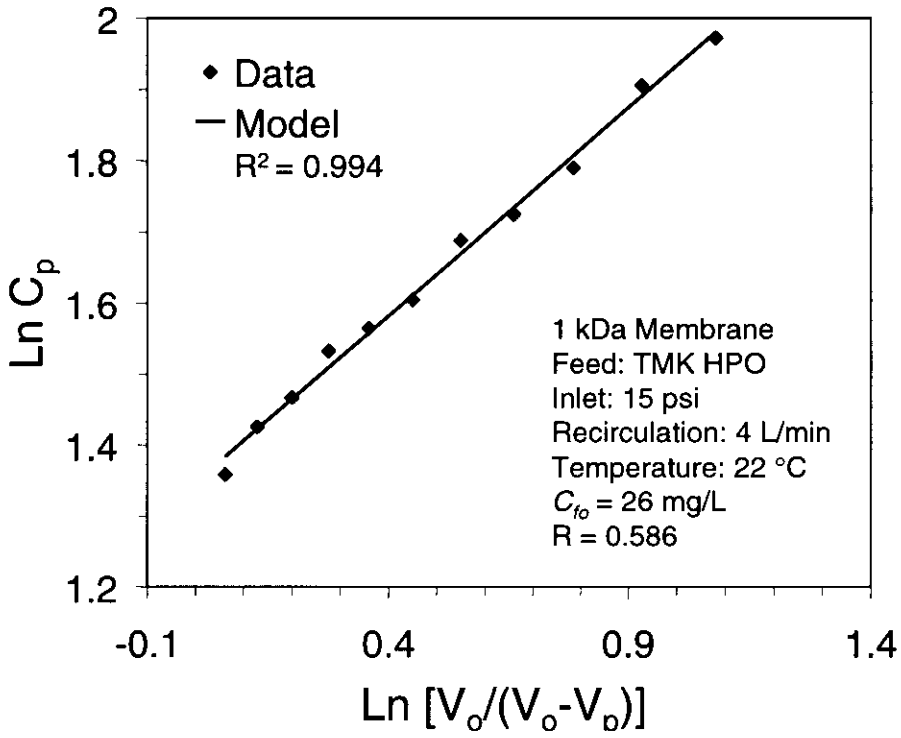

Figure 3-5. Verification of the solute permeation model for Tomhannock NOM.

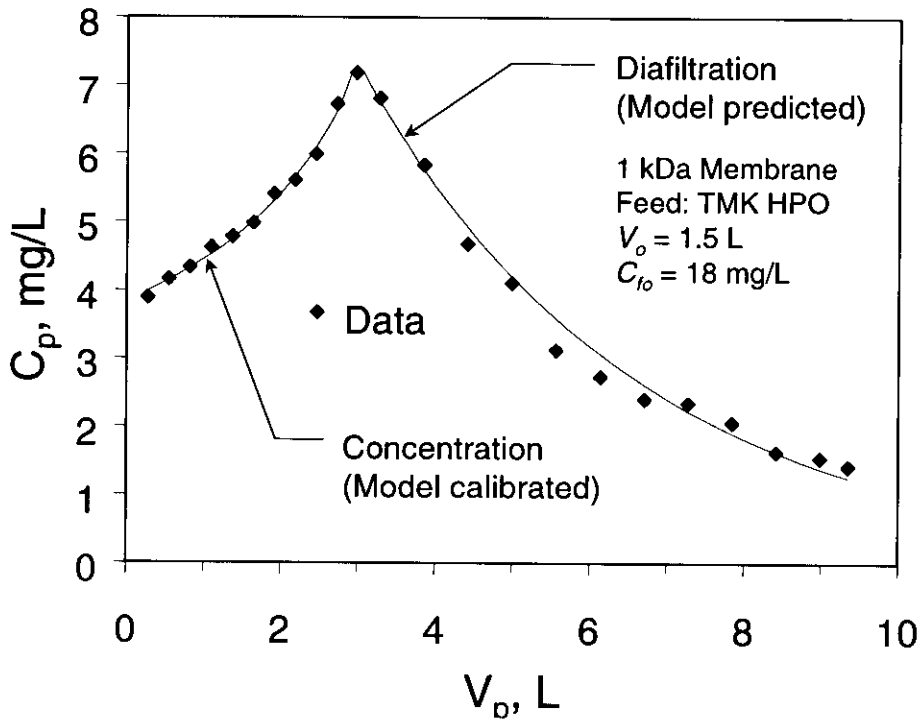

Figure 3-6. Verification of the solute permeation model in the concentration and diafiltration modes of operation.

3.7 Molecular Weight Distribution Determination

The results for NOM (as DOC) molecular weight fraction distributions and experimental mass balance calculations are summarized in Table 3-1 and Figure 3-7. Because the MB and CT samples contained significant mass in the >5K fraction, further fractionation on the 10K, 30K, and 100K membranes was performed and results are presented in Figure 3-8. The percentage of mass in a given fraction as depicted in Figures 3-7 and 3-8 was calculated based on the total mass of organic carbon (OC) recovered for all fractions, and does not include OC mass in base wash and sample volumes removed for DOC analysis.

Table 3-1. Molecular Weight Fractionation Summary.

Fraction	TMK		TMK HPO		MB	
	%C (a)	%C (b)	%C (a)	%C (b)	%C (a)	%C (b)
<1K	51.7	56.4	64.5	65.0	45.0	38.3
1-3K	34.5	37.7	13.3	13.4	13.8	11.7
3-5K	3.2	3.4	7.1	7.1	16.8	14.3
>5K	10.6	11.5	15.1	15.3	24.5	20.8
5-10K	NA	NA	NA	NA	9.1	7.8
10-30K	NA	NA	NA	NA	2.5	2.1
30-100K	NA	NA	NA	NA	7.3	6.2
>100K	NA	NA	NA	NA	5.6	4.8
% Recovery*	109.1		105.5		98.1	

Notes: %C (a) is the percent of total organic carbon mass recovered in fractions, %C (b) is the percent of the initial organic carbon mass; *overall DOC mass recovery including fractions, base wash, and DOC samples

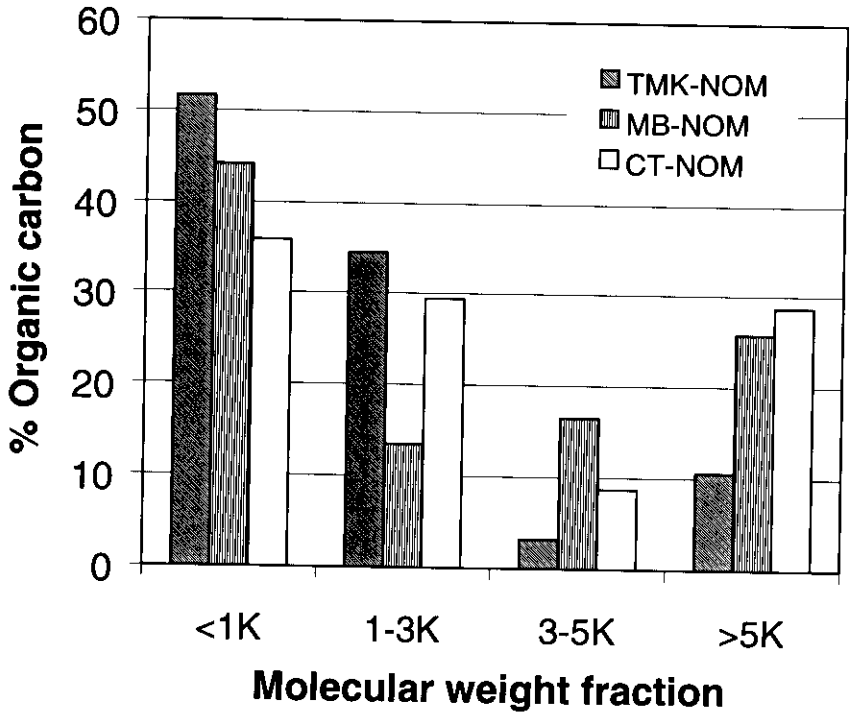

Figure 3-7. Source water molecular weight distributions.

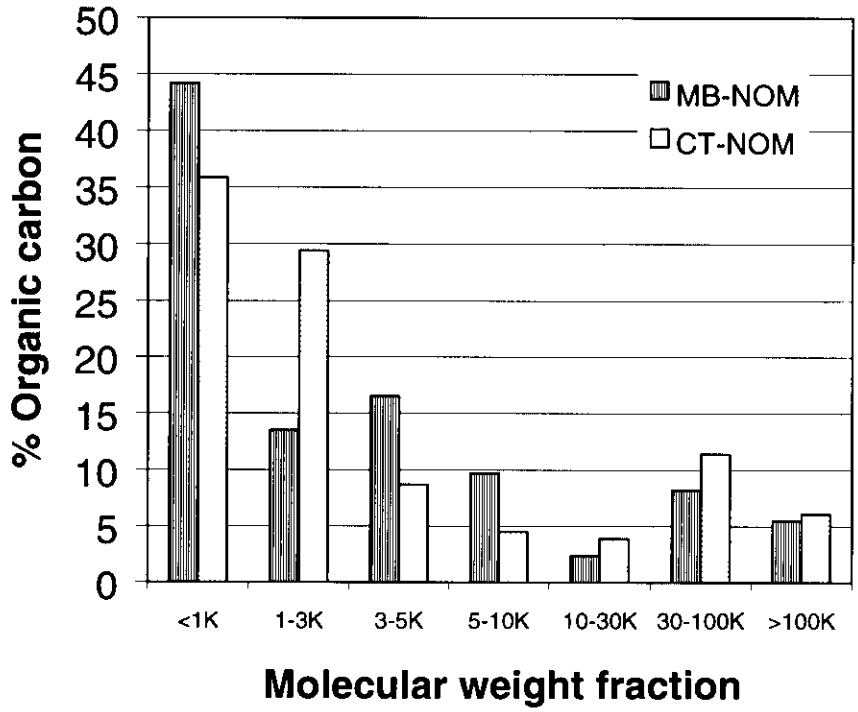

Figure 3-8. Detailed molecular weight distribution of MB and CT waters.

4.0 Organic Matter Fractionation by XAD Resin Adsorption

4.1 Introduction

Dissolved natural organic matter (NOM) may be classified into three major subgroups, aquatic humic substances, hydrophilic acids, and simple identifiable compounds that account for approximately 50%, 30%, and 20% of the total NOM (as organic carbon) of a natural water respectively. The simple identifiable compounds include carbohydrates, carboxylic acids, amino acids, and hydrocarbons. The remaining 80% of NOM, humic substances and hydrophilic acids, are larger molecular weight macromolecules with heterogeneous structures and functional groups. For this reason they are further classified operationally based on their adsorption and precipitation behavior.

Aquatic humic substances are those compounds that can be removed by a reversed phase adsorptive process, and are further classified into humic acids (HAs), which precipitates out of solution at pH 1, and fulvic acids (FAs), which remain in solution at any pH. In general, the HAs (~10% of total NOM) are larger molecular weight (>2000) and often exist as colloids or are associated with mineral particles. The FAs (~40% of total NOM) are lower molecular weight (800-2000) and contain more carboxyl and phenolic acid functional groups, thus enhancing aqueous solubility relative to HAs (Thurman, 1985). Based on this operational definition, those compounds not sorbed are termed hydrophilic acids, thought to be a mixture of simple organic acids and polyelectrolytic acids with many carboxyl and hydroxyl groups (Thurman, 1985) and possibly including proteinaceous material (Leenheer, 1981).

Humic substances are considered to be the most biologically, physically and chemically reactive fraction of NOM in natural water systems, (Mantoura and Riely, 1975; Aiken et al., 1979) and have therefore received the greatest attention. As a group, fresh surface water humic substances have an average elemental composition of 52% C, 5% H, 40% O, 1.5% N, <1% P, and S, and about 5% ash. The primary functional groups present include carboxyl (4-6 meq/g), phenolic hydroxyl (0.5-2 meq/g), hydroxyl (6-8 meq/g), and carbonyl (1-4 mM/g) (Thurman, 1985). To effectively study aquatic humic substances, it is necessary to isolate reasonable quantities, which is a challenge given the often dilute concentrations found in natural systems.

Historically, attempts to separate humic substances from natural water have included co-precipitation, electrodialysis, liquid/liquid extraction, and freeze concentration; all having met with limited success suffering from low yield, solute corruption, process volume constraints, or some combination of these. Adsorption onto inorganic supports such as activated carbon, silica, alumina, magnesia, and calcium carbonate can overcome some of these limitations; however, inefficiency in the desorption step can result in low recoveries, and solute alteration can be a concern using some of these materials. Anion exchange is an effective means of adsorbing humic substances but also is subject to poor elution characteristics. The development of

synthetic, non-ionic, macroporous, XAD resins in the late 1960's prompted investigation into reversed phase (RP) separation using synthetic organic stationary phase materials.

Mantoura and Riley (1975) conducted a detailed study of humic substance concentration by adsorption onto microporous polystyrene beads (Amberlite XAD-2). They established the thermodynamic driving force, identified the effects of pH and ionic strength, and quantified factors governing column dynamics. XAD-2 is a macroreticular, non-polar, styrene-divinyl benzene polymer whose properties are summarized in Table 4-1. Humic substances used in this study were base-extracted from garden peat, separated into humic acid and fulvic acid fractions.

Table 4-1. Resin Properties

Resin	Polymer Matrix	Pore Size, Å	Surface Area	Polarity	Mesh	Specific Pore vol, cm^3/g
XAD1	SDB	200	100	low		0.69
XAD2	SDB	90	330	low	20/50	0.69
XAD4	SDB	50	750	low	20/50	0.99
XAD 7	acrylic ester	80	450	medium		1.08
XAD8	acrylic ester	250	250	medium	20/40	0.82

Notes: SDB = styrene divinyl benzene polymer

Thermodynamic adsorption data was calculated by linearization of the Langmuir isotherm to calculate the equilibrium adsorption constant K as a function of temperature, and determine the enthalpy, Gibbs free energy, and entropy of sorption. It was concluded based on the relatively small ΔH° value (-5.4kJ/mole) that adsorption was dominated by hydrophobic interactions. This is consistent with 85% of the adsorption driving force, ΔG° (-36.4kJ/mole), being provided by the positive entropy gain. This is in contrast to reported ΔH° values greater than 40 kJ/mol for inorganic adsorbents and explains some of the desorption inefficiency noted for these materials.

Because humic acids are anionic at natural pH values, they must be protonated to facilitate the hydrophobic bonding needed for efficient column separation. By varying pH, it was determined by Mantoura and Riley (1975) that good recoveries could be achieved at pH equal to or below 2.2. They found that lowering the pH from 2.2 to 1.5 increased the efficiency by only ~2%, and increased the risk of macromolecule denaturation. Adsorption efficiency was also improved by increasing the aqueous ionic strength. This was attributed to decreased coulombic repulsion between adjacent hydrophilic groups on sorbed molecules, favoring a more spherocoidal configuration, and increasing the effective surface area available to sorbed molecules.

Mantoura and Riley (1975) found that the percent adsorption in fixed beds of XAD-2 resin decreased linearly with increased flow over the range 5-130 bed volumes per hour (bvh). Given the practicalities of concentrating NOM from a feed stream of natural water, where concentrations are typically on the order of 1.5-5 mg/L, the authors determined an acceptable flow rate of 35 bvh based on uptakes of >92% and >75% for humic acid and fulvic acid respectively. From column geometry experiments for a constant resin volume of 8cm (Mantoura and Riley, 1975), it was determined that maximum uptake occurred at a column length to cross sectional area ratio of ~14. It was also determined that leakage >5% occurs if more than 20% of the theoretical resin capacity is used.

Using the optimum column parameters determined, desorption experiments were performed using various eluant mobile phase conditions. Maximum recovery (~95%) was obtained using four bed volumes of 0.2 M NaOH at 3 mL/min. The authors noted higher recovery when the resin was soaked in the eluant solution overnight. However, this may have been due to resin bleed, because XAD resins are not stable in basic solutions. Recoveries using organic solvent eluants were poor, with the exception of a solution of methanol and 2-M ammonia hydroxide (1:1 v/v), which resulted in recovery of ~91%.

From batch isotherm experiments, it was found that there was a near linear relationship between number-averaged molecular weight and the Langmuir K, consistent with increasing hydrophobicity of the larger molecular weight components. The authors claim that this potential for selective uptake of larger molecules should not significantly alter the final molecular weight distribution of the concentrate relative to the feed, under optimum column operating conditions. However, it was shown that this phenomenon can be exploited to fractionate the concentrate on elution. By using a series of eluants with increasing pH, smaller molecules were eluted preferentially.

Given these promising results for the quantitative isolation of humic substances from natural water using XAD resin, a study was performed by Aiken et al. (1979) to compare the concentration of fulvic acid using five different XAD resins (Table 4-1).

Column adsorption was performed using soil-extracted fulvic acid adjusted to 10 mg/L and pH 2, pumped onto resin columns 0.9 × 30 cm (ten times the optimum length to cross sectional area ratio determined previously) at a flow rate of 12 bvh. Desorption was performed using ~8 bed volumes of 0.1N NaOH eluant, and fulvic acid concentrations were determined by DOC analysis and visible absorbance at 460 nm. Resin capacity, adsorption rate, and optimum pH data was generated using batch experiments. As previously, adsorption was found to be most efficient at low pH, constrained by concerns of organic molecule denaturation and precipitation.

The selection of a weaker base desorption eluant was made due to results indicating resin bleed, with significant bleed from XAD-7 even when elution duration was short. Limited trials using organic solvent eluants gave results consistent with Mantoura and Riley (1975).

Based on pore size, batch distribution coefficients, and breakthrough profiles, the authors conclude that size exclusion of fulvic acid occurs on the styrene-divinyl benzene (SDB) resins at 100 Å. Because XAD-4 has more than twice the surface area of XAD-2, it would be expected to have the larger adsorption capacity, which it does for low molecular weight model compounds tested. For fulvic acids, however, the measured distribution coefficient (K_d) for XAD-2 is nearly twice that for XAD-4. This result is consistent with other cited studies which indicate that the dimensions of rod-shaped fulvic acid conglomerates are on the order of 40 Å by 7 Å, which are large enough to encounter steric resistance to diffusion into pores smaller than 100 Å.

Adsorption rate data show that the order of adsorption rate by SDB resins is consistent with pore size, (XAD7 > XAD 8 > XAD 1 > XAD 2 > XAD 4). Adsorption rate is likely controlled by intraparticle diffusion of the relatively large fulvic acid molecules into small pores. The acrylic-ester resins reach equilibrium faster than the SDB resins, but not necessarily in order of pore size. The proposed mechanism for this is based on the more hydrophilic character of the acrylic-ester resins, which allows them to absorb water (twice the specific pore volume for XAD-7), and thus change the resin properties measured using dry beads.

The desorption efficiencies of the two classes of resins studied were related to differences in their respective chemical composition. The acrylic ester resins, XAD-7 and XAD-8, give elution recoveries of ~98%. These resins are non-aromatic with ion exchange capacities on the order of 10^{-2} meq/gram resin. Breakthrough curves for fulvic acid solution at pH 13, at which all acidic groups will be ionized, are as expected for the acrylic ester resins showing almost immediate breakthrough. Conversely, breakthrough curves under the same conditions for the SDB resins, which are aromatic and hydrophobic, with no ion-exchange capacity, indicate higher adsorption capacities consistent with poorer elution recoveries of 70-75%. The authors hypothesize charge-transfer complexation as a possible explanation. In this scenario, a donor aromatic compound (resin) can contribute available π electron pairs to phenol or quinone groups present in fulvic acid molecules.

These results indicated that the acrylic-ester resins may be the most useful for the quantitative isolation and recovery of fulvic acids from natural water sources. Experiments were performed using two natural water sources, which confirmed the superior recovery efficiency of the XAD-8 resin. The highest SDB resin recovery was found to be XAD-1, which was 80% as efficient as the XAD-8. The excessive resin bleed from the XAD-7 made its utility for NOM isolation questionable at best.

Based in part on the above, an accepted operational definition for aquatic humic substances has been established as colored polyelectrolytic acids isolated from water by sorption onto XAD-8 resin. In order to study these substances in detail, preparative isolation and fractionation schemes have been developed to isolate gram quantities of humic substances needed for research purposes (Leenheer, 1981; Thurman and Malcolm, 1981). These procedures are basically scaled up versions of the analytical techniques outlined above with process design and control additions.

The hydrophobic-hydrophilic split of a water sample on XAD-8 resin is an operationally defined designation controlled by the characteristics of the NOM, and by the ratio of resin to process water throughput. Assuming frontal chromatography and neglecting mass transfer limitations, the elution volume, V_e for solute breakthrough on a chromatographic column is:

$$V_e = V_o(k' + 1) \qquad (27)$$

where V_o is the column void volume and k' is the column distribution coefficient defined as the mass of solute sorbed divided by the mass of solute in the void volume aqueous phase. For this fractionation procedure, a column distribution coefficient $k'_{0.5r}$ is defined for hydrophobic solutes which are greater than 50% retained, and hydrophilic solutes greater than 50% eluted at a constant resin to process water throughput. The effluent volume necessary for this split ($V_{0.5r}$) is two times the breakthrough volume or $2V_e$ and:

$$V_{0.5r} = 2V_o(k'_{0.5r} + 1) \qquad (28)$$

From this equation the amount of resin needed to process a known amount of water with a defined $k'_{0.5r}$ can be calculated. The choice of the operational $k'_{0.5r}$ parameter has consequence as to the character of the hydrophobic (HPO) and hydrophilic (HPL) fractions produced. Thurman et al. (1978) conducted research to experimentally measure and compare the capacity factors for a number of organic solutes on XAD-8 resin. The capacity factor, k', was determined for twenty aqueous organic solvents by adsorption onto an XAD-8 column in non-ionized form, and then desorbing in ionized form, in similar fashion as that used to isolate aquatic humic substances from natural water. Feed concentrations were in the range 5-10 mg/L. Consistent with other cited studies, a strong linear correlation between log k' and log(molar solubility) was observed. Capacity factors generally increased with decreasing solubility. The controlling influence of solubility is illustrated by structurally dissimilar aniline (an aromatic amine) and pentanoic acid (an aliphatic carboxylic acid), which have similar solubilities and identical k' values. The following dependency on carbon backbone structure and functional group content were noted:

$$k' \text{ (aliphatic)} > k' \text{ (aromatic)} > k' \text{ (cyclic)}$$

$$k' (CH_3) > k' (COOH) > k' (CHO)\ k' (OH) > k' (NH_2)$$

For example, short chain (four carbon) aliphatic alcohols and acids had k' values on the order of 25 to 40; increasing the number of carbon atoms to six increased k' to a value on the order of 300 to 400. Aromatic compounds exhibited k' values from 126 for aniline to 1406 for toluene.

The XAD-8 chromatographic protocol involves processing a heterogeneous mixture of naturally occurring NOM into fractions that have distinct, albeit still diverse, structural and functional properties. This makes possible a more detailed understanding of how NOM may interact with physical, chemical and biological processes. The ability

to target specific solutes and change the relative makeup of a fraction by varying k' is also a valuable analytical tool. It is possible to design a fractionation scheme to produce a matrix of target fractions with predetermined characteristics that can be evaluated for reactivity; for example, this approach is amenable to the study of enhanced solubility and drinking water disinfectant-by-product formation. Caution must be employed, however, to avoid separation of groups that may have synergistic effects that will not be taken into account when testing the reactivity of individual fractions. For example, it may be possible that coagulation and precipitation of large macromolecules depends on the presence of a particular group of smaller molecules. If these groups were in separate fractions, the effects of one fraction may not be representative of the natural system.

4.2 Materials and Methods

NOM was isolated from the Tomhannock Reservoir (TMK), and the intake to the Myrtle Beach, SC municipal drinking water treatment plant (MB), using the field scale RO system as discussed above. Each water type was fractionated into HPO and HPL fractions using techniques based on minor modifications to the methods developed by researchers at the USGS (Leenheer, 1981; Thurman and Malcolm, 1981).

The acrylic ester resin employed, Supelite DAX-8 (Supelco Inc.; formerly XAD-8 Rohm and Haas) was received with the following manufacturer supplied physical parameters: 40/60 mesh size, mean surface area 160 m^2/g, mean pore diameter 225Å. To remove impurities and methylmethacrylate monomers, the following clean-up procedure was followed. As-received resin was slurried in 0.1-M NaOH solution and stored for five days, after which the resin was rinsed with fresh NaOH solution, and fines decanted. The resin was sequentially soxhlet extracted using acetone and hexane for 24 hours each, slurried in methanol and left overnight. The resin was vacuum filtered, placed in a drying oven at 48°C and dried to constant weight (10 days) with intermittent vacuum applied. The resin was then 24-hour soxhlet extracted using methanol, packed in a 450-mL glass chromatographic column (3.7 cm id. × 45 cm, teflon end fittings) and rinsed with one liter of HPLC-grade methanol applied at 3.5 bed volumes per hour (BVH). Methanol rinse was followed by >115 bed volumes of deionized (DI) water rinse, applied at a flow rate of 3.8 BVH. After this rinse, the effluent DOC was found to equal influent DOC at 0.15 mg/L. All DOC measurements were made using an O.I. Analytical (College Station, TX) Model 1010 TOC analyzer that employs a high-temperature sodium persulfate wet oxidation method. Next, back elution with 2L of 0.1N NaOH solution at 3.8 BVH, in order to desorb any organic matter concentrated during the DI water rinse, was followed by 0.01N HCl solution until effluent pH = 2. The resin was stored in the column at pH 2, jacketed to exclude light. This base elution/acid wash sequence was performed immediately prior to all sample fractionation runs, and once weekly if the column remained idle.

All system tubing consisted of 1/8" i.d. PTFE with stainless steel valves and Swagelock fittings except the peristaltic pump head tubing, which was a peroxide cured silicon (Cole-Parmer), chosen for low organic leachables and acid-base stability characteristics. The sample was introduced onto the resin using a variable speed (10-600 rpm) peristaltic pump (Masterflex L/S, Cole-Parmer). The resin bed was packed to

approximately 95% of the column volume to allow for expansion due to resin swell during fractionation/rinsing procedures. A tracer test was conducted using an NaCl solution, and the data were fitted with a plug flow with diffusion model (per Teefy and Singer, 1990) to determine a system void volume of 332 mL ± 3.6%.

Water samples were adjusted to pH 2 using concentrated HCl immediately prior to each fractionation run. At pH 2, essentially all NOM acidic functional groups are protonated, facilitating hydrophobic interactions with the resin. The fraction designated HPO was adsorbed on the column using flow rates of 4.5-13 BVH, and the non-sorbed effluent (HPL) was collected in glass carboys and sampled intermittently for DOC and UV analysis. UV measurements were made using a 1-cm quartz cell and a Diode Array spectrophotometer (HP 8452A, Hewlett-Packard) with a wavelength accuracy of 2 nm, a wavelength reproducibility of 0.05 nm, a spectral bandwidth of 2 nm, a stability of <0.001 AU and a baseline noise of < 0.0002 AU rms.

Following sample application, one bed volume of 0.01-N HCl was passed through the column to flush any non-sorbed components from the resin bed voids, and then the HPO fraction was recovered by back elution in the reverse direction, using 0.1-N NaOH, at a flow rate of 5 BVH. HPO and HPL fractions were subsequently adjusted to pH ~ 4, sampled for DOC and UV analysis, and stored in the dark at 4°C. Those components of the NOM that do not desorb from the resin during back elution are deemed the hydrophobic neutral fraction and are not recovered using this protocol.

4.3 XAD Fractionation Results

The conditions and recovery results for ten fractionation runs for six water samples from two different sources are outlined in Table 4-2; hydrophobic/hydrophilic splits for three source waters are shown in Figure 4-1. Tomhannock Reservoir water designations reference fractionation runs for the natural water (TMK1), and four separate RO concentration runs of the same source (TMK2-5).

Table 4-2. XAD Fractionation Results Summary

WATER	TMK1	TMK2		TMK3			TMK4		TMK5	MB
RUN #	1	2	3	4	5	6	7	8	9	10
$SUVA_{254}$	2.15	2.26		2.96			1.97		1.92	4.56
k'	53	44	50	52	31	95	95	82	96	96
Feed conc mg/L	3	25	30	30	31	35	37	36	34	33
Vol. applied, L	18	15	17	18	11	32	32	28	32	32
Mass applied, mgC	55	375	510	533	322	1134	1155	992	1105	1058
HPL conc, mg/L	2	14	16	16	14	24	24	24	22	11
HPL mass, mg C	31	211	268	280	151	763	775	643	703	361
Mass sorbed, mg C	24	164	242	252	171	371	380	348	403	698
HPO recovered, mg	19	134	241	239	163	339	346	316	362	737
% HPO recovered	80	82	100	95	95	91	91	91	90	106
% Mass recovered	91	92	100	98	98	97	97	97	96	104
Hydrophobic-Hydrophilic split (%)										
% HPO (mass)	43	44	47	47	53	33	33	35	36	66
% HPL (mass)	57	56	53	53	47	67	67	65	64	34

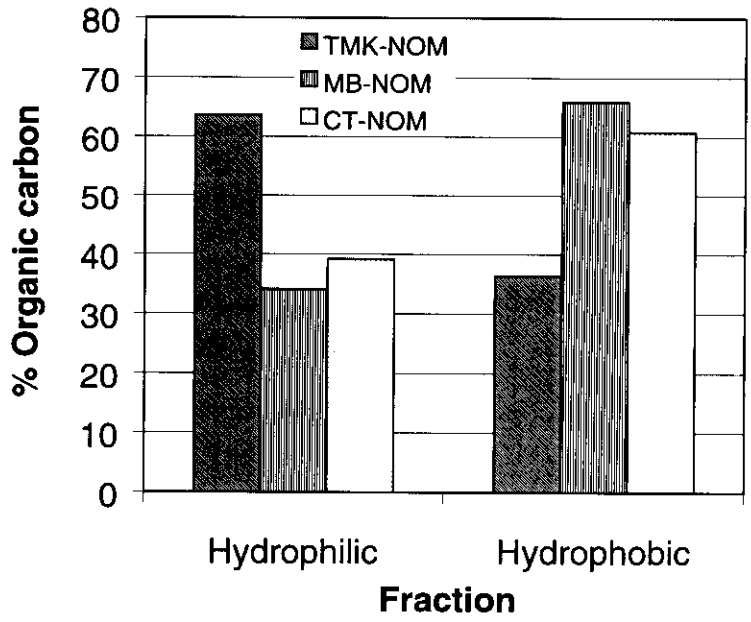

Figure 4-1. Hydrophobic/hydrophilic splits for three source waters.

As given by Equation 27, for the same column conditions (i.e., constant V_o), the column distribution coefficient k' for a given run is determined by the volume of water processed (V_e). It can be seen from the data in Table 4-2 that for a given water source, the operationally designated hydrophobic-hydrophilic split is a function of k'; as k' increases, mass is shifted from the hydrophobic to the hydrophilic fraction. As illustrated in Figure 4-2, over the range of k' studied, the correlation of k' to fraction of mass in the hydrophilic fraction is found to be linear. The four k' values for the single XAD run on Myrtle Beach water (MB) were obtained by collecting the HPL column effluent in four separate volumes. Initially, as k' gets larger, the HPL fraction contains increasingly greater proportions of more hydrophobic components until the column reaches a steady state, at which point the hydrophobic-hydrophilic split becomes relatively constant and is controlled by the NOM characteristics of the water. This phenomenon is illustrated in Figure 4.3, where the column effluent organic carbon normalized specific UV absorbance at 254 nm ($SUVA_{254}=100 \times UV_{254}/DOC$), a surrogate for NOM hydrophobicity, is shown to rise sharply and then plateau as throughput volume increases. In contrast, the $SUVA_{254}$ removed, calculated as:

$$SUVA_{254,removed} = 100 \times \frac{UV_{feed} - UV_{effluent,V_e}}{DOC_{feed} - DOC_{effluent,V_e}} \tag{29}$$

remains relatively constant over the course of a fractionation run (Figure 4.3). The data presented in Figure 4-3 distinguishes between water samples (TMK1-5, MB) and exemplifies the consistency between fractionation runs of the same water sample (TMK3, TMK4). Normalized NOM breakthrough curves (as DOC) in Figure 4-4 show consistency between fractionation runs of the same water sample, distinguish between water samples consistent with $SUVA_{removed}$, in that the water samples with higher initial SUVA show greater affinity for the resin and so have lower effluent DOC. Based on empirical observations, the number of bed volumes of a water sample that may be processed before breakthrough occurs, is dependent in part on initial sample concentration (Thurman, 1981). For an initial concentration of 25 mg/L, the reported number of bed volumes to breakthrough (30), is exceeded for runs on TMK4, TMK5, and MB however, based on typical results shown in Figure 4-4, breakthrough is not apparent.

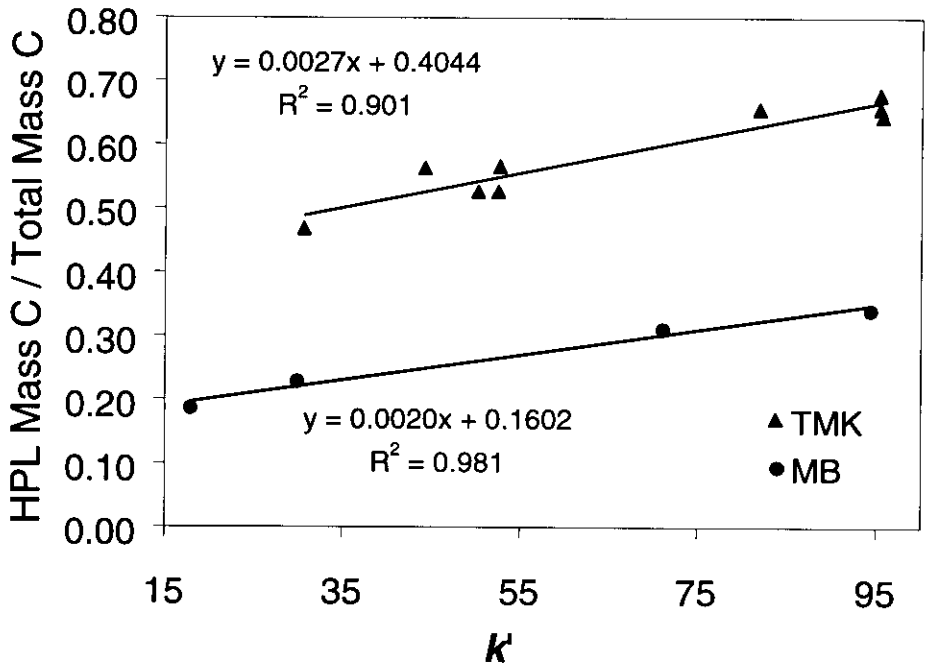

Figure 4-2. The column distribution coefficient, k', for two different waters.

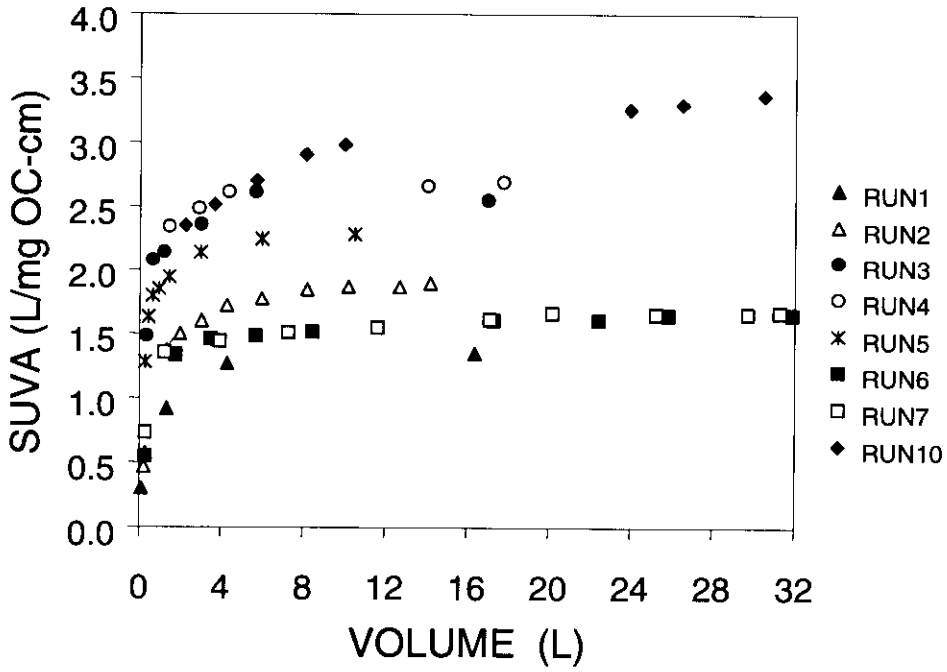

Figure 4-3. Breakthrough of Specific UV Absorbance for Runs 1 through 10 (see Table 4-2).

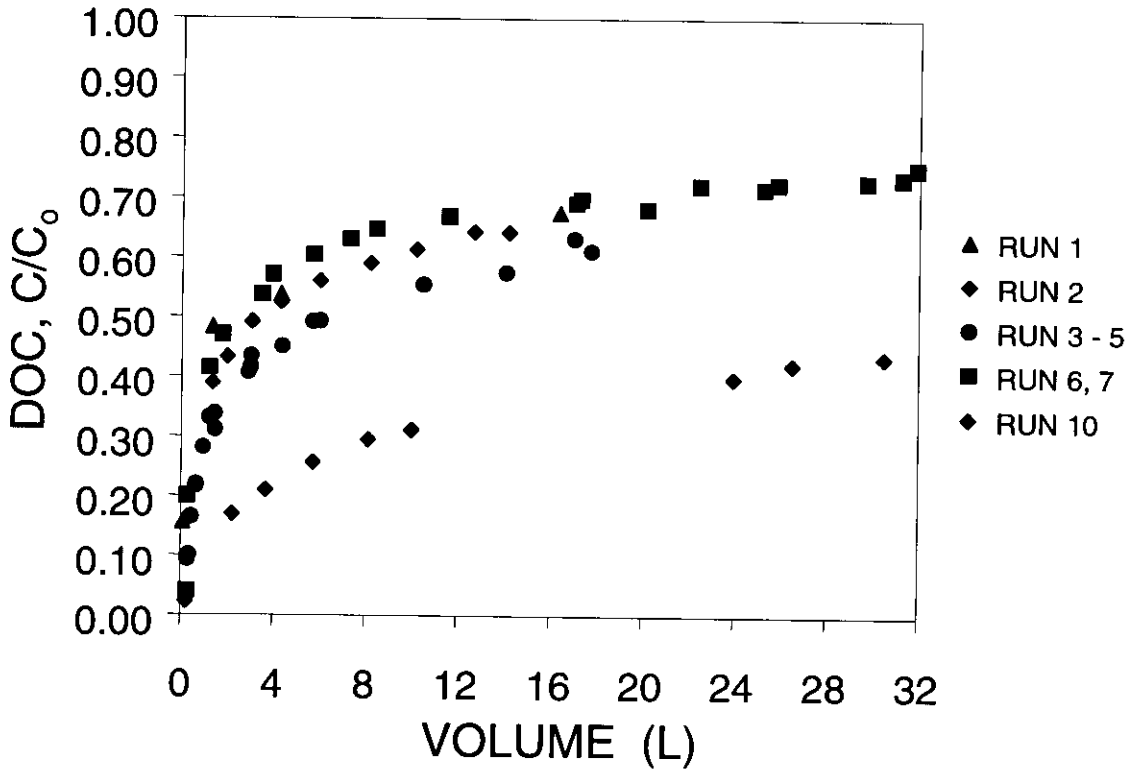

Figure 4-4. Normalized breakthrough of DOC for Runs 1 through 10 (see Table 9).

4.4 Organic Acidity

Organic acidity titrations were performed in a closed vessel, purged and maintained under positive Ascarite-scrubbed N_2 pressure to exclude CO_2, using a Ross Sure-Flow semi-micro combination electrode (Model No. 8175). Carbon dioxide free NaOH analytical concentrate (J.T. Baker 4687-01) titrant was diluted in Milli-Q water, which was previously boiled for 30 minutes, and stored in a container fitted with an Ascarite CO_2 trap. Diluted titrant was standardized against a certified 0.01 N HCl solution (Fisher Scientific SA62-1). Delivery of titrant to HCl standard and samples employed a Class A 5 mL microburet with 70 mL integral reservoir, graduated at 0.01 mL. Sample ionic strength (as NaCl) was determined by conductance at pH 7, followed by adjustment of pH to 3.0 using HCl, a purge of CO_2 by bubbling Ascarite scrubbed N_2 through the sample while in the titration vessel for at least 15 minutes, and subsequent titration to pH > 11. Measured H^+ activity was converted to molar H^+ concentration by calculating an activity coefficient using the Debye-Hückel model:

$$\log \gamma_i = \frac{-Az_i^2\sqrt{0.5\sum m_i z_i^2}}{1+Ba_0\sqrt{0.5\sum m_i z_i^2}} \quad (30)$$

where m is the molar concentration; z is the ion charge; and model parameter values for H^+ used were $A = 0.506$, $B = 0.3275$, $a_o = 9$ (Drever 1997). Ion molar

concentrations used to calculate ionic strength following sample pH adjustment to 3.0 were determined from the initial ionic strength at pH 7, plus the measured Cl^- added to lower the pH, and solving for H^+ and OH^- iteratively under charge balance constraints with $K_w = 10^{-14}$. Replacing H^+ with Na^+ in the course of the titration will not change the ionic strength, and the assumption that the concentration of divalent ions is negligible is justified because all water samples were ion exchanged in the softening unit prior to reverse osmosis. Buffering curves were determined by subtracting a theoretical pure water titration, corresponding to the actual volume additions of base titrant, from the measured sample titration. Because all alkalinity was stripped from the sample prior to titration, all difference between measured and theoretical H^+ consumption is attributable to organic acid functionality protonation.

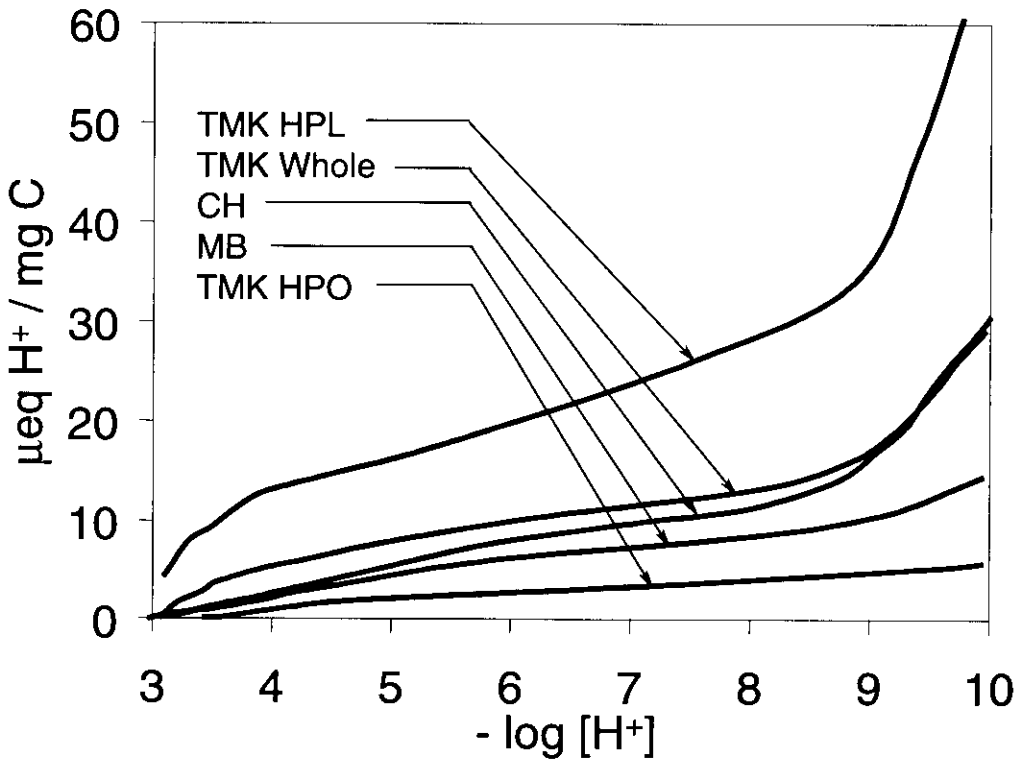

Figure 4-5. Organic acidity titrations of natural organic matter from different sources.

Table 4-3. Acidity of Natural Waters and Organic Matter Fractions

Water	Endpoint pH	Acidity ueq H / mg C
TMK	7.0	11.2
	10.0	28.8
MB	7.0	8.6
	10.0	14.3
CH	7.0	8.2
	10.0	24.5
TMK HPO	7.0	10.6
	10.0	12.6
TMK HPL	7.0	12.4
	10.0	37.0

5.0 Membrane Selection, Characterization, and Modification

5.1 Membrane Selection

Asymmetric cellulose acetate membranes produced by wet-phase inversion techniques, and polyamide thin film composite membranes produced from interfacial polymerization on a non-desalting support membrane are widely used in water treatment and desalting applications. Indeed, the thin film composites are considered state of the art technology for water and wastewater applications. In part, this is because of the hydrophilic nature of these materials, imparted by the carbonyl group, as shown in Figure 5.1. We have selected one aromatic polyamide thin film composite membrane for this research, the NF-70 produced by Dow-Film Tec. However, this type of polymer does have limitations. Polyamide membranes are susceptible to oxidative degradation, but more importantly, cannot tolerate exposure to free chlorine because of their amide functionality. While this membrane can be operated over a wide range of pH, 3-9 for continuous operation and 1-11 for short-term cleaning, it is sensitive to chlorine with a maximum chlorine tolerance of 0.1 ppm. In addition, these membranes have relatively low temperature thresholds (e.g. < 40 °C).

Ultrafiltration and nanofiltration membranes manufactured from polysulfone and polyethersulfone are also commercially available, and offer attractive characteristics that address some of the deficiencies of polyamide membranes.

Polysulfone and polyethersulfone membranes (structures also shown in Figure 5-1) can tolerate wide pH ranges (2 to12), exhibit good resistance to oxidants, including chlorine, and have high temperature limits (on the order of 75 °C). These materials are more hydrophobic than both cellulose acetate and polyamide membranes, and are therefore potentially more susceptible to fouling by natural organic matter and other colloidal material. However, surface modification of such materials offers a promising approach to developing physically and chemically robust materials that have a lower fouling potential than the native polymers. UV photochemical modification is currently practiced by the millions of feet per day in the paper and other industries, and the process is relatively inexpensive. In this research, we have extended the UV photochemical modification approach to directly compare the performance of commercial polyamide (PA) and polysulfone membranes. The reaction was conducted in a UV photochemical reactor at a wavelength of 254 nm. The effects of reaction time, modification protocol, and the amount of graft monomer was investigated. This work has focused on one monomer, N-vinylpyrolidinone (NVP). No initiator is required for the polysulfone membranes because the UV radiation is sufficient to break the ether bond; this provides an economic advantage for these membranes.

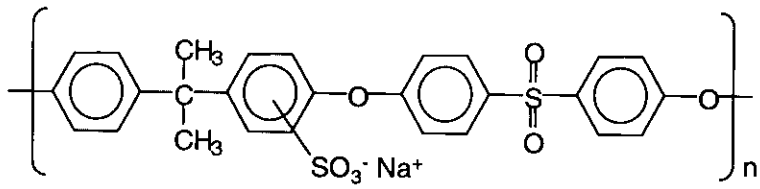

Sulfonated Polysulfone(PSf)
NTR7450 Nitto-Denko America, Inc

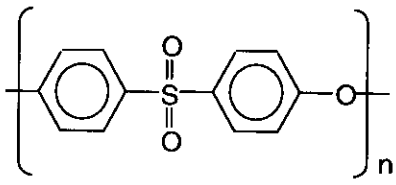

Polyethersulfone (PES)
NF PES 10, Hoechst AG (Celgard)

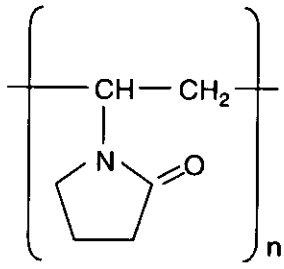

Poly-vinyl pyrrolidone

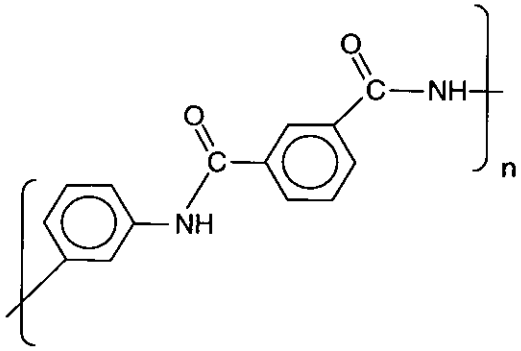

Aromatic Polyamide (PA)
NF 70, Dow Liquid Separations (FilmTec)

Figure 5-1. Structures of membrane and graft polymers used in this research.

5.2 Membrane Modification

5.2.1 Materials

A commercial poly(ether sulfone) (PES) membrane (NF-PES-10, Hoechst AG/Celgard, Lot 548, Roll 6) and a commercial sulfonated poly(sulfone) (sPSf) membrane (NTR7450, Nitto-Denko America, Inc., Roll 8011501) were used in this research. Membrane sheets were cleaned by soaking in 0.1 M NaOH for 30 minutes, followed by rinsing with reagent-grade water 3 times (30-minute each). *N*-vinyl-2-pyrrolidone (NVP) was obtained from Aldrich (Milwaukee, WI) and vacuum distilled to remove the inhibitor before use. Deionized, reagent-grade water was produced from tap water pretreated by mixed-bed ion-exchange and activated carbon, and processed in a Milli-Q system (Millipore, Bedford MA) that included microfiltration (0.2-μm pore size). Natural organic matter was isolated from the Tomhannock reservoir, the drinking water supply for the city of Troy, NY, as described in Chapter 2.

5.2.2 Bench Scale Membrane Testing

Solution flux experiments were conducted using the cross-flow bench scale membrane test system depicted schematically in Figure 5-2. The system consists of a stainless steel cell (SEPA, Osmonics Inc. Minnetonka, MN), a high-pressure stainless-steel piston feed pump, and a high capacity booster (gear) pump to maintain high flow rates in a recycle loop. Using the recycle loop, the desired cross-flow velocity was maintained independent of the feed flow rate and recovery.

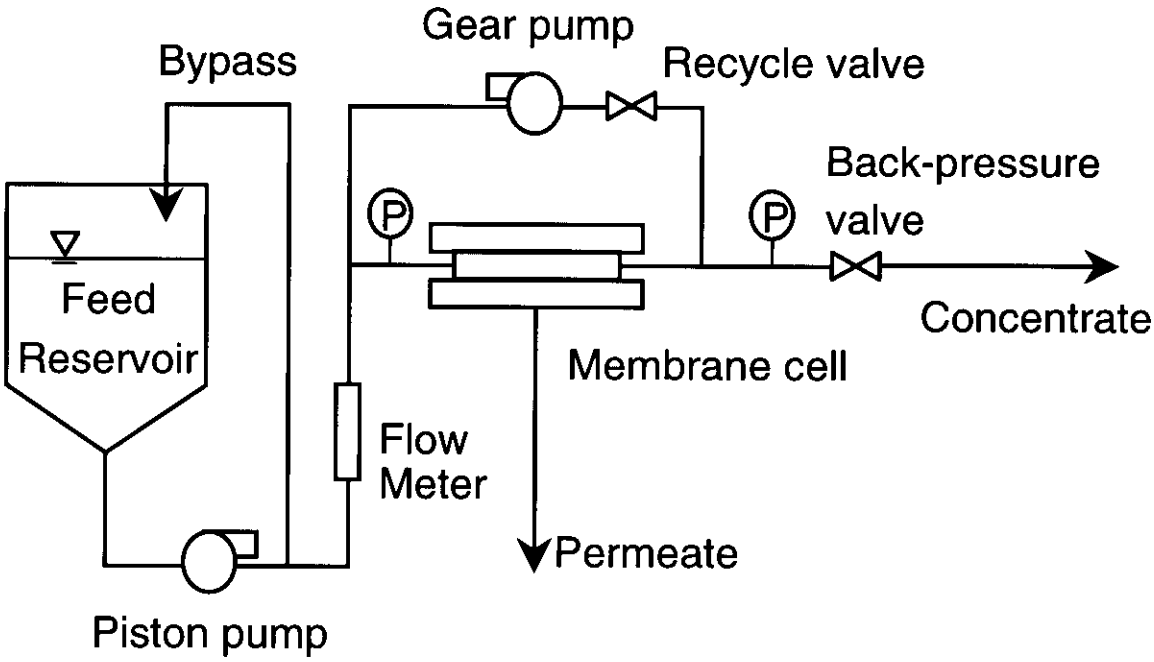

Figure 5-2. Schematic diagram of the nanofiltration system

A 155 cm^2 membrane sheet and a feed channel spacer (0.086 cm high with 3 to 4 strands per cm) were mounted between halves of the stainless steel cell, and were sealed with an o-ring. Recovery was maintained at 85% with a cross-flow velocity of 0.1 m/s, typical of full-scale systems. Permeate and concentrate flowrate were measured directly, while the feed flowrate was calculated by continuity. Clean water flux, J_o, as a function of transmembrane pressure (206 to 620 kPa; 30 to 90 psi) was measured using Milli-Q water to determine the membrane permeability. As shown in Figure 5-3, plots of membrane flux versus transmembrane pressure were linear over the pressure range studied, and the clean water permeability was taken as the slope of the line. The system was then run for 5 hours to allow for membrane compaction; over the 5-hour run, the initial flux of about 45 L/(m^2-hr) (LMH) was reduced by 3% on average. Solution flux can impact the rate and extent of fouling; therefore, prior to the start of all membrane performance experiments, the transmembrane pressure was adjusted to yield approximately the same initial solution flux, 45.3 (± 0.7) LMH. The transmembrane pressure was then held constant throughout the run, while changes in flux were monitored. Inlet temperature was directly measured in the recycle loop during membrane operation. Over the 10-hour filtration experiments conducted in this research, the temperature increased a maximum of less than 3° C, and no attempt was made to correct for this effect.

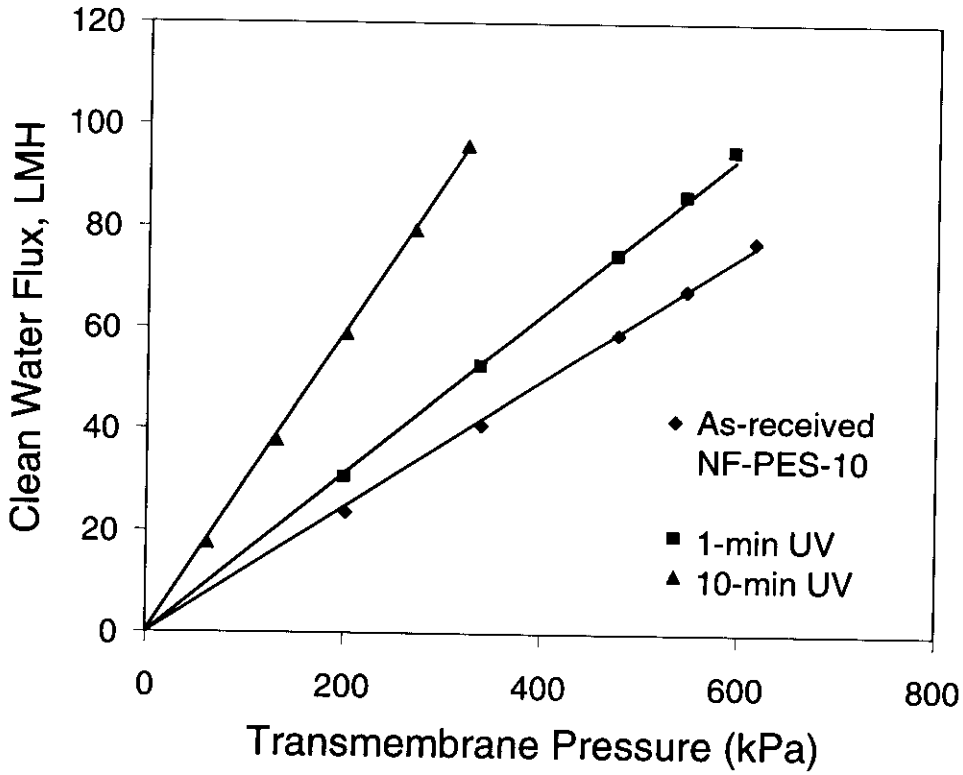

Figure 5-3. Clean water permeability determination for as-received and UV-irradiated NF-PES-10 poly(ether sulfone) membranes. The permeability is calculated from the slope of the permeation flux versus transmembrane pressure.

After a filtration run, the membrane was cleaned in two steps. First, a hydrodynamic cleaning was performed, followed by chemical cleaning. The mass recovered from each step was calculated from measured concentrations to determine the total mass of NOM deposited, the NOM recovered by cleaning, and the mass remaining on the membrane as "irreversibly bound" foulant. During hydrodynamic cleaning, Milli-Q water was recirculated in the system at a velocity 2.5 times higher than the velocity of operation (i.e., 0.25 m/s) for 30 minutes. For chemical cleaning, solutions of Milli-Q with pH adjusted to pH 10 (using NaOH) and pH 3 (using HCl) were recirculated sequentially at a crossflow velocity of 0.25 m/s for 30-min each.

5.2.3 Membrane Modification

Membranes were photochemically modified in a Rayonet photochemical chamber reactor system (Model RPR-100, Southern New England Ultraviolet Company, CT) as described by Pieracci et al. (1999). The quartz photochemical reaction vessel was equipped with sixteen UV lamps with an emission maximum at 254 nm and an intensity of 2.5 mW/cm^2 at the center of the reactor. For membrane modification, a pre-cleaned membrane coupon (of sufficient size for subsequent filtration experiments) was placed in the quartz reaction vessel, sealed, and placed in the photochemical reactor. For irradiation-only experiments, the reaction vessel was partially filled with distilled de-ionized water, and purged for 30 minutes with a stream of ultra-high purity nitrogen to remove oxygen that could terminate the free radicals formed during photochemical modification. For irradiation and grafting experiments using the dip technique, the membrane was first dipped in monomer solution prior to mounting in the reaction vessel. The vessel was then partially filled with distilled de-ionized water, and purged with nitrogen. For irradiation and grafting experiments using the immersion technique, the reaction vessel was filled with monomer solution, and then purged with nitrogen. Following the purge step, the UV lamps were then turned on for a predetermined time. Cooling fans maintained a reaction temperature of 22°C in the reactor system. After irradiation was complete, the quartz vessel was removed from the reactor, and the membranes were washed to remove any unreacted monomer or physically adsorbed polymer by shaking them in bottles of de-ionized water for 2 hours at room temperature.

System variables include monomer type, monomer solution concentration, and irradiation time. N-vinylpyrolidinone (NVP) was chosen as the monomer type because previous studies have identified it as superior to several other hydrophilic monomers, and NVP-modified PES membranes were shown to outperform commercial regenerated cellulose membranes in terms of low fouling by BSA and high flux (Pieracci et al., 2000). Furthermore, N-vinylpyrolidinone is non-toxic and hydrophilic; its polymer, polyvinyl pyrolidinone, is water-soluble and is often added to the casting solution during manufacture of commercially available polysulfone membranes. A 3% (w/w) concentration of NVP in aqueous solution was chosen to minimize the chance of exhausting the monomer available for grafting at the surface, thus minimizing possible consequences including subsequent trunk polymer scission and possible loss of previously grafted polymer.

5.2.4 FTIR Analysis

Attenuated total reflection-Fourier transform infrared spectra (FTIR/ATR) of the unmodified and monomer-modified membranes were obtained using a Nicolet Magna-IR 550 Series II spectrometer (Nicolet Instrument Corp., Madison, WI). Multiple scans (256) were performed at a resolution of $\pm$ 4 cm^{-1} using a germanium crystal at an incident angle of 45°. The IR penetration depth for this incident angle is 0.1 to 1 μm, depending on the index of refraction of the polymer and the wavelength (SpectraTech, Inc., 1995).

5.2.5 Contact Angle

Static contact angles of the membrane surface were measured using the captive air bubble technique. Membranes were inverted in deionized water and air bubbles were placed in contact with the surface. The static angle was measured using an SIT camera (SIT66 Dage-MTI, Michigan City, IN) connected to a video screen. The contact angles were averages of measurements on 10 different bubbles; the measurement error was ±3°.

5.2.6 Filtration Parameters

The filtration parameters employed in this research, previously discussed by Pieracci et al. (1999), are shown in Figure 5-4. The clean water permeability, L_p, is used to evaluate changes in membrane flow characteristics as a result of membrane modification. Goals of this work are to produce modified membranes that exhibit (i) a low tendency to foul, having a fouling flux ratio, J_{om}/J_o, larger than that for unmodified membranes (i.e., $(J_{om}/J_o)_{modified}/(J_{om}/J_o)_{as\text{-}received} > 1$) and as close to unity as possible; (ii) solution flux during natural organic matter filtration, J_{om}, greater than as-received membranes; (iii) observed solute rejection ($R = 1 - C_{permeate}/C_{feed}$) greater than as-received membranes; and, (iv) flux loss due to fouling ($J_o - J_{om}$) that is completely recoverable by hydrodynamic cleaning with water only (i.e., $J_1 \approx J_o$).

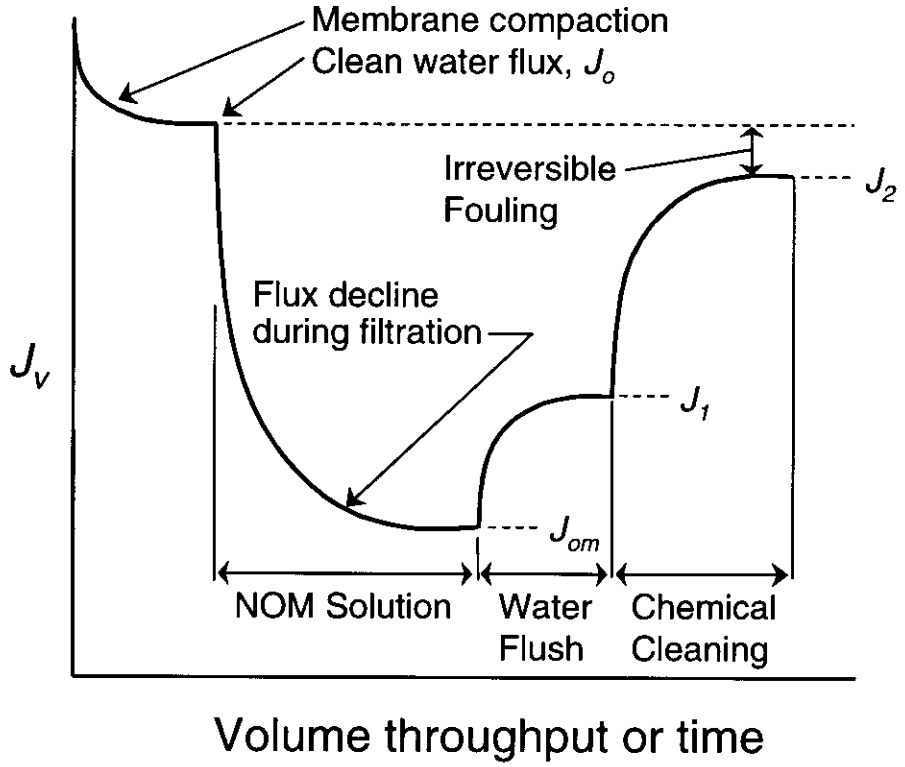

Figure 5-4. Schematic depiction of the filtration protocol employed and definition of the filtration parameters.

5.3 Results and Discussion

5.3.1 UV Irradiation

The effects of UV irradiation on membrane surfaces were characterized by FTIR spectroscopy and wettability. Wettability was quantified by measuring contact angles using the captive air bubble technique. Exposure of the poly(ether sulfone) membranes to UV radiation caused an increase in the OH-stretch region (between 3200 and 3600 cm^{-1}) of the FTIR spectra (data not shown). This is consistent with the previous results of Pieracci et al., (1999), who attributed their findings to an increase in the amount of surface hydroxyl groups present; such groups increased linearly with irradiation time. UV light at a wavelength of 254 nm has sufficient energy to break the sulfur-carbon bond of the trunk polymer, forming a radical at that position. The radical terminates with a hydroxyl group, as suggested by FTIR analysis. Surface hydroxyl groups, which can bind water through hydrogen bonds, may be responsible, in part, for the observed increase in hydrophilicty of UV-irradiated membranes. Another possibility exists for the NF-PES-10 membranes studied here. As will be discussed in greater detail below, it is possible that the manufacturer added a (presumably) hydrophilic monomer to the casting solution. UV irradiation may expose such moieties or promote their migration to the surface, resulting in a greater surface concentration. The observed increase in hydrophilicty of UV-irradiated membranes, and the effect of UV radiation on the OH-

stretch region of the FTIR spectra, could be due, in part, to an increase in water absorption by these hydrophilic moieties.

As is evident from examination of the data tabulated in Table 5-1, UV irradiation had a notable effect on surface energy, lowering contact angles significantly. The as-received NTR7450 sulfonated poly(sulfone) membrane had a lower contact angle (28.6°) than the NF-PES-10 poly(ether sulfone) membrane (39.6°). Contact angles for both membranes were lowered significantly after 1 min irradiation time, and after 10 min, contact angles of the NF-PES-10 and NTR7450 were lowered 51% and 42% respectively. It should be noted that the contact angles of both membrane types were lower (suggesting a more hydrophilic surface) than commercially available polyamide membranes ($\theta \cong$ 28°). Indeed, for both the sPSf and PES materials, achieving contact angles less than 20° was shown to be possible, making the UV irradiated surfaces as hydrophilic as the most hydrophilic membranes manufactured. The kinetics of the surface hydroxyl formation were faster than those observed in previous research (Pieracci et al., 1999), in which it was found that significant changes in contact angle occurred only after 7 min of irradiation time. This is likely due to the fact that for the UF membranes studied previously, modification occurred at a greater depth in the pores, while for the NF membranes studied here, modification was localized at the membrane surface.

As shown in Figure 5-3 for the NF-PES-10 membrane, UV irradiation had a marked effect on clean water permeability (slope of the flux vs. pressure curve). Clean water permeability values for all membranes are tabulated in Table 5-2. The effect was significant for an irradiation time of 1 min (increases of 76% for the sPSf membrane and 26% for the PES membrane were observed) and dramatic for the 10 min irradiation time (increases by a factor of 6.7 for the sPSf membrane and 2.4 for the PES membrane were observed). Pieracci et al. (1999) found similar results, and attributed their findings to facile bond cleavage along the backbone of the polymer chain, and subsequent increase in pore size. Examination of the data in Table 5-2 also shows that the increase in clean water flux was accompanied by a decrease in rejection, and an increase in solute flux. This finding is in contrast to those of Pieracci et al. (1999), who observed that solute flux of BSA decreased upon UV irradiation of fully retentive 10 kDa UF membranes. To explain this, they cited the possibility that UV irradiation formed negatively charged surface functional groups, which increased the electrostatic repulsion between BSA and the membrane surface. The increase in solute flux observed here suggests that if electrostatic repulsion was increased, any tendency for this to reduce solute flux was secondary to the effects of pore enlargement. The impact of UV irradiation on solute flux appears to depend on the solute molecular size (or size distribution) relative to the nominal membrane molecular weight cutoff. In Pieracci's work, the BSA was much larger than the nominal membrane pore size, and changes in surface charge were important in decreasing solute flux. In this work, it is likely that the much lower molecular weight NOM was not significantly larger than the nominal membrane pore size, and changes in pore size were important in increasing solute flux. In addition, the broad size distribution of NOM may have played a role to exacerbate this effect.

Table 5-1. Summary of Contact Angle Measurements

Membrane	Contact Angle[a] [°]	95% CI[b] [°]	Cos θ ± 95% CI [–]
As-received[c]			
NTR7450	28.6	2.6	0.855 - 0.899
NF-PES-10	39.6	2.3	0.745 - 0.795
UV Irradiated			
NTR7450-1min	17.8	1.1	0.946 - 0.958
NTR7450-10 min	16.6	1.0	0.953 - 0.963
NF-PES-10-1 min	27.0	1.8	0.876 - 0.905
NF-PES-10-10 min	19.3	1.3	0.936 - 0.951
Graft Polymerized (Dip method)			
NF-PES-10-10 s	29.0	1.0	0.866 - 0.883
NF-PES-10-30 s	24.4	0.90	0.904 - 0.917
NF-PES-10-60 s	ND	ND	
NF-PES-10-180 s	21.0	0.62	0.930 - 0.938
Graft Polymerized (Immersion method)			
NF-PES-10-3 min	24.7	0.72	0.903 - 0.914
NF-PES-10-5 min	22.4	0.72	0.920 - 0.930
NF-PES-10-10 min	22.0	0.72	0.922 - 0.932

(a) Values are averages of 10 replicate measurements
(b) Confidence Interval
(c) NTR 7450 - poly(sulfone) membrane
NF-PES-10 - poly(ethersulfone) membrane

Table 5-2. Summary of Membrane Filtration Experiments

Membrane	L_p LMH/ kPa	TMP, ΔP kPa	R^a (DOC) %	Fluxes[b] J_o LMH	J_{om}[c] LMH	J_1 LMH	J_2 LMH	J_s (DOC) mg/(m^2-hr)	Flux Ratios J_{om}/J_o	J_1/J_o	J_2/J_o	$(J_1-J_{om})/(J_o-J_{om})$	$(J_2-J_1)/(J_o-J_{om})$
As-received													
NTR7450	0.097	457	83.3	45.8	35.1	35.1	38.7	55.9	0.766	0.766	0.845	0.0	33.6
NF-PES-10	0.123	374	57.9	45.4	36.9	42.5	44.3	139	0.813	0.936	0.976	65.9	21.2
UV Irradiated													
NTR7450-1min	0.171	274	71.5	45.0	34.5	34.5	40.8	88.1	0.767	0.767	0.907	0.0	60.0
NTR7450-10 min	0.646	76	33.0	45.6	35	40.9	40.9	223	0.768	0.897	0.897	55.7	0.0
NF-PES-10-1 min	0.155	322	57.7	45.1	38.4	41.3	42.1	154	0.851	0.916	0.933	43.3	11.9
NF-PES-10-10 min	0.295	159	28.7	45.8	41.3	45.2	45.2	289	0.902	0.987	0.987	86.7	0.0
Graft Polymerized (Dip method)													
NF-PES-10-10 s	0.052	896	72.9	44.6	35.8	40.3	41.1	96.0	0.803	0.904	0.922	51.1	9.1
NF-PES-10-60 s	0.074	643	49.8	45.1	42.2	44.0	44.0	207.3	0.936	0.976	0.976	62.1	0.0
NF-PES-10-180 s	0.383	124	29.3	45.3	39.5	42.2	42.2	263	0.872	0.932	0.932	46.6	0.0

(a) R is the observed solute rejection, $1-C_{permeate}/C_{feed}$. (b) Flux in LMH is L/(m^2-hr) except solute flux, J_s, in mg/(m^2-hr). J_o is the initial NOM solution flux. J_{om} is the volumetric solution flux after 10 hours of natural organic matter filtration. J_1 is the volumetric solution flux after hydrodynamic cleaning with water only. J_2 is the volumetric solution flux after cleaning with caustic (see Figure 3). J_s is the solute flux, natural organic matter as dissolved organic carbon; $J_s = J_{om}C_{permeate}$. (c) Natural organic matter filtration solution: 10 mg DOC/L, 10 mM NaCl, pH 7, T = 20 °C.

As shown in Figure 5-5 and Table 5-2, the tendency for the NF-PES-10 membrane to foul was reduced by UV irradiation, for both irradiation times. This effect is related, in part, to an increased solute flux (reduced rejection) that resulted from irradiation for 10 min; however, for the membrane irradiated for 1 min, solute flux and rejection were similar to the as-received membrane. In contrast, UV irradiation did not reduce the tendency for the sPSf (NTR7450) membrane to foul, even though solute flux was increased and rejection was decreased for both irradiation times. Also, an increase in reversible fouling, from increased membrane permeability, was observed. Pieracci et al. (1999) observed an *increase* in the tendency to foul after UV irradiation; possible explanations cited were an increase in available surface area and surface roughness.

Examination of the data in Table 5-2 reveals that little of the flux lost by the as-received NTR7450 membrane was recoverable by hydrodynamic cleaning, and only about 34% was recovered by the caustic cleaning. UV irradiation for 1 min improved the flux recovered by caustic cleaning to 60%, but did not increase the flux recovered by hydrodynamic cleaning. In contrast, after UV irradiation for 10 min, about 57% of the flux loss was recovered by hydrodynamic cleaning only. The as-received PES membrane exhibited higher overall flux recovery, and flux recovered by hydrodynamic cleaning; this was likely due, in part, to lower solute rejection. While the overall recovery of flux was relatively high for the as-received membrane (98%), cleaning by caustic was required to recover 21% of this. The overall recovery was not improved by UV irradiation; however, the same overall recovery could be achieved without caustic when the PES membrane was irradiated for 10 min. The continuous decrease in the fraction of fouling recovered by caustic cleaning, $(J_2 - J_1)/(J_o - J_{om})$, with increasing UV irradiation time was consistent with the findings of Pieracci *et al.* (1999). One potential limitation of surface modification by UV-irradiation is the surface restructuring characteristic of small moieties such as hydroxyls (Lee et al., 1987). The likelihood of surface restructuring increases as the glass transition temperature (T_g) of the polymer decreases. When such restructuring occurs, the beneficial surface characteristics measured prior to restructuring (e.g., surface hydrophilicity) can be reduced. To overcome these limitations, polymer grafting was pursued.

5.3.2 Polymer grafting

The NF-PES-10 membrane was chosen for further studies to evaluate the effects of surface modification using UV assisted graft polymerization. FTIR was employed to verify graft polymerization of NVP to the NF-PES-10 membrane surface. As demonstrated by the spectra shown in Figure 5-6, the OH stretch absorbance peak at 3417 cm^{-1} and the amide I carbonyl stretch at 1670 cm^{-1} are significantly increased as a result of modification. The presence of the amide I carbonyl peak is taken as evidence that grafting has occurred. The degree of grafting is quantified by normalizing the peak height of the carbonyl stretch at 1670 cm^{-1} by the benzene carbon-carbon double bond absorbance peak at 1487 cm^{-1}, which remains constant after modification.

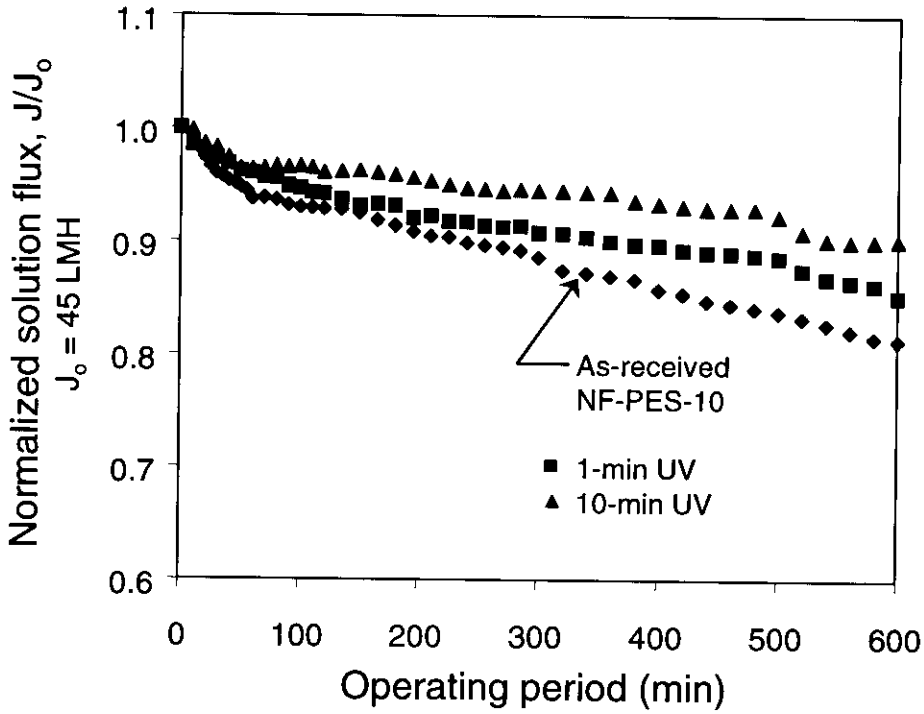

Figure 5-5. Effect of UV irradiation on the performance of the of the NF-PES10 membrane flux. Solution conditions: Tomhannock reservoir organic matter, 10 mg/L as organic carbon, pH = 7, 10 mM NaCl; T = 20 °C

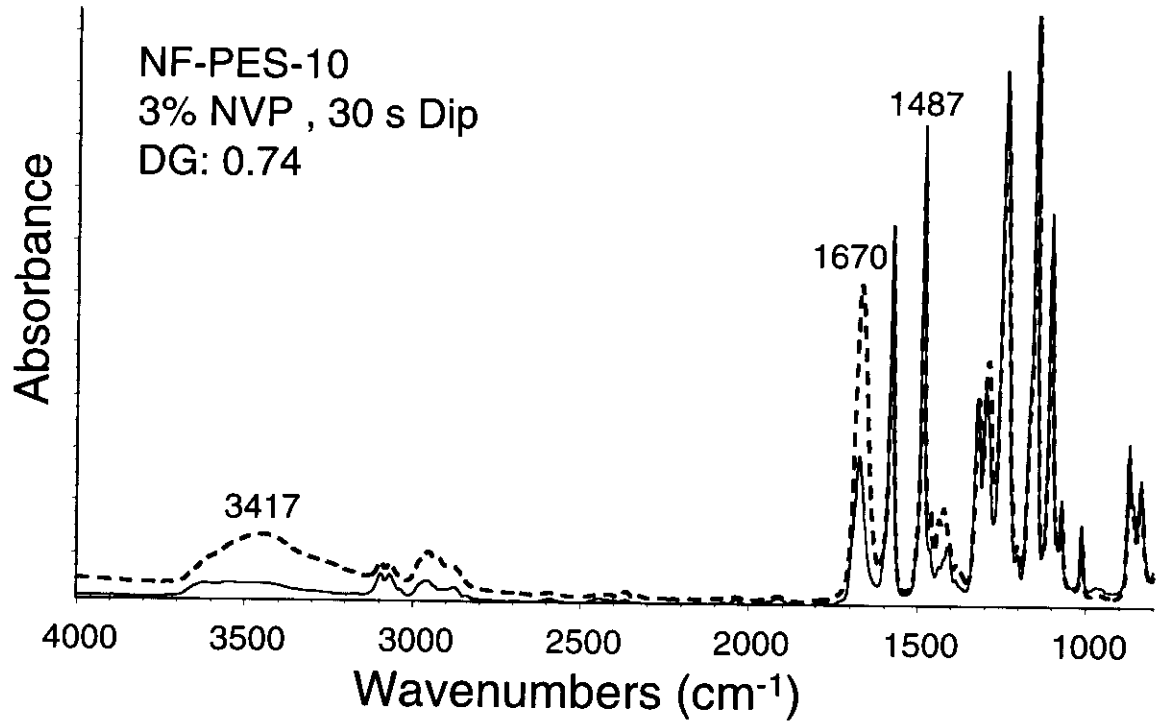

Figure 5-6. FTIR spectra of as-received (solid line) and NVP-graft polymerized (dashed line) NF-PES-10 membrane.

Note that the as-received NF-PES-10 membrane displays a degree of grafting of 0.31; this suggests that the manufacturer has incorporated a hydrophilic moiety with a carbonyl group into the membrane polymer, onto the membrane surface, or both. This could provide an explanation for the lower contact angle of this membrane as compared to the PES UF membrane studied by Pieracci et al. (1999). The effects of reaction time, and modification technique (dip vs. immersion) on the degree of grafting are shown in Figure 5-7.

Examination of Figure 5-7 shows that both the dip and immersion modification techniques can produce high degrees of grafting on the NF-PES-10 membrane surface. However, it is evident that the immersion technique requires a significantly longer reaction time to produce the same degree of grafting. Pieracci et al. (2000) used energy absorbance measurements to show that when the dip technique is used, a larger fraction of the energy emitted by the UV lamps reaches the membrane surface. This causes, in turn, the bond cleavage and free radical production required to promote graft polymerization. In contrast, the energy reaching the membrane surface is lower when the immersion technique is used, because the NVP monomer solution absorbs strongly in the UV, thus shielding the membrane.

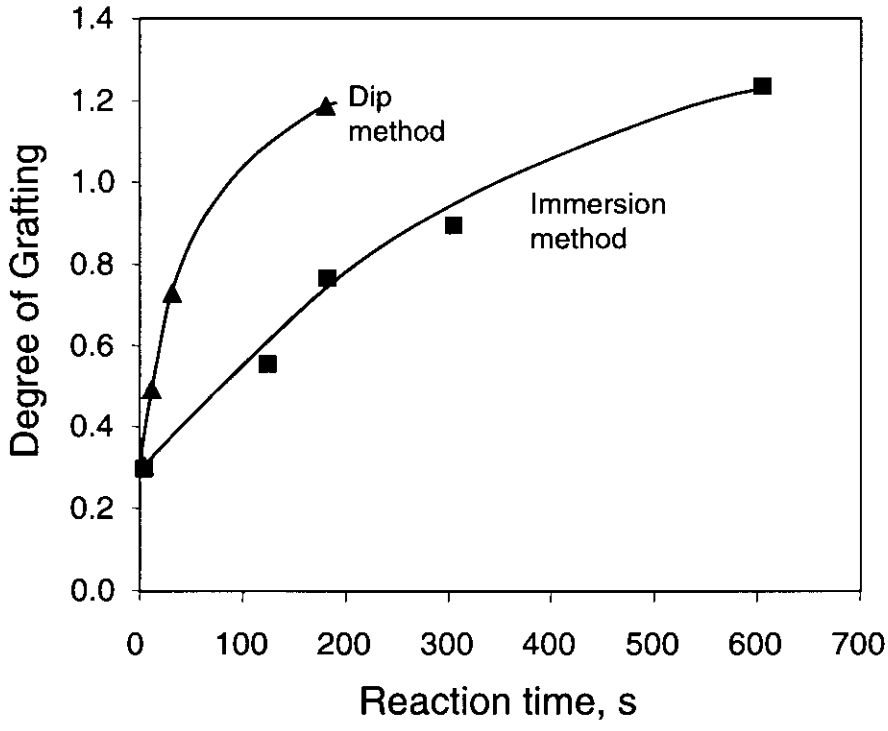

Figure 5-7. A comparison of the degree of grafting achieved using the dip (▲) and immersion (■) methods of photo-assisted graft polymerization.

Both the dip and immersion techniques are effective in producing membranes that have hydrophilic surfaces, as measured by either the contact angle, θ, or surface wettability (cos θ)(Table 5-1). Using the dip method, the contact angle was lowered to below 25° (cos θ > 0.90) using a reaction time of only 30 s; increasing the reaction time to 3 min lowered the contact angle to 21°. Using the immersion method, about 3 min were required to lower the contact angle below 25° (cos θ > 0.90), and 10 min were required to lower the contact angle to 22°. The trend of surface wettability with degree of grafting is shown in Figure 5-8; features of this plot are similar to those found by Pieracci et al. (2000). The surface wettability increases most significantly as the degree of grafting is increased from 0.31 (as-received membrane) to about 0.7 to 0.8, above which cos θ approaches an asymptotic value of about 0.94. As shown in Figure 5-8, the relationship between cos θ and degree of grafting does not appear to be influenced by the modification technique (dip versus immersion); differences in the two techniques appear to be confined to kinetic effects only. It should be noted that the similarity of cos θ for the two modification techniques at a given degree of grafting does not preclude the possibility that other properties, not measured here, are different.

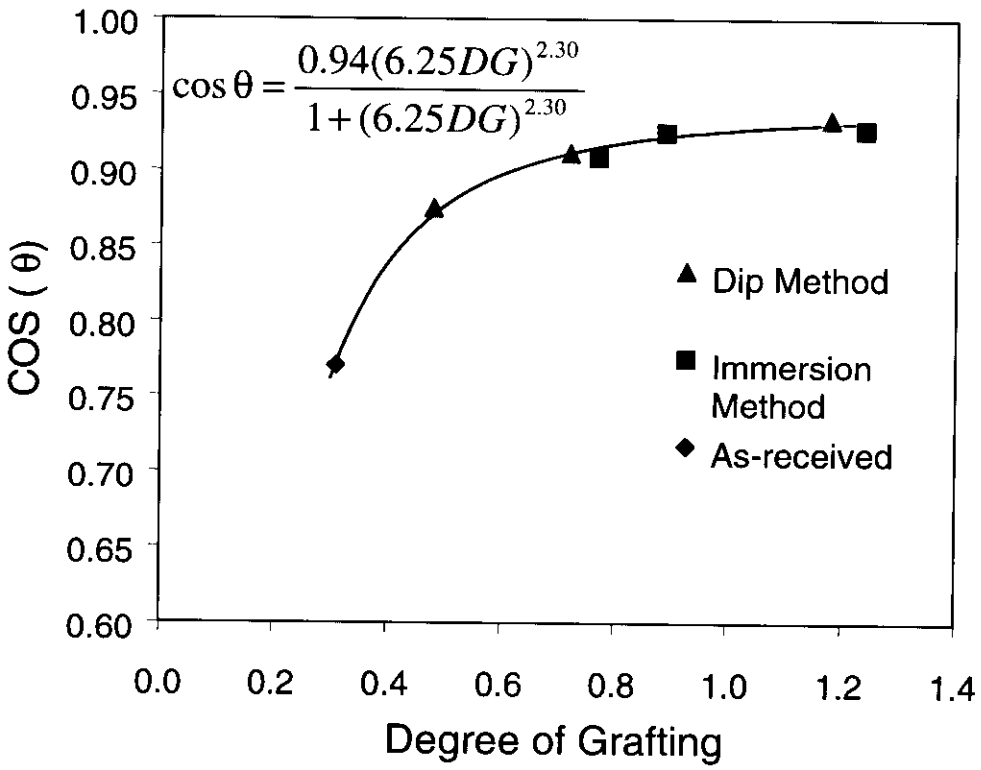

Figure 5-8. The effect of degree of grafting (*DG*) on membrane wettability, defined as the cosine of the contact angle, θ

The effects of graft polymerization on the clean water permeability, NOM rejection, and NOM solution flux decline were evaluated employing the dip method. We have focused on the dip technique because this method requires significantly shorter reaction times to achieve the same degree of grafting, making it better suited for integration into a membrane manufacturing process. For irradiation times of 10 or 60 s using the dip method, graft modification reduced clean water permeability 58 and 40%, respectively, as compared to the as-received NF-PES-10 membrane. However, for the longest irradiation time, 180 s, the clean water permeability was increased by a factor of about 3 (Table 5-2). A reduction in clean water permeability is consistent with the findings of Pieracci et al. (2000), who modified a 50 kDa UF membrane using the dip technique with a 5% NVP solution. It was assumed that grafted poly(vinyl pyrolidinone) (PVP) chains blocked pores, and thus decreased permeability. Pieracci *et al.* (2000) also observed increases in membrane permeability when lower concentrations (1%) of NVP were employed, citing the possibility that during the longer irradiation time, NVP was exhausted from the surface, and either previously grafted polymer was lost, trunk polymer scission occurred, or both. It should be noted that in this study, a decline in the degree of grafting (Figure 5-7) with increasing irradiation time was not observed; therefore, there is no direct evidence that exhaustion of monomer on the membrane surface occurred.

As shown in Table 5-2, significant changes in membrane rejection for natural organic matter were observed as a function of irradiation time during dip modification. Pieracci et al. (2000) observed only decreases in rejection; however, we observed both increases and decreases depending on irradiation time. For the shortest irradiation time, 10 s, we observed an increase in rejection from 57.9% (as-received membrane) to 72.9%. For the longest irradiation time, 180 s, we observed a significant decrease in rejection, to 29.3%. For their system, Pieracci et al. (2000) conclude that irradiation times greater than 10 s should be avoided. Based on interpolation of the data in Table 5-2, it appears that for the NF membrane studied here, longer irradiation times on the order of 40 s appear feasible without causing significant decreases in rejection. The magnitude of the change in rejection that results from graft modification of the membrane should depend, in part, on the pore size (and/or size distribution) relative to the solute molecular size (or, in the case of natural organic matter, size distribution). It is likely that the different results obtained in this study relate, in part, to the smaller size of the NF membrane pores relative to the NOM solutes, as compared to the 50 kDa UF membrane employed by Pieracci et al. (2000) to filter 67 kDa BSA.

The flux decline observed for the polymer-grafted membranes using the dip method are compared to the as-received membrane in Figure 5-9; filtration results are tabulated in Table 5-2. As depicted in this Figure, the graft polymerization approach using irradiation times 60 s or greater produced membranes with a significantly lower propensity to foul (higher J_{om}/J_o). In contrast, the membrane irradiated for only 10 s shows a slightly greater fouling tendency than the as-received NF-PES-10 membranes. In part, the results are correlated to changes in solute rejection. The J_{om}/J_o for the membrane irradiated for 10 s decreased modestly from 0.813 to 0.803 while rejection increased 26% and solute flux decreased more than 30%.

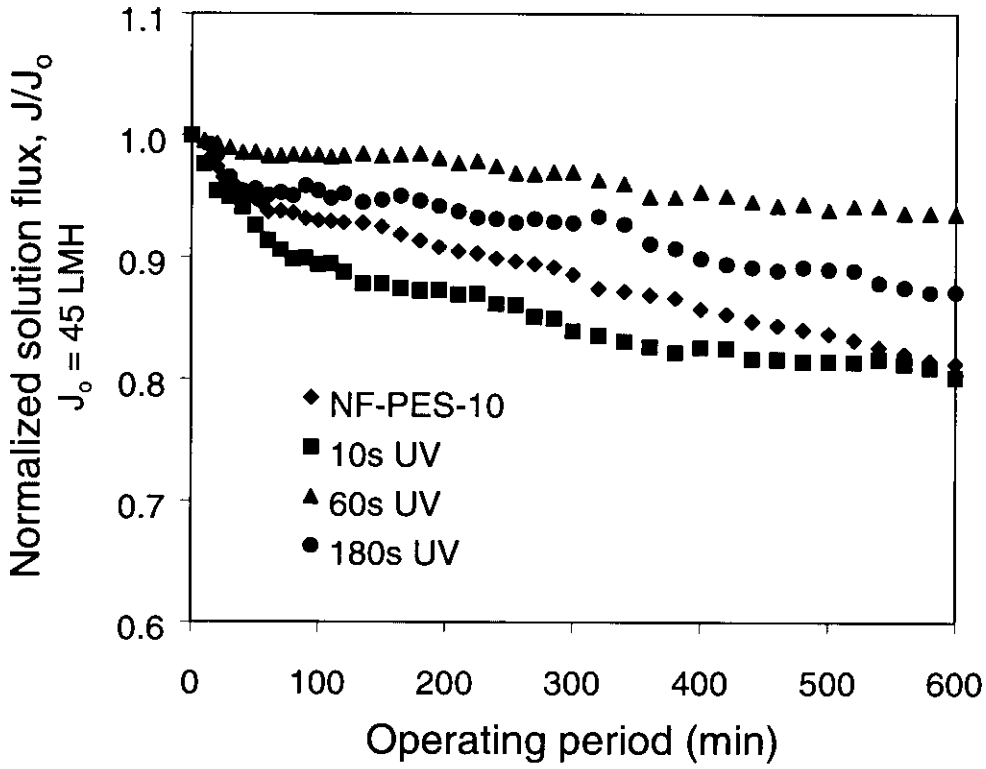

Figure 5-9. Effect of graft polymerization, using the dip method, on the performance of the of the NF-PES10 membrane flux. Reaction conditions: 3% NVP solution, dip method. As-received NF-PES-10 membrane (◆); after photooxidative treatment of the NF-PES-10 membrane with reaction times of 10 s (■), 60 s (▲), and 180 s (●). Solution conditions: Tomhannock reservoir organic matter, 10 mg/L as organic carbon, pH = 7, 10 mM NaCl; T = 20 °C

The increase in J_{om}/J_o for membranes irradiated for 60 and 180 s was not in proportion to irradiation time; the best performance was observed for the membrane irradiated for 60 s. It is possible that the enlargement of the membrane pore structure caused by long irradiation times allowed additional pore fouling by larger molecular weight natural organic matter components that were previously rejected. Under this hypothesis, the decrease in rejection of the membrane irradiated for 180 s could result in a lower fouling tendency as compared to the as-received membrane, but a higher fouling tendency as compared to the membrane irradiated for 60 s, as a result of a change in the fouling mechanism. While the rejection by the 60 s-irradiated membrane was lower than the as-received membrane, it appears possible, using shorter irradiation times, to produce membranes that have both higher J_{om}/J_o and higher rejection than the as-received membranes. The optimum range of reaction time is depicted schematically as the cross-hatched area in Figure 5-10.

Examination of the flux parameters in Table 5-2 shows that in addition to a lower fouling tendency, the graft modified membrane irradiated for 60 s was also easier to clean. Hydrodynamic cleaning alone recovered the same fraction of the initial flux (J_1/J_o = 0.976) as achieved by cleaning the as-received membrane with caustic.

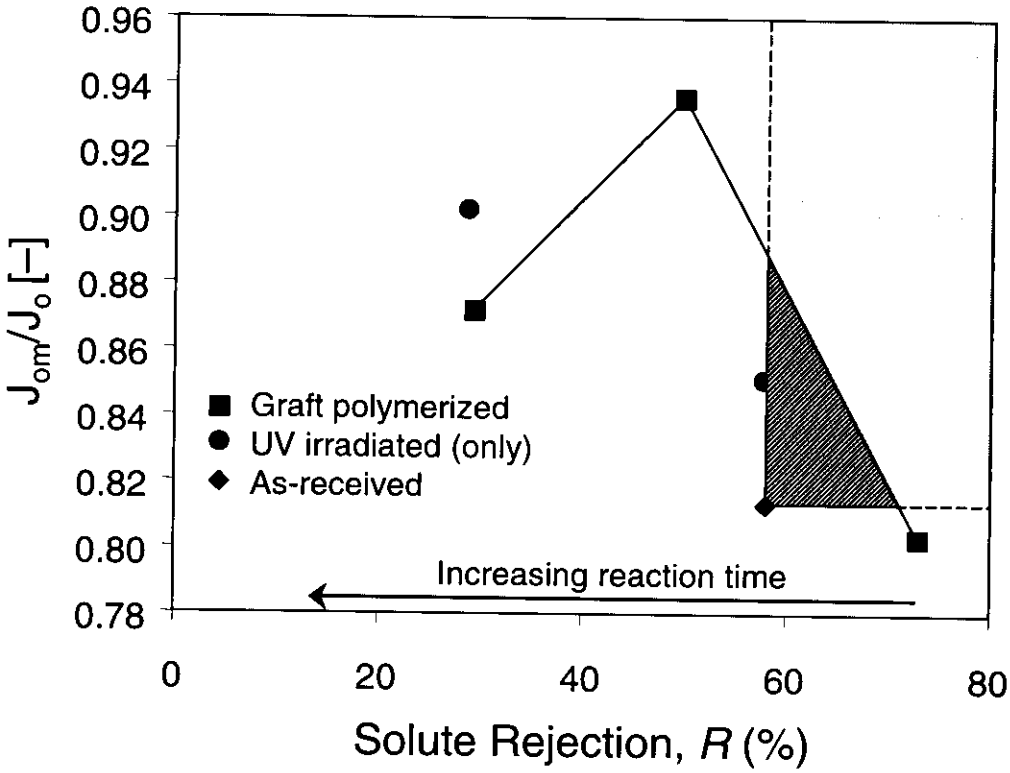

Figure 5-10. Propensity to foul (J_{om}/J_o) versus solute rejection for the as-received (◆), UV irradiated (●), and graft polymerized (using the dip modification method) (■) membranes. J_o = 45 LMH. The gray shaded area represents the locus of conditions with both improved solute rejection and resistance to fouling relative to the as-received membrane (square). The cross-hatched area within this shaded area represents the locus of conditions possible through optimization of the graft polymerization technique. For comparison, conditions achieved using UV irradiation alone are also shown.

5.4 Conclusions

Both UV irradiation and UV-assisted graft polymerization of N-vinyl-2-pyrrolidinone (NVP) can be employed to mitigate fouling by naturally occurring organic compounds (NOM) present in surface waters. Using both techniques, membrane hydrophilicity was increased, and fouling by natural organic matter was reduced significantly. However, graft polymerization was found to be superior for mitigating fouling (higher J_{om}/J_o), maintaining flux, and minimizing loss of rejection. Under the conditions studied here, using the dip technique and an irradiation time between 10 and 60 s, the UV-assisted graft polymerization appears promising as a strategy to significantly reduce fouling by NOM, while maintaining clean water permeability and solute rejection similar to as-received membranes (Figure 5-10). Irradiation conditions that are too long result in unacceptably large reductions in solute rejection, and do not improve resistance to fouling, possibly due to exacerbated pore fouling.

6.0 Effects of Organic Matter Characteristics on Flux Decline

6.1 Introduction

Membrane fouling, which can include concentration polarization, reversible and irreversible solute accumulation (cake formation), pore blockage, and pore constriction, causes significant reductions in solution flux over time as resistance to flow increases. Membrane fouling can be influenced by membrane characteristics (pore size, permeability, charge, surface roughness, and surface energy). Most work has focused on the effects of surface energy, often characterized in terms of hydrophobicity. There is a general consensus that hydrophobic membranes foul to a greater extent than hydrophilic ones. For example, Jucker and Clark (1994) found preferential adsorption of hydrophobic compounds onto hydrophobic polysulfone UF membranes.

Feed solution chemistry (pH, ionic strength, and calcium concentration) can affect NOM configuration, electrostatic interactions between NOM molecules, and interactions between NOM and the membrane surface. Hong and Elimelech (1997), using commercial humic acid and Suwannee fulvic acid, indicated that membrane fouling increased with increasing electrolyte (NaCl) concentration and addition of divalent cation (Ca^{2+}). They explained this effect in terms of interactions between calcium and humic carboxyl functional groups, resulting a reduction of NOM charge and electrostatic repulsion between humic macromolecules.

Operating parameters such as initial flux rate, crossflow velocity, recovery, and the mass transfer characteristics of the fluid boundary layer, can also impact fouling. For example, Hong and Elimelech (1997) found that increased initial flux rates caused more membrane fouling. Increased crossflow velocity can result in decreased membrane fouling due to the disruption of cake layer formation on the membrane (Braghetta et al., 1997; Connell et al., 1999).

In this research, we have focused on the effects of NOM composition on membrane fouling. One way to characterize NOM composition is to separate it into hydrophilic and hydrophobic fractions based on preferential adsorption to synthetic resins as discussed in Chapter 4. Cho et al. (1999) demonstrated the NOM aromaticity and membrane hydrophobicity significantly influenced the permeate flux decline of high flux UF membrane. It is possible for hydrophobic effects to dominate over electrostatic repulsion to cause fouling of hydrophobic membranes (Manttari et al., 2000). Nilson and DiGiano (1996 found a greater degree of fouling caused by hydrophobic NOM fractions as compared to hydrophilic fractions. However, there are also examples of research that have found otherwise. Lin et al. (2000) showed that a hydrophilic NOM fraction, both before and after treatment by powdered activated carbon, exhibited faster permeate flux decline than a hydrophobic fraction. Braghetta et al. (1998) reported that the effect of NOM hydrophobicity on membrane fouling was in the order: hydrophobic fraction < hydrophilic fraction < unfractionated fraction. Cho et al. (2000b) found that larger hydrophilic NOM fractions lead to a significant reduction in long-term flux while DOC

rejection was controlled primarily by size exclusion, electrostatic repulsion, and aromaticity /hydrophobicity interactions between NOM and the membrane surface and pores.

Molecular weight appears to be a significant NOM property related to fouling. Nilson and DiGiano (1996) indicated that the membrane fouling was significantly caused by large NOM molecular weight, but as the hydrophobic fraction was also the higher molecular weight fraction, it is difficult to separate these effects. Lin et al. (2000) confirmed that the worst membrane fouling was caused by NOM having the largest molecular weights. One reason molecular weight can have an impact is related to rejection; small molecular weight components can more readily pass through the membrane, providing less mass to build a cake layer (Nilson and DiGiano, 1996; Lin et al., 2000).

The objectives of this study are to better understand the effect of NF membrane characteristics (membrane pore size), NOM properties (NOM composition and molecular weight) on permeate flux decline. The RO-concentrated NOM solutions were initially fractionated by adsorption to XAD8 resin (to yield hydrophobic and hydrophilic fractions) and by ultrafiltration (to yield several molecular weight fractions). Fouling experiments were conducted using a crossflow bench-scale test cell under controlled crossflow velocity similar to the full-scale operation. Membrane performance parameters included permeate flux decline and rejection observed during filtration experiments. Feed solution chemistry was also investigated to probe the interaction between NOM composition and solution ionic strength. The hydraulic resistances-in-series model was used to help interpret filtration data. Moreover, the water flux recovery was used to distinguish between reversible and irreversible fouling after hydrodynamic and chemical cleaning, respectively.

6.2. Materials and Methods

6.2.1 Source Waters

Three different water sources were employed in these experiments, Tomhannock (TMK) reservoir, NY; Intercoastal Waterway Myrtle beach (MB), SC; and Edisto River Charleston (CT), SC. The characteristics of these waters are shown in Table 2-2 (Chapter 2). Tomhannock (TMK) NOM has a lowest DOC concentration of 2.99 mg/L and UV (254 nm) of 0.074 cm^{-1}, corresponding to a 2.5 L/mg-m of SUVA. Myrtle Beach (MB) NOM contains a highest DOC concentration of 23.8 mg/L and UV_{254} of 1.06 cm^{-1} with a 4.5 L/mg-m of SUVA. The DOC concentration and UV_{254} of Charleston (CT) NOM are found between TMK- and MB-NOM solution but it has a highest SUVA of 4.7 L/mg-m. SUVA has been correlated with aromaticity, and for surface waters, molecular weight. These natural water sources were isolated with a field reverse osmosis (RO) system, as described in Chapter 2. Concentrated NOM solutions were also fractionated by ultrafiltration as described in Chapter 3, and were fractionated using acrylic ester resins as described in Chapter 4.

6.2.2 Fractionation by Polarity

As discussed in Chapter 4, concentrated NOM solutions of three different source waters were fractionated with XAD8 resin to yield hydrophobic and hydrophilic fraction. Figure 4-1 shows the percent organic carbon in the hydrophobic fraction of each water. It was found that the TMK-NOM water, having lowest SUVA, contained the largest hydrophilic fraction (about 63.6%) and lowest hydrophobic fraction (about 36.4%). As shown in Figure 3-7, the TMK water also had the largest fraction of organic carbon in the <3 kDa size range. The MB and CT waters were more hydrophobic, containing 65.9 and 60.8% carbon in that fraction, respectively. In addition, they also contained larger molecular weight components.

6.2.3 Molecular Weight Fractionation

Concentrated NOM solution was fractionated with ultrafiltration (UF) membrane to yield several molecular weight fractions. Figure 3.7 presents the molecular weight fraction for three different natural sources. The TMK-NOM water had the largest <1 kDa fraction, about 51.7%, and the largest 1 to 3 kDa fraction, about 34.5%. The fraction of organic carbon in the larger size fractions is correspondingly lower (the 3-5K and >5K contain only 3.2% and 10.6%, respectively). Still, the MB and CT waters had a sizeable fraction of their organic carbon in the small molecular weight range. The MB water had 44.2% in the <1 kDa fraction and 13.5% in the 1 to 3 kDa fraction, with 42.3% of the carbon greater than 3 kDa. Similarly, the CT water had had 35.9% in the <1 kDa fraction and 29.4% in the 1 to 3 kDa fraction, with 37.4% of the carbon greater than 3 kDa.

6.2.4 NF Membranes

As discussed in Chapter 6, three nanofiltration membranes were used in this study for the crossflow filtration experiments: (1) an aromatic polyamide thin-film composite (NF-70 membrane, Dow-FilmTec.); (2) a sulfonated polyethersulfone (NTR7450 membrane, Nitto Denko America, Inc., Roll 8011501); (3) a hydrophilic polyethersulfone (NF-PES-10, Hoechst AG/Celgard, Lot 548, Roll 6).

The thin-film composite NF-70 membrane has an isoelectric point at pH 4 (Childress and Elimelech, 1996), a molecular weight cut off (MWCO) of about 200 Da (Fu et al., 1995), and contact angle of 28.4°. The clean water permeability (L_p) of this membrane is approximately 0.118 L/m^2/h/kPa (LMH/kPa) at 23 °C. The salt (NaCl) rejection is about 70% (Petersen, 1993) and the magnesium sulfate rejection is 95%, as reported by the manufacturer (conditions: 2000 mg/L $MgSO_4$, 70 psi (483 kPa), and 25 °C).

The as-received NTR7450 membrane has a molecular weight cut-off between 500 and 1000 Da (Fu et al., 1995; Manttari et al., 2000). It has a contact angle about 28.6, and a salt rejection of 51% (conditions: 5000 mg/L NaCl, 147 psi (1013 kPa), and 25 °C)

(Nystrom et al., 1995; Petersen, 1993). This membrane has a clean water permeability of 0.097 LMH/kPa at 23 °C.

The as-received NF-PES-10 membrane has a contact angle of 39.6°. According to the manufacturer, salt rejection was about 10-20% (conditions: 5000 mg/L NaCl, 580 psi (4000 kPa), and 20 °C). The clean water permeability is approximately 0.124 LMH/kPa at 23 °C. Based on MWCO and salt rejection, the tightest membrane were: NF-70 > NTR7450 > NF-PES-10. These membranes were stored as flat sheets in 1% sodium *meta*-bisulfite ($Na_2S_2O_5$) to prevent microbial activity and refrigerated at 4 °C.

6.2.5 Crossflow Bench-Scale Test Cell and Test Conditions

A schematic diagram of the crossflow bench-scale test cell with recycle loop is shown in Figure 5-2. During filtration, permeate and concentrate flow were directly measured using an analytical balance (S-110, Denver Instrument Co.) and intermittently sampled for DOC, UV absorbance at 254 nm, and conductivity analysis.

Membrane sheets were rinsed with filtered (0.2 μm) DI water and then transferred to the bench scale test cell. Filtered DI water was subsequently rinsed in the system and operated for membrane compaction. After membrane compaction, water flux was then determined with the function of transmembrane pressure ranging from 30 to 70 psi (207 to 483 kPa). Feed NOM solution was pumped through the system with adjusting initial solution flux of 45 LMH. Transmembrane pressure was kept constant during filtration.

After a filtration run, hydrodynamic cleaning was done by recirculating filtered DI water for 30 minutes. The crossflow velocity was adjusted to about 0.25 m/s, a factor of 2.5 times higher than the velocity during filtration. After this cleaning, clean water flux was determined as a function of operating pressure to determine water flux recovery. A chemical cleaning was subsequently employed by using filtered DI water adjusted to pH 10 (using NaOH) and followed with a solution adjusted to pH 3 (using HCl) at a crossflow velocity of 0.25 m/s for 30-min each. Water flux was determined after the chemical cleaning.

For all fouling experiments, the recovery, which is defined as ratio of permeate to feed flow, was adjusted to 85%, crossflow velocity of 0.1 m/s (similar to that of full-scale membrane (Allgeier and Summers, 1995)), corresponding to a flowrate of 530 mL/min in the recycle loop. The Reynolds number was approximately 104. Inlet temperature was about 23 °C. For most fouling experiments, the feed NOM solution contained 10 mg/L DOC, and had an ionic strength of 0.01 M NaCl, which corresponded to a conductivity of 1070 μS/cm at 25 °C (analyzed by advanced portable AP50, Denver Instrument Co.). All experiments were conducted at pH 7 (adjusted by NaOH or HCl). The effect of ionic strength on the permeate flux decline was studied by varying NaCl concentration (0.01 M and 0.05 M).

6.2.6 Membrane Performance Evaluation

Membrane performance parameters include permeate flux decline as a function of time, rejection, and water flux recovery after hydrodynamic and chemical cleaning (further characterized by membrane hydraulic resistances-in-series model). Equations (31) and (32) define the feed rejection (R_{feed}) and bulk rejection (R_{bulk}), respectively.

$$R_{feed} = \frac{C_{feed} - C_{perm}}{C_{feed}} \qquad (31)$$

$$R_{bulk} = \frac{C_{bulk} - C_{perm}}{C_{bulk}} \qquad (32)$$

where, C_{feed} is the DOC concentration in the sample reservoir (mg/L), C_{perm} is the permeate DOC concentration passing through the membrane (mg/L), and C_{bulk} is the bulk DOC concentration accumulating on the membrane surface (mg/L), sampled from the retentate line.

A membrane resistances-in-series model was used to quantify solution flux decline. Figure 5-4 illustrates the schematic of filtration protocol used to determine hydraulic resistances-in-series. The membrane resistance can be found from the clean-water flux (after membrane compaction) using the following form of Eq. 6:

$$J_o = \frac{\Delta P}{\mu R_m} \qquad (33)$$

where J_o is the initial solution flux (45 LMH), ΔP is the transmembrane pressure (kPa), μ is viscosity (kg/m.s), and R_m is the clean membrane hydraulic resistance (m^{-1}). The solution flux after fouling has occurred can be expressed as:

$$J_v = \frac{\Delta P}{\mu (R_T)} = \frac{\Delta P}{\mu (R_m + R_f)} = \frac{\Delta P}{\mu (R_m + R_{c1} + R_{c2} + R_{irr})} \qquad (34)$$

where J_v is the solution flux (m/s or LMH), R_T is the total hydraulic resistance after filtration (m^{-1}), determined from $J_o - J_{om}$; and R_f accounts for concentration polarization and NOM fouling. R_f can be written as the sum of a labile cake and polarization resistance ($R_{c,1}$) recoverable by hydrodynamic cleaning (m^{-1}), determined from $J_1 - J_{om}$; an adsorbed NOM layer resistance, recoverable by chemical cleaning ($R_{c,2}$), determined from $J_2 - J_1$; and an "irreversible" (non-recoverable) resistance (R_{irr}) that remains after hydrodynamic and chemical cleaning, determined from $J_o - J_2$.

6.2.7 Membrane Cleaning

After a solution filtration run, the membrane was cleaned in two steps; first, a hydrodynamic cleaning was performed, followed by chemical cleaning. The mass recovered from each step was measured to determine the total mass of NOM deposited, the NOM recovered by cleaning, and the mass remaining on the membrane as

"irreversibly bound" foulant. Before hydrodynamic cleaning, 200-mL (3 times the total beach scale system volume of 70 mL) of filtered DI (passing a 0.2 μm hydrophilic membrane) was used to flush the concentrate volume from the recycle loop; the mass of NOM flushed is $V_{sys}C_{reten,f}$. Then, 800-mL of filtered DI was recirculated in the system at high velocity, 2.5 times higher than the velocity of operation (i.e., 0.25 m/s). The recirculation was maintained for 30 minutes to complete the hydrodynamic cleaning. Finally, 200 ml of filtered DI was flushed through the system. The total volume was measured gravimetrically, and the organic carbon concentration was measured to estimate NOM recovery. The overall mass of the hydrodynamically labile "cake" was determined as $M_{d,1}$. Filtered DI water was then used to determine water flux after hydrodynamic cleaning.

For chemical cleaning, filtered DI with pH adjusted to 10 (using NaOH) was used first; 800 mL of this solution was recirculated at a crossflow velocity of 0.25 m/s for 30-min. The total volume of this solution was then drained, and its TOC concentration was measured. Then, 800-mL of filtered water with pH adjusted to pH 3 (using HCl) was recirculated at a crossflow velocity of 0.25 m/s for 30-min. Finally, 200 ml of filtered DI was flushed through the system and collected for organic carbon analysis. The total mass NOM recovered from chemical cleaning was determined as $M_{d,2}$. Filtered DI water was then used to determine water flux after chemical cleaning.

The mass of NOM remaining on the membrane after hydrodynamic and chemical cleaning, $M_{d,3}$, was determined by mass balance. The total mass fed to the system over the duration if the run, t_f, is equated to the retentate bled off during the run, the organic carbon in the permeate, the organic carbon remaining in the system volume at the conclusion of the run, the mass of NOM recovered by hydrodynamic and chemical cleaning, and the NOM irreversibly bound:

$$\int_0^{t_f} Q_{feed}(t)C_{feed}dt = \int_0^{t_f} Q_{reten}(t)C_{reten}dt + \int_0^{t_f} Q_{perm}(t)C_{perm}dt + V_{sys}C_{reten,f} + \sum_{i=1}^{3} M_{d,i} \quad (35)$$

where C_{feed} is the feed DOC concentration, C_{reten} is the retentate DOC concentration, $C_{reten,}$ is the retentate DOC concentration, at the end of the run; C_{perm} is the DOC concentration in the permeate; V_{sys} is the bench scale system holdup volume, about 70 ml. In practice, the integrals were evaluated as discrete summations, and the individual masses were computed from the final volume and concentration of the total volume of solution and flush, as discussed above.

6.3 Results and Discussion

6.3.1 Effects of NOM concentration

NOM concentration was varied to determine its effect on membrane fouling and solution flux decline. Tomhannock RO concentrate was diluted to yield feed NOM concentrations of 0, 5, 10, and 25 mg DOC/L. Figure 6-1 shows the effect of NOM

concentration on normalized solution flux decline, and Table 6-1 summarizes relevant parameters. Significant concentration polarization caused by salt (0.01-M NaCl) was observed in the NOM-free solution; this provides a baseline for assessing the effects of natural organic matter. With a low NOM concentration, the initial flux decline is similar to the NOM-free solution, but the solution flux curves diverge significantly after about 200 minutes of filtration. The 10-mg/L NOM solution exhibits a flux decline significantly greater than the 5 mg/L solution, but markedly less than the 25 mg/L solution. Solution flux was sharply reduced for the highest DOC concentration, suggesting a possible shift in the fouling mechanism.

The lowest normalized solution flux was observed during filtration of the solution having the highest NOM concentration; however, the mean DOC rejection was not significantly different from 10-mg/L NOM. However, the rejection of feed DOC during filtration of the 5-mg/L NOM solution was significantly lower than that observed during filtration of the more concentrated 10- and 25-mg/L solutions. Statistical significance was assessed using single-factor ANOVA ($F = 13.79 > F_{0.05, 2,17} = 3.59$) at a 95% confidence interval. This is evidence that the fouling layer of NOM increases with increased concentration, as expected, and that increased NOM rejection is observed as a result.

As shown by the data in Table 6-1, the DOC concentration has an effect on the rejection of NaCl by the NF-70 membrane. As the NOM concentration increases, the rejection of salt increases significantly, to a greater extent than NOM rejection increases. The possibility that NOM is forming a secondary membrane that rejects salt must be considered; it seems most likely that the mechanism of rejection by this secondary membrane is mostly due to charge exclusion between acidic moieties on the NOM molecules that have accumulated on, or adsorbed to, the membrane. Salt rejection reaches a maximum during filtration of the 10 mg/L NOM solution; it is lower for both higher and lower NOM concentrations. A less dense cake layer formed may explain the lower salt rejection at low NOM concentrations, or lower density of charged functional groups in the vicinity of the membrane surface. The lower rejection at high NOM concentrations suggests that charged moieties on the NOM molecules are being more effectively screened. This suggests that the conformation of the NOM at the surface has changed, perhaps due to a coiling or coagulation mechanism. The existence of a denser cake layer would also explain the more rapid decrease in solution flux observed during the run with the highest NOM concentration.

Table 6-1. Effect of NOM Concentration on Normalized Solution Flux and Feed Rejection

Concentration	J_{om}/J_o at t = 10 h	Rejection, %		
		DOC	UV	Conductivity
0 mg/L	0.744	-	-	52.2 - 61.6
5 mg/L	0.683	96.4 - 97.5	95.6 - 97.0	63.8 - 72.6
10 mg/L	0.646	97.7 - 98.4	97.8 - 98.2	70.9 - 79.5
25 mg/L	0.351	97.4 - 97.9	95.0 - 97.1	61.9 - 75.8

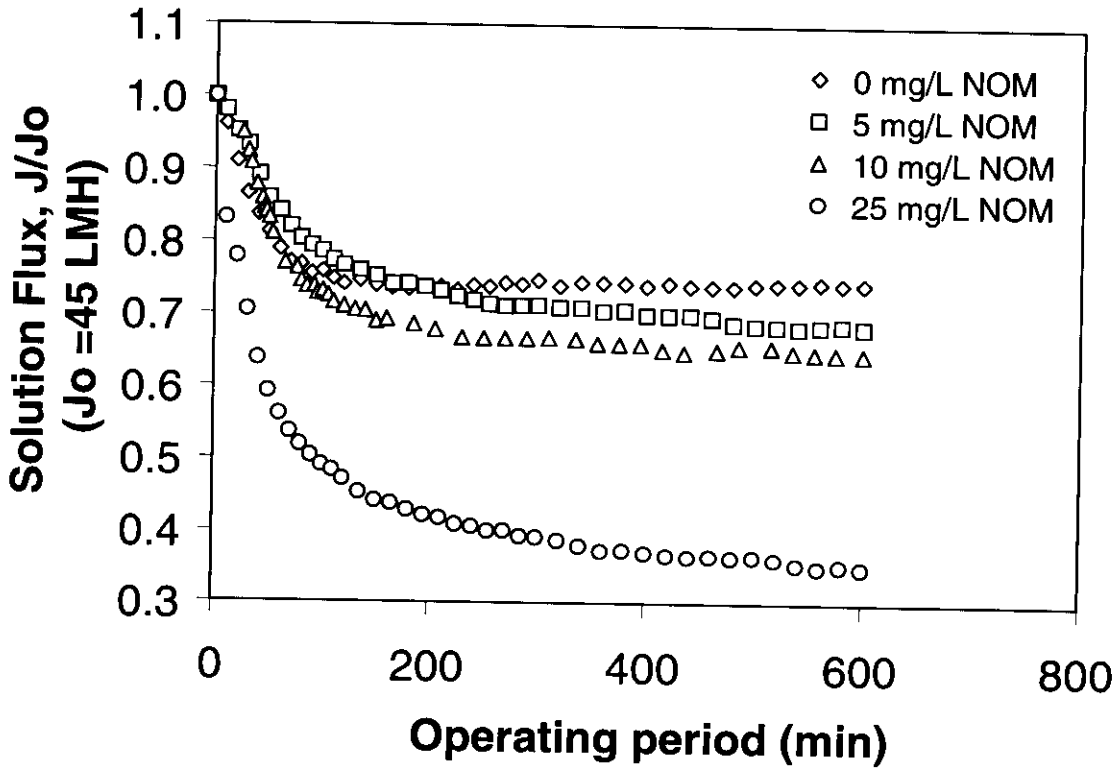

Figure 6-1. Effect of NOM concentration on normalized solution flux; pH = 7, I.S. = 0.01 M, 10 mg/L TMK NOM , T = 23 °C, r = 0.85.

6.3.1.1 DOC Accumulation

The DOC concentration in the retentate was measured during membrane operation. Because the membrane rejects NOM, DOC in the retentate stream increases, and this increase can be predicted by employing a mass balance model for the system. The bench scale system can be modeled as a completely mixed flow reactor, because the recycle ratio was high ($Q_{recycle}/Q_{feed} > 40$). A simple balance of mass input and output from the system yields:

$$V_{sys}\frac{dC_{reten}}{dt} = Q_{feed}C_{feed} - Q_{reten}C_{reten} - Q_{perm}C_{perm} - k_a C_{reten}V_{sys} \qquad (36)$$

where, C_{reten} = DOC concentration in the concentrate stream (mg/L); C_{feed} = DOC concentration in the feed stream (mg/L); C_{perm} = DOC permeate in the permeate stream (mg/L) = $(1-R)C_r$; Q_r = flow of the retentate stream (L/min); Q_{feed} = flow of the feed stream (L/min); Q_{perm} = flow of the permeate feed stream, $J_v A_m$ (L/min). This model takes into account loss of mass from the liquid phase to the membrane surface (or cake layer) as a result of fouling through the sink term, $-k_a C_r V_{sys}$. The rate of fouling is approximated as a first-order process, $r = -k_a C_{reten}$, where k_a is a first-order adhesion rate constant. This is a simplified approach consistent with that used by Cohen and Probstein (1986).

The time profile of measured retentate concentration was fitted to a model based on Equation 36. Model equations were solved using a Fourth-order Runge-Kutta routine; the adhesion rate constant was determined by minimizing sum of square error (SSE). It was found that good fits to the data were not possible unless a fouling mechanism was included in the model (i.e., $k_a > 0$). The finding of a fouling rate constant greater than zero for all runs indicates significant mass accumulation to the membrane surface. When the fouling rate constant was employed as a fitting parameter, the data from filtration runs using the 5 and 10 mg/L solutions were fitted quite satisfactorily. Figure 6-2 shows the measured retentate concentration profiles, and model fits to the data; fitted rate constants are tabulated in Table 6-2.

With increasing feed NOM concentration, DOC in the retentate and permeate stream were also increased; however, the rate of retentate DOC increase for the 25 mg/L solution filtration run is slower than for the lower concentrations, suggesting a different (non-first order) adhesion mechanism. This is reflected in an adhesion rate constant that is significantly larger, by a factor of about 3.

Table 6-2. Adhesion Coefficient

NOM Concentration, mg/L	k_a (1/min)
5	0.0037
10	0.0022
25	0.0099

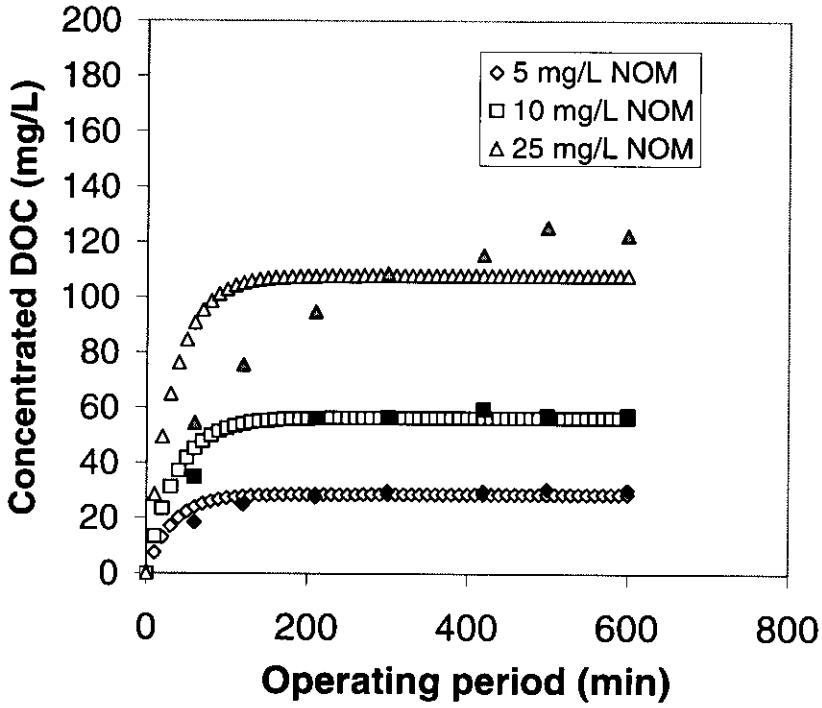

Figure 6-2. Effect of feed NOM concentration on DOC build-up on the membrane surface; pH = 7, I.S. = 0.01 M, T = 23 °C, r = 0.85.

The extent and rate of the mass of NOM accumulated on the membrane surface during a filtration run was calculated using Equation 35. Figure 6-3 illustrates how the accumulation of NOM varies with NOM feed concentration. The accumulated NOM includes the mass of the hydrodynamically labile cake, $M_{d,1}$, the mass of the NOM that can be removed by chemical cleaning, $M_{d,2}$, and the mass of NOM irreversible bound to the membrane, $M_{d,3}$. For the same cross flow velocity of 0.1 m/s, both the amount of NOM that accumulates, and the initial rate of accumulation, increases with increasing feed NOM concentration. This is consistent with a larger first-order adhesion rate constant (Figure 6-2), and a sharper rate of solution flux decline (Figure 6-1). Further experiments were conducted to elucidate the fouling mechanism by evaluating the relative magnitude of $M_{d,1}$, $M_{d,2}$, and $M_{d,3}$.

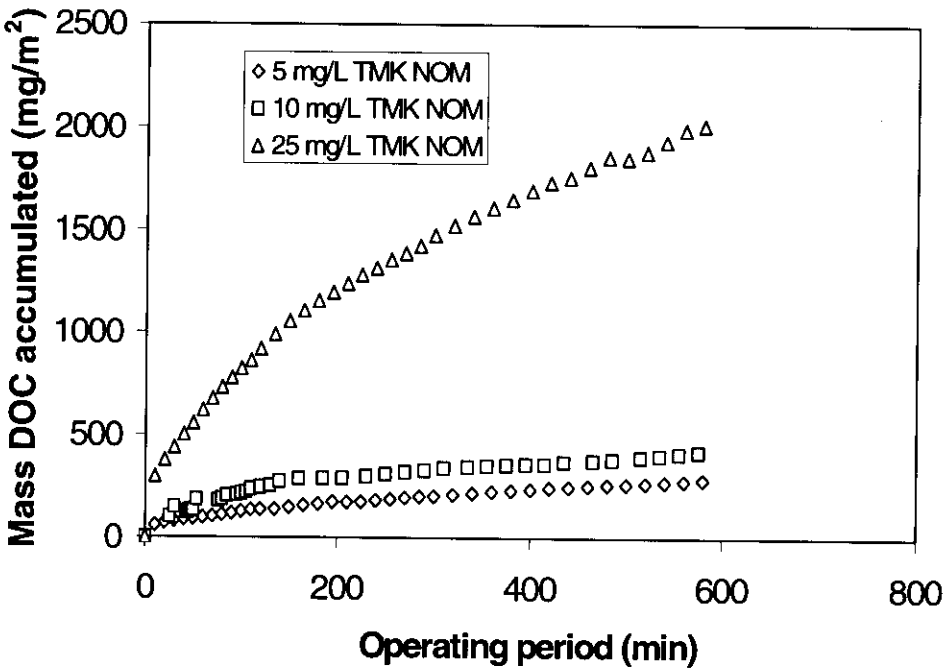

Figure 6-3. Mass DOC accumulated with function of feed NOM concentration; pH = 7, I.S. = 0.01 M, T = 23 °C, r = 0.85.

6.3.1.2 Water flux and Mass DOC recovered

Clean water flux was determined after hydrodynamic and chemical cleaning. A comparison was made between initial water flux and flux after cleaning; Figure 6-4 shows representative data for clean water flux as a function of membrane operating pressures used to determine water permeability. Generally, as shown in Figure 6-4, good correlation was found (> 0.99) and this parameter was determined with high confidence. As discussed above, at the conclusion of a 10-h run, filtered DI water was used to remove the mass of NOM cake by a 30-min hydrodynamic cleaning. This was followed by a 30-min chemical cleaning, which was subsequently used to evaluate the mass DOC left on the membrane as a result of "irreversible" fouling. Table 6-3 shows water flux recovered (J_2/J_o) as a function of different NOM concentrations, and Figure 6-5 illustrates that the trends observed are not linear, with significant deviations from linearity as the concentration is increased from 10 to 25 mg NOM/L.

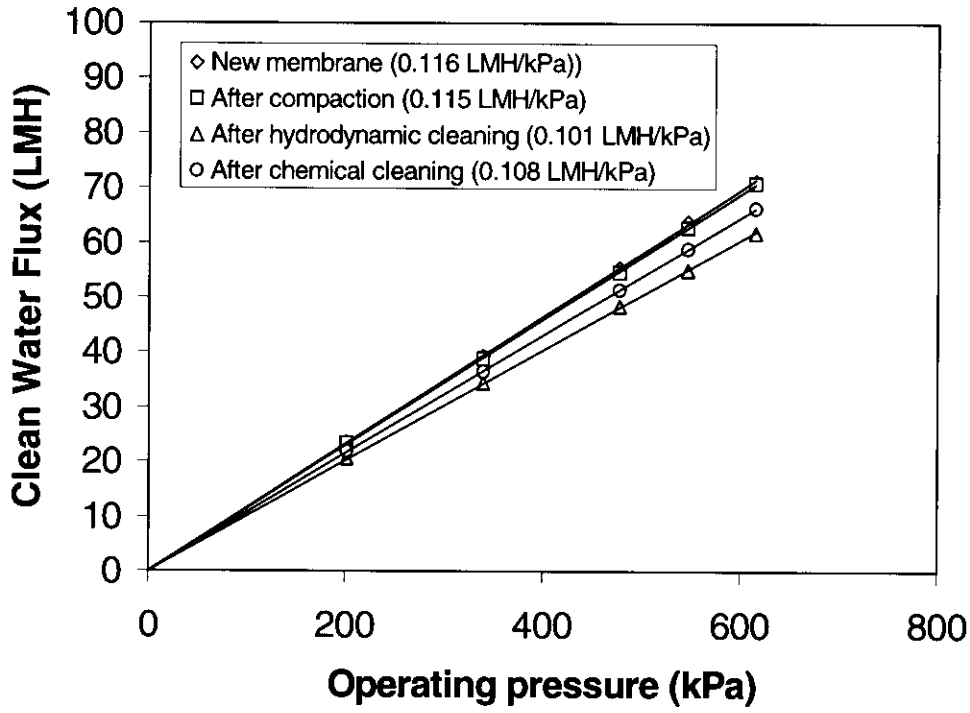

Figure 6-4. Comparison of clean water flux with membrane operating pressures; pH = 7, 10 mg/L TMK NOM, I.S. = 0.01 M, T = 23 °C, r = 0.85.

Table 6-3. Water Flux Recovered

Concentration, mg NOM/L	J_1/J_o	J_2/J_o
0	0.928	0.944
5	0.906	0.939
10	0.851	0.924
25	0.712	0.780

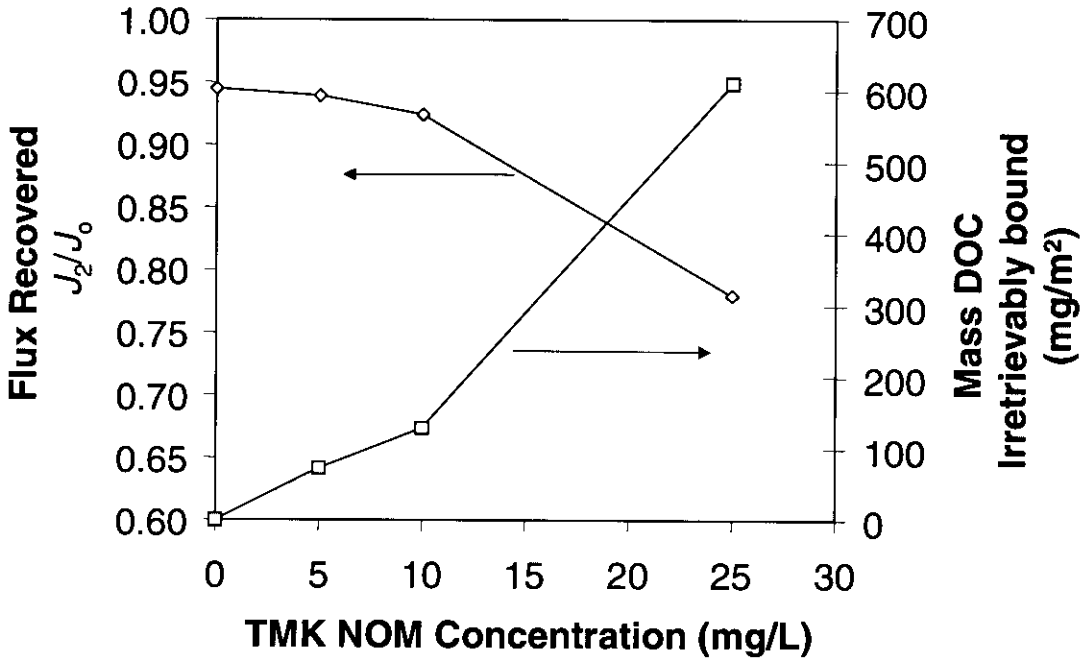

Figure 6-5. Effect of feed NOM concentration on water flux recovery and mass DOC irretrievably bound; pH = 7, I.S. = 0.01 M, T = 23 °C, r = 0.85.

Hydrodynamic cleaning was effective in recovering membrane clean water flux to 93% of its original value (after membrane compaction) when the filtration solution contained salt but no NOM. This indicates that the concentration polarization layer, caused by NaCl solution, can easily be removed from membrane surface. However, a small amount (<2%) of additional flux was recovered with chemical cleaning. When the filtration solution contained a low NOM concentration (5 mg/L), the recovery of clean water flux after hydrodynamic cleaning was comparable (within a few percent) to that observed when the filtration solution contained salt only. As in the salt-only case, further improvement was seen upon chemical cleaning (<4%). When the filtration solution contained higher concentrations of NOM, the mass accumulated on the membrane was significantly less hydrodynamically labile. In the case of the 10 mg/L NOM solution, chemical cleaning restored the membrane clean water flux to near the performance of the membrane after filtering a solution containing salt only. While after filtering the 25 mg/L NOM solution, this membrane showed the greatest degree of irreversible fouling, on the order of 22%.

As mention previously, experiments were conducted to further elucidate the fouling mechanism by evaluating the relative magnitude of $M_{d,1}$, $M_{d,2}$, and $M_{d,3}$ for different runs conducted with NOM concentrations ranging from 5 to 25 mg/L. Results of this analysis are shown in Figure 6-6.

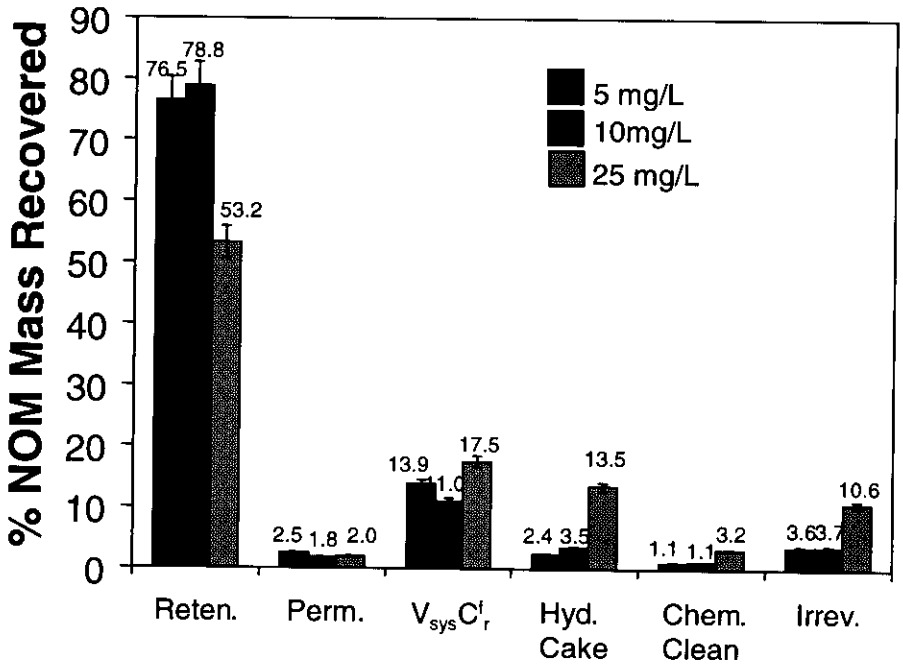

Figure 6-6. Percent of mass DOC distributed during membrane filtration and cleaning; pH = 7, I.S. = 0.01 M, T = 23 °C, r = 0.85, (Error bars indicate 5% estimated analytical error).

The mass that permeated the membrane was similar for all runs, because differences in NOM rejection were not too dramatic. The significantly lower mass present in the permeate of the 25 mg/L solution run is an artifact of the rapid flux decline during this run, and the lower retentate bleed rate required to keep the recovery constant. The mass present in the system at the conclusion of a run, $V_{sys}C^f_r$ is higher for the 25 mg/L solution, in part because of the higher feed concentration. What is most significant is the higher amount of mass found in the hydrodynamically labile cake layer, and the amount of mass irreversibly bound to the membrane. These characteristics of the high NOM concentration solution appear to contribute to the rapid solution flux decline, high fouling rate, and lower flux recovery.

6.3.2 Effects of membrane properties

The concentrated TMK-NOM solution was used to investigate the fouling of three membranes having different characteristics. Figure 6-7 shows the normalized solution flux with the three different membranes. Table 6-4 shows the normalized solution flux and rejection characteristics of the three membranes. The NF-70 membrane exhibited the most rapid solution flux decline, which is likely related primarily to its low molecular weight cut-off and corresponding high solute (both salt and NOM) rejection. Normalized solution flux is inversely related to both salt and NOM rejection. Increased salt rejection increased salt concentration polarization on the membrane surface, thus decreasing the driving force (ΔP -$\sigma\Delta\pi$) for solution flux.

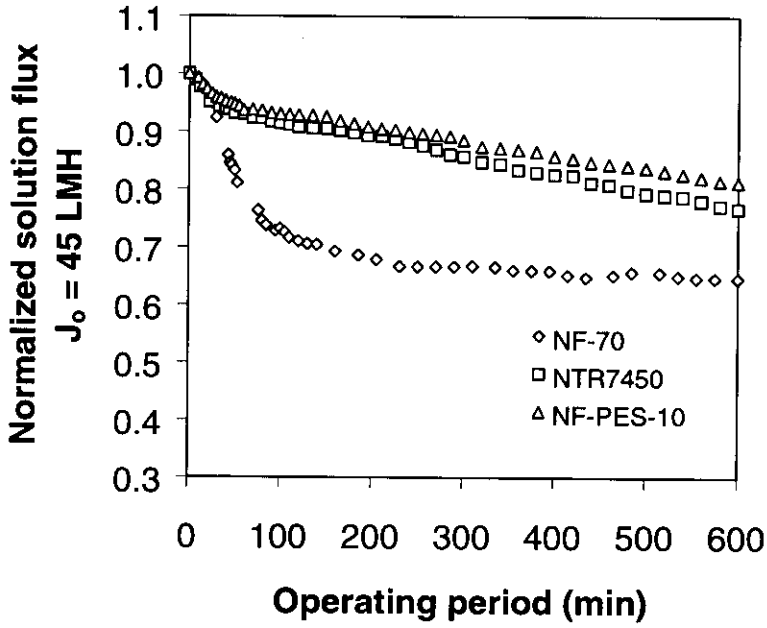

Figure 6-7. Effect of membrane type on normalized solution flux. Feed solution conditions: 10 mg/L TMK-NOM concentration, ionic strength = 0.01 M NaCl as a background, and pH 7. Experimental conditions: initial solution flux = 45 LMH, crossflow velocity = 0.1 m/s, recovery = 0.85, and temperature = 23 °C.

Table 6-4. Normalized solution flux, rejection, and conductivity

Parameter	Membrane Type		
	NF-70	NTR7450	NF-PES-10
J_{om}/J_o at 10 hour	0.646	0.767	0.813
% DOC rejection	97.7 - 98.4 (97.9)	82.2 - 84.2 (83.3)	53.6 - 63.0 (57.9)
% UV rejection	97.8 - 98.2 (97.9)	85.4 - 87.4 (86.4)	55.4 - 65.1 (60.4)
% Conductivity rejection	70.1 - 79.5 (72.7)	15.4 - 24.1 (17.0)	2.4 - 4.8 (3.7)
Conductivity (retentate) µS/cm	6458	2530	1528
Conductivity (permeate) µS/cm	327	1028	1201

Feed solution conditions: 10 mg/L TMK-NOM concentration, ionic strength of 0.01 M as NaCl (1070 µS/cm at 25 °C), and pH 7. Experimental conditions: initial solution flux = 45 LMH, crossflow velocity = 0.1 m/s, recovery = 0.85, temperature = 23 °C. The average values are presented in the parenthesis, N = 7.

Figure 6-8 shows the DOC concentration in the retentate and permeate line. Solid lines are model fits using the mass balance model. Reasonably good fits to the experimental data were obtained after incorporating the fouling term (NOM adhesion/adsorption). Due to a high DOC rejection (97.9%), the system employing the NF-70 membrane had the highest DOC concentration in the retentate line. The adhesion rate constants for the NF-70, NTR7450, and NF-PES-10 membrane were 0.0022, 0.0044, and 0.0055 min^{-1}, respectively. It is interesting that the adhesion rates of the NF-PES-10 and NTR7450 membranes were higher than that of the NF-70 membrane, despite the lower rate of flux decline for those membranes. The higher adhesion coefficients are consistent with both 1) higher contact angle (lower wettability) and 2) membrane openness.

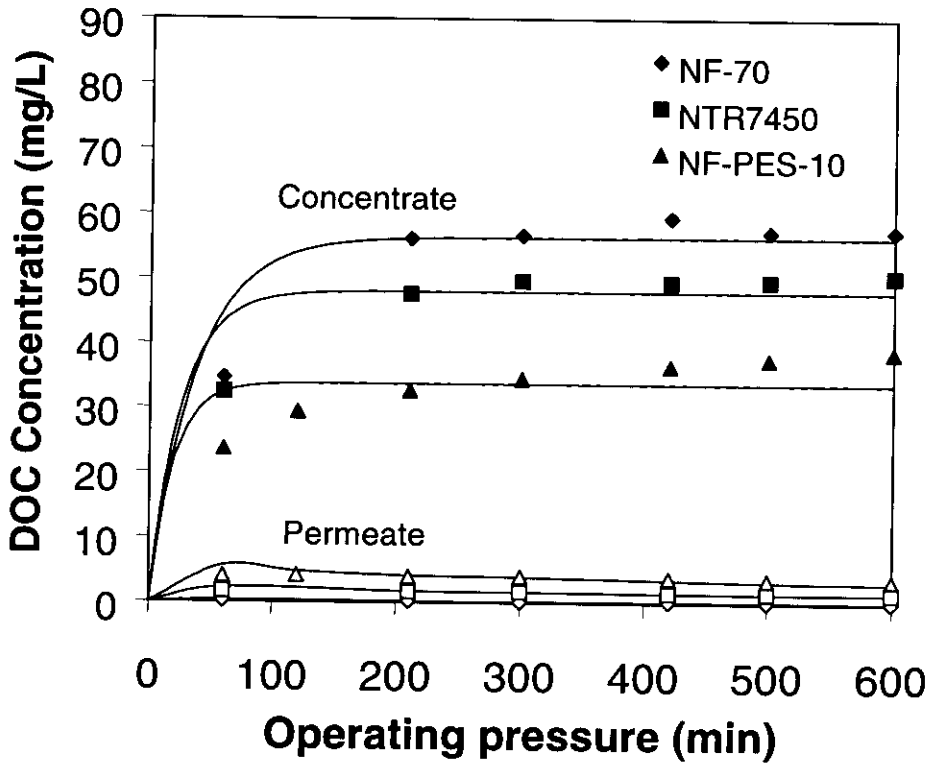

Figure 6-8. Concentrate and permeate DOC accumulation as a function of different membrane characteristics. Feed solution conditions: 10 mg/L TMK-NOM concentration, ionic strength = 0.01 M NaCl as a background, and pH 7. Experimental conditions: initial solution flux = 45 LMH, crossflow velocity = 0.1 m/s, recovery = 0.85, and temperature = 23 °C. Lines represent mass balance model.

The contact angle (air/water) of the NF-70, NTR7450, and NF-PES-10 membrane were measured as 28.4, 28.6, and 39.6 degrees, respectively. The greater adhesion coefficient for the less-wettable NF-PES-10 membrane is consistent with the findings of Jucker and Clark (1994) [20], who observed that NOM absorbed more favorably onto

hydrophobic membranes. The lower solute rejection exhibited by the NF-PES-10 and NTR7450 membranes is evidence of a more open membrane structure; it seems likely that NOM could adsorb into membrane pores, in addition to the membrane surface. This would represent an additional fouling mechanism not present for the NF-70 membrane. It was found that water flux recovery (J_2 / J_o) of the NF-70, NTR7450, and NF-PES-10 membrane were 92.6%, 82.2%, and 82.7%, respectively. The higher irreversible fouling (after hydrodynamic and chemical cleaning) for the more open membranes suggests that it is more difficult to remove adsorbed NOM from membrane pores

6.3.3 Solution flux and rejection

Effects of NOM composition on solution flux were investigated using unfractionated NOM, hydrophobic fractions, and hydrophilic fractions for three different water sources. Figure 6-9 illustrates the effect of TMK-NOM composition on normalized solution flux. The effect of composition appears to depend strongly on solution ionic strength. At high ionic strength (0.05 M), fouling was most severe for the hydrophobic TMK fraction as compared to the hydrophilic TMK fraction.

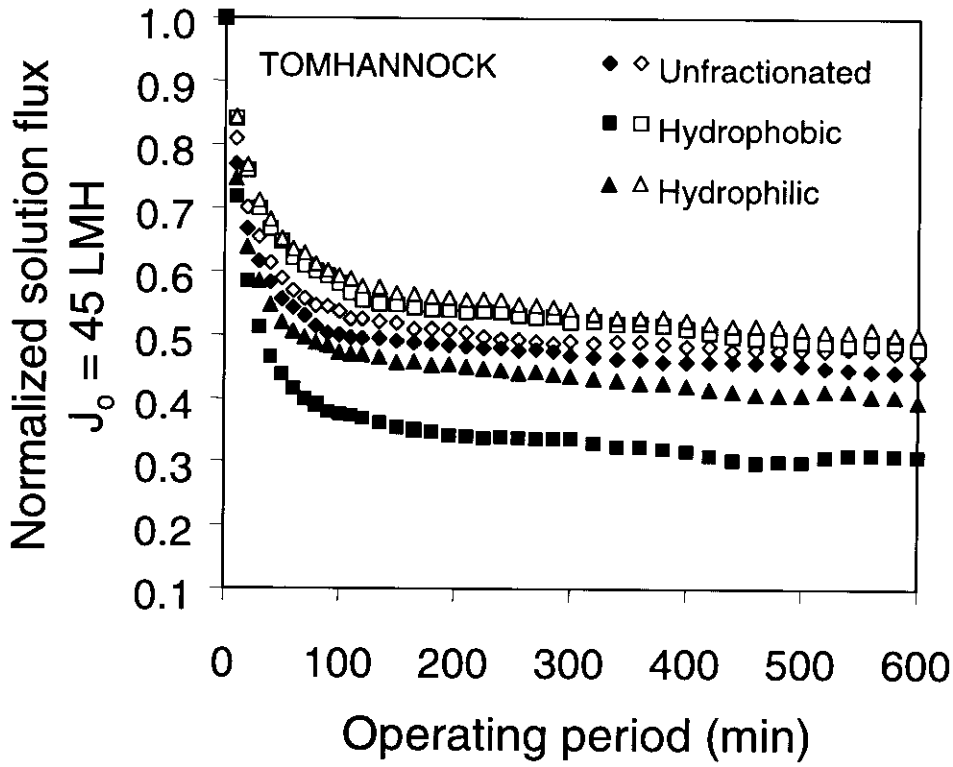

Figure 6-9. Effect of TMK-NOM composition on normalized solution flux. NF-70 membrane. Filled data points: 10 mg/L NOM, I.S. = 0.05 M; open data points: 12 mg/L NOM, 0.018 M. NaCl, and pH 7. Experimental conditions: initial solution flux = 45 LMH, crossflow velocity = 0.1 m/s, recovery = 0.85, and temperature = 23 °C.

A similar result was observed by Nilson and DiGiano (1996). Their feed NOM solutions contained about 11.7-mg/L NOM, an ionic strength of 0.051 M, and a pH of 7. In addition, the permeate flux decline of unfractionated TMK-NOM solution was less severe than either of the fractions. This is consistent with previous studies (Nilson and DiGiano, 1996; Lin et al., 2000). In contrast to these results, at a lower ionic strength (0.018 M NaCl), the permeate flux decline of the unfractionated NOM was more severe than either the hydrophobic or hydrophilic fractions, which were similar. This result is consistent with a previous study by Braghetta et al. (1998); their feed NOM solution contained a 6-mg/L NOM, ionic strength of 0.016 M and pH 7.

Table 6-5 shows the rejection of TMK-NOM fractions at two different ionic strengths. At both ionic strengths, the rejection of the hydrophilic NOM was lower than either the hydrophobic fraction or the unfractionated water, consistent with a lower molecular weight of this fraction. A lower DOC rejection of hydrophilic fraction was also observed by Lin et al., 2000. Their experiments contained feed solution of 5 mg/L-NOM solution, ionic strength about 0.014 M (~ 1500 µS/cm), and pH 7. However, the severity of fouling does not appear to correlate with NOM rejection, because at low ionic strength, the fouling tendencies of the hydrophilic and hydrophobic fractions are similar, but the rejection of the hydrophobic fraction is greater. Furthermore, at high ionic strength, the unfractionated NOM has the highest rejection but the lowest fouling tendency. The extent of fouling does not correlate with rejection of salt, either.

Table 6-5. Effect of Ionic Strength and Composition on Rejection of TMK NOM

	I.S. = 0.018 M NaCl, 12 mg/L DOC			
Sources	J/J_o at t = 10 hr	% DOC	% UV	% Conductivity
Unfractionated	0.469	92.5 – 94.2 (93.1)	92.5 – 93.8 (92.9)	42.4 – 54.4 (45.6)
Hydrophobic	0.481	94.6 – 95.4 (95.1)	94.3 – 94.7 (94.5)	43.1 – 51.9 (45.6)
Hydrophilic	0.503	90.1 – 91.8 (90.8)	91.1 – 91.7 (91.4)	44.6 – 51.5 (45.8)
	I.S. = 0.05 M NaCl, 10 mg/L DOC			
Unfractionated	0.443	95.7 - 96.9 (96.1)	91.3 - 93.4 (92.1)	33.4 - 38.6 (35.5)
Hydrophobic	0.308	90.5 - 91.9 (91.3)	88.4 – 90.8 (89.1)	30.4 – 41.0 (33.3)
Hydrophilic	0.395	90.9 - 91.9 (91.3)	87.5 – 90.5 (88.7)	29.9 – 35.6 (31.6)

NF-70 membrane; Feed solution conditions: pH 7. Experimental conditions: initial solution flux = 45 LMH, crossflow velocity = 0.1 m/s, recovery = 0.85, temperature = 23 °C. The average values are presented in the parenthesis, N = 7.

Figure 6-10 shows the normalized solution flux of the MB-NOM fractions. At low ionic strength of 0.01 M, the hydrophilic MB fraction caused more membrane fouling than the unfractionated and hydrophobic MB-NOM solutions. This is consistent

with the results of Lin et al., 2000 but different from the trends observed for the TMK water. The water flux recovery of hydrophilic MB fraction was only 69% (data not shown), significantly lower than the unfractionated MB-NOM solution and the hydrophobic MB faction (both greater than 92%). Moreover, the water flux recovery after hydrodynamic cleaning was not significantly different from that after chemical cleaning. This suggests that the hydrophilic MB fraction caused a pore plugging, thus increased irreversible fouling of the membrane surface. However, at high ionic strength of 0.05 M NaCl, the hydrophobic MB fraction showed a more significant effect on solution flux decline.

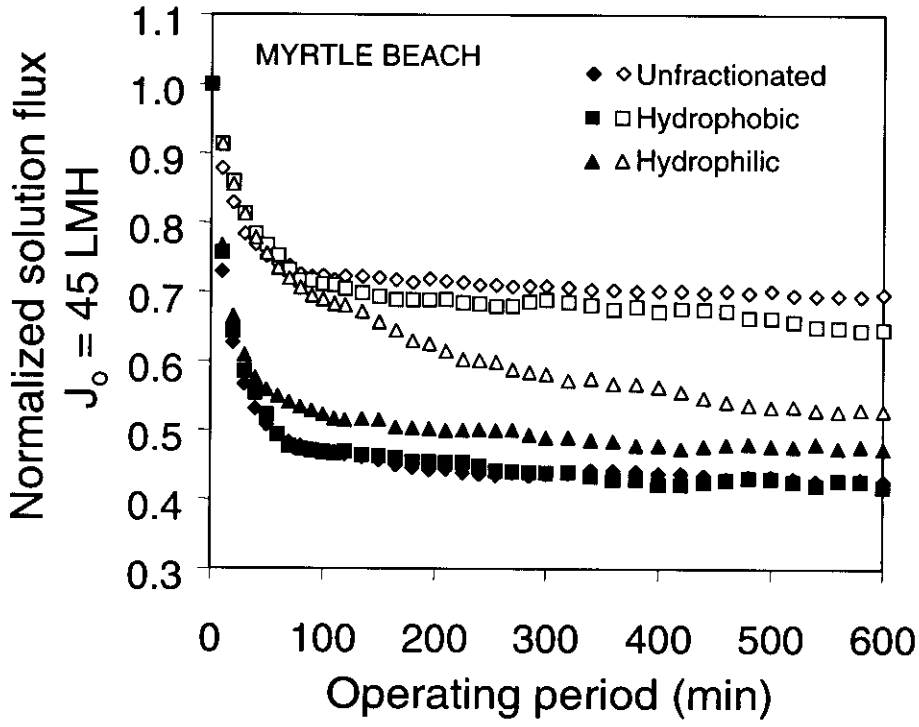

Figure 6-10. Effect of MB-NOM composition on normalized solution flux. NF-70 membrane. Open symbols: 10 mg/L MB-NOM concentration, ionic strength = 0.01 M NaCl, pH 7; closed symbols: 10 mg/L MB-NOM concentration, ionic strength = 0.05 M NaCl, pH 7. Experimental conditions: initial solution flux = 45 LMH, crossflow velocity = 0.1 m/s, recovery = 0.85, and temperature = 23 °C.

Table 6-6 shows the rejection of MB-NOM composition with different ionic strengths. Again, fouling tendency does not correlate well with NOM rejection. At low ionic strength, the hydrophobic MB fraction showed higher NOM rejection (96.6%) than the unfractionated and hydrophilic MB-NOM solutions (each about 93.3%), yet the greatest fouling was observed for the hydrophilic fraction. At higher ionic strength, the NOM rejection of the hydrophilic MB fraction (86.2%) was much lower than the hydrophobic MB fraction (94.9%), and the rejection

of the unfractionated NOM was intermediate between the two fractions. This is similar to the trends observed by Nilson and DiGiano (1996). They suggested that increased NOM rejection of the hydrophobic MB fraction could shift the molecular size distribution to values greater than either the unfractionated MB-NOM solution or the hydrophilic MB fraction.

Table 6-6. Effect of Ionic Strength and Composition on Rejection of MB NOM.

Sources	J/J_o at t = 10 hr	% DOC	% UV	% Conductivity
	I.S. = 0.01 M NaCl, 10 mg/L DOC			
Unfractionated	0.696	92.3 – 94.1 (93.3)	92.3 – 94.1 (93.3)	38.9 – 45.6 (40.4)
Hydrophobic	0.646	96.3 – 97.0 (96.6)	97.1 – 97.5 (97.4)	54.1 – 62.6 (56.2)
Hydrophilic	0.528	91.1 – 94.7 (93.0)	92.5 – 95.9 (94.2)	53.6 – 61.5 (56.7)
	I.S. = 0.05 M NaCl, 10 mg/L DOC			
Unfractionated	0.426	90.1 – 91.7 (90.9)	90.5 – 92.1 (91.2)	24.2 – 34.4 (26.8)
Hydrophobic	0.418	90.3 – 97.1 (94.9)	96.1 – 97.2 (96.5)	29.6 – 50.4 (36.1)
Hydrophilic	0.473	84.6 – 87.0 (86.2)	91.4 – 92.9 (92.0)	28.4 – 35.1 (30.1)

NF-70 membrane; Feed solution conditions: pH 7. Experimental conditions: initial solution flux = 45 LMH, crossflow velocity = 0.1 m/s, recovery = 0.85, temperature = 23 °C. The average values are presented in the parenthesis, N = 7.

Figure 6-11 illustrates the normalized solution flux of CT-NOM fractions at high and low ionic strengths. At low ionic strength, the greater fouling exhibited by the hydrophilic fraction is similar to the effects observed for the MB water. At higher ionic strength, both the hydrophobic and hydrophilic fractions exhibited more fouling than the unfractionated NOM. As shown in Table 6-7, fouling tendency does not correlate with either NOM or salt rejection.

Conclusions from this set of experiments are that:

1) the hydrophilic fraction generally exhibits lower NOM rejection than either the unfractionated NOM or the hydrophobic fraction;

2) the hydrophobic fraction does not appear to be the primary contributor to fouling under low ionic strengths conditions, but is always a significant contributor at high ionic strength conditions;

3) the hydrophobic fraction may not be the only contributor to fouling at high ionic strength conditions, and;

4) fouling tendency cannot be predicted by either NOM or salt rejection alone.

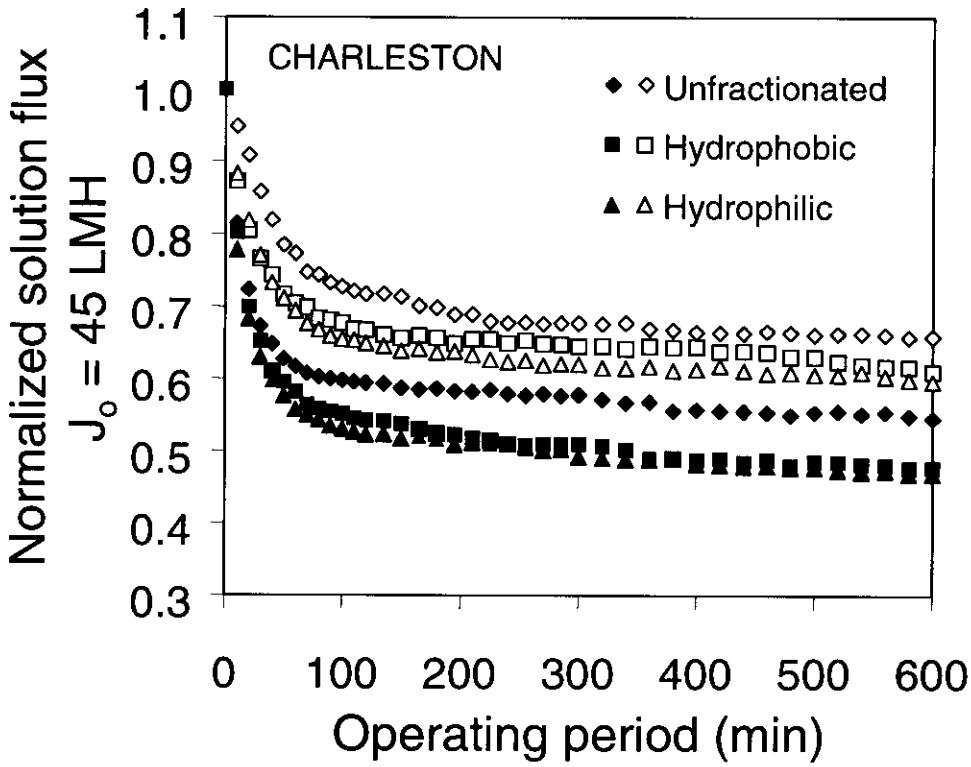

Figure 6-11. Effect of CT-NOM composition on normalized solution flux. NF-70 membrane. Open symbols: 10 mg/L NOM, ionic strength = 0.01 M, pH 7. Filled symbols: 10 mg/L NOM, ionic strength = 0.05 M, pH 7. Experimental conditions: initial solution flux = 45 LMH, crossflow velocity = 0.1 m/s, recovery = 0.85, and temperature = 23 °C.

Table 6-7. Effect of Ionic Strength and Composition on Rejection of CH NOM.

	I.S. = 0.01 M NaCl, 10 mg/L DOC			
Sources	J/J_o at t = 10 hr	% DOC	% UV	% Conductivity
Unfractionated	0.658	95.8 – 96.4	97.6 – 97.8	58.9 – 65.6
Hydrophobic	0.610	92.3 – 93.7	94.1 – 95.3	38.8 – 46.6
Hydrophilic	0.596	94.7 – 95.6	96.1 – 97.0	54.9 – 63.8
	I.S. = 0.05 M NaCl, 10 mg/L DOC			
Unfractionated	0.545	90.7 – 91.5	92.2 – 93.2	27.8 – 32.1
Hydrophobic	0.477	93.1 – 94.8	94.3 – 95.5	27.8 – 33.3
Hydrophilic	0.468	89.1 – 90.7	90.6 – 91.7	27.4 – 33.8

NF-70 membrane; Feed solution conditions: NOM concentration = 10 mg/L, ionic strength = varied and pH 7. Experimental conditions: initial solution flux = 45 LMH, crossflow velocity = 0.1 m/s, recovery = 0.85, temperature = 23 °C. The average values are presented in the parenthesis, N = 7.

6.3.4 Effect of ionic strength

Feed solution chemistry can significantly affect membrane fouling. Braghetta and co-authors (1997) found that increased ionic strength caused more membrane fouling and reduced DOC and conductivity rejection. In this research, it was found that upon increasing ionic strength from 0.01 M to 0.05 M NaCl, the normalized solution flux of the unfractionated TMK-NOM, MB-NOM, and CT-NOM solution were decreased from 0.469 to 0.443, 0.696 to 0.426, and 0.658 to 0.545, respectively. In part, this is due to a greater degree of concentration polarization caused by the increased salt in the feed. However, it is also likely that increasing electrolyte concentration decreased the electrostatic repulsion between 1) negatively charged moieties on single humic molecules; and 2) negative charges on the membrane surface and NOM molecules. These effects could serve to increase the adsorption of NOM to the membrane, and cause the NOM to adopt more compact configurations, increasing the cake density. At high ionic strength, the permeate flux decline of MB-NOM solution was more pronounced but it was not the worst fouling at low ionic strength. It was observed that increased ionic strength decreased NOM and salt rejection. Part of the decrease in NOM rejection could be due to a decrease in NOM molecular size, previously observed by Ghosh and Schnitzer, 1980. Reduced charge repulsion in membrane pores could also contribute.

Increased ionic strength caused more irreversible fouling, possibly due to a decrease in electrostatic charge repulsion (Bacchin et al. (1996)), thus causing a more densely compacted cake on the membrane surface, a greater mass of NOM accessing membrane pores, or both. Braghetta et al. (1997) suggested that the change of membrane pore size and clean membrane resistance induced by changes in ionic strength could be caused by charge screening at the membrane surface and in membrane pores. Table 6-8 tabulates the effect of ionic strength on water flux recovery. At low ionic strength, the TMK-NOM solution, having the lowest aromaticity (SUVA), caused the worst membrane fouling, and had the highest irreversible fouling. The water flux recovery after hydrodynamic cleaning was about 89% and increased to only about 91.7% after chemical cleaning.

Table 6-8. Effect of ionic strength on water flux recovery.

NOM	I.S. = 0.01 M		I.S. = 0.05 M	
	J_1/J_o	J_2/J_o	J_1/J_o	J_2/J_o
TMK	0.890	0.917	0.808	0.861
MB	0.996	0.997	0.944	0.971
CT	0.895	0.924	0.914	0.922

NF-70 membrane; Feed solution conditions: NOM concentration = 10 mg/L, ionic strength = varied and pH 7. Experimental conditions: initial solution flux = 45 LMH, crossflow velocity = 0.1 m/s, recovery = 0.85, temperature = 23 °C. The average values are presented in the parenthesis, N = 7.

The high-SUVA MB-NOM solution exhibited the highest water flux recovery. It is possible that the larger MB-NOM caused a looser cake layer, and that components of the MB water were too large to become trapped in the membrane pores. At high ionic strength, the water flux recovery of TMK-NOM solution after hydrodynamic cleaning was lowest, dropping to about 80.8%, and it had the highest irreversible fouling, but the percent increase in flux after chemical cleaning was significantly higher (about 6.6%) as compared with the MB- and CT-NOM solutions. The water flux recovery for the CT solution did not depend significantly on ionic strength.

6.3.5 Resistances- in-Series Model

The hydraulic resistances-in-series model described by Eq. 34 is one approach to describe changes in membrane performance. Table 6-9 tabulates the hydraulic resistances calculated for different NOM solutions. The dominant resistance for all fractions under both ionic strength conditions was R_{cl}, the hydrodynamically labile cake layer, in combination with any concentration polarization. The resistance that was removed by chemical cleaning was generally less than 2% of the total, and in many cases, less than 1%, even at high ionic strength. The irretrievable resistance, R_{irr}, was a slightly higher proportion of the total, and generally increased significantly with increasing ionic strength, except for the MB hydrophobic and hydrophilic fractions.

Nilson and DiGiano (1996) indicated that hydrophobic fraction isolated in their study corresponded to larger NOM molecular weight, and caused more membrane fouling. This is consistent with our results for the hydrodynamically labile cake resistance at high ionic strength (0.05 M); for all waters, the resistance was greatest for the hydrophobic fraction. However, this was not a general trend. The labile cake resistance was not correlated to solution hydrophobicity at low ionic strength, and neither were other resistances at high or low ionic strength. At low ionic strength, for the MB and CH waters, the hydrophilic fraction appeared quite reactive, exhibiting the highest labile cake and irretrievable resistances.

Table 6-9. Resistances-in-series for NOM composition.

Sources	I.S. = 0.01 M NaCl, (x 10^{-13} m^{-1})				
	SUVA (L/mg-m)	R_{c1}	R_{c2}	R_{irr}	R_T
TMK-Unfractionated	2.26	7.13	0.17	0.068	10.65
TMK-Hydrophobic	2.88	7.11	0.11	0.263	10.76
TMK-Hydrophilic	1.68	6.80	0.25	0.114	10.44
MB-Unfractionated	4.46	2.87	0.05	0.006	6.21
MB-Hydrophobic	4.71	3.37	0.04	0.213	6.90
MB-Hydrophilic	3.14	3.83	0.07	1.340	8.51
CT-Unfractionated	4.64	3.51	0.12	0.166	7.08
CT-Hydrophobic	4.88	3.28	0.05	0.151	6.76
CT-Hydrophilic	3.44	3.87	0.03	0.233	7.41
	I.S. = 0.05 M NaCl, (x 10^{-13} m^{-1})				
TMK-Unfractionated	2.03	14.01	0.28	0.487	18.06
TMK-Hydrophobic	3.02	16.60	0.08	0.456	20.42
TMK-Hydrophilic	1.73	12.86	0.15	0.361	16.65
MB-Unfractionated	4.39	10.41	0.08	0.095	13.87
MB-Hydrophobic	4.58	12.60	0.06	0.153	16.09
MB-Hydrophilic	3.24	10.20	0.06	0.206	13.75
CT-Unfractionated	4.40	9.51	0.08	0.204	13.07
CT-Hydrophobic	5.28	11.31	0.13	0.302	15.02
CT-Hydrophilic	3.38	10.39	0.07	0.249	13.99

Note: R_m = 3.28 x 10^{13} m^{-1}, N = 18 samples, Feed solution conditions: NOM concentration = 10 mg/L (except for the first three row; 12mg/L TMK with ionic strength of 0.018 M NaCl), ionic strength = varied and pH 7. Experimental conditions: initial solution flux = 45 LMH, crossflow velocity = 0.1 m/s, recovery = 0.85, temperature = 23 °C.

6.3.5.1 Contact angle measurements

Static contact angles of the membrane surface were measured using the captive air bubble placed in the contact with the membrane surface. The static angle was measured using an SIT camera (SIT66 Dage-MTI, Michigan City, IN) connected to a video screen. The membrane contact angle was determined after TMK-NOM filtration and cleaning procedure based on 10 different bubbles. The contact angle of the as-received NF-70 membrane was about 28.4. The contact angle of the membrane fouled by the hydrophilic TMK fraction and unfractionated NOM were approximately 27.6 and 27.3, respectively.

Apparently, hydrophilic components served to reduce the contact angle of the fouled membrane. In contrast, the contact angle of the membrane fouled by the hydrophobic TMK fraction increased to 33.9, significantly higher than that of the as-received NF-70 membrane. The experimental results are similar to observations reported previously (Cho et al., 1999; Childress and Elimelech, 1996; Childress and Deshmukh, 1998). It has been found that humic macromolecules adsorbed on the membrane surface, and that the negatively charged functional groups of NOM changed the contact angle and the zeta potential of the membrane. For the TMK water, both the hydrodynamically labile cake and the irretrievable resistances were greater for the hydrophobic fraction. Still, the hydrophilic fraction exhibited significant resistances as well. This again supports the conclusion that hydrophobicity is important in assessing membrane fouling, but is not sufficient.

6.3.6 Effects of NOM Molecular Weight

Concentrated NOM solution was fractionated with several different ultrafiltration membranes (1-, 3-, and 5-K UF membrane). The fractionation was done to selectively shift the molecular weight distribution to either higher or lower values by removing either high or low molecular weight components. Figure 6-12 shows the effect of TMK-NOM molecular weight on normalized solution flux using the NF-70 membrane. Figure 6-12 (a) presents TMK molecular weight fractions starting with the smallest (<1K) and progressively shifting the molecular weight distribution to larger values by fractionating on a larger MWCO membrane, which has the effect of "adding" larger fractions. In all solutions shown in this figure, however, the largest components are absent. Figure 6-12 (b) shows TMK molecular weight fractions starting with the largest components (>5K), and shifting the molecular weight distribution to smaller values, by fractionating on a smaller MWCO membrane, which has the effect of "adding" smaller fractions. In all solutions shown in this figure, however, the smallest components are absent.

As shown in Figure 6-12 (a), individual molecular weight fractions, absent the largest components, exhibit less flux decline than the unfractionated water. For this water, the larger MW components appear to play a significant role in fouling. This conclusion is confirmed in Figure 6-12 (b), which shows that the greatest fouling is observed for the larger MW fractions. The >3K and >5K fractions are expected to behave similarly, because the 3-5K fraction for this water is small. The >1K fraction exhibits fouling similar to the unfractionated water; i.e., the smallest <1K components do not appear to play a significant role in fouling, consistent with the data shown in Figure 6-12 (a). These results are consistent with those observed in previous studies (Nilson and DiGiano, 1996; Lin et al., 2000).

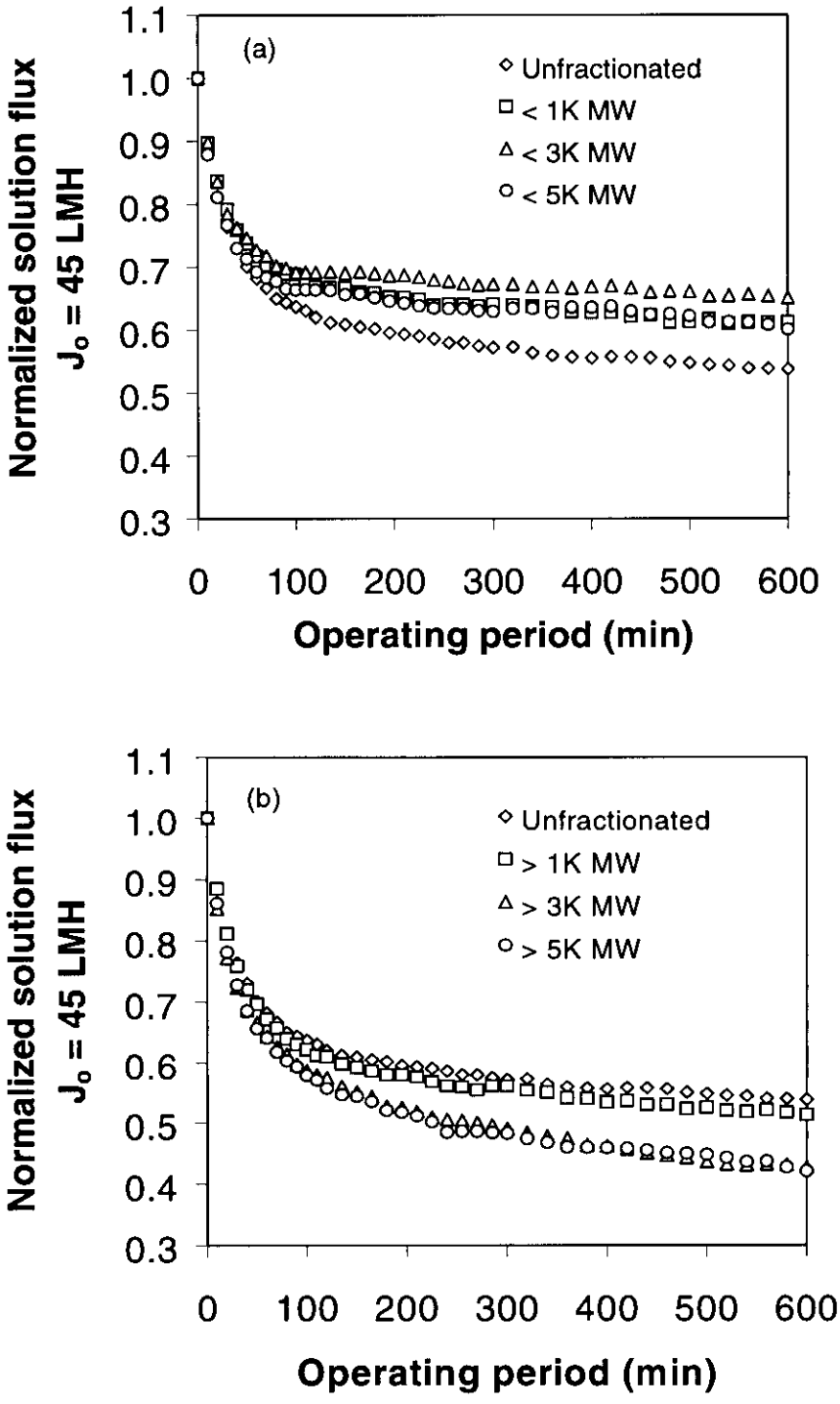

Figure 6-12. Effect of TMK-NOM molecular weight on normalized solution flux. (a) NOM molecular weight less than particular membranes (b) NOM molecular weight more than particular membranes. NF-70 membrane. Feed solution: 10 mg/L TMK-NOM concentration, ionic strength = 0.01 M NaCl as a background, and pH 7. Experimental conditions: initial solution flux = 45 LMH, crossflow velocity = 0.1 m/s, recovery = 0.85, and temperature = 23 °C.

The TMK-NOM solutions that had the smallest components removed (Fig. 6-12 (b) exhibited more irreversible fouling (water flux recovery from 88% to 90%) than the solutions that had the largest components removed (Fig. 6-12 (a)), which had water flux recoveries ranging from 92% to 97%. In comparison, the hydrophobic fraction caused the most irreversible fouling (water flux recovery of 84.2%) and the water flux recovery of unfractionated NOM was about 91.7%.

Figure 6-13 shows the effect of MB-NOM molecular weight on normalized solution flux. Two trends are consistent with the TMK water. First, the solution containing only the smallest components (<1K) exhibits less fouling than the unfractionated water. Second, all solutions containing the largest MW components, shown in Fig 6-13 (b), exhibit fouling greater than the unfractionated water. In contrast to the TMK water, the solution containing the lowest MW components (<1K) exhibited significantly less fouling than the <3K and <5K solutions, which also contained the lowest MW components but which had their MW distribution shifted to higher values. Furthermore, the <3K and <5K solutions exhibited fouling similar to the unfractionated MB water, where in the case of the TMK water, fouling by these fractions was less than the unfractionated water. In part, this may be attributed to higher MW components in the 1-3K and 3-5K fractions of the MB water. While both the TMK and MB waters were fractionated on the same UF membranes, differences in the MW of the same fraction could be due to differences in molecular shape or conformation. Another explanation is that the difference in the fouling of these fractions is caused by other NOM properties. When the highest MW components are present (Fig. 6-13 (b)), all solutions exhibit fouling greater than the unfractionated solution, and similar to each other. It appears that the fouling behavior of the solution having the lowest MW distribution of those containing the highest MW components (>1K) is dominated by the largest MW components in the MB water, which are significantly larger than those in the TMK water.

It was found that the unfractionated NOM and MW fractions of MB-NOM solution showed higher water flux recovery than those of TMK-NOM solution. This was possibly due to larger MB-NOM molecular size distribution than the TMK-NOM solution.

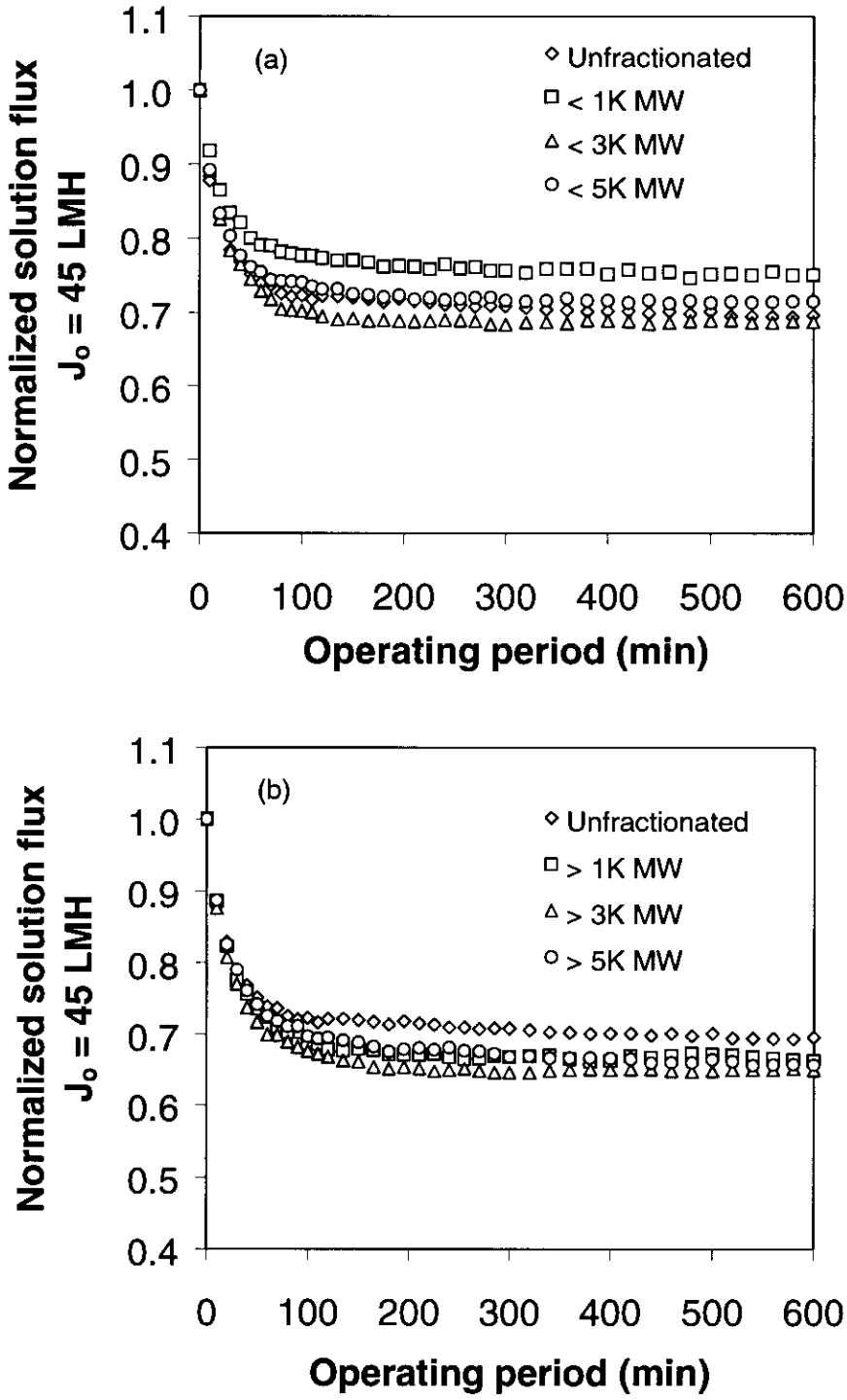

Figure 6-13. Effect of MB-NOM molecular weight on normalized solution flux. (a) NOM molecular weight less than particular membranes (b) NOM molecular weight more than particular membranes. NF-70 membrane. Feed solution: 10 mg/L MB-NOM concentration, ionic strength = 0.01 M NaCl as a background, and pH 7. Experimental conditions: initial solution flux = 45 LMH, crossflow velocity = 0.1 m/s, recovery = 0.85, and temperature = 23 °C.

Figure 6-14 presents the effect of CT-NOM molecular weight on normalized solution flux. As shown in Fig. 12-14 (b), the fouling behavior of the unfractionated water and all fractions appears to be dominated by the high molecular weight components in the CT water. This is consistent with the behavior of the MB water; however, the fractions do not exhibit greater fouling than the unfractionated water, as they did for the MB water. This may be due to the larger proportion of low molecular weight (<1K) components in the MB water, which had a significant influence on the fouling behavior of the unfractionated water, in contrast to the lower proportion of <1K components in the CT water, which did not. The fouling trends for the CT water with the highest MW components removed, shown in Figure 6-14 (a), are not consistent with either the TMK or MB waters. The smallest components do not exhibit the least flux decline, and the solution with the MW distribution shifted to the highest values (<5K) does not exhibit the greatest fouling; rather it fouls the least. The reasons for this behavior are not readily apparent.

A trend seen in much of the data presented suggests that fouling increases with molecular weight, but this does not appear to be a general conclusion. This is based on the behavior of the CT water, and the fact that among the different waters, which have significantly different molecular weight distribution, there does not seem to be a consistent trend. It appears that factors other than molecular weight dominate fouling. This may be due, in part, to the possibility that high molecular weight components could aggregate or form loose cake layers that do not cause significant flux decline. Another possibility is the synergistic effects between NOM acidity and enhancement of salt rejection, which would cause increase concentration polarization and manifest as flux decline. This effect may be counterbalanced by the likelihood that acidic NOM, with significant intra-molecular charge repulsion, would form less dense cake layers.

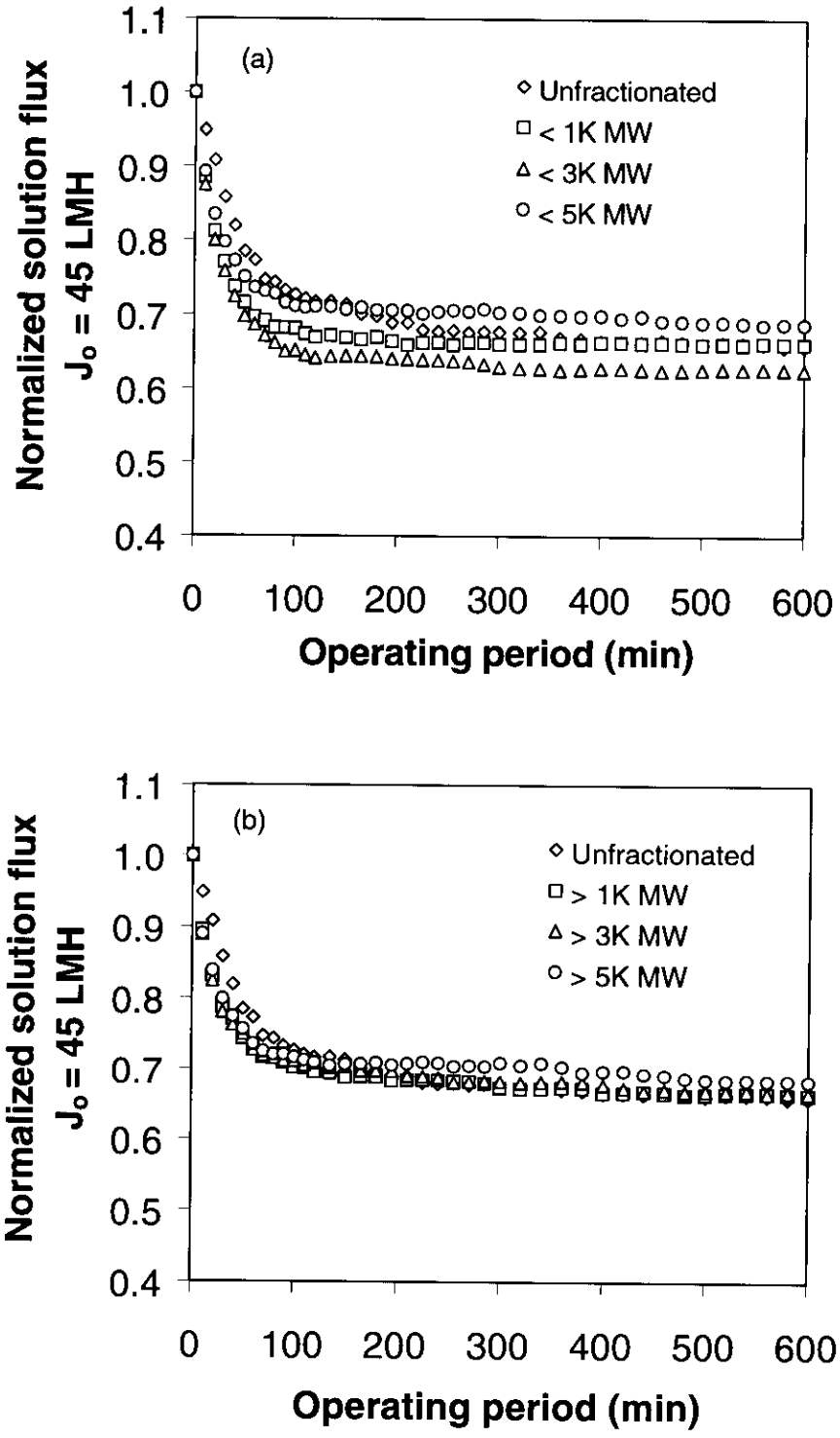

Figure 6-14. Effect of CT-NOM MW on normalized solution flux. (a) large components absent; (b) smallest components absent. NF-70 membrane. Feed solution: 10 mg/L CT-NOM concentration, ionic strength = 0.01 M NaCl as a background, and pH 7. Experimental conditions: initial solution flux = 45 LMH, crossflow velocity = 0.1 m/s, recovery = 0.85, and temperature = 23 °C.

6.4 Conclusions

Membrane fouling was dependent on the characteristics of NF membrane, natural organic matter properties and feed solution chemistry. The characteristics of the NF membranes that were important included membrane pore size, which appeared to control the fouling mechanism, and membrane wettability, measured by contact angle. The tightest NF membrane (NF-70) showed the worst membrane fouling but lower fouling irreversibility. Increased membrane openness showed a decreased DOC and salt rejection, thus reducing NOM accumulation and salt concentration polarization on the membrane surface. The decreased wettability (increased contact angle) and membrane openness of the NF-PES-10 membrane correlated with an increased rate of NOM adhesion, and increased irreversible fouling. The rate of membrane fouling was significantly influenced by natural water properties (i.e. NOM source, concentration, polarity, and NOM molecular weight). Moreover, feed solution chemistry also caused a marked effect on the membrane fouling, consistent with the effects previously observed by others (Nilson and DiGiano, 1996; Lin et al., 2000; Braghetta et al., 1998). In this study, it was found that increased ionic strength exacerbated membrane fouling and decreased DOC rejection due to a decreased electrostatic charge repulsion, thus reducing NOM molecular size and causing a more densely compacted NOM cake layer. At high ionic strength, fouling by the hydrophobic fraction was pronounced (increased total hydraulic resistance on the membrane) for most natural waters, but this trend did not hold at lower ionic strengths. Indeed, the hydrophobic fractions of MB-and CT-NOM solution showed less membrane fouling than the hydrophilic fractions, possibly due to larger molecular weight from hydrophobic components, thus producing a looser cake layer on the membrane surface. In addition, the hydrophilic MB- and CT-NOM fractions caused significant membrane fouling and increased "irreversible" fouling at high ionic strength. Larger NOM molecular weight fractions (those retained by a 5 kDa UF membrane) of the MB- and CT waters exhibited less membrane fouling, increased DOC rejection and decreased irreversible fouling. However, the larger NOM molecular weight fractions of the TMK water caused more membrane fouling, and increased irreversible fouling. For the TMK-NOM solution, large TMK-NOM molecular weight (5-K UF membrane) showed the worst reversible and irreversible fouling.

7.0 References

Aiken, G. R; Brown, P. A.; Noyes ,T. I.; Pinckney, D. J., Molecular Size and Weight of Fulvic and Humic Acids from the Suwannee River, In R. C. Averett, J. A. Leenheer, D. M. McKnight, and K. A. Thorn (Eds), *Humic Substances in the Suwannee River, Georgia: Interactions, Properties, and Proposed Structures*, U. S. Geological Survey Water-Supply Paper 2373 (1995) 89.

Aiken, G.R.; Malcolm, R.L.; Molecular Weight of Aquatic Fulvic Acids by Vapor Pressure Osmometry. *Geochim. Cosmochim. Acta 51* (1987) 2177.

Aiken, G.R.; Thurman, E.M.; Malcolm, R.L.; Walton, H. F. Comparison of XAD Macroporous Resins for the Concentration of Fulvic Acid From Aqueous Solution, *Anal. Chem.* 51(11) (1979) 1799

Alborzfar, M.; Jonsson, G.; Gron, C. Removal of Natural Organic Matter from Two Types of Humic Groundwaters by Nanofiltration. *Wat. Res.* 32 (1998) 2983-2994.

Allegeir, S.C.; Summers, R.S. Evaluating NF for DBP Control with the RBSMT. *J. AWWA*, 87 (Mar. 1995) 87-99.

Bacchin, P.; Aimar ,P.; Sanchez, V. Influence of Surface Interaction on Transfer During Colloid Ultrafiltration, *J. Membrane Sci.*, 115 (1996) 49-63.

Beck, K. C., J. H. Reuter, and E. M. Purdue. 1974. "Organic and Inorganic Geochemistry of Some Coastal Plain Rivers of the Southeastern United States", *Geochim. Cosmochim. Acta.*, 38: 341-364.

Beckett, R.; Jue, Z.; Giddings, C. Determination of Molecular Weight Distributions of Fulvic and Humic Acids Using Flow Field-Flow Fractionation. *Environ. Sci. Techno.* 21(1987) 289-295.

Belfer, S.; Purinson, Y.; Fainshtein, R.; Radchenko, Y.; Kedem, O. Surface Modification of Commercial Composite Polyamide Reverse Osmosis Membranes. *J. Membrane Sci.* 139 (1998) 175-181.

Blau, T.J.; Taylor, J.S.; Morris, K.E.; Mulford, L.A. DBP Control by Nanofiltration: Cost and Performance. *J. AWWA*, 84 (Dec 1992) 104-116.

Braghetta, A.; DiGiano, F. A.; Ball, W. P. Nanofiltration of Natural Organic Matter: pH and Ionic Strength Effects, *J. Environ. Eng.* 123(7) (1997) 628-641.

Braghetta, A.; DiGiano ,F. A.; Ball, W. P. NOM Accumulation at NF Membrane Surface: Impact of Chemistry and Shear, *J. Environ. Eng.* 124(11) (1998) 1087-1098.

Buffle, J. The Analytical Challenge Posed by Fulvic and Humic Acids. *Anal. Chim. Acta*, 232 (1990) 1-2.

Buffle, J., P. Deladoey, and W. Haerdi. 1978. The Use of Ultrafiltration for the Separation and Fractionation of Organic Ligands in Fresh Waters, *Anal. Chim. Acta*, 101: 339-357.

Cadotte, J. R., R. J. Petersen, R. E. Larson, and E. E. Erickson. 1980. A New Thin-Film Sea Water Reverse Osmosis Membrane, Presented at 5th Seminar on Membrane Separation Technology, Clemson University, Clemson, South Carolina.

Cameron, R.S.; Thornton, B.K.; Swift, R.S.; Posner, A.M. Molecular Weight and Shape of Humic Acid from Sedimentation and Diffusion Measurements on Fractionated Extracts. *J. Soil Sci.* 23 (1972) 394-408.

Chellam, S. Effects of Nanofiltration on Trihalomethane and Haloacetic Acid Precursor Removal and Speciation in Waters Containing Low Concentrations of Bromide Ion. *Environ. Sci. Technol.* 34 (2000) 1813-1820.

Chellam, S.; Wiesner, M.R. Particle Back-Transport and Permeate Flux Behavior in Crossflow Membrane Filters. *Environ. Sci. Technol.* 31 (1997) 819.

Childress, A.E.; Elimelech, M. Effect of Solution Chemistry on the Surface Charge of Polymeric Reverse Osmosis and Nanofiltration Membranes. *J. Membrane Sci.*, 119 (1996) 253-268.

Childress, A.E.; Deshmukh, S.S. Effect of Humic Substances and Anionic Surfactants on the Surface Charge and Performance of Reverse Osmosis Membranes, *Desalination*, 118 (1998) 167-174

Chin, Y.P.; Aiken, G.; O'Laughlin, E. Molecular Weight, Polydispersity, and Spectroscopic Properties of Aquatic Humic Substances. *Environmental Sci. and Technology*, 28 (1994) 1853-1858.

Chin, Y.P.; Gschwend, P.M. The Abundance, Distribution, and Configuration of Porewater Organic Colloids in Recent Sediments. *Geochim. Cosmochim. Acta*, 55 (1991) 1309-1317.

Chiou, C. T., D. E. Kile, T. I. Brinton, R. L. Malcolm. 1987. A Comparison of Water Solubility Enhancements of Organic Solutes by Aquatic Humic Materials and Commercial Humic Acids, *Environ. Sci. Technol.*, 21: 1231-1236.

Cho, J.; Amy, G.; Pellegrino, J. Membrane Filtration of Natural Organic Matter: Comparison of Flux Decline, NOM Rejection, and Foulants During Filtration with Three UF membranes. *Desalination* 127 (2000a) 283-298.

Cho, J.; Amy, G.; Pellegrino, J. Membrane Filtration of Natural Organic Matter: Factors and Mechanisms Affecting Rejection and Flux Decline with Charged Ultrafiltration (UF) Membrane. *J. Membrane Sci.* 164 (2000b) 89-110.

Cho, J.; Amy, G.L.; Pellegrino, J. Membrane Filtration of Natural Organic Matter: Initial Comparison of Rejection and Flux Decline Characteristics with Ultrafiltration and Nanofiltration Membranes. *Wat. Res.* 33: 2517 (1999).

Clair, T. A., J. R. Kramer, M. Sydor, and D. Eaton. 1991. Concentration of Aquatic Dissolved Organic Matter by Reverse Osmosis, *Wat. Res.*, 25(9): 1033-1037.

Cohen, R.D.; Probstein, R.F. Colloidal Fouling of Reverse Osmosis Membranes. *J. Colloid Interface Sci.* 114 (1986) 194-207.

Combe, C.; Molis, E.; Lucas, P.; Riley, R.; Clark, M.M. The Effect of CA Membrane Properties on Adsorptive Fouling by Humic Acid. J. *Membrane Sci.* 154 (1999) 73-87.

Connell, H.; Zhu, J.; Bassi, A. Effect of Particle Shape on Crossflow Filtration Flux. *J. Membr. Sci.*, 153 (1999) 121-139.

Cornel, P.K.; Summers, R.S.; Roberts, P. V. Diffusion of Humic Acid in Aqueous Solution. *J. Colloid Interface Sci.*, 110 (1986) 149-164.

Danielsson, L. G. 1982. On the Use of Filters for Distinguishing Between Dissolved and Particulate Fractions in Natural Waters, *Wat. Res.*, 16, 179-182.

Drever, J. I. 1997. *The Geochemistry of Natural Waters: Surface and Ground water Environments*, 3rd Edition, Prentice-Hall, Eaglewood Cliffs, NJ.

Eaton, A. D.; Clesceri, L. S.; Greenberg (Eds), A. E. *Standard Methods for the Examination of Water and Wastewater*, 19th Edition (1995), Washington, D.C.

Eriksson P., Nanofiltration Extends the Range of Membrane Filtration, *Environ. Prog.*, 7(1) (1988) 58-62.

Eriksson, P. 1988. Nanofiltration Extends the Range of Membrane Filtration, *Environ. Prog.*, 7(1): 58-62.

Federal Register, 59(145), 38668, 1994

Field, R. W.; Wu, D.; Howell J. A.; Gupta, B. B, Critical Flux Concept for Microfiltration Fouling, *J. Membrane Sci.*, 100 (1995) 259-272.

Fu, P.; Ruiz, H.; Lozier , J.; Thompson, K.; Spangenberg , C. A Pilot Study on Groundwater Natural Organics Removal By Low-Pressure Membranes, *Desalination.*, 102 (1995) 47-56.

Ghosh K.; M. Schnitzer, Macromolecular Structures of Humic Substances, *Soil Sci.*, 129(5) (1980) 266-276.

Glaze, W.H.; Andelman, J.B.; Bull, R.J.; Conolly, R.B.; Hertz, C.D.; Hood, R.D.; Pegram, R.A. Determining Health Risks Associated with Disinfectants and Disinfection By-Products. Research needs. *J. AWWA*, 85 (Mar. 1993) 53-56.

Hong S., R. S. Faibish and M. Elimelech, Kinetics of Permeate Flux Decline in Crossflow Membrane Filtration of Colloidal Suspensions, *J. Colloid and Interface Sci.*, 196 (1997) 267-277.

Hong, S.; Elimelech, M. Chemical and Physical Aspects of Natural Organic Matter (NOM) Fouling of Nanofiltration Membranes. *J. Membrane Sci.* 132 (1997) 159-181

Hong, S.; Elimelech, M.; Chemical and Physical Aspects of Natural Organic Matter (NOM) Fouling of Nanofiltration Membranes, *J. Membrane Sci.*, 132 (1997) 159-181.

Jolley, R. L., and I. H. Suffet. 1987. Concentration Techniques for Isolating Organic Constituents in Environmental Water Samples, In *Organic Pollutants in Water; Sampling, Analysis, and Toxicity Testing*, I. H. Suffet and M. Malaiyandi, eds., American Chemical Society, Washington, D. C.

Jucker, C.; Clark, M.M. Adsorption of Aquatic Humic Substances on Hydrophobic Ultrafiltration Membranes. *J. Membrane Sci.*, 97 (1994) 37-52.

Kabsch-Korbutowicz, M.; Majewska-Nowak, K.; Winnicki, T. Analysis of Membrane Fouling in the Treatment of Water Solutions Containing Humic Acids and Mineral Salts. *Desalination*, 126 (1999) 179-185.

Kaiya, Y.; Itoh ,Y.; Fujita, K; Takizawa , S. Study on Fouling Materials in the Membrane Treatment Process For Potable Water, *Desalination*, 106 (1996) 71-77.

Kilduff, J.; W. J. Weber, Jr. Transport and Separation of Organic Macromolecules in Ultrafiltration Processes, *Environ. Sci. Technol.*, 26 (1992), 569-577.

Kim, J.-S. 1988. Characteristics of Humic Substances and Their Removal Behavior in Water Treatment, Ph.D. Thesis, Georgia Institute of Technology.

Kim, J.-S., E. S. K. Chian, F. M. Saunders, E. M. Perdue, and M. F. Giabbai. 1989. Characteristics of Humic Substances and Their Removal Behavior in Water Treatment, In *Aquatic Humic Substances: Influence on Fate and Treatment of Pollutants*, I. H. Suffet, and P. McCarthy, American Chemical Society, Washington, D. C.

Krasner, S. W., J.-P. Croue, J. Buffle, and E. M. Perdue. 1996. Three Approaches for Characterizing NOM, *J. AWWA*, 88(6): 66-79.

Krasner, S.W.; Westrick, J.J.; Regli, S. Bench and Pilot Testing Under the ICR. *J. AWWA*, 8 (1995) 60.

Lawrence, J. 1989. Humic Acid and Related Substances in the Environment, In *Analysis of Trace Organics in the Aquatic Environment*, B. K. Afghan, and A. S. Y. Chau, eds., CRC Press Inc., Boca Raton, Florida, 313-337.

Lee, S.; Ruckenstein, E. Surface Restructuring of Polymers. *J. Colloid Interface Sci.*, 120 (1987) 529-536.

Leenheer, Jerry A, Comprehensive Approach to the Preparative Isolation and Fractionation of Dissolved Organic Carbon From Natural Waters and Wastewaters, *Environ. Sci. Technol.* 15(5) 1981 p578

Levenspiel, O. 1972. *Chemical Reaction Engineering*, 2nd Edition, John Wiley & Sons, New York.

Lin, C-F.; Huang, Yuh-Jay.; Hao, O.J. Ultrafiltration Processes for Removing Humic Substances: Effect of Molecular Weight Fractions and PAC Treatment. *Wat. Res.* 33 (1999) 1252-1264.

Lin, C-F; Lin, Y-T; Hao, O.J. Effects of Humic Substance Characteristics on UF Performance. *Wat. Res.*, 34(4) (2000) 1097-1106.

Logan, B.E., and Jiang, Q. (1990) Molecular Size Determination of Dissolved Organic Matter. *J. Environ. Eng.*, 116: 1046-1062.

Maartens, A.; Swart, P.; Jacobs, E.P. Membrane Pretreatment: A Method for Reducing Fouling by Natural Organic Matter. *J. Colloid Interface Sci.* 221 (2000) 137-142.

Malcolm, R.L. (1990) The Uniqueness of Humic Substances in Each of Soil Stream and Marine Environments. *Anal. Chim. Acta*, 232: 19-30.

Malcolm, R.L.; MacCarthy, P. (1986) Limitations in the Use of Commercial Humic Acids in Water and Soil Research. *Environ. Sci. Technol.*, 20: 904-911.

Mallevialle, J.; Anselme, C.; Marsigny, O. Effects of Humic Substances on Membrane Processes. *In: Aquatic Humic Substances, Influence on Fate and Treatment of Pollutants*, I.H. Suffet and P. McCarthy, Eds. Advances in Chemistry Series 219, American Chemical Society, Washington D.C. (1989).

Mallubhotla, H.; Belfort, G. Semiempirical Modeling of Cross-Flow Microfiltration with Periodic Reverse Filtration *Ind. Eng. Chem. Res.* 35 (1998) 2920-2928

Mantoura, R.F.C.; Riley, J.P. The Analytical Concentration of Humic Substances from Natural Waters, *Anal. Chim. Act.* 76 (1975) 97-106

Manttari, M.; Puro, L.; Nuortila-Jokinen, J.; Nystrom, M. Fouling Effects of Polysaccharides and Humic Acid in Nanofiltration. *J. Membrane Sci.* 165 (2000) 1-17.

Miles, C. J., J. R. Tuschall, and P. L. Brezonik. 1983. Isolation of Aquatic Humus with Diethylaminoethylcellulose, *Anal. Chem.*, 55: 410-411.

Morel, F.M.M. *Principles of Aquatic Chemistry.* John Wiley, New York (1983).

Nabe, A.; Staube, E.; Belfort, G. Surface Modification of Polysulfone Ultrafiltration Membranes and Fouling by BSA solutions. *J. Membrane Sci.* 133 (1997) 57-72.

Nilson, J.A.; DiGiano, F.A. Influence of NOM Composition on Nanofiltration. *J. AWWA*, 88 (1996) 53-66.

Nystrom, M.; Kaipia, L.; Luque, S. Fouling and Retention of Nanofiltration Membranes. *J. Membr. Sci.*, 98 (1995) 249-262.

Odegaard, H., and S. Koottatep. 1982. Removal of Humic Substances from Natural Waters by Reverse Osmosis, *Water Res.*, 16, 613-620.

Petersen, R. J. Composite Reverse Osmosis and Nanofiltration Membranes, *J. Membrane Sci.*, 83 (1993) 81-150.

Pieracci, J; Crivello, J.V.; Belfort, G.Photochemical Modification of 10 kDa Polyethersulfone Ultrafiltration Membranes for Reduction of Biofouling. *J. Membrane Sci.*, 156 (1999) 223-240.

Pieracci, J; Wood, D.W.; Crivello, J.V.; Belfort, G. UV-Assisted Graft Polymerization of *N*-vinyl-2-pyrrolidinone onto Poly(ether sulfone) Ultrafiltration Membranes: Comparison of Dip versus Immersion Modification Techniques. *Chem. Mat.* 12 (2000) 2123-2134.

Potts, D. E.; Ahlert,R. C.; Wang, S. S. Critical Review of Fouling of Reverse Osmosis Membranes. *Desalination* 36 (1981) 235-264.

Putnam, S.W.; Graham, J.D. Chemicals Versus Microbials in Drinking Water. A Decision Sciences Perspective. *J. AWWA* 85 (1993) 57-61.

Rautenbach, R.; Linn, T.; Al-Gobaisi, D.M.K. Present and Future Pretreatment Concepts - Strategies for Reliable and Low-Maintenance Reverse Osmosis Seawater Desalination. *Desalination* 110 (1997) 97-106.

Reid, P.M., Wilkinson, A.E., Tipping, E., and Jones, M.N. Determination of Molecular Weights of Humic Substances by Analytical (UV Scanning) Ultracentrifugation. *Geochim. Cosmochim. Acta*, 54 (1990) 131-138.

Schafer, A.; Fane, G.; Waite T. D. Nanofiltration of Natural Organic Matter: Removal, Fouling and the Influence of Multivalent Ions, *Desalination*, 118 (1998) 109-122.

Schnitzer, M. Soil Organic Matter -- The Next 75 Years. *Soil Sci.* 151(1991) 41-58.

Schulten, H.R.; Schnitzer, M. A State of the Art Structural Concept for Humic Substances. *Naturwissenschaften*, 80 (1993) 29-30.

Serkiz, S.M.; Perdue, E.M. Isolation of Dissolved Organic Matter From the Suwannee River Using Reverse Osmosis. *Wat. Res.* 24 (1990) 911-916.

Sigal, G.B.; Mrksich, M.; Whitesides, G. M. Effect of Surface Wettability on the Adsorption of Proteins and Detergents. *J. Am. Chem. Soc.* 120 (1998) 3464-3473.

SpectraTech, Inc. *Contact Sampler Users Manual for Model #0012-490T Nicolet Magna-IR Spectrophotometer* (1995).

Sun, L.; Perdue, E.M.; McCarthy, J.F. Using reverse osmosis to obtain organic matter from surface and ground waters. *Wat. Res.* 29 (1995) 1471-1477.

Symons, J.M.; Bellar, T.A.; Carswell, J. K.; DeMarco, J.; Kropp, K.L.; Robeck, G.G.; Seeger, D.R.; Slocum, C.J.; Smith, B.L.; Stevens, A. A. National Organics Reconnaissance Survey for Halogenated Organics. *J. AWWA*, 11 (1975) 634-647.

Taylor, J. S., Thompson , D. M.; Carswell, J. K. Applying Membrane Processes to Groundwater Sources for Trihalomethane Precursor Control, *J. AWWA*, 79 (8) (1987) 72-82.

Teefy, S. M.; Singer, P.C. Performance and Analysis of Tracer Tests to Determine Compliance of a Disinfection Scheme With the SWTR, *J. AWWA*, Dec 1990.

Thurman, E. M. (1985) *Organic Geochemistry of Natural Waters* Martinus Nijhofff/Junk Publishers: Dordrecht, The Netherlands.

Thurman, E. M.; Malcolm , R. L. Preparative Isolation of Aquatic Humic Substances, *Environ. Sci. Technol.*, 15 (1981) 463-466.

Thurman, E. M.; Wershaw , R. L.; . Malcolm, R. L; Pinckney , D. J. Molecular Size of Aquatic Humic Substances, *Org. Geochem.*, 4 (1982) 27-35.

Thurman, E.M.; Aiken, G.R.; Malcolm R.L. Prediction of Capacity Factors for Aqueous Organic Solutes Adsorbed on a Porous Acrylic Resin, *Anal. Chem.* 50(6) 1978 p775

Ulbricht, M.; Belfort, G. Surface Modification of Ultrafiltration Membranes by Low Temperature Plasma. II. Graft Polymerization onto Polyacrylonitrile and Polysulfone *J. Membrane Sci.* 111(1996) 193-215

Visvanathan, C.; Marsono, B.D.; Basu, B. Removal of THMFP by Nanofiltration: Effects of Interference Parameters. *Wat. Res.* 32:3527 (1998).

Weber, J. H., and S. A. Wilson. The Isolation and Characterization of Fulvic Acid and Humic Acid from River Water. *Wat Res.* 9 (1975) 1079-1084.

Yamagishi, H.; Crivello, J; Belfort, G. Development of a Novel Photochemical Technique for Modifying poly(arylsulfone) Ultrafiltration Menbranes. *J. Membrane Sci.*, 105 (1995a) 237-247.

Yamagishi, H.; Crivello, J.;Belfort, G. Evaluation of Photochemically Modified Poly(arylsulfone) Ultrafiltration Membranes. *J. Membrane Sci.*, 105 (1995b) 249-259.

Yamagishi; Crivello; Belfort US Patent Number 5,468,390 (1995).

Yoon, S-H.; Lee, C-H.; Kim, K-J.; Fane, A.G. Effect of Calcium Ion on the Fouling of Nanofilter by Humic Acid in Drinking Water Production. *Wat. Res.* 32 (1998) 2180-2186.

Yuan W.; Zydney, A. L. Humic Acid Fouling During Microfiltration, *J. Membrane Sci.*, 157 (1999) 1-12.

Yuan, W.; Zydney, A. L. Effects of Solution Environment on Humic Acid Fouling During Microfiltration. *Desalination* 122 (1999a) 63-76.

Zeeman; Zydney, A. L. *Microfiltration and Ultrafiltration: Principles and Applications.* Marcel Dekker, Inc., New York, 1996.

8.0 APPENDIX I. Nomenclature

A_f	cross sectional flow area [m^2]
A_m	effective membrane area [m^2]
b	channel width [m]
C	solute concentration [mg L^{-1}]
C_i	molar concentration [M]
C_{feed}	feed concentration [mg L^{-1}]
C_{flush}	concentration of NOM flush [mg L^{-1}]
C_{NaOH}	concentration in NaOH cleaning solution [mg L^{-1}]
C_{perm}	permeate concentration [mg L^{-1} or mol L^{-1}]
C_r^f	concentrate DOC concentration, [mg L^{-1}], at the end of the run
C_{reten}	retentate concentration [mg L^{-1} or mol L^{-1}]
C_s	pretreated source water concentration [mg L^{-1}]
C_{sample}	concentration of NOM sample [mg L^{-1}]
C_{ss}	Steady state concentration [mg L^{-1} or mol L^{-1}]
D	solute diffusivity [m^2 min^{-1}]
d_h	hydraulic diameter [m]
d_f	diameter of filaments [m]
F	F curve for tracer test
J_o	clean (initial) water flux [L m^{-2} hr^{-1} or LMH]
J_{om}	solution flux after 10 hours of filtration [L m^{-2} hr^{-1} or LMH]
J_s	solute flux [mg m^{-2} min^{-1}]
J_v	solution flux [L m^{-2} hr^{-1}]
J_1	solution flux after hydrodynamic cleaning [L m^{-2} hr^{-1} or LMH]
J_2	solution flux after cleaning with caustic solution [L m^{-2} hr^{-1} or LMH]
k_a	first order adhesion rate coefficient [min^{-1}]
L	length [m]
L_p	permeability [L m^{-2} hr^{-1} kPa^{-1} or LMH kPa^{-1}]
m_{cake}	cake mass [mg]

$M_{d,1}$	mass NOM recovered from hydrodynamic cleaning [mg]
$M_{d,2}$	mass NOM recovered from chemical cleaning [mg]
$M_{d,3}$	mass NOM remaining on the membrane after all cleaning [mg]
N_{Pe}	Peclet number
N_{Re}	Reynolds number
N_{Sc}	Schmidt number
N_{Sh}	Sherwood number
P	transmembrane pressure [kPa]
Q	flow rate [L min^{-1}]
Q_{feed},	feed flow rate [L min^{-1}]
Q_{perm}	permeate flow rate [L min^{-1}]
Q_{reten}	retentate (concentrate) flow rate [L min^{-1}]
Q_s	pretreated source water flow to the sample reservoir
r	water recovery
R_c	hydraulic resistance of the cake [m^{-1}]
R_{c1}	resistance recoverable with hydrodynamic cleaning [m^{-1}]
R_{c2}	resistance recoverable using chemical cleaning [m^{-1}]
R_f	resistance due to sum of a polarization resistance and fouling [m^{-1}]
R_{feed}	feed rejection
R_m	intrinsic membrane hydraulic resistance [m^{-1}]
R_{mem}	intrinsic membrane rejection
$R_{non\text{-}rec}$	"non-recoverable" resistance [m^{-1}]
R_{reten}	retentate rejection
R_T	total hydraulic resistance [m^{-1}]
t	time [min]
$\bar{t}$	mean residence time [min]
v	crossflow velocity [m]
V	volume [L]
V_c	volume of isolate [L]
V_{flush}	volume of flush after isolation [L]
V_{NaOH}	volume of NaOH cleaning solution [L]
V_{reten}	volume of retentate [L]

V_{sample}	volume of sample [L]
V_{sys}	system volume of the crossflow bench-scale test cell [L]
Z_i	ionic valence
ρ	water density [$kg.m^{-3}$]
μ	viscosity [$kg.m^{-1}.s^{-1}$]
μ_T	viscosity at specific temperature
π	osmotic pressure [kPa]
π_{mem}	osmotic pressure at the membrane surface [kPa]
π_{perm}	osmotic pressure in the permeate line [kPa]
σ	osmotic reflection coefficient (= $1-C_{perm}/C_{mem}$)
θ	hydrodynamic angle [degree]
θ_i	ratio between the time (t) and the mean residence time ($\bar{t}$)

9.0 APPENDIX II. Data Record

Figure 2-2

Sample	pH	Turbidity (NTU)		average (NTU)
Raw	6.74	2.13	2.14	2.135
10-WS	7.43	0.61	0.63	0.62
5-0.45	7.84	0.45	0.43	0.44

Figure 2-3

(1) RO Perm

Initial permeate (Temp. 19.4 -21)

Ave. P (psi)	P(kPa)	Flux(L/m^2/h)
54.5	375.6607143	11.30573876
60	413.5714286	13.1391018
76	523.8571429	15.88914636
92.5	637.5892857	20.47255397
97.5	672.0535714	21.38923549
107.5	740.9821429	22.91703802
118.5	816.8035714	26.2782036
123.5	851.2678571	27.19488512
139	958.1071429	31.16717171
150	1033.928571	32.38941374
155	1068.392857	33.91721627
160	1102.857143	35.1394583
170	1171.785714	37.27838185
180	1240.714286	40.63954742

(2) Raw TMK

Pressure (psi)	P(kPa)	Water flux (L/m^/h)
59.887	412.7932028	11.1578869
102.500	706.5178571	20.72718772
123.5	851.2678571	25.15144923
144.3	994.6392857	30.39308509
55	379.1071429	9.930716476
65.5	451.4821429	12.83354129
76	523.8571429	15.12524509
86.5	596.2321429	17.4169489
97	668.6071429	19.40309219
108	744.4285714	21.84757625
118.5	816.8035714	24.44484056
129	889.1785714	26.43098385
139	958.1071429	28.87546791
150	1033.928571	30.5560507
160	1102.857143	33.91721627
170	1171.785714	36.20892007
175	1206.25	37.58394236

(3) RO Perm after cleaning

Ave. P	P(kPa)	Ave. Flux
55	379.1071429	11.45851901
65.5	451.4821429	14.81968459
76	523.8571429	16.95860814
86.5	596.2321429	19.25031194
97.5	672.0535714	22.45869726
108	744.4285714	24.59762081
118.5	816.8035714	26.58376411
129	889.1785714	29.33380867
139	958.1071429	31.77829272
150	1033.928571	34.52833729
160	1102.857143	37.27838185
170	1171.785714	39.7228659
175	1206.25	41.86178945

(4) DI water

Pave (psi)	P(kPa)	Ave. Flux
55	379.1071429	11.61129926
65.5	451.4821429	14.66690433
76	523.8571429	17.11138839
86.5	596.2321429	18.94475143
97.5	672.0535714	21.38923549
108	744.4285714	24.44484056
118.5	816.8035714	27.19488512
129	889.1785714	28.72268765
139	958.1071429	30.8616112
149.5	1030.482143	33.30609526
160	1102.857143	36.05613982
170	1171.785714	38.80618438
180	1240.714286	42.16734996

Figure 2-4.

Feed Flow

(1) RO Perm

Ave. P (psi)	P(kPa)	Qf (L/h)
54.5	375.6607143	16.4269
60	413.5714286	15.9727
76	523.8571429	14.79935
92.5	637.5892857	13.5503
97.5	672.0535714	13.20965
107.5	740.9821429	12.3391
118.5	816.8035714	11.61995
123.5	851.2678571	11.24145
139	958.1071429	10.2195
150	1033.928571	9.34895
155	1068.392857	8.97045
160	1102.857143	8.6298
170	1171.785714	7.75925
180	1240.714286	7.00225

(2) Raw TMK

Pressure (psi)	P(kPa)	Qf(L/m)
59.887	412.7932028	15.94583871
102.500	706.5178571	12.93418611
123.5	851.2678571	11.49457188
144.3	994.6392857	10.03277333
55	379.1071429	16.1998
65.5	451.4821429	15.5185
76	523.8571429	14.553325
86.5	596.2321429	13.720625
97	668.6071429	12.869
108	744.4285714	12.055225
118.5	816.8035714	11.373925
129	889.1785714	10.579075
139	958.1071429	9.859925
150	1033.928571	9.065075
160	1102.857143	8.36485
170	1171.785714	7.57
175	1206.25	7.1158

Recovery

(1) RO Perm

P(kPa)	R
375.6607143	8.525345622
413.5714286	10.18957346
523.8571429	13.29923274
637.5892857	18.7150838
672.0535714	20.05730659
740.9821429	23.00613497
816.8035714	28.01302932
851.2678571	29.96632997
958.1071429	37.77777778
1033.928571	42.91497976
1068.392857	46.83544304
1102.857143	50.43859649
1171.785714	59.51219512
1240.714286	71.89189189

(2) Raw TMK

P(kPa)	% R
412.7932028	8.669282909
706.5178571	19.84924867
851.2678571	27.10560675
994.6392857	37.52667121
379.1071429	7.593457944
451.4821429	10.24390244
523.8571429	12.87386216
596.2321429	15.72413793
668.6071429	18.67647059
744.4285714	22.44897959
816.8035714	26.62229617
889.1785714	30.94812165
958.1071429	36.27639155
1033.928571	41.75365344
1102.857143	50.22624434
1171.785714	59.25
1206.25	65.42553191

(3) RO Perm after cleaning

P(kPa)	Recovery
379.1071429	8.844339623
451.4821429	12.00349233
523.8571429	14.4309988
596.2321429	17.52329217
672.0535714	21.71135316
744.4285714	25.15041413
816.8035714	28.95179869
889.1785714	34.40860215
958.1071429	39.92454832
1033.928571	47.08333333
1102.857143	54.95495495
1171.785714	65
1206.25	72.87234043

Figure 2-6

Flow = 1.71 L; Volume reactor = 6.8 L

Volume (L)	Time	V/Vr	Conductivity (μS/cm)	F(V/Vr)
0	0.00	0.00	3946.127341	-3.2271E-05
1	0.58	0.13	3935.488184	0.002663917
2	1.17	0.27	3924.706024	0.005396345
3	1.75	0.40	3855.526397	0.022927928
4	2.34	0.53	3916.543981	0.007464779
5	2.92	0.67	3857.170177	0.022511359
6	3.51	0.80	3695.104203	0.06358231
7	4.09	0.93	2478.740452	0.371834655
8	4.68	1.07	1087.166865	0.724488884
9	5.26	1.20	429.0374278	0.891272826
10	5.85	1.33	181.5568664	0.953989644
11	6.43	1.47	113.300498	0.971287253
12	7.02	1.60	81.52526959	0.979339769
13	7.60	1.73	68.20839288	0.982714548
14	8.19	1.87	60.337761	0.984709133
15	8.77	2.00	57.5005072	0.985428153
16	9.36	2.13	54.26524853	0.986248036
17	9.94	2.27	52.95091494	0.986581116
18	10.53	2.40	50.42831177	0.987220397
19	11.11	2.53	45.70037472	0.988418557
20	11.70	2.67	46.50634713	0.988214306
21	12.28	2.80	44.23077133	0.988790985
22	12.87	2.93	46.16587991	0.988300588
23	13.45	3.07	43.50324132	0.988975357
24	14.04	3.20	41.7455346	0.989420797
25	14.62	3.33	40.53711123	0.989727037
26	15.20	3.47	41.41596459	0.989504317
27	15.79	3.60	39.10897452	0.990088957
28	16.37	3.73	38.99911785	0.990116797
29	16.96	3.87	37.6019803	0.990470862
30	17.54	4.00	36.1012805	0.990851171
31	18.13	4.13	35.58936424	0.990980901
32	18.71	4.27	37.93086059	0.990387516
33	19.30	4.40	36.39608589	0.990776461
34	19.88	4.53	34.13211975	0.991350198
35	20.47	4.67	33.98429706	0.991387659
36	21.05	4.80	32.64177886	0.991727882
37	21.64	4.93	31.63872096	0.991982078
38	22.22	5.07	33.8746703	0.991415441
39	22.81	5.20	33.68678773	0.991463054
40	23.39	5.33	30.93975137	0.992159212
41	23.98	5.47	32.28885589	0.99181732
42	24.56	5.60	31.52783908	0.992010178
43	25.15	5.73	30.30319606	0.992320528
44	25.73	5.87	30.41259388	0.992292804
45	26.32	6.00	29.99087091	0.992399678
46	26.90	6.13	29.16071941	0.992610056
47	27.49	6.27	28.3340353	0.992819555
48	28.07	6.40	27.954825	0.992915655

Figure 2-7.

60 psi

Time (minutes)	% DOC rej.
0	96.58709432
27	99.45832515
54	99.36704079
81	99.8089146
108	99.88149188
135	99.82556582
162	99.91615561
189	99.91694919
216	99.7632996
243	99.93796064
270	99.97892041
283.5	99.87480683
297	99.8811092
310.5	99.92127793
324	99.8936395
337.5	99.82672285
351	99.81584048
364.5	99.86977312
378	99.7762152
391.5	99.80617165
405	99.8416139

103 psi

Time (minutes)	% DOC
0	98.35475082
34	99.61278847
68	99.8683088
102	99.65251557
136	99.91630631
170	99.88088926
178.5	99.9358327
187	99.9344402
195.5	99.90147224
204	99.90873508
212.5	99.83510423
221	99.87053356
226	99.86424231

124 psi

Time (minutes)	% DOC
0	98.18557274
38	99.52961069
76	99.48560727
114	99.67786571
152	99.80622739
161.5	99.87378886
171	99.77728807
180.5	99.65157859
190	99.8833901
199.5	99.68441129
209	99.84201186
217	99.86398933

145 psi

Time (minutes)	% DOC
0	97.36481163
44	99.66252046
88	99.65930701
132	99.8040382
143	99.7371414
148.5	99.95203923
154	99.78462332
159.5	99.87747029
165	99.8604021
170.5	99.89726658
176	99.86874274
179	99.87597827

Figure 2-8.

Data		R = 99%		R= 90%	
Time	TOC	Time	TOC	Time	TOC
0	5.759585502	0	5.76	0	5.76
27	7.002370706	10	6.187877965	10	6.150905824
54	8.240310909	20	6.615460796	20	6.539123682
81	9.343036895	30	7.042748697	30	6.924672057
108	10.52945675	40	7.469741871	40	7.307569305
135	11.82089505	50	7.896440521	50	7.687833656
162	12.99717536	60	8.322844851	60	8.065483215
189	14.07310899	70	8.748955063	70	8.44053596
216	15.22306315	80	9.17477136	80	8.81300975
243	16.67345135	90	9.600293946	90	9.182922317
270	17.57385438	100	10.02552302	100	9.550291272
283.5	18.42753268	110	10.45045879	110	9.915134107
297	20.002723	120	10.87510146	120	10.27746819
310.5	22.17671016	130	11.29945122	130	10.63731078
324	25.33188197	140	11.72350828	140	10.99467899
337.5	29.00600394	150	12.14727284	150	11.34958986
351	33.472588	160	12.57074511	160	11.70206027
364.5	39.99079413	170	12.99392528	170	12.052107
378	48.91481539	180	13.41681356	180	12.39974673
391.5	62.46930935	190	13.83941015	190	12.74499599
406	86.37054486	200	14.26171524	200	13.08787124
		210	14.68372905	210	13.42838879
		220	15.10545176	220	13.76656486
		230	15.52688359	230	14.10241555
		240	15.94802473	240	14.43595684
		250	16.36887538	250	14.76720462
		260	16.78943575	260	15.09617465
		270	17.20970603	270	15.42288261
		280	18.29687314	280	16.30611439
		290	19.53150038	290	17.30338807
		300	20.94583789	300	18.43881835
		310	22.58229079	310	19.74391715
		320	24.49776094	320	21.26068813
		330	26.77042572	330	23.04642553
		340	29.51071543	340	25.18142824
		350	32.87987378	350	27.78193838
		360	37.12301139	360	31.0229794
		370	42.63183835	370	35.18127388
		380	50.0736586	380	40.72250897
		390	60.68578874	390	48.49794368
		400	77.05041778	400	60.25389694
		404	86.38531899	404	66.85518406

Figure 2-8. Continued

R= 80%

Time	TOC
0	5.76
10	6.110090817
20	6.455383564
30	6.795943999
40	7.13183698
50	7.463126474
60	7.789875575
70	8.112146508
80	8.430000648
90	8.743498528
100	9.052699852
110	9.357663505
120	9.658447565
130	9.955109315
140	10.24770525
150	10.5362911
160	10.82092181
170	11.1016516
180	11.37853392
190	11.65162152
200	11.92096639
210	12.18661983
220	12.44863243
230	12.70705409
240	12.96193403
250	13.21332078
260	13.46126222
270	13.70580557
280	14.40131944
290	15.18163092
300	16.06399221
310	17.07079287
320	18.23165671
330	19.58666915
340	21.1915231
350	23.12607298
360	25.5092859
370	28.52703097
380	32.48788454
390	37.94706067
400	46.02209897
404	50.4777176

Figure 3.7

% Carbon Recovered

Fraction	TMK-NOM	MB-NOM	CT-NOM
<1K	51.7	44.2	35.9
1-3K	34.5	13.5	29.4
3-5K	3.2	16.5	8.7
>5K	10.6	25.8	28.7

Figure 3.8

% Carbon Recovered

Fraction	MB-NOM	CT-NOM
<1K	44.2	35.9
1-3K	13.5	29.4
3-5K	16.5	8.7
5-10K	9.7	4.5
10-30K	2.4	3.9
30-100K	8.2	11.4
>100K	5.5	6.1

Figure 4.1

	TMK-NOM	MB-NOM	CT-NOM
Hydrophilic	63.6	34.1	39.2
Hydrophobic	36.4	65.9	60.8

Figure 5-3.

As-received NF-PES-10		1-min UV		10-min UV	
Pressure kPa	Flux(L/m2/h)	Pressure kPa	Flux(L/m2/h)	Pressure kPa	Flux(L/m2/h)
201.6160714	23.62010974	201.6160714	30.3006231	62.03571429	17.58284767
339.4732143	40.77089404	339.4732143	52.08591667	130.9642857	37.81426313
477.3303571	58.78580507	477.3303571	74.24321099	201.6160714	58.83811768
546.2589286	67.60338521	546.2589286	85.8023591	270.5446429	79.249721
615.1875	77.11265423	594.5089286	94.55600161	322.2410714	95.82506665

Figure 5-5.

As-received NF-PES-10			1-min UV		
Time (min)	Flux (L/m2/h)	J/Jo	Time (min)	Flux (L/m2/h)	J/Jo
0	45.39571579	1	0	45.09734019	1
10	45.09346519	0.993341869	10	44.42308885	0.985048977
15	44.55871412	0.9815621	22	44.04721309	0.976714212
20	44.22158844	0.974135723	30	43.90771282	0.973620897
25	43.83408767	0.965599659	40	43.67133734	0.968379447
30	43.55508711	0.959453692	50	43.37683675	0.961849115
35	43.46208692	0.957405036	60	43.28383657	0.959786905
40	43.26446153	0.953051643	70	43.13658627	0.956521739
46	43.14046128	0.950320102	80	43.1017112	0.95574841
50	43.02033604	0.947673922	90	42.79171058	0.948874377
55	42.86146072	0.944174136	100	42.69096038	0.946640316
60	42.54371009	0.937174563	110	42.51271003	0.942687747
70	42.57471015	0.937857448	120	42.47783496	0.941914418
80	42.501085	0.936235595	135	42.25308451	0.936930744
90	42.30733461	0.931967563	150	42.001209	0.931345592
100	42.22595945	0.930174989	165	42.08258417	0.933150026
110	42.19108438	0.929406743	180	42.02058404	0.931775219
120	42.14458429	0.928382416	195	41.51683303	0.920604915
135	42.13295927	0.928126334	210	41.5982082	0.922409349
150	42.00508401	0.925309432	225	41.38895778	0.917769376
165	41.71058342	0.918822023	240	41.36183272	0.917167898
180	41.48195796	0.913785745	255	41.20683241	0.913730882
195	41.23783248	0.908408024	270	41.1487073	0.912442
210	41.07508215	0.904822877	285	41.20295741	0.913644956
225	41.00920702	0.903371746	300	40.94333189	0.907887953
240	40.80383161	0.898847631	320	40.90458181	0.907028699
255	40.70695641	0.896713615	340	40.77283155	0.904107235
270	40.61395623	0.894664959	360	40.59458119	0.900154666
285	40.48995598	0.891933419	380	40.47058094	0.897405052
300	40.21870544	0.885958173	400	40.43183086	0.896545798
320	39.69557939	0.874434486	420	40.24195548	0.892335453
340	39.59095418	0.872129748	440	40.16445533	0.890616944
360	39.45532891	0.869142125	460	40.12958026	0.889843616
380	39.31970364	0.866154503	480	40.0482051	0.888039182
400	38.92832786	0.857533077	500	39.92807986	0.885375494
420	38.7500775	0.853606487	520	39.44370389	0.874634817
440	38.47107694	0.847460521	540	39.12595325	0.867588933
460	38.32382665	0.844216816	560	38.99032798	0.864581543
480	38.16882634	0.84080239	580	38.87020274	0.861917855
500	38.01770104	0.837473325	600	38.40907682	0.851692731
520	37.78132556	0.832266325			
540	37.52945006	0.826717883			
560	37.26982454	0.82099872			
580	37.002449	0.815108835			
600	36.9016988	0.812889458			

Fig 5-5 Continued

10-min UV

Time (min)	Flux (L/m2/h)	J/Jo
0	45.76771654	1
10	45.68634137	0.998221996
20	45.12834026	0.986029972
30	44.99271499	0.983066633
40	44.56646413	0.973753281
50	44.14021328	0.964439929
60	44.0975882	0.963508594
70	44.1479633	0.964609263
80	44.2487135	0.9668106
90	44.17508835	0.96520193
100	44.22158844	0.966217932
110	44.17121334	0.965117264
120	43.98133796	0.960968589
135	44.00458801	0.96147659
150	44.04721309	0.962407925
165	43.96583793	0.960629921
180	43.88446277	0.958851918
195	43.7488375	0.955888578
210	43.61708723	0.953009906
225	43.46983694	0.949792566
240	43.33808668	0.946913894
255	43.29546159	0.945982559
270	43.22958646	0.944543222
285	43.27996156	0.945643891
300	43.22571145	0.944458556
320	43.22958646	0.944543222
340	43.17146134	0.94327322
360	43.14433629	0.942680552
380	42.82658565	0.935737871
400	42.71808544	0.9333672
420	42.62508525	0.931335196
440	42.52821006	0.929218525
460	42.50496001	0.928710524
480	42.50883502	0.928795191
500	42.21433443	0.922360511
520	41.55945812	0.908051816
540	41.26495753	0.901617137
560	41.20295741	0.900262467
580	41.23008246	0.900855135
600	41.26883254	0.901701803

Figure 5-9 Dip method

As-received NF-PES-10

Time (min)	Flux (L/m2/h)	J/Jo
0	45.39571579	1
10	45.09346519	0.993341869
15	44.55871412	0.9815621
20	44.22158844	0.974135723
25	43.83408767	0.965599659
30	43.55508711	0.959453692
35	43.46208692	0.957405036
40	43.26446153	0.953051643
46	43.14046128	0.950320102
50	43.02033604	0.947673922
55	42.86146072	0.944174136
60	42.54371009	0.937174563
70	42.57471015	0.937857448
80	42.501085	0.936235595
90	42.30733461	0.931967563
100	42.22595945	0.930174989
110	42.19108438	0.929406743
120	42.14458429	0.928382416
135	42.13295927	0.928126334
150	42.00508401	0.925309432
165	41.71058342	0.918822023
180	41.48195796	0.913785745
195	41.23783248	0.908408024
210	41.07508215	0.904822877
225	41.00920702	0.903371746
240	40.80383161	0.898847631
255	40.70695641	0.896713615
270	40.61395623	0.894664959
285	40.48995598	0.891933419
300	40.21870544	0.885958173
320	39.69557939	0.874434486
340	39.59095418	0.872129748
360	39.45532891	0.869142125
380	39.31970364	0.866154503
400	38.92832786	0.857533077
420	38.7500775	0.853606487
440	38.47107694	0.847460521
460	38.32382665	0.844216816
480	38.16882634	0.84080239
500	38.01770104	0.837473325
520	37.78132556	0.832266325
540	37.52945006	0.826717883
560	37.26982454	0.82099872
580	37.002449	0.815108835
600	36.9016988	0.812889458

10-s UV NF-PES-10

Time (min)	Flux (L/m2/h)	J/Jo
0	44.61296423	1
10	43.57058714	0.976635108
20	42.58633517	0.954573091
30	42.38095976	0.9499696
40	41.98958398	0.941196908
50	41.32308265	0.926257274
60	40.76508153	0.913749674
70	40.42020584	0.906019283
80	40.07920516	0.898375749
90	40.10633021	0.898983757
100	39.88545477	0.894032832
110	39.91257983	0.894640841
120	39.60257921	0.887692174
135	39.19182838	0.878485191
150	39.19182838	0.878485191
165	39.01745303	0.874576566
180	38.93995288	0.872839399
195	38.94382789	0.872926257
210	38.80432761	0.869799357
225	38.81595263	0.870059932
240	38.45557691	0.861982107
255	38.40907682	0.860939807
270	37.97507595	0.851211674
285	37.91307583	0.84982194
300	37.4480749	0.83939894
320	37.29307459	0.835924607
340	37.06832414	0.830886824
360	36.88619877	0.826804482
380	36.67307335	0.822027274
400	36.87069874	0.826457049
420	36.81257363	0.825154174
440	36.44444789	0.816902632
460	36.43282287	0.816642057
480	36.33982268	0.814557457
500	36.34369769	0.814644315
520	36.32819766	0.814296882
540	36.43282287	0.816642057
560	36.26619753	0.812907148
580	36.13057226	0.809867107
600	35.77407155	0.80187614

Figure 5-9 Dip method

60-s UV			180-s UV		
Time (min)	Flux (L/m2/h)	J/Jo	Time (min)	Flux (L/m2/h)	J/Jo
0	45.04696509	1	0	45.26009052	1
10	44.86096472	0.995870968	15	44.90746481	0.992208904
20	44.7485895	0.993376344	20	44.55483911	0.984417808
30	44.57808916	0.989591398	30	43.71396243	0.965839041
40	44.40758882	0.985806452	40	43.19083638	0.954280822
50	44.43083886	0.986322581	50	43.27996156	0.95625
60	44.29521359	0.983311828	60	43.04358609	0.951027397
70	44.28746357	0.983139785	70	43.14046128	0.953167808
80	44.33396367	0.984172043	80	43.03196106	0.950770548
90	44.30683861	0.983569892	90	43.39621179	0.958818493
100	44.31846364	0.983827957	100	43.21408643	0.954794521
110	44.25258851	0.982365591	110	42.93896088	0.948715753
120	44.30683861	0.983569892	120	43.10558621	0.95239726
135	44.36496373	0.984860215	135	42.78008556	0.945205479
150	44.30296361	0.983483871	150	42.87308575	0.947260274
165	44.34171368	0.984344086	165	43.02808606	0.950684932
180	44.38433877	0.985290323	180	42.85371071	0.946832192
195	44.22158844	0.981677419	195	42.65608531	0.942465753
210	44.02783806	0.977376344	210	42.45458491	0.938013699
225	44.1014632	0.979010753	225	42.21045942	0.932619863
240	43.91546283	0.97488172	240	42.16783434	0.931678082
255	43.67133734	0.969462366	255	42.03220906	0.928681507
270	43.63646227	0.968688172	270	42.15620931	0.931421233
285	43.68296237	0.96972043	285	42.0515841	0.929109589
300	43.71008742	0.970322581	300	42.01670903	0.928339041
320	43.40396181	0.963526882	320	42.24533449	0.933390411
340	43.26446153	0.960430108	340	41.95858392	0.927054795
360	42.79558559	0.950021505	360	41.22620745	0.910873288
380	42.77621055	0.949591398	380	41.05958212	0.907191781
400	42.97383595	0.953978495	400	40.67983136	0.89880137
420	42.83046066	0.950795699	420	40.47445595	0.894263699
440	42.60958522	0.945892473	440	40.36983074	0.891952055
460	42.46620993	0.942709677	460	40.24195548	0.889126712
480	42.54371009	0.944430108	480	40.36983074	0.891952055
500	42.29183458	0.93883871	500	40.28845558	0.89015411
520	42.42745985	0.941849462	520	40.24583049	0.889212329
540	42.46620993	0.942709677	540	39.79245458	0.879195205
560	42.19495939	0.936688172	560	39.61807924	0.875342466
580	42.17945936	0.936344086	580	39.43595387	0.871318493
600	42.16008432	0.935913978	600	39.4514539	0.871660959

UV irradiated only

Figure 5-10

As-received NF-PES-10		1-min UV	10-min UV
Time (min)	% DOC (Feed)	% DOC (Feed)	% DOC (Feed)
58	54.63539697	55.17142411	28.29766399
120	53.62191396	54.13604429	27.727091
215	55.53389393	55.62424417	26.19227239
305	57.35342265	57.30323974	29.06009006
425	59.52421415	59.69453579	28.66641948
500	61.8759053	60.69673039	30.71699561
595	63.01949297	61.3569514	30.20372867
Average	**57.93774856**	**57.71188141**	**28.69489446**
Jom/Jo	**0.812889458**	**0.851692731**	**0.901701803**

Dip technique

	10s UV	60s UV	180s UV
Time (min)	% DOC (Feed)	% DOC (Feed)	% DOC (Feed)
58	71.9956501	50.15758425	27.47420597
120	70.51100915	47.14974532	26.42582619
215	71.45733918	48.97956384	27.6671975
305	72.9065499	49.80716803	29.471357
425	73.90659674	50.45537824	30.87832749
500	74.37290429	50.6084611	31.16345691
595	75.220944	51.50662692	31.94413877
Average	**72.91014191**	**49.80921824**	**29.28921569**
Jom/Jo	**0.80187614**	**0.935913978**	**0.871660959**

Figure 6-1.

NOM-Free (salt only)

5 mg/L NOM

Time (min)	Flux (L/m2/h)	J/Jo	Time (min)	Flux (L/m2/h)	J/Jo
0	44.81058962	1	0	45.95759192	1
10	43.08621117	0.961518506	10	45.05859012	0.980438449
20	40.78445657	0.910152196	20	43.72171244	0.951349073
30	38.79270259	0.865703909	30	42.88083576	0.933052277
40	37.49457499	0.836734694	40	40.97820696	0.891652614
50	36.43669787	0.813126946	50	39.501829	0.859527825
60	35.36719573	0.789259772	60	38.66482733	0.841315346
70	34.5495691	0.77101349	70	37.71157542	0.820573356
80	34.43719387	0.768505707	80	36.96757394	0.804384486
90	33.86369273	0.755707368	90	36.51032302	0.794435076
100	34.01481803	0.759079903	100	36.14607229	0.786509275
110	33.53431707	0.74835697	110	35.58032116	0.774198988
120	33.23594147	0.741698374	120	35.25482051	0.767116358
135	33.46456693	0.746800415	135	34.95256991	0.760539629
150	33.17394135	0.74031477	150	34.62319425	0.753372681
165	33.01506603	0.736769284	165	34.11169322	0.742242833
180	32.93369087	0.734953303	180	34.13494327	0.742748735
195	33.10806622	0.73884469	195	33.92181784	0.738111298
210	33.06931614	0.737979938	210	33.67769236	0.732799325
225	32.89494079	0.734088551	225	33.2979416	0.724536256
240	33.17006634	0.740228295	240	33.08481617	0.71989882
255	33.08869118	0.738412314	255	32.81744063	0.714080944
270	33.34056668	0.744033207	270	32.71281543	0.711804384
285	33.22431645	0.741438948	285	32.73606547	0.712310287
300	33.48006696	0.747146316	300	32.7515655	0.712647555
320	33.14681629	0.739709443	320	32.62756526	0.70994941
340	33.37544175	0.744811484	340	32.62369025	0.709865093
360	33.35606671	0.744379108	360	32.39118978	0.704806071
380	33.32119164	0.74360083	380	32.46093992	0.706323777
400	33.17394135	0.74031477	400	32.16256433	0.699831366
420	33.34056668	0.744033207	420	32.14706429	0.699494098
440	33.18169136	0.740487721	440	32.15868932	0.699747049
460	33.16231632	0.740055344	460	31.98431397	0.695952782
480	33.12744125	0.739277067	480	31.63943828	0.688448567
500	33.25919152	0.742217226	500	31.53868808	0.686256324
520	33.27856656	0.742649602	520	31.46506293	0.6846543
540	33.31731663	0.743514355	540	31.37981276	0.682799325
560	33.39481679	0.74524386	560	31.47668795	0.684907251
580	33.3018166	0.743168454	580	31.55806312	0.686677909
600	33.34444169	0.744119682	600	31.40693781	0.683389545

Figure 6-1. continued

10 mg/L NOM

Time (min)	Flux (L/m2/h)	J/Jo
0	45.2988406	1
25	43.02421105	0.949786142
30	41.86558373	0.924208725
43	38.93607787	0.859538067
45	38.33932668	0.846364414
47	38.11070122	0.841317365
50	37.71932544	0.832677502
53	36.73894848	0.811035073
76	34.59606919	0.763729683
80	33.8016926	0.746193328
85	33.42581685	0.737895637
95	32.99569099	0.728400342
100	33.15844132	0.731993157
105	32.87944076	0.725834046
110	32.44543989	0.716253208
120	32.17806436	0.710350727
130	31.97268895	0.705816938
140	31.90293881	0.70427716
160	31.38756278	0.692899914
185	31.08531217	0.686227545
205	30.73268647	0.678443114
230	30.21731043	0.667065868
250	30.19018538	0.666467066
270	30.19406039	0.666552609
290	30.19018538	0.666467066
310	30.2521855	0.667835757
335	30.16306033	0.665868263
355	29.91118482	0.660307956
375	29.89180978	0.65988024
395	29.86468473	0.659281437
415	29.52368405	0.651753636
435	29.35318371	0.647989735
465	29.49655899	0.651154833
485	29.75618451	0.656886228
515	29.72130944	0.656116339
535	29.43455887	0.649786142
555	29.31443363	0.647134303
575	29.30280861	0.646877673
600	29.27568355	0.646278871

25 mg/L NOM

Time (min)	Flux (L/m2/h)	J/Jo
0	45.43834088	1
10	37.77357555	0.831315026
20	35.39044578	0.778867474
30	32.05793912	0.705526181
40	28.97730795	0.637728126
50	26.91580383	0.592358861
60	25.47817596	0.560719768
70	24.38542377	0.536670646
80	23.59492219	0.51927341
90	22.91292083	0.504264029
100	22.30841962	0.490960259
110	22.002294	0.484223094
120	21.44041788	0.471857411
135	20.58404117	0.453010404
150	20.0996652	0.442350333
165	19.92528985	0.438512707
180	19.49516399	0.429046563
195	19.18516337	0.422224117
210	19.01466303	0.418471772
225	18.62716225	0.409943715
240	18.499287	0.407129456
255	18.23191146	0.401245096
270	18.24741149	0.401586219
285	17.90641081	0.394081528
300	17.83278567	0.392461197
320	17.63516027	0.388111888
340	17.29028458	0.380521917
360	16.98028396	0.373699471
380	17.03065906	0.374808119
400	16.87178374	0.371311615
420	16.70515841	0.367644551
440	16.61990824	0.365768378
460	16.66253333	0.366706464
480	16.56953314	0.364659731
500	16.59665819	0.365256695
520	16.45328291	0.362101313
540	16.12778226	0.354937745
560	15.94178188	0.350844278
580	16.05803212	0.353402695
600	15.92628185	0.350503155

Figure 6-2.

5 mg/L	model	10mg/L		25 mg/L	
t	cp (adhesion)	t	cp(adhesion)	t	cp(adhesion)
0.00	0.00	0.00	0.00	0.00	0.00
10.00	7.47	10.00	13.24	10.00	28.45
20.00	12.99	20.00	23.36	20.00	49.40
30.00	17.07	30.00	31.11	30.00	64.84
40.00	20.08	40.00	37.04	40.00	76.20
50.00	22.30	50.00	41.58	50.00	84.58
60.00	23.94	60.00	45.05	60.00	90.74
70.00	25.15	70.00	47.70	70.00	95.29
80.00	26.05	80.00	49.73	80.00	98.63
90.00	26.71	90.00	51.28	90.00	101.10
100.00	27.19	100.00	52.47	100.00	102.91
110.00	27.55	110.00	53.38	110.00	104.25
120.00	27.82	120.00	54.08	120.00	105.23
130.00	28.02	130.00	54.61	130.00	105.96
140.00	28.16	140.00	55.02	140.00	106.49
150.00	28.27	150.00	55.33	150.00	106.89
160.00	28.35	160.00	55.57	160.00	107.18
170.00	28.41	170.00	55.75	170.00	107.39
180.00	28.45	180.00	55.89	180.00	107.55
190.00	28.48	190.00	56.00	190.00	107.66
200.00	28.50	200.00	56.08	200.00	107.75
210.00	28.52	210.00	56.14	210.00	107.81
220.00	28.54	220.00	56.19	220.00	107.86
230.00	28.54	230.00	56.23	230.00	107.89
240.00	28.55	240.00	56.25	240.00	107.92
250.00	28.56	250.00	56.27	250.00	107.94
260.00	28.56	260.00	56.29	260.00	107.95
270.00	28.56	270.00	56.30	270.00	107.96
280.00	28.57	280.00	56.31	280.00	107.97
290.00	28.57	290.00	56.32	290.00	107.97
300.00	28.57	300.00	56.33	300.00	107.98
310.00	28.57	310.00	56.33	310.00	107.98
320.00	28.57	320.00	56.33	320.00	107.98
330.00	28.57	330.00	56.34	330.00	107.98
340.00	28.57	340.00	56.34	340.00	107.98
350.00	28.57	350.00	56.34	350.00	107.98
360.00	28.57	360.00	56.34	360.00	107.98
370.00	28.57	370.00	56.34	370.00	107.99
380.00	28.57	380.00	56.34	380.00	107.99
390.00	28.57	390.00	56.34	390.00	107.99

Figure 6.2 continued

Experimental

400.00	28.57	400.00	56.34	400.00	107.99
410.00	28.57	410.00	56.34	410.00	107.99
420.00	28.57	420.00	56.34	420.00	107.99
430.00	28.57	430.00	56.34	430.00	107.99
440.00	28.57	440.00	56.34	440.00	107.99
450.00	28.57	450.00	56.34	450.00	107.99
460.00	28.57	460.00	56.34	460.00	107.99
470.00	28.57	470.00	56.34	470.00	107.99
480.00	28.57	480.00	56.34	480.00	107.99
490.00	28.57	490.00	56.34	490.00	107.99
500.00	28.57	500.00	56.34	500.00	107.99
510.00	28.57	510.00	56.34	510.00	107.99
520.00	28.57	520.00	56.34	520.00	107.99
530.00	28.57	530.00	56.34	530.00	107.99
540.00	28.57	540.00	56.34	540.00	107.99
550.00	28.57	550.00	56.34	550.00	107.99
560.00	28.57	560.00	56.34	560.00	107.99
570.00	28.57	570.00	56.34	570.00	107.99
580.00	28.57	580.00	56.34	580.00	107.99
590.00	28.57	590.00	56.34	590.00	107.99
600.00	28.57	600.00	56.34	600.00	107.99

5 mg/L

t	Measured
60.00	18.43
120.00	24.83
210.00	27.64
300.00	29.74
420.00	29.74
500.00	30.51
600.00	30.35

10 mg/L

t	Measured
60.00	34.66
210.00	56.14
300.00	56.67
420.00	59.42
500.00	57.27
600.00	57.37

25 mg/L

t	Measured
60.00	54.33
120.00	75.56
210.00	94.77
300.00	108.65
420.00	115.48
500.00	125.48
600.00	122.49

Figure 6-3.

5 mg/L		10 mg/L		25 mg/L	
Time (min)	Md mg/m^2	Time (min)	Md mg/m^2	Time (min)	Md mg/m^2
0	0	0	0	0	0
10	58.84503754	25	100.6153239	10	295.4266073
20	70.56022036	30	147.2228173	20	376.1433133
30	81.1416684	43	122.3273094	30	439.151263
40	87.53478964	45	124.7665655	40	501.946279
50	91.90340378	47	130.5881728	50	556.9696884
60	97.79468924	50	133.4868293	60	619.6493883
70	104.0074068	53	184.7735328	70	677.0393409
80	111.063353	76	179.2917667	80	730.2322417
90	118.8299375	80	187.5053212	90	778.5074924
100	126.5149675	85	204.1553542	100	822.3675205
110	134.5375765	95	208.2061525	110	862.2024518
120	136.6873014	100	214.7815418	120	920.5656132
135	138.6818227	105	220.665592	135	988.7007944
150	147.9649219	110	235.3507922	150	1055.521247
165	156.8867463	120	245.2105369	165	1105.972442
180	165.7541565	130	253.4154468	180	1154.527342
195	174.2244357	140	274.4523669	195	1195.254307
210	172.7432486	160	287.5630279	210	1237.835052
225	174.8656867	185	288.775418	225	1280.12389
240	181.5778228	205	290.3897433	240	1314.733139
255	187.8416876	230	298.8310663	255	1354.826129
270	194.0042396	250	309.3193572	270	1387.82875
285	200.4168292	270	319.0610542	285	1423.432678
300	203.3076878	290	327.3032368	300	1474.165738
320	210.2345206	310	339.2499279	320	1522.025019
340	217.2183188	335	345.0754946	340	1566.100154
360	223.9648072	355	350.2878725	360	1607.5214
380	230.6540372	375	354.7859635	380	1646.727544
400	236.7147297	395	358.0889035	400	1692.83473
420	243.1241411	415	358.0261503	420	1732.109216
440	247.4499961	435	369.5382439	440	1756.832276
460	252.8759636	465	374.0363433	460	1805.383428
480	257.8807604	485	381.2507455	480	1856.532639
500	261.422669	515	394.1060199	500	1848.875012
520	267.0149994	535	401.9175555	520	1880.503371
540	272.2683125	555	409.7157513	540	1932.797852
560	277.8104427	575	418.9330235	560	1987.644342
580	283.2971102			580	2010.473678

Figure 6-4.

New membrane		After compaction	Flushing	Cleaning
Pressure (kPa)	Flux(L/m2/h)	Flux(L/m2/h)	Flux(L/m2/h)	Flux (L/m2/h)
201.6160714	23.62592225	23.37598425	20.66154132	21.95966892
339.4732143	39.35264121	38.82370265	34.48175646	36.50451051
477.3303571	55.39129828	54.56398413	48.36203422	51.37679025
546.2589286	63.87562775	62.81581313	55.00379751	58.88461777
615.1875	71.19357989	70.84482919	61.82768616	66.37500775

Figure 6-5.

		Mass/area
NOM (mg/L)	J/Jo	(mg/m^2)
0	0.944441407	0
5	0.939028585	72.537793
10	0.92361089	129.1959181
25	0.779510457	611.1405381

Figure 6-6.

	5 mg/L	10mg/L	25 mg/L
Mass solution	% Mass DOC	% Mass DOC	% Mass DOC
Concentrate	76.50797383	78.81154814	53.2493091
Permeate	2.508560746	1.814279994	1.968312908
Mass DOC fluid	13.86043923	11.02311287	17.53389771
Cake	2.430204748	3.514042594	13.4511449
Clean	1.076222493	1.145517602	3.152287293
Left	3.616598958	3.691498804	10.64504808

Figure 6-7.

NF-70 membrane			NF-PES-10		
Time (min)	Flux (L/m2/h)	J/Jo	Time (min)	Flux (L/m2/h)	J/Jo
0	45.2988406	1	0	45.39571579	1
25	43.02421105	0.949786142	10	45.09346519	0.993341869
30	41.86558373	0.924208725	15	44.55871412	0.9815621
33	41.15258231	0.908468777	20	44.22158844	0.974135723
38	39.8002046	0.8786142	25	43.83408767	0.965599659
43	38.93607787	0.859538067	30	43.55508711	0.959453692
45	38.33932668	0.846364414	35	43.46208692	0.957405036
47	38.11070122	0.841317365	40	43.26446153	0.953051643
50	37.71932544	0.832677502	46	43.14046128	0.950320102
53	36.73894848	0.811035073	50	43.02033604	0.947673922
65	34.91769484	0.770829769	55	42.86146072	0.944174136
76	34.59606919	0.763729683	60	42.54371009	0.937174563
80	33.8016926	0.746193328	70	42.57471015	0.937857448
85	33.42581685	0.737895637	80	42.501085	0.936235595
92	33.46069192	0.738665526	90	42.30733461	0.931967563
95	32.99569099	0.728400342	100	42.22595945	0.930174989
100	33.15844132	0.731993157	110	42.19108438	0.929406743
105	32.87944076	0.725834046	120	42.14458429	0.928382416
110	32.44543989	0.716253208	135	42.13295927	0.928126334
120	32.17806436	0.710350727	150	42.00508401	0.925309432
130	31.97268895	0.705816938	165	41.71058342	0.918822023
140	31.90293881	0.70427716	180	41.48195796	0.913785745
150	31.27131254	0.690333618	195	41.23783248	0.908408024
160	31.38756278	0.692899914	210	41.07508215	0.904822877
185	31.08531217	0.686227545	225	41.00920702	0.903371746
205	30.73268647	0.678443114	240	40.80383161	0.898847631
230	30.21731043	0.667065868	255	40.70695641	0.896713615
250	30.19018538	0.666467066	270	40.61395623	0.894664959
270	30.19406039	0.666552609	285	40.48995598	0.891933419
290	30.19018538	0.666467066	300	40.21870544	0.885958173
310	30.2521855	0.667835757	320	39.69557939	0.874434486
335	30.16306033	0.665868263	340	39.59095418	0.872129748
355	29.91118482	0.660307956	360	39.45532891	0.869142125
375	29.89180978	0.65988024	380	39.31970364	0.866154503
395	29.86468473	0.659281437	400	38.92832786	0.857533077
415	29.52368405	0.651753636	420	38.7500775	0.853606487
435	29.35318371	0.647989735	440	38.47107694	0.847460521
465	29.49655899	0.651154833	460	38.32382665	0.844216816
485	29.75618451	0.656886228	480	38.16882634	0.84080239
515	29.72130944	0.656116339	500	38.01770104	0.837473325
535	29.43455887	0.649786142	520	37.78132556	0.832266325
555	29.31443363	0.647134303	540	37.52945006	0.826717883
575	29.30280861	0.646877673	560	37.26982454	0.82099872
600	29.27568355	0.646278871	580	37.002449	0.815108835
			600	36.9016988	0.812889458

Figure 6-7. Continued

NTR-7450

Time (min)	Flux (L/m2/h)	J/Jo
0	45.80259161	1
7	45.30659061	0.989170897
12	44.7524645	0.977072758
23	43.54733709	0.950761421
33	43.2024614	0.94323181
40	43.08233616	0.940609137
44	42.99321099	0.938663283
50	42.67158534	0.931641286
60	42.59021018	0.929864636
70	42.31895964	0.92394247
80	42.26083452	0.922673435
90	41.99733399	0.916920474
100	41.89658379	0.914720812
110	41.76870854	0.911928934
120	41.54395809	0.907021997
135	41.48970798	0.905837563
150	41.45870792	0.905160745
165	41.29208258	0.901522843
180	41.13708227	0.898138748
195	40.9007068	0.892978003
210	40.84258169	0.891708968
225	40.63720627	0.887225042
240	40.39695579	0.881979695
255	40.12183024	0.875972927
270	39.78470457	0.868612521
285	39.40495381	0.860321489
300	39.2499535	0.856937394
320	38.81982764	0.847546531
340	38.63770228	0.84357022
360	38.16882634	0.833333333
380	37.99057598	0.829441624
400	37.80845062	0.825465313
420	37.74257549	0.824027073
440	37.15744931	0.811252115
460	37.00632401	0.807952623
480	36.58782318	0.798815567
500	36.31269763	0.792808799
520	36.17707235	0.789847716
540	36.06857214	0.787478849
560	35.73919648	0.780287648
580	35.36332073	0.772081218
600	35.14244528	0.767258883

Figure 6-8. Model

NF-70		NTR-7450		NF-PES-10	
t	cp(adhesion)	t	cp(adhesion)	t	cp(adhesion)
0.00	0.00	0.00	0.00	0.00	0.00
10.00	13.24	10.00	15.44	10.00	13.71
20.00	23.36	20.00	25.92	20.00	21.85
30.00	31.11	30.00	33.03	30.00	26.69
40.00	37.04	40.00	37.85	40.00	29.56
50.00	41.58	50.00	41.13	50.00	31.26
60.00	45.05	60.00	43.35	60.00	32.27
70.00	47.70	70.00	44.86	70.00	32.87
80.00	49.73	80.00	45.88	80.00	33.23
90.00	51.28	90.00	46.57	90.00	33.44
100.00	52.47	100.00	47.05	100.00	33.57
110.00	53.38	110.00	47.37	110.00	33.64
120.00	54.08	120.00	47.58	120.00	33.69
130.00	54.61	130.00	47.73	130.00	33.71
140.00	55.02	140.00	47.83	140.00	33.73
150.00	55.33	150.00	47.90	150.00	33.74
160.00	55.57	160.00	47.94	160.00	33.75
170.00	55.75	170.00	47.97	170.00	33.75
180.00	55.89	180.00	48.00	180.00	33.75
190.00	56.00	190.00	48.01	190.00	33.75
200.00	56.08	200.00	48.02	200.00	33.75
210.00	56.14	210.00	48.03	210.00	33.75
220.00	56.19	220.00	48.03	220.00	33.75
230.00	56.23	230.00	48.03	230.00	33.75
240.00	56.25	240.00	48.04	240.00	33.75
250.00	56.27	250.00	48.04	250.00	33.75
260.00	56.29	260.00	48.04	260.00	33.75
270.00	56.30	270.00	48.04	270.00	33.75
280.00	56.31	280.00	48.04	280.00	33.75
290.00	56.32	290.00	48.04	290.00	33.75
300.00	56.33	300.00	48.04	300.00	33.75
310.00	56.33	310.00	48.04	310.00	33.75
320.00	56.33	320.00	48.04	320.00	33.75
330.00	56.34	330.00	48.04	330.00	33.75
340.00	56.34	340.00	48.04	340.00	33.75
350.00	56.34	350.00	48.04	350.00	33.75
360.00	56.34	360.00	48.04	360.00	33.75
370.00	56.34	370.00	48.04	370.00	33.75
380.00	56.34	380.00	48.04	380.00	33.75
390.00	56.34	390.00	48.04	390.00	33.75
400.00	56.34	400.00	48.04	400.00	33.75
410.00	56.34	410.00	48.04	410.00	33.75
420.00	56.34	420.00	48.04	420.00	33.75

Figure 6-8. Continued

430.00	56.34	430.00	48.04	430.00	33.75
440.00	56.34	440.00	48.04	440.00	33.75
450.00	56.34	450.00	48.04	450.00	33.75
460.00	56.34	460.00	48.04	460.00	33.75
470.00	56.34	470.00	48.04	470.00	33.75
480.00	56.34	480.00	48.04	480.00	33.75
490.00	56.34	490.00	48.04	490.00	33.75
500.00	56.34	500.00	48.04	500.00	33.75
510.00	56.34	510.00	48.04	510.00	33.75
520.00	56.34	520.00	48.04	520.00	33.75
530.00	56.34	530.00	48.04	530.00	33.75
540.00	56.34	540.00	48.04	540.00	33.75
550.00	56.34	550.00	48.04	550.00	33.75
560.00	56.34	560.00	48.04	560.00	33.75
570.00	56.34	570.00	48.04	570.00	33.75
580.00	56.34	580.00	48.04	580.00	33.75
590.00	56.34	590.00	48.04	590.00	33.75
600.00	56.34	600.00	48.04	600.00	33.75

Concentrate

NF-70		NTR-7450		NF-PES-10	
Time	DOC (mg/L)	Time	DOC (mg/L)	Time	DOC (mg/L)
60.00	34.66	60.00	32.46	60.00	23.71
210.00	56.14	210.00	47.62	120.00	29.39
300.00	56.67	300.00	49.73	210.00	32.66
420.00	59.42	420.00	49.49	300.00	34.50
500.00	57.27	500.00	49.68	420.00	36.52
600.00	57.37	600.00	50.49	500.00	37.60
				600.00	38.77

Permeate

NF-70		NTR-7450		NF-PES-10	
Time	DOC (mg/L)	Time	DOC (mg/L)	Time	DOC (mg/L)
0.00	0.00	0.00	0.00	0.00	0.00
60.00	0.21	60.00	1.68	60.00	4.09
210.00	0.21	210.00	1.71	120.00	4.19
300.00	0.19	300.00	1.74	210.00	4.01
420.00	0.22	420.00	1.58	300.00	4.07
500.00	0.18	500.00	1.55	420.00	3.86
600.00	0.15	600.00	1.56	500.00	3.64
				600.00	3.53

Figure 6.9

I.S. = 0.18 M ; 12 mg/L TMK NOM

Unfractionated			Hydrophobic		
Time (min)	Flux (L/m2/h)	J/Jo	Time (min)	Flux (L/m2/h)	J/Jo
0	45.01209002	1	0	44.99658999	1
10	36.42119784	0.809142562	10	37.84332569	0.841026524
20	31.55806312	0.701101928	20	34.17369335	0.759472959
30	29.47718395	0.65487259	30	31.47668795	0.699534964
40	27.63655527	0.613980716	40	30.03518507	0.667499139
50	26.54380309	0.589703857	50	29.14393329	0.647692043
60	25.67967636	0.570506198	60	27.98143096	0.6218567
70	25.1023002	0.557679063	70	27.44667989	0.609972442
80	24.61017422	0.546745868	80	27.03205406	0.600757837
90	24.5481741	0.545368457	90	26.69492839	0.593265587
100	24.19554839	0.537534435	100	26.16405233	0.581467447
110	23.65692231	0.525568182	110	25.501426	0.566741302
120	23.66079732	0.52565427	120	25.00155	0.555632105
135	23.47092194	0.52143595	135	24.72642445	0.54951774
150	23.37792176	0.519369835	150	24.66829934	0.548225973
165	22.93617087	0.509555785	165	24.48229896	0.544092318
180	22.96717093	0.51024449	180	24.34667369	0.541078195
195	22.91679583	0.509125344	195	24.31567363	0.540389252
210	22.69592039	0.50421832	210	24.1490483	0.536686187
225	22.39366979	0.497503444	225	24.2497985	0.53892525
240	22.23091946	0.493887741	240	24.1490483	0.536686187
255	22.22316945	0.493715565	255	23.92042284	0.531605236
270	22.07591915	0.490444215	270	23.79642259	0.528849466
285	21.95579391	0.487775482	285	23.8506727	0.530055115
300	22.11466923	0.491305096	300	23.4515469	0.521184981
320	21.98291897	0.488378099	320	23.5484221	0.523337926
340	22.07979416	0.490530303	340	23.31979664	0.518256976
360	22.06429413	0.49018595	360	23.34692169	0.5188598
380	21.94029388	0.487431129	380	23.22292145	0.51610403
400	21.74266849	0.483040634	400	22.99429599	0.51102308
420	21.75429351	0.483298898	420	22.71142042	0.50473648
440	21.45591791	0.47667011	440	22.47116994	0.499397175
460	21.53729307	0.478477961	460	22.32779466	0.496210816
480	21.46366793	0.476842287	480	22.32004464	0.496038581
500	21.52566805	0.478219697	500	22.06429413	0.490354805
520	21.49079298	0.477444904	520	22.02554405	0.489493627
540	21.57991816	0.479424931	540	21.8976688	0.48665174
560	21.56441813	0.479080579	560	21.998419	0.488890803
580	21.33191766	0.473915289	580	21.97516895	0.488374096
600	21.14591729	0.469783058	600	21.62254325	0.480537375

Figure 6-9. Continued

I.S. = 0.05 M; 10 mg/L TMK NOM

Hydrohilic TMK NOM			Unfractionated		
Time (min)	Flux (L/m2/h)	J/Jo	Time (min)	Flux (L/m2/h)	J/Jo
0	45.65534131	1	0	45.80259161	1
10	38.50982702	0.84349007	10	35.23932048	0.769373942
20	35.03782008	0.76744186	20	30.56218612	0.667258883
30	32.49969	0.711848583	30	28.22555645	0.616243655
40	31.1511873	0.682312001	40	26.70655341	0.583079526
50	29.77943456	0.652266169	50	25.48980098	0.556514382
60	29.03155806	0.635885249	60	24.89304979	0.543485618
70	28.72543245	0.629180105	70	24.3001736	0.530541455
80	27.95818092	0.612374809	80	23.53679707	0.513874788
90	27.49317999	0.602189781	90	23.04467109	0.503130288
100	27.10567921	0.593702258	100	22.92842086	0.500592217
110	26.88092876	0.588779494	110	22.70754542	0.495769882
120	26.3500527	0.577151587	120	22.67654535	0.495093063
135	26.28805258	0.575793583	135	22.66879534	0.494923858
150	25.86955174	0.566627058	150	22.47891996	0.490778342
165	25.78430157	0.564759803	165	22.37041974	0.488409475
180	25.60992622	0.560940418	180	22.32779466	0.487478849
195	25.53630107	0.559327788	195	22.21929444	0.485109983
210	25.38130076	0.555932779	210	22.0991692	0.48248731
225	25.41617583	0.556696656	225	21.98679397	0.480033841
240	25.38905078	0.556102529	240	21.98679397	0.480033841
255	25.06742513	0.549057885	255	21.84341869	0.476903553
270	24.98217496	0.54719063	270	21.88216876	0.477749577
285	24.87754976	0.544898998	285	21.77366855	0.475380711
300	24.72254945	0.541503989	300	21.49079298	0.469204738
320	24.38542377	0.534119844	320	21.37066774	0.466582064
340	24.12192324	0.528348328	340	21.22341745	0.463367174
360	24.12967326	0.528518078	360	21.20404241	0.462944162
380	24.16842334	0.529366831	380	20.998667	0.458460237
400	23.9475479	0.524528942	400	20.99479199	0.458375635
420	23.71892244	0.519521304	420	20.99479199	0.458375635
440	23.54067208	0.515617043	440	20.98316697	0.458121827
460	23.54454709	0.515701918	460	20.95991692	0.457614213
480	23.47092194	0.514089289	480	20.98704197	0.45820643
500	23.29654659	0.510269903	500	20.76229152	0.453299492
520	23.13379627	0.506705143	520	20.58404117	0.449407783
540	23.0989212	0.505941266	540	20.46391593	0.44678511
560	23.31592163	0.510694279	560	20.33991568	0.444077834
580	22.94004588	0.502461382	580	20.31279063	0.443485618
600	22.9516709	0.502716007	600	20.27404055	0.442639594

Figure 6-9. Continued I.S. = 0.05 M; 10 mg/L TMK NOM

Hydrophobic TMK			Hydrophilic TMK		
Time (min)	Flux (L/m2/h)	J/Jo	Time (min)	Flux (L/m2/h)	J/Jo
0	46.09321719	1	0	46.000217	1
10	33.11194122	0.718369063	10	34.3015686	0.745682756
20	27.001054	0.58579235	20	29.38030876	0.638699351
30	23.64529729	0.512988651	30	26.93517887	0.585544604
40	21.46754294	0.465741908	40	25.19142538	0.547637099
50	20.21591543	0.438587642	50	23.92429785	0.520090978
60	19.18903838	0.416309374	60	23.27329655	0.505938843
70	18.43728687	0.4	70	22.83929568	0.496504086
80	18.00716101	0.390668348	80	22.46729493	0.488417151
90	17.45303491	0.37864649	90	22.24254449	0.483531295
100	17.32903466	0.375956284	100	21.76591853	0.47316991
110	17.2011594	0.373182009	110	21.62641825	0.470137309
120	16.99190898	0.368642287	120	21.57991816	0.469126443
135	16.63540827	0.360907945	135	21.41716783	0.465588409
150	16.30603261	0.353762085	150	21.03354207	0.457248757
165	16.12778226	0.349894914	165	21.07616715	0.458175385
180	15.99215698	0.346952501	180	20.82041664	0.452615618
195	15.70540641	0.3407314	195	20.89404179	0.454216157
210	15.65890632	0.339722573	210	20.74291649	0.45093084
225	15.53490607	0.337032367	225	20.58016616	0.447392806
240	15.62015624	0.338881883	240	20.48716597	0.445371072
255	15.56978114	0.337788987	255	20.28566557	0.440990649
270	15.45740591	0.335350988	270	20.37479075	0.442928144
285	15.48065596	0.335855401	285	20.22366545	0.439642827
300	15.48453097	0.33593947	300	20.06866514	0.436273271
320	15.16290533	0.328961749	320	19.87878976	0.432145565
340	14.91490483	0.323581337	340	19.77803956	0.429955353
360	14.90715481	0.323413199	360	19.57653915	0.425574931
380	14.73277947	0.319630097	380	19.57653915	0.425574931
400	14.56615413	0.316015132	400	19.35566371	0.420773313
420	14.2484035	0.30912148	420	19.11153822	0.415466262
440	13.93840288	0.302395965	440	18.93716287	0.411675512
460	13.73302747	0.297940311	460	18.75503751	0.407716283
480	13.84152768	0.300294241	480	18.69303739	0.406368461
500	13.77177754	0.298781	500	18.73566247	0.407295089
520	14.15540331	0.307103825	520	18.98366297	0.412686379
540	14.28327857	0.3098781	540	18.999163	0.413023334
560	14.31040362	0.310466583	560	18.64266229	0.405273355
580	14.27165354	0.309625893	580	18.59228718	0.40417825
600	14.18640337	0.307776377	600	18.18928638	0.395417404

Figure 6-10. I.S. = 0.01 M; 10 mg/L MB NOM

Unfractionated MB			Hydrophobic MB		
Time (min)	Flux (L/m2/h)	J/Jo	Time (min)	Flux (L/m2/h)	J/Jo
0	45.27946556	1	0	45.62821626	1
10	39.74595449	0.877792041	10	41.67183334	0.91329087
20	37.51782504	0.828583654	20	39.21895344	0.859532909
30	35.49119598	0.783825417	30	37.07607415	0.812569002
40	34.78594457	0.768249893	40	35.76632153	0.783864119
50	34.02256805	0.751390672	50	35.01844504	0.767473461
60	33.46069192	0.7389816	60	34.34031868	0.752611465
70	33.35606671	0.736670946	70	33.36769174	0.731295117
80	32.8484407	0.725459991	80	32.69731539	0.716602972
90	32.66244032	0.721352161	90	32.65856532	0.715753715
100	32.72831546	0.722807018	100	32.42993986	0.7107431
110	32.45318991	0.716730852	110	32.3524397	0.709044586
120	32.68956538	0.72195122	120	32.13931428	0.704373673
135	32.67406535	0.7216089	135	31.87968876	0.698683652
150	32.59656519	0.719897304	150	31.62393825	0.693078556
165	32.48806498	0.71750107	165	31.43406287	0.688917197
180	32.32143964	0.713821138	180	31.43018786	0.688832272
195	32.51906504	0.718185708	195	31.42243784	0.68866242
210	32.39118978	0.715361575	210	31.4495629	0.6892569
225	32.31368963	0.713649979	225	31.23643747	0.684585987
240	32.14706429	0.709970047	240	31.17443735	0.683227176
255	32.13931428	0.709798887	255	31.00393701	0.679490446
270	32.04243908	0.707659392	270	31.02718705	0.68
285	32.08893918	0.70868635	285	31.3023126	0.686029724
300	32.07343915	0.708344031	300	31.42631285	0.688747346
320	31.97656395	0.706204536	320	31.29456259	0.685859873
340	31.85256371	0.703465982	340	31.08531217	0.681273885
360	31.82543865	0.702866923	360	30.79468659	0.674904459
380	31.74406349	0.701069748	380	30.96131192	0.678556263
400	31.77506355	0.701754386	400	30.64743629	0.671677282
420	31.77118854	0.701668806	420	30.84506169	0.676008493
440	31.63943828	0.698759093	440	30.79468659	0.674904459
460	31.75568851	0.701326487	460	30.7016864	0.672866242
480	31.61618823	0.698245614	480	30.2521855	0.663014862
500	31.75956352	0.701412067	500	30.22506045	0.662420382
520	31.47668795	0.695164741	520	29.98480997	0.657154989
540	31.45343791	0.694651262	540	29.66705933	0.650191083
560	31.43406287	0.694223363	560	29.61280923	0.649002123
580	31.40693781	0.693624305	580	29.41130882	0.644585987
600	31.52318805	0.696191699	600	29.48880898	0.646284501

Figure 6-10. Continued

I.S. = 0.05 M; 10 mg/L MB NOM

Hydrophilic MB			Unfractionated MB		
Time (min)	Flux (L/m2/h)	J/Jo	Time (min)	Flux (L/m2/h)	J/Jo
0	45.43446587	1	0	45.94209188	1
10	41.50520801	0.913518124	10	33.49556699	0.729082321
20	38.8508277	0.855095949	20	28.7990576	0.626855601
30	36.9016988	0.812196162	30	26.03617707	0.566717274
40	35.37107074	0.778507463	40	24.38542377	0.5307861
50	34.31319363	0.755223881	50	23.31592163	0.507506748
60	33.35994172	0.73424307	60	22.67654535	0.493589744
70	32.66631533	0.718976546	70	22.16504433	0.48245614
80	32.06956414	0.705842217	80	21.8976688	0.476636302
90	31.55418811	0.694498934	90	21.68066836	0.471912955
100	31.31781264	0.689296375	100	21.41716783	0.466177463
110	31.01168702	0.682558635	110	21.51016802	0.468201754
120	30.91093682	0.680341151	120	21.37841776	0.465334008
135	30.52343605	0.671812367	135	21.16529233	0.460695007
150	29.82205964	0.656375267	150	20.96766694	0.456393387
165	29.28343357	0.644520256	165	20.65766632	0.449645749
180	28.5975572	0.629424307	180	20.49491599	0.446103239
195	28.41543183	0.625415778	195	20.32829066	0.442476383
210	27.93105586	0.614754797	210	20.38254077	0.44365722
225	27.39242978	0.602899787	225	20.12679025	0.438090418
240	27.32655465	0.601449893	240	20.06091512	0.436656545
255	27.21030442	0.598891258	255	19.97953996	0.43488529
270	26.72592845	0.588230277	270	20.15391531	0.438680837
285	26.5476781	0.584307036	285	19.93691487	0.43395749
300	26.42367785	0.581577825	300	20.07254015	0.436909582
320	26.01292703	0.572537313	320	20.10741521	0.437668691
340	26.14080228	0.575351812	340	20.3011656	0.441885965
360	25.79592659	0.567761194	360	20.27016554	0.441211201
380	25.77267655	0.567249467	380	20.22754046	0.440283401
400	25.58667617	0.56315565	400	20.11516523	0.437837382
420	25.26892554	0.556162047	420	20.10741521	0.437668691
440	24.85817472	0.547121535	440	19.9524149	0.434294872
460	24.6024242	0.541492537	460	19.77416455	0.43041498
480	24.37767376	0.536545842	480	19.89041478	0.432945344
500	24.25754852	0.533901919	500	19.89041478	0.432945344
520	24.29242358	0.53466951	520	19.77803956	0.430499325
540	24.0521731	0.529381663	540	19.63078926	0.427294197
560	23.97467295	0.527675906	560	19.64241428	0.427547233
580	24.0986732	0.530405117	580	19.71603943	0.429149798
600	24.00954802	0.528443497	600	19.57653915	0.42611336

Figure 6-10. Continued

I.S. = 0.05 M; 10 mg/L MB NOM

Hydrophobic MB			Hydrophilic MB		
Time (min)	Flux (L/m2/h)	J/Jo	Time (min)	Flux (L/m2/h)	J/Jo
0	45.70571641	1	0	45.58171616	1
10	34.59219418	0.756846121	10	34.9486949	0.766726175
20	29.41905884	0.643662569	20	30.31031062	0.66496642
30	26.73755348	0.584993641	30	27.7489305	0.608773272
40	25.32317565	0.554048326	40	26.22992746	0.57544844
50	23.84679769	0.521746503	50	25.46655093	0.558701012
60	22.54479509	0.493259856	60	25.03642507	0.549264643
70	21.78529357	0.476642645	70	24.64117428	0.540593386
80	21.63804328	0.473420941	80	24.31567363	0.533452351
90	21.51404303	0.470707927	90	24.07154814	0.528096574
100	21.4016678	0.468249258	100	23.82354765	0.522655785
110	21.29316759	0.465875371	110	23.55617211	0.516789935
120	21.4520429	0.46935142	120	23.4476719	0.514409589
135	21.23504247	0.464603646	135	23.52129704	0.516024824
150	21.13816728	0.462484103	150	23.45542191	0.514579614
165	21.01804204	0.459855871	165	22.96329593	0.503783049
180	20.80879162	0.45527766	180	22.92842086	0.503017938
195	20.7506665	0.454005935	195	22.88192076	0.50199779
210	20.70804142	0.453073336	210	22.76567053	0.49944742
225	20.73904148	0.45375159	225	22.79279559	0.500042506
240	20.49491599	0.448410343	240	22.84704569	0.501232679
255	20.15779032	0.441034337	255	22.77342055	0.499617445
270	20.11129022	0.440016956	270	22.80442061	0.500297543
285	20.09191518	0.439593048	285	22.47504495	0.493071495
300	20.0492901	0.438660449	300	22.3006696	0.489245941
320	20.08416517	0.439423485	320	22.31616963	0.48958599
340	19.82453965	0.433743111	340	22.14179428	0.485760435
360	19.58816418	0.428571429	360	22.06816914	0.484145201
380	19.59591419	0.428740992	380	21.77754356	0.477769277
400	19.25878852	0.421364985	400	21.78141856	0.477854289
420	19.26266353	0.421449767	420	21.57991816	0.473433648
440	19.42153884	0.424925816	440	21.75429351	0.477259203
460	19.56878914	0.42814752	460	21.82791866	0.478874437
480	19.68891438	0.430775752	480	21.90541881	0.480574683
500	19.66178932	0.430182281	500	21.74654349	0.477089178
520	19.44478889	0.425434506	520	21.72329345	0.476579104
540	19.19678839	0.420008478	540	21.9015438	0.480489671
560	19.55328911	0.427808393	560	21.62641825	0.474453796
580	19.499039	0.42662145	580	21.73879348	0.476919153
600	19.11541323	0.418228063	600	21.56054312	0.473008586

Figure 6-11. I.S. = 0.01 M; 10 mg/L CT NOM

Unfractionated CT NOM			Hydrophobic CT NOM		
Time (min)	Flux (L/m2/h)	J/Jo	Time (min)	Flux (L/m2/h)	J/Jo
0	44.9500899	1	0	45.68246636	1
10	42.64446029	0.948706897	10	39.85445471	0.872423446
20	40.82320665	0.908189655	20	36.76607353	0.804818051
30	38.56795214	0.858017241	30	34.96419493	0.765374502
40	36.83582367	0.819482759	40	33.96056792	0.743404869
50	35.27032054	0.784655172	50	32.72831546	0.716430571
60	34.74719449	0.773017241	60	32.17806436	0.704385444
70	33.56919214	0.746810345	70	31.91843884	0.69870218
80	33.42194184	0.743534483	80	31.22868746	0.683603359
90	32.92206584	0.732413793	90	31.11631223	0.681143439
100	32.66631533	0.726724138	100	30.93806188	0.677241496
110	32.3989398	0.720775862	110	30.5505611	0.668759013
120	32.21681443	0.716724138	120	30.51956104	0.668080414
135	32.2478145	0.717413793	135	30.2018104	0.661124777
150	32.06956414	0.713448276	150	29.97705995	0.656204937
165	31.499938	0.700775862	165	30.15531031	0.660106879
180	31.37981276	0.698103448	180	30.00806002	0.656883535
195	30.97681195	0.689137931	195	29.6476843	0.648994826
210	30.98068696	0.689224138	210	29.91893484	0.654932564
225	30.5505611	0.679655172	225	29.91118482	0.654762915
240	30.46143592	0.677672414	240	29.67480935	0.6495886
255	30.51181102	0.678793103	255	29.85693471	0.653575367
270	30.40331081	0.67637931	270	29.64380929	0.648910001
285	30.44593589	0.677327586	285	29.60505921	0.648061752
300	30.44206088	0.677241379	300	29.47330895	0.645177708
320	30.38781078	0.676034483	320	29.49268399	0.645601832
340	30.4498109	0.677413793	340	29.32993366	0.642039189
360	30.08168516	0.669224138	360	29.49268399	0.645601832
380	30.02743505	0.668017241	380	29.41518383	0.643905335
400	29.87243474	0.664568966	400	29.44618389	0.644583934
420	29.84143468	0.66387931	420	29.15943332	0.638306896
440	29.81430963	0.663275862	440	29.18655837	0.63890067
460	29.92668485	0.665775862	460	29.1013082	0.637034524
480	29.82980966	0.66362069	480	28.82618265	0.63101196
500	29.71355943	0.661034483	500	28.7990576	0.630418186
520	29.78718457	0.662672414	520	28.50843202	0.624056324
540	29.77555955	0.662413793	540	28.30305661	0.619560607
560	29.72518445	0.661293103	560	28.1984314	0.617270337
580	29.58180916	0.658103448	580	28.17130634	0.616676563
600	29.6011842	0.658534483	600	27.86130572	0.609890576

Figure 6-11. Continued

I.S. = 0.05 M; 10 mg/L CT NOM

Hydrophilic CT NOM			Unfractionated CT NOM		
Time (min)	Flux (L/m2/h)	J/Jo	Time (min)	Flux (L/m2/h)	J/Jo
0	45.01984004	1	0	45.93821688	1
10	39.73820448	0.882682045	10	37.40544981	0.814255588
20	36.84357369	0.818385264	20	33.21656643	0.723070434
30	34.68131936	0.770356344	30	30.90318681	0.672711936
40	32.96856594	0.73231193	40	29.79493459	0.648587094
50	31.99593899	0.710707523	50	28.83005766	0.627583298
60	31.22093744	0.693492856	60	28.33018166	0.616701814
70	30.45368591	0.676450336	70	27.9000558	0.607338676
80	30.07781016	0.668101222	80	27.68305537	0.60261493
90	29.67868436	0.659235669	90	27.56680513	0.600084353
100	29.46943394	0.654587709	100	27.46992994	0.597975538
110	29.41518383	0.653382682	110	27.36917974	0.59578237
120	29.22918346	0.649251162	120	27.30330461	0.594348376
135	29.0509331	0.645291789	135	27.25680451	0.593336145
150	28.75643251	0.638750215	150	26.97005394	0.587094053
165	28.89593279	0.641848855	165	26.87705375	0.585069591
180	28.66343233	0.636684455	180	26.93517887	0.58633488
195	28.70993242	0.637717335	195	26.78792858	0.583129481
210	28.50455701	0.633155448	210	26.73755348	0.582032898
225	28.21393143	0.626699948	225	26.86542873	0.584816533
240	28.06668113	0.623429162	240	26.61742823	0.579417967
255	28.15580631	0.625408848	255	26.501178	0.576887389
270	27.85355571	0.618695128	270	26.6019282	0.579080557
285	27.96593093	0.621191255	285	26.48567797	0.576549979
300	27.92330585	0.620244448	300	26.5476781	0.57789962
320	27.6985554	0.615252195	320	26.24542749	0.571320118
340	27.68305537	0.614907902	340	26.03230206	0.566680725
360	27.77605555	0.616973662	360	26.09042718	0.567946014
380	27.53580507	0.611637115	380	25.52467605	0.555630536
400	27.6016802	0.613100362	400	25.57505115	0.556727119
420	27.81868064	0.617920468	420	25.52080104	0.555546183
440	27.53580507	0.611637115	440	25.48980098	0.554871362
460	27.32655465	0.606989155	460	25.41617583	0.553268663
480	27.38855478	0.608366328	480	25.23017546	0.549219739
500	27.27617955	0.605870201	500	25.42780086	0.553521721
520	27.26842954	0.605698055	520	25.501426	0.55512442
540	27.41955484	0.609054915	540	25.31155062	0.550991143
560	27.15605431	0.603201928	560	25.42780086	0.553521721
580	26.94680389	0.598553968	580	25.18755038	0.54829186
600	26.84217868	0.596229988	600	25.03255007	0.544917756

Figure 6-11. Continued

I.S. = 0.05 M; 10 mg/L CT NOM

Hydrophobic CT NOM			Hydrophilic CT NOM		
Time (min)	Flux (L/m2/h)	J/Jo	Time (min)	Flux (L/m2/h)	J/Jo
0	45.63209126	1	0	45.19034038	1
10	36.61107322	0.802309783	10	35.14244528	0.777653919
20	31.91843884	0.699473505	20	30.86443673	0.682987481
30	29.76393453	0.652258832	30	28.48130696	0.630252101
40	27.83805568	0.610054348	40	26.97392895	0.596895901
50	27.17542935	0.595533288	50	26.03617707	0.576144744
60	26.56705313	0.582201087	60	25.18367537	0.557280055
70	25.73780148	0.564028533	70	24.81554963	0.549133939
80	25.497551	0.558763587	80	24.51329903	0.54244555
90	25.31542563	0.554772418	90	24.14129828	0.534213685
100	25.15267531	0.551205842	100	23.96692293	0.530354999
110	24.87367475	0.545091712	110	23.76154752	0.525810324
120	24.76517453	0.542713995	120	23.60267221	0.522294632
135	24.70704941	0.541440217	135	23.62204724	0.522723375
150	24.52879906	0.537533967	150	23.34692169	0.516635226
165	24.20329841	0.530400815	165	23.47867196	0.519550677
180	23.90879782	0.523947011	180	23.32367165	0.516120734
195	23.83904768	0.522418478	195	22.97104594	0.508317613
210	23.61042222	0.517408288	210	23.10667121	0.511318813
225	23.46317193	0.514181386	225	23.02142104	0.509432344
240	23.25392151	0.509595788	240	23.01367103	0.509260847
255	23.18029636	0.507982337	255	22.81992064	0.504973418
270	23.23454647	0.509171196	270	22.62617025	0.500685989
285	23.21904644	0.508831522	285	22.70754542	0.502486709
300	23.23454647	0.509171196	300	22.22704445	0.491853884
320	23.12992126	0.506878397	320	22.14179428	0.489967416
340	22.88967078	0.501613451	340	22.04491909	0.487823701
360	22.31616963	0.489045516	360	22.07591915	0.48850969
380	22.33166966	0.48938519	380	22.06816914	0.488338192
400	22.26579453	0.487941576	400	21.74266849	0.481135311
420	22.31229462	0.488960598	420	21.70779342	0.480363574
440	22.11466923	0.484629755	440	21.61091822	0.478219859
460	22.27741955	0.488196332	460	21.65354331	0.479163094
480	21.87441875	0.47936481	480	21.55666811	0.477019379
500	22.14179428	0.485224185	500	21.56054312	0.477105128
520	22.12629425	0.484884511	520	21.37841776	0.473074944
540	21.99066898	0.481912364	540	21.29316759	0.471188475
560	21.91316883	0.480213995	560	21.3512927	0.472474704
580	21.73879348	0.476392663	580	21.13816728	0.467758532
600	21.78529357	0.477411685	600	21.13816728	0.467758532

Figure 6.12 (a) TMK NOM molecular weight

Unfractionated TMK NOM			< 1 K MW		
Time (min)	Flux (L/m2/h)	J/Jo	Time (min)	Flux (L/m2/h)	J/Jo
0	44.9500899	1	0	45.5507161	1
10	39.77695455	0.884913793	10	40.88520677	0.8975755
20	36.52194804	0.8125	20	38.12232624	0.836920459
30	34.32094364	0.763534483	30	36.05307211	0.791492982
40	32.81744063	0.730086207	40	34.58444417	0.759251382
50	31.49606299	0.700689655	50	33.59631719	0.737558486
60	30.64356129	0.681724138	60	32.66244032	0.717056572
70	29.96155992	0.666551724	70	31.99206398	0.70233943
80	29.2020584	0.649655172	80	31.72081344	0.696384517
90	28.93080786	0.64362069	90	31.3991878	0.689323692
100	28.64405729	0.637241379	100	31.34493769	0.688132709
110	28.35343171	0.630775862	110	30.85281171	0.677328796
120	27.88455577	0.620344828	120	30.45368591	0.668566567
135	27.52418005	0.612327586	135	30.38781078	0.667120374
150	27.39242978	0.609396552	150	30.37231074	0.666780094
165	27.21030442	0.605344828	165	30.05843512	0.659889409
180	27.07080414	0.602241379	180	29.98868498	0.658358145
195	26.78405357	0.595862069	195	29.71743443	0.652403233
210	26.67942836	0.593534483	210	29.68643437	0.651722671
225	26.5515531	0.590689655	225	29.53530907	0.648404934
240	26.35780272	0.58637931	240	29.12068324	0.639302425
255	26.08655217	0.580344828	255	29.18655837	0.640748618
270	26.07880216	0.580172414	270	29.17493335	0.640493407
285	25.85792672	0.575258621	285	29.03930808	0.637515951
300	25.73005146	0.572413793	300	29.17880836	0.640578477
320	25.77267655	0.573362069	320	29.14005828	0.639727775
340	25.36192572	0.564224138	340	29.03543307	0.63743088
360	25.16042532	0.559741379	360	28.98505797	0.636324968
380	25.05967512	0.5575	380	28.64405729	0.628838792
400	24.98992498	0.555948276	400	28.62080724	0.628328371
420	25.09455019	0.558275862	420	28.60918222	0.62807316
440	25.06355013	0.557586207	440	28.33793168	0.622118248
460	24.99379999	0.556034483	460	28.41155682	0.623734581
480	24.73029946	0.550172414	480	27.90393081	0.612590387
500	24.62954926	0.547931034	500	27.93880588	0.613356019
520	24.50554901	0.545172414	520	28.11318123	0.617184177
540	24.4512989	0.543965517	540	27.7993056	0.610293492
560	24.25754852	0.539655172	560	27.90780582	0.612675457
580	24.23042346	0.539051724	580	27.9000558	0.612505317
600	24.17229834	0.537758621	600	27.89618079	0.612420247

Figure 6.12 (a) TMK NOM molecular weight (continued)

< 3 K TMK NOM			< 5 K TMK NOM		
Time (min)	Flux (L/m2/h)	J/Jo	Time (min)	Flux (L/m2/h)	J/Jo
0	45.89171678	1	0	45.60884122	1
10	41.21845744	0.898167694	10	40.07533015	0.878674596
20	38.36257673	0.83593684	20	36.99469899	0.811129992
30	35.99494699	0.784345183	30	34.97969496	0.766949873
40	34.97581995	0.762137972	40	33.27856656	0.729651657
50	34.23956848	0.74609474	50	32.51131502	0.712829227
60	33.37544175	0.727265051	60	31.56581313	0.692098556
70	32.95694091	0.71814574	70	31.13956228	0.682752761
80	32.20518941	0.701764756	80	30.89156178	0.677315208
90	32.0501891	0.698387233	90	30.35293571	0.665505523
100	31.71306343	0.691041121	100	30.27156054	0.663721325
110	31.72081344	0.691209997	110	30.27931056	0.663891249
120	31.73243846	0.691463312	120	30.26381053	0.663551402
135	31.77118854	0.692307692	135	30.23281047	0.662871708
150	31.68206336	0.690365617	150	29.92280985	0.656074766
165	31.78281357	0.692561007	165	29.97318495	0.657179269
180	31.65493831	0.68977455	180	29.69418439	0.651062022
195	31.49218798	0.686228152	195	29.44618389	0.645624469
210	31.51931304	0.686819218	210	29.30280861	0.642480884
225	31.38756278	0.683948324	225	29.12068324	0.638487681
240	31.17443735	0.67930423	240	28.95405791	0.634834325
255	31.07368715	0.677108841	255	28.91530783	0.633984707
270	30.91481183	0.67364688	270	28.92305785	0.63415463
285	30.80631161	0.671282614	285	28.76030752	0.630586236
300	30.87218674	0.672718061	300	28.7021824	0.62931181
320	30.88381177	0.672971375	320	28.92305785	0.63415463
340	30.69006138	0.668749472	340	28.93080786	0.634324554
360	30.7016864	0.669002786	360	28.65568231	0.628292268
380	30.60481121	0.666891835	380	29.01218302	0.636108751
400	30.6978114	0.668918348	400	28.99280799	0.635683942
420	30.75981152	0.670269357	420	29.07030814	0.637383178
440	30.60481121	0.666891835	440	28.72543245	0.62982158
460	30.30256061	0.660305666	460	28.49293199	0.624723874
480	30.36068572	0.661572237	480	28.53168206	0.625573492
500	30.34131068	0.661150046	500	28.38830678	0.622429907
520	30.01968504	0.654141687	520	27.9504309	0.612829227
540	30.02743505	0.654310563	540	27.95430591	0.612914189
560	30.13206026	0.656590391	560	27.91943084	0.612149533
580	30.01581003	0.654057249	580	27.74505549	0.608326253
600	29.86855974	0.650848603	600	27.41180482	0.601019541

Figure 6.12 (b) TMK NOM molecular weight

Unfractionated TMK NOM			> 1 K TMK-NOM		
Time (min)	Flux (L/m2/h)	J/Jo	Time (min)	Flux (L/m2/h)	J/Jo
0	44.9500899	1	0	45.2988406	1
10	39.77695455	0.884913793	10	40.07920516	0.884773311
20	36.52194804	0.8125	20	36.75444851	0.811377246
30	34.32094364	0.763534483	30	34.36744373	0.758682635
40	32.81744063	0.730086207	40	32.61594023	0.720017109
50	31.49606299	0.700689655	50	31.54256309	0.696321642
60	30.64356129	0.681724138	60	30.42268585	0.671599658
70	29.96155992	0.666551724	70	29.76005952	0.656971771
80	29.2020584	0.649655172	80	28.97343295	0.639606501
90	28.93080786	0.64362069	90	28.55880712	0.630453379
100	28.64405729	0.637241379	100	28.16743133	0.621813516
110	28.35343171	0.630775862	110	27.7489305	0.61257485
120	27.88455577	0.620344828	120	27.64043028	0.610179641
135	27.52418005	0.612327586	135	27.09405419	0.59811805
150	27.39242978	0.609396552	150	26.83442867	0.592386655
165	27.21030442	0.605344828	165	26.57867816	0.586740804
180	27.07080414	0.602241379	180	26.26480253	0.579811805
195	26.78405357	0.595862069	195	26.27642755	0.580068435
210	26.67942836	0.593534483	210	26.0981772	0.576133447
225	26.5515531	0.590689655	225	25.74167648	0.568263473
240	26.35780272	0.58637931	240	25.41230082	0.560992301
255	26.08655217	0.580344828	255	25.33867568	0.55936698
270	26.07880216	0.580172414	270	25.07517515	0.553550043
285	25.85792672	0.575258621	285	25.42392585	0.561248931
300	25.73005146	0.572413793	300	25.4006758	0.560735672
320	25.77267655	0.573362069	320	25.07130014	0.5534645
340	25.36192572	0.564224138	340	24.92404985	0.550213858
360	25.16042532	0.559741379	360	24.48617397	0.540547476
380	25.05967512	0.5575	380	24.44354889	0.539606501
400	24.98992498	0.555948276	400	24.1994234	0.53421728
420	25.09455019	0.558275862	420	24.29242358	0.536270317
440	25.06355013	0.557586207	440	23.99017298	0.529597947
460	24.99379999	0.556034483	460	24.00954802	0.530025663
480	24.73029946	0.550172414	480	23.67629735	0.522668948
500	24.62954926	0.547931034	500	23.79642259	0.525320787
520	24.50554901	0.545172414	520	23.56004712	0.520102652
540	24.4512989	0.543965517	540	23.45542191	0.517792985
560	24.25754852	0.539655172	560	23.58717217	0.520701454
580	24.23042346	0.539051724	580	23.41279683	0.51685201
600	24.17229834	0.537758621	600	23.21904644	0.51257485

Figure 6.12 (b) TMK NOM molecular weight (continued)

> 3K TMK NOM			> 5K TMK NOM		
Time (min)	Flux (L/m2/h)	J/Jo	Time (min)	Flux (L/m2/h)	J/Jo
0	45.97696695	1	0	46.20946742	1
10	39.15695331	0.85166456	10	39.78470457	0.860964361
20	35.47182094	0.771512853	20	36.09182218	0.781048218
30	33.25919152	0.723388116	30	33.61181722	0.727379455
40	31.53093806	0.685798567	40	31.6510633	0.684947589
50	30.63968628	0.666413822	50	30.31806064	0.656100629
60	29.58180916	0.643404973	60	29.60893422	0.640754717
70	28.77580755	0.625874421	70	28.54718209	0.617777778
80	28.21780644	0.613737885	80	27.87293075	0.603186583
90	27.46992994	0.597471555	90	27.43117986	0.593626834
100	26.99330399	0.58710493	100	26.74142848	0.57870021
110	26.68330337	0.58036241	110	26.38880278	0.571069182
120	26.44692789	0.575221239	120	25.72230144	0.556645702
135	25.76492653	0.560387695	135	25.22242544	0.545828092
150	25.33480067	0.551032448	150	25.11005022	0.543396226
165	24.9511749	0.54268858	165	24.70704941	0.534675052
180	24.22267345	0.526843658	180	24.04054808	0.520251572
195	24.14129828	0.525073746	195	23.87779776	0.51672956
210	23.82354765	0.518162663	210	23.60654721	0.510859539
225	23.39729679	0.508891698	225	23.15317131	0.501048218
240	23.22292145	0.505099031	240	22.35491971	0.483773585
255	23.1492963	0.503497682	255	22.43629487	0.485534591
270	22.98654597	0.499957859	270	22.4479199	0.485786164
285	22.8005456	0.495912347	285	22.34329469	0.483522013
300	22.55254511	0.490518331	300	22.28516957	0.482264151
320	22.22316945	0.483354404	320	21.90541881	0.474046122
340	21.96741893	0.477791825	340	21.62254325	0.467924528
360	21.81629363	0.474504846	360	21.26991754	0.460293501
380	21.30479261	0.463379688	380	21.25441751	0.459958071
400	21.24666749	0.462115466	400	21.21566743	0.459119497
420	21.03741707	0.457564265	420	21.16916734	0.458113208
440	20.73516647	0.450990308	440	21.02966706	0.45509434
460	20.52204104	0.446354825	460	20.83591667	0.450901468
480	20.37091574	0.443067847	480	20.79716659	0.450062893
500	20.07641515	0.436662453	500	20.69641639	0.4478826
520	19.89041478	0.432616941	520	20.47166594	0.443018868
540	19.80516461	0.430762748	540	20.16166532	0.436310273
560	19.87103974	0.432195533	560	20.18879038	0.436897275
580	19.84391469	0.431605563	580	19.75478951	0.427505241
600	19.64241428	0.427222925	600	19.45253891	0.420964361

Figure 6.13 (a) MB NOM molecular weight

Unfractionated MB NOM			< 1K MB NOM		
Time (min)	Flux (L/m2/h)	J/Jo	Time (min)	Flux (L/m2/h)	J/Jo
0	45.27946556	1	0	45.85296671	1
10	39.74595449	0.877792041	10	42.07870916	0.917687822
20	37.51782504	0.828583654	20	39.65682931	0.864869433
30	35.49119598	0.783825417	30	38.25407651	0.834277022
40	34.78594457	0.768249893	40	37.6495753	0.821093552
50	34.02256805	0.751390672	50	36.66144832	0.799543649
60	33.46069192	0.7389816	60	36.2506975	0.79058565
70	33.35606671	0.736670946	70	36.20419741	0.789571537
80	32.8484407	0.725459991	80	35.82832166	0.781374123
90	32.66244032	0.721352161	90	35.72369645	0.779092369
100	32.72831546	0.722807018	100	35.5996962	0.776388067
110	32.45318991	0.716730852	110	35.58032116	0.77596552
120	32.68956538	0.72195122	120	35.44082088	0.772923181
135	32.67406535	0.7216089	135	35.28969558	0.769627313
150	32.59656519	0.719897304	150	35.31682063	0.770218879
165	32.48806498	0.71750107	165	35.17344535	0.767092031
180	32.32143964	0.713821138	180	34.91381983	0.761429899
195	32.51906504	0.718185708	195	34.95644491	0.762359503
210	32.39118978	0.715361575	210	34.91769484	0.761514409
225	32.31368963	0.713649979	225	34.76656953	0.758218541
240	32.14706429	0.709970047	240	35.05332011	0.764472239
255	32.13931428	0.709798887	255	34.80531961	0.759063636
270	32.04243908	0.707659392	270	34.88669477	0.760838333
285	32.08893918	0.70868635	285	34.66581933	0.756021296
300	32.07343915	0.708344031	300	34.68131936	0.756359334
320	31.97656395	0.706204536	320	34.53406907	0.753147976
340	31.85256371	0.703465982	340	34.77431955	0.75838756
360	31.82543865	0.702866923	360	34.77819456	0.75847207
380	31.74406349	0.701069748	380	34.78206956	0.758556579
400	31.77506355	0.701754386	400	34.43331887	0.750950731
420	31.77118854	0.701668806	420	34.71619443	0.757119919
440	31.63943828	0.698759093	440	34.49531899	0.752302882
460	31.75568851	0.701326487	460	34.59219418	0.754415617
480	31.61618823	0.698245614	480	34.18919338	0.745626637
500	31.75956352	0.701412067	500	34.44106888	0.75111975
520	31.47668795	0.695164741	520	34.47206894	0.751795825
540	31.45343791	0.694651262	540	34.37906876	0.749767599
560	31.43406287	0.694223363	560	34.60381921	0.754669146
580	31.40693781	0.693624305	580	34.39456879	0.750105637
600	31.52318805	0.696191699	600	34.41394383	0.750528184

Figure 6.13 (a) MB NOM molecular weight (continued)

< 3K MB NOM			< 5K MB NOM		
Time (min)	Flux (L/m2/h)	J/Jo	Time (min)	Flux (L/m2/h)	J/Jo
0	45.63984128	1	0	46.04284209	1
10	40.67595635	0.891237901	10	41.06733213	0.891937384
20	37.71157542	0.826286296	20	38.36257673	0.833193065
30	35.75857152	0.783494651	30	36.96757394	0.802895135
40	34.89056978	0.764476142	40	35.72757146	0.775963642
50	33.98381797	0.744608592	50	35.03394507	0.760898839
60	33.25531651	0.728646629	60	34.73169446	0.754334287
70	32.7476905	0.717524198	70	34.23181846	0.743477529
80	32.14318929	0.704279165	80	34.16206832	0.741962633
90	32.09281419	0.703175412	90	34.13494327	0.741373506
100	32.03856408	0.701986755	100	34.07294315	0.740026931
110	31.95331391	0.700118866	110	33.83269267	0.734808955
120	31.68981338	0.69434539	120	33.66219232	0.731105874
135	31.51931304	0.690609611	135	33.67769236	0.731442518
150	31.56581313	0.69162846	150	33.35994172	0.724541323
165	31.41468783	0.688317202	165	33.29406659	0.723110587
180	31.45731291	0.689251146	180	33.17006634	0.720417438
195	31.41468783	0.688317202	195	33.29019158	0.723026427
210	31.37593775	0.687468161	210	33.02669105	0.717303484
225	31.3991878	0.687977585	225	33.12356625	0.719407507
240	31.46506293	0.689420954	240	32.99181598	0.716546036
255	31.43793788	0.688826626	255	33.06156612	0.718060933
270	31.39143778	0.687807777	270	33.13131626	0.719575829
285	31.20931242	0.683817286	285	33.15456631	0.720080794
300	31.17831236	0.683138054	300	32.95694091	0.715788588
320	31.31006262	0.686024792	320	32.90656581	0.714694496
340	31.33718767	0.68661912	340	32.95694091	0.715788588
360	31.25968752	0.684921039	360	33.10419121	0.718986703
380	31.4495629	0.689081338	380	32.9491909	0.715620266
400	31.41468783	0.688317202	400	32.96469093	0.71595691
420	31.39531279	0.687892681	420	32.82131564	0.712842956
440	31.21706243	0.683987095	440	32.97244094	0.716125231
460	31.31006262	0.686024792	460	32.77094054	0.711748864
480	31.3991878	0.687977585	480	32.93756588	0.715367783
500	31.43793788	0.688826626	500	32.81356563	0.712674634
520	31.46118792	0.68933605	520	32.88331577	0.71418953
540	31.31006262	0.686024792	540	32.82906566	0.713011278
560	31.31781264	0.6861946	560	32.86781574	0.713852887
580	31.39143778	0.687807777	580	32.90269081	0.714610335
600	31.35268771	0.686958737	600	32.8988158	0.714526174

Figure 6.13 (b) MB NOM molecular weight

Unfractionated MB NOM			> 1K MB NOM		
Time (min)	Flux (L/m2/h)	J/Jo	Time (min)	Flux (L/m2/h)	J/Jo
0	45.27946556	1	0	45.08571517	1
10	39.74595449	0.877792041	10	39.9513299	0.886119467
20	37.51782504	0.828583654	20	37.09157418	0.822690159
30	35.49119598	0.783825417	30	34.94481989	0.775075204
40	34.78594457	0.768249893	40	34.07681815	0.755822948
50	34.02256805	0.751390672	50	33.16619133	0.735625269
60	33.46069192	0.7389816	60	32.63144026	0.723764504
70	33.35606671	0.736670946	70	31.99593899	0.709669102
80	32.8484407	0.725459991	80	31.68206336	0.702707349
90	32.66244032	0.721352161	90	30.95743691	0.686635153
100	32.72831546	0.722807018	100	30.94193688	0.686291362
110	32.45318991	0.716730852	110	30.9496869	0.686463257
120	32.68956538	0.72195122	120	30.62031124	0.679157714
135	32.67406535	0.7216089	135	30.53893608	0.677352815
150	32.59656519	0.719897304	150	30.6513113	0.679845294
165	32.48806498	0.71750107	165	30.56218612	0.6778685
180	32.32143964	0.713821138	180	30.2986856	0.672024065
195	32.51906504	0.718185708	195	30.28318557	0.671680275
210	32.39118978	0.715361575	210	30.25993552	0.67116459
225	32.31368963	0.713649979	225	30.34518569	0.673055436
240	32.14706429	0.709970047	240	30.13593527	0.668414267
255	32.13931428	0.709798887	255	30.00031	0.665406102
270	32.04243908	0.707659392	270	30.05843512	0.666695316
285	32.08893918	0.70868635	285	30.22118544	0.670305114
300	32.07343915	0.708344031	300	30.16693533	0.669101848
320	31.97656395	0.706204536	320	30.19406039	0.669703481
340	31.85256371	0.703465982	340	30.26381053	0.671250537
360	31.82543865	0.702866923	360	30.01968504	0.66583584
380	31.74406349	0.701069748	380	29.85693471	0.662226042
400	31.77506355	0.701754386	400	29.90343481	0.663257413
420	31.77118854	0.701668806	420	30.22893546	0.670477009
440	31.63943828	0.698759093	440	30.11656023	0.667984529
460	31.75568851	0.701326487	460	30.23281047	0.670562957
480	31.61618823	0.698245614	480	30.37231074	0.673657069
500	31.75956352	0.701412067	500	30.31418563	0.672367856
520	31.47668795	0.695164741	520	30.27931056	0.671594327
540	31.45343791	0.694651262	540	30.1514353	0.668758058
560	31.43406287	0.694223363	560	30.06231012	0.666781263
580	31.40693781	0.693624305	580	29.97705995	0.664890417
600	31.52318805	0.696191699	600	29.93055986	0.663859046

Figure 6.13 (b) MB NOM molecular weight

> 3K MB NOM			> 5K MB NOM		
Time (min)	Flux (L/m2/h)	J/Jo	Time (min)	Flux (L/m2/h)	J/Jo
0	45.46546593	1	0	45.85684171	1
10	39.81182962	0.875649876	10	40.66820634	0.886851445
20	36.71182342	0.807466121	20	37.82782566	0.824911273
30	35.01457003	0.770135515	30	36.21582243	0.789758323
40	33.51881704	0.737236853	40	34.87894476	0.760605036
50	32.60431521	0.717122646	50	34.00706801	0.741592023
60	31.81768864	0.699821018	60	33.26694153	0.725452087
70	31.7983136	0.699394869	70	32.9491909	0.7185229
80	31.36043772	0.689763914	80	32.61206522	0.711171202
90	31.03106206	0.68251939	90	32.63144026	0.711593713
100	30.78693657	0.677149919	100	31.97656395	0.697312827
110	30.59706119	0.672973664	110	31.82931366	0.694101741
120	30.40718581	0.668797409	120	31.90293881	0.695707284
135	30.17856036	0.663768857	135	31.72468845	0.691820179
150	30.09331019	0.661893804	150	31.6006882	0.689116106
165	29.7523095	0.654393591	165	31.32168764	0.683031942
180	29.63605927	0.6518367	180	31.00781202	0.676187257
195	29.74455949	0.654223131	195	31.15893732	0.679482846
210	29.6476843	0.652092389	210	31.22481245	0.680919385
225	29.46555893	0.648086593	225	31.11631223	0.678553321
240	29.54693409	0.649876417	240	31.26743753	0.68184891
255	29.63993428	0.65192193	255	31.05818712	0.677285787
270	29.500434	0.648853661	270	31.03106206	0.676694271
285	29.3996838	0.646637689	285	30.87218674	0.673229677
300	29.40355881	0.646722918	300	30.66681133	0.668751056
320	29.40355881	0.646722918	320	30.72106144	0.669934088
340	29.51980904	0.649279809	340	30.58543617	0.666976508
360	29.57793416	0.650558254	360	30.59318619	0.667145513
380	29.6011842	0.651069633	380	30.61643623	0.667652527
400	29.57793416	0.650558254	400	30.58156116	0.666892006
420	29.60505921	0.651154862	420	30.52731105	0.665708974
440	29.61280923	0.651325322	440	30.28318557	0.66038533
460	29.49268399	0.648683201	460	30.2986856	0.66072334
480	29.45393391	0.647830904	480	30.29481059	0.660638837
500	29.48493397	0.648512742	500	30.49243598	0.664948454
520	29.56243412	0.650217336	520	30.38006076	0.662497887
540	29.56630913	0.650302565	540	30.11656023	0.656751732
560	29.55855912	0.650132106	560	30.16306033	0.65776576
580	29.62055924	0.651495781	580	30.18631037	0.658272773
600	29.53530907	0.649620728	600	30.1514353	0.657512253

Figure 6.14 (a) CT NOM molecular weight

Unfractionated CT NOM			< 1K CT NOM		
Time (min)	Flux (L/m2/h)	J/Jo	Time (min)	Flux (L/m2/h)	J/Jo
0	44.9500899	1	0	45.12834026	1
10	42.64446029	0.948706897	10	39.9513299	0.8852825
20	40.82320665	0.908189655	20	36.6498233	0.812124335
30	38.56795214	0.858017241	30	34.75494451	0.770135669
40	36.83582367	0.819482759	40	33.26306653	0.737077108
50	35.27032054	0.784655172	50	32.29431459	0.71561051
60	34.74719449	0.773017241	60	31.44181288	0.696719904
70	33.56919214	0.746810345	70	31.2015624	0.691396188
80	33.42194184	0.743534483	80	30.78306157	0.682122617
90	32.92206584	0.732413793	90	30.77143654	0.681865018
100	32.66631533	0.726724138	100	30.73656147	0.681092221
110	32.3989398	0.720775862	110	30.41881084	0.674051176
120	32.21681443	0.716724138	120	30.1979354	0.669156792
135	32.2478145	0.717413793	135	30.33356067	0.672162116
150	32.06956414	0.713448276	150	30.18243536	0.668813326
165	31.499938	0.700775862	165	30.07781016	0.666494934
180	31.37981276	0.698103448	180	30.21731043	0.669586124
195	30.97681195	0.689137931	195	29.97318495	0.664176541
210	30.98068696	0.689224138	210	29.74455949	0.659110424
225	30.5505611	0.679655172	225	29.88793478	0.662287481
240	30.46143592	0.677672414	240	29.8995598	0.66254508
255	30.51181102	0.678793103	255	29.76005952	0.65945389
270	30.40331081	0.67637931	270	29.91505983	0.662888545
285	30.44593589	0.677327586	285	29.89180978	0.662373347
300	30.44206088	0.677241379	300	29.80268461	0.66039842
320	30.38781078	0.676034483	320	29.79493459	0.660226687
340	30.4498109	0.677413793	340	29.79105958	0.660140821
360	30.08168516	0.669224138	360	29.88793478	0.662287481
380	30.02743505	0.668017241	380	29.82980966	0.660999485
400	29.87243474	0.664568966	400	29.90730981	0.662716813
420	29.84143468	0.66387931	420	29.91893484	0.662974412
440	29.81430963	0.663275862	440	29.87243474	0.661944015
460	29.92668485	0.665775862	460	29.88793478	0.662287481
480	29.82980966	0.66362069	480	29.84530969	0.66134295
500	29.71355943	0.661034483	500	29.80655961	0.660484286
520	29.78718457	0.662672414	520	29.85305971	0.661514683
540	29.77555955	0.662413793	540	29.79493459	0.660226687
560	29.72518445	0.661293103	560	29.88018476	0.662115748
580	29.58180916	0.658103448	580	29.85305971	0.661514683
600	29.6011842	0.658534483	600	29.83368467	0.661085351

Figure 6.14 (a) CT NOM molecular weight

< 3K CT NOM			< 5K CT NOM		
Time (min)	Flux (L/m2/h)	J/Jo	Time (min)	Flux (L/m2/h)	J/Jo
0	45.63596627	1	0	45.94596689	1
10	39.92032984	0.87475588	10	41.01695703	0.892721599
20	36.51032302	0.800033965	20	38.35482671	0.834781142
30	34.61156922	0.758427443	30	36.63819828	0.797419246
40	33.05381611	0.724293114	40	35.47957096	0.772202075
50	31.84481369	0.697800798	50	34.48756898	0.750611453
60	31.34106268	0.686762333	60	33.82494265	0.736189593
70	30.6513113	0.671648128	70	33.58469217	0.730960614
80	30.20568541	0.661883332	80	33.4490669	0.728008771
90	29.69030938	0.650590133	90	32.88719077	0.715779708
100	29.72130944	0.651269423	100	32.68569037	0.711394113
110	29.45780892	0.645495457	110	32.59269019	0.709369992
120	29.27180854	0.641419716	120	32.66244032	0.710888083
135	29.38030876	0.643797232	135	32.64694029	0.71055073
150	29.40355881	0.644306699	150	32.48031496	0.70692418
165	29.39193378	0.644051966	165	32.59656519	0.709454331
180	29.36868374	0.643542498	180	32.44156488	0.706080796
195	29.24080848	0.640740426	195	32.42218984	0.705659104
210	29.2020584	0.639891314	210	32.3989398	0.705153074
225	29.17105834	0.639212023	225	32.21293943	0.701104833
240	29.12843326	0.638277999	240	32.33306467	0.703719322
255	29.08193316	0.637259064	255	32.43768988	0.705996458
270	29.02768306	0.636070307	270	32.36018972	0.70430969
285	28.88818278	0.633013501	285	32.50744001	0.707514548
300	28.72543245	0.629447228	300	32.2981896	0.702960277
320	28.63243226	0.627409357	320	32.27493955	0.702454246
340	28.64018228	0.62757918	340	32.14706429	0.69967108
360	28.53943208	0.625371487	360	32.11993924	0.699080712
380	28.5975572	0.626645156	380	32.07343915	0.698068651
400	28.66343233	0.628088647	400	32.11218922	0.698912035
420	28.64018228	0.62757918	420	31.94556389	0.695285485
440	28.58980718	0.626475333	440	32.07731415	0.69815299
460	28.50843202	0.624692197	460	31.8021886	0.692164966
480	28.55493211	0.625711132	480	31.75956352	0.691237244
500	28.58593217	0.626390422	500	31.68981338	0.689719153
520	28.62468225	0.627239535	520	31.72468845	0.690478199
540	28.60530721	0.626814978	540	31.67431335	0.6893818
560	28.62855726	0.627324446	560	31.56581313	0.687020326
580	28.5975572	0.626645156	580	31.62781326	0.688369739
600	28.55493211	0.625711132	600	31.60456321	0.687863709

Figure 6.14 (b) CT NOM molecular weight

Unfractionated CT NOM			> 1K CT NOM		
Time (min)	Flux (L/m2/h)	J/Jo	Time (min)	Flux (L/m2/h)	J/Jo
0	44.9500899	1	0	45.36859074	1
10	42.64446029	0.948706897	10	40.6023312	0.894943628
20	40.82320665	0.908189655	20	37.70382541	0.831055688
30	38.56795214	0.858017241	30	35.72757146	0.787495729
40	36.83582367	0.819482759	40	34.97969496	0.771011274
50	35.27032054	0.784655172	50	33.73194246	0.743508712
60	34.74719449	0.773017241	60	33.2010664	0.731807311
70	33.56919214	0.746810345	70	32.49581499	0.716262385
80	33.42194184	0.743534483	80	32.43381487	0.714895798
90	32.92206584	0.732413793	90	32.16256433	0.70891698
100	32.66631533	0.726724138	100	31.86031372	0.702254868
110	32.3989398	0.720775862	110	31.83318867	0.701656987
120	32.21681443	0.716724138	120	31.55418811	0.695507345
135	32.2478145	0.717413793	135	31.48056296	0.693884523
150	32.06956414	0.713448276	150	31.18218736	0.687307824
165	31.499938	0.700775862	165	31.22093744	0.688161941
180	31.37981276	0.698103448	180	31.22868746	0.688332764
195	30.97681195	0.689137931	195	30.96906194	0.682610181
210	30.98068696	0.689224138	210	31.00781202	0.683464298
225	30.5505611	0.679655172	225	31.01168702	0.68354971
240	30.46143592	0.677672414	240	31.000062	0.683293475
255	30.51181102	0.678793103	255	30.96518693	0.682524769
270	30.40331081	0.67637931	270	30.94193688	0.682012299
285	30.44593589	0.677327586	285	30.7985616	0.678852067
300	30.44206088	0.677241379	300	30.50406101	0.672360779
320	30.38781078	0.676034483	320	30.45368591	0.671250427
340	30.4498109	0.677413793	340	30.44593589	0.671079604
360	30.08168516	0.669224138	360	30.52343605	0.672787837
380	30.02743505	0.668017241	380	30.49631099	0.672189956
400	29.87243474	0.664568966	400	30.1979354	0.665613256
420	29.84143468	0.66387931	420	30.21343543	0.665954903
440	29.81430963	0.663275862	440	30.26381053	0.667065255
460	29.92668485	0.665775862	460	30.17856036	0.665186197
480	29.82980966	0.66362069	480	30.07393515	0.662880082
500	29.71355943	0.661034483	500	30.09718519	0.663392552
520	29.78718457	0.662672414	520	30.1514353	0.664588316
540	29.77555955	0.662413793	540	30.17468535	0.665100786
560	29.72518445	0.661293103	560	30.16693533	0.664929962
580	29.58180916	0.658103448	580	30.11268523	0.663734199
600	29.6011842	0.658534483	600	30.07006014	0.66279467

Figure 6.14 (b) CT NOM molecular weight

> 3K CT NOM			> 5 K CT NOM		
Time (min)	Flux (L/m2/h)	J/Jo	Time (min)	Flux (L/m2/h)	J/Jo
0	45.5507161	1	0	45.73671647	1
10	40.50933102	0.889323692	10	40.6992064	0.889858511
20	37.57207514	0.824840493	20	38.33932668	0.838261459
30	35.55707111	0.780603998	30	36.53744807	0.798864695
40	34.74331949	0.76273926	40	35.40982082	0.774209947
50	34.15431831	0.749808592	50	34.59219418	0.756333136
60	33.11969124	0.727094853	60	33.64281729	0.735575701
70	32.76706553	0.719353467	70	33.15844132	0.724985173
80	32.6004402	0.715695449	80	32.96469093	0.720748962
90	32.44156488	0.712207571	90	32.96469093	0.720748962
100	32.39506479	0.711186729	100	32.78644057	0.716851648
110	32.12768926	0.705316886	110	32.59656519	0.712700161
120	32.26331453	0.708294343	120	32.45318991	0.709565365
135	31.99206398	0.70233943	135	32.22843946	0.70465136
150	32.03081406	0.703190132	150	32.32531465	0.706769465
165	31.74406349	0.696894938	165	32.34468969	0.707193087
180	31.74018848	0.696809868	180	32.42993986	0.709057019
195	31.73243846	0.696639728	195	32.26718953	0.705498602
210	31.39531279	0.689238622	210	32.37181474	0.707786156
225	31.37593775	0.688813271	225	32.46093992	0.709734813
240	31.3023126	0.687196937	240	32.41056482	0.708633398
255	30.98843698	0.680306253	255	32.18968938	0.703804118
270	31.02718705	0.681156954	270	32.22843946	0.70465136
285	31.09306219	0.682603148	285	32.18581437	0.703719393
300	31.05431211	0.681752446	300	32.42218984	0.708887571
320	30.96131192	0.679710761	320	32.25556451	0.705244429
340	31.01556203	0.680901744	340	32.40281481	0.70846395
360	31.04268709	0.681497235	360	32.15868932	0.703126324
380	31.00393701	0.680646533	380	31.78281357	0.694908074
400	30.82568665	0.676733305	400	31.87968876	0.69702618
420	30.62031124	0.672224585	420	31.89131378	0.697280352
440	30.43818588	0.668226287	440	31.68206336	0.692705244
460	30.53506107	0.670353041	460	31.60456321	0.69101076
480	30.40331081	0.667460655	480	31.41081282	0.686774549
500	30.44593589	0.668396427	500	31.31393763	0.684656443
520	30.41881084	0.667800936	520	31.26743753	0.683639753
540	30.47306095	0.668991918	540	31.2984376	0.684317546
560	30.31806064	0.665589111	560	31.25581251	0.68338558
580	30.38781078	0.667120374	580	31.25968752	0.683470304
600	30.31031062	0.665418971	600	31.22093744	0.682623062